2013

Development of a Guide for Prioritization of Railway Bridges for Repair and Replacement

Anna Maria Rakoczy
University of Nebraska-Lincoln, arakoczy1@gmail.com

Andrzej S. Nowak
University of Nebraska-Lincoln, asn0007@auburn.edu

MID-AMERICA
TRANSPORTATION CENTER

Report # MATC-UNL: #052

Final Report
25-1121-0003-052

Development of a Guide for Prioritization of Railway Bridges for Repair and Replacement

Anna M. Rakoczy
Post-Doctoral Research Associate
Department of Civil Engineering
University of Nebraska-Lincoln

Andrzej S. Nowak
Professor

2013

A Coopertative Research Project sponsored by
U.S. Department of Tranportation-Research, Innovation and Technology Innovation Administration

Development of a Guide for Prioritization of Railway Bridges for Repair and Replacement

Anna M. Rakoczy, Ph.D.
Post-Doctoral Research Associate
Department of Civil Engineering
University of Nebraska-Lincoln

Andrzej S. Nowak, Ph.D.,
Professor
Department of Civil Engineering
University of Nebraska-Lincoln

A Report on Research Sponsored by

Mid-America Transportation Center

University of Nebraska-Lincoln

September 2013

Technical Report Documentation Page

1. Report No. 25-1121-0003-052	2. Government Accession No.	3. Recipient's Catalog No.
4. Title and Subtitle Development of a Guide for Prioritization of Railway Bridges for Repair and Replacement		5. Report Date September 2013
		6. Performing Organization Code
7. Author(s) Anna M. Rakoczy and Andrzej S. Nowak		8. Performing Organization Report No. 25-1121-0003-052
9. Performing Organization Name and Address Mid-America Transportation Center 2200 Vine St. PO Box 830851 Lincoln, NE 68583-0851		10. Work Unit No. (TRAIS)
		11. Contract or Grant No.
12. Sponsoring Agency Name and Address Research and Innovative Technology Administration 1200 New Jersey Ave., SE Washington, D.C. 20590		13. Type of Report and Period Covered August 2012 - August 2013
		14. Sponsoring Agency Code MATC TRB RiP No. 28686
15. Supplementary Notes		

16. Abstract

The objective of this study was to develop evaluation bases for the repair, rehabilitation, and replacement of existing railway bridges. Considering the importance of bridges to the railway network, the research involved the review and analysis of major factors that influence structural performance, e.g., degree of corrosion, loss of material (section loss, holes), fatigue problems, and loose connections. In particular, the research focused on connections, and their importance relative to the evaluation of bridge performance. The relationship between various conditions and the ability to perform the required function (i.e., carry a freight train) was established in the form of maximum capacity. Sensitivity analysis was performed to establish the relationship between load and resistance factors. Results were presented in the form of graphs and tables. The outcomes of this study served as a basis for the development of a decision-making spread sheet. This report provides research documentation and offers a tool for bridge owners for the prioritization of structures for repair/rehabilitation or replacement. The study involved the nonlinear finite element method (FEM) analysis of stringer-to-floorbeam connections, the development of the resistance capacity of typical bridge connections, and the calculation of reduced capacity based on deterioration and other conditions. The findings and final conclusions of this research could serve as a basis for the development of more accurate provisions for the evaluation of railway bridges.

17. Key Words railway bridges, FEM analysis, bolted connections	18. Distribution Statement		
19. Security Classif. (of this report) Unclassified	20. Security Classif. (of this page) Unclassified	21. No. of Pages 158	22. Price

Table of Contents

List of Figures

List of Tables

Disclaimer

The contents of this report reflect the views of the authors, who are responsible for the facts and the accuracy of the information presented herein. This document is disseminated under the sponsorship of the U.S. Department of Transportation's University Transportation Centers Program, in the interest of information exchange. The U.S. Government assumes no liability for the contents or use thereof.

Abstract

The objective of this study was to develop evaluation bases for the repair, rehabilitation, and replacement of existing railway bridges. Considering the importance of bridges to the railway network, the research involved the review and analysis of major factors that influence structural performance, e.g., degree of corrosion, loss of material (section loss, holes), fatigue problems, and loose connections. In particular, the research focused on connections, and their importance relative to the evaluation of bridge performance. The relationship between various conditions and the ability to perform the required function (i.e., carry a freight train) was established in the form of maximum capacity. Sensitivity analysis was performed to establish the relationship between load and resistance factors. Results were presented in the form of graphs and tables. The outcomes of this study served as a basis for the development of a decision-making spread sheet. This report provides research documentation and offers a tool for bridge owners for the prioritization of structures for repair/rehabilitation or replacement. The study involved the nonlinear finite element method (FEM) analysis of stringer-to-floorbeam connections, the development of the resistance capacity of typical bridge connections, and the calculation of reduced capacity based on deterioration and other conditions. The findings and final conclusions of this research could serve as a basis for the development of more accurate provisions for the evaluation of railway bridges.

Chapter 1 Introduction

1.1 Problem Statement

The performance of the railway transportation network depends upon the reliability of railway bridges, which can be affected by various forms of deterioration and extreme environmental conditions. More than half of railway bridges in the U.S. were built prior to 1950, and many show signs of distress. Bridge owners are in need of evaluation criteria for existing structures to enable rational decisions regarding bridge repair, rehabilitation, or replacement. With limited available resources, this decision-making is important and has potentially serious financial consequences. The objective of the current research was to formulate rational acceptability criteria for critical bridge components based upon the resulting theoretical and analytical findings.

The design and rating procedures for railway bridges are included in the Manual for Railway Engineering published by the American Railway Engineering and Maintenance-of-Way Association (AREMA) and Federal Railway Administration (FRA). According to FRA 49 CFR Part 237 (2010), "Each bridge management program shall include a provision for scheduling an inspection for each bridge in railroad service at least once in each calendar year, with not more than 540 days between any successive inspections." However, the rated condition of a single bridge is not adequate criteria by which to provide general guidelines for the prioritization of structures for reair and replacement, as this prioritization relies upon many factors. On one hand are load rating criteria; on the other hand, structural deterioration. Environmental and climatic conditions also have a considerable influence on structural members.

Inspectors have to deal with the serviceability of bearings, severely corroded bracings, loose fastener connections, holes in web, and many other problems. Each determination of an

inspection can have a different impact on the evaluation of the entire bridge. The question is how to measure the level of safety, which, of the above determinations, is most important. For example, what is a low, medium, and high level of corrosion? How many loose connections can lead to failure? Probability of failure is therefore proposed as a prioritization criterion for bridge repair.

Closure of a railway bridge can cause the stoppage of railway traffic and serious logistical problems in terms of detouring trains. Moreover, since freight trains constitute the majority of railway traffic, their stoppage can have severe consequences on the regional or even national economy, such as interruptions in production due to the deficiency or late delivery of raw materials (e.g., coal or iron ore). Costs related to the interruption of the manufacturing process and the resumption of production can be very high. Therefore, the consequences of railway bridge closure can be unacceptably high.

An important question facing the owners and administrators of railway bridges is how to assure the safety of existing structures under their jurisdiction. The development of a rational ranking system requires the consideration of many factors, including:

(1) Identification of critical parameters that affect the resistance capacity of railway bridges.

(2) Evaluation of structural capacity based upon degree of deterioration.

(3) Development of accurate and efficient procedures for the assessment of existing bridges.

(4) Development of procedures for the prediction of the remaining life time of existing bridges.

The current study addressed items 1 and 2, primarily.

During bridge evaluation, both the primary and secondary bridge components must be considered. However, each component can entail a component-specific inspection procedure. The proposed inspection guidelines were developed for the prioritization of bridge repairs.

This research focused on the estimation of bridge capacity based upon the findings of a bridge inspection. This involved determining how to prioritize inspection findings: for example, what is a low, medium, or high level of corrosion? Or, how many loose connections can lead to failure? Accordingly, it was proposed that probability of failure be used as a prioritization criterion for bridge repair.

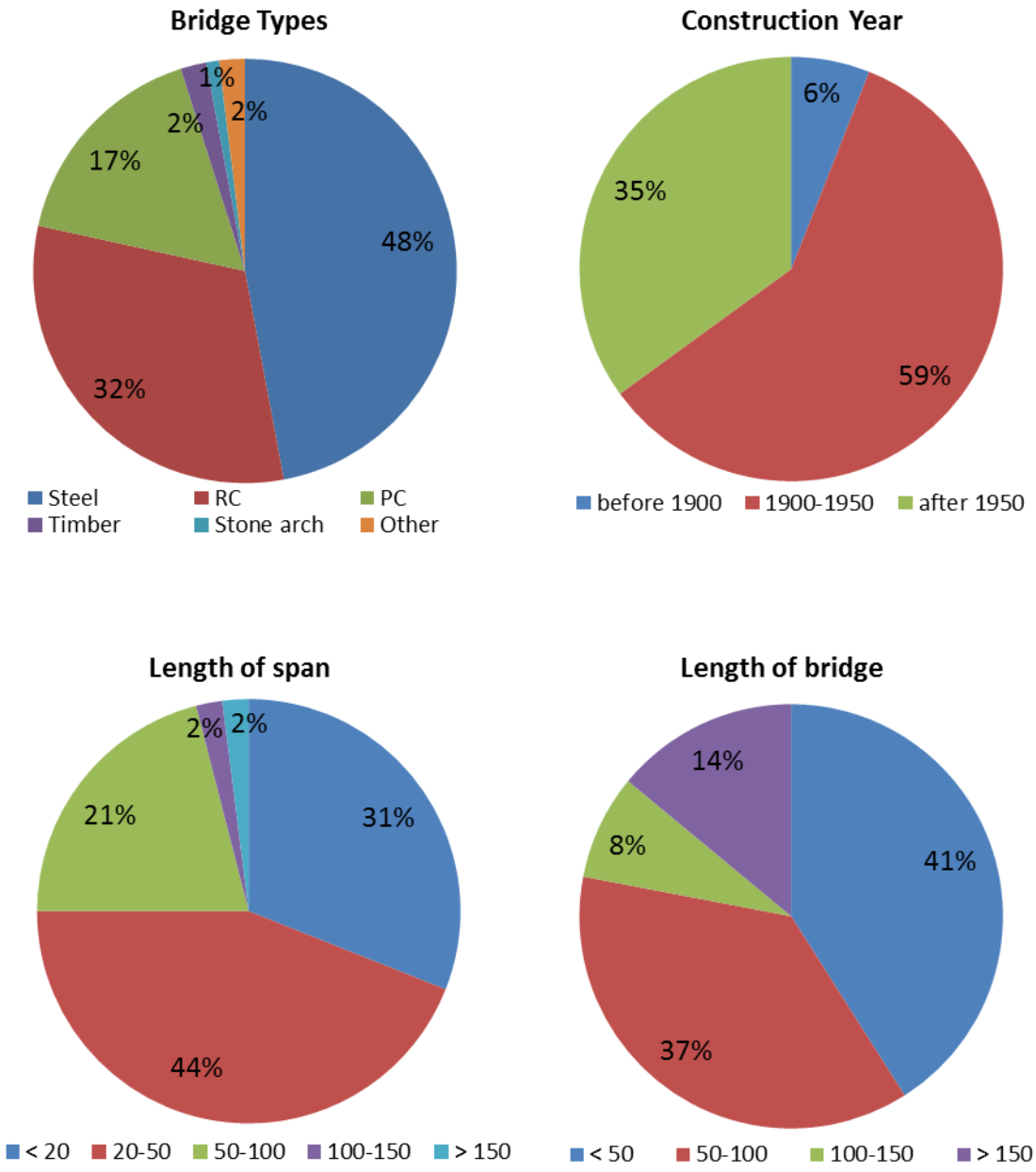

Figure 1.1 Characteristics of railway bridges on main lines in Nebraska and Iowa

Figure 1.1, based on data provided by Union Pacific, illustrates the characteristics of railway bridges on main lines in Nebraska and Iowa. The figure reveals that over 60% of railway bridges in Nebraska and Iowa were constructed prior to 1950. As such, these bridges require special attention. Such statistics are true for the entire nation. As summarized in fig. 1.1,

approximately 50% of railway bridges are steel structures, while approximately 40% are short bridges with a total length of less than 50 ft.; approximately 75% have span lengths of less than 50 ft.

According to data from one heavy-duty main line, approximately 50% of railway bridges are steel structures, and about 25% of all steel bridges are through plate girder bridges. Based on the characteristic of one secondary main line, 20% of all steel bridges are through plate girder bridges—all of the same turn of the 20th century vintage—and all are steel. These data were provided by two separate railroads, and concern the number of TPGs relative to the total number of steel bridges on mainline subdivisions.

The development of a rational ranking system requires the consideration of many factors, including: the identification of critical loads and other parameters that affect the safety and durability of railway bridges; the development of a statistical load model for rating existing railway bridges; the development of accurate and efficient procedures for assessing existing bridges; and the development of procedures for predicting the remaining life time of existing bridges.

When evaluating bridges, both the primary and secondary components must be considered. A need exists for efficient methods to evaluate the safety reserve in railway bridges by identifying the most sensitive parts of a bridge. Different types of bridges have unique performance functions relative to their service. Each part of a bridge system influences bridge safety with a different importance ratio. This approach can be used to optimize the prioritization of repair and reconstruction of railway bridges.

1.2 Objective and Scope of the Research

The objective of this study was to develop a rational guide for the prioritization of bridge repair and replacement based on bridge condition. The resulting analysis involved the calculation of capacity demonstrated on typical bridge connections. The research involved a review and analysis of the major factors that influence structural performance. A sensitivity analysis was performed to establish the relationship between load carrying capacity and degree of deterioration, and is presented in the form of graphs and tables. The results served as a basis for the development of general conclusions regarding through-plate girder railway bridges. The research involved the development of advanced analytical procedures for modeling structural behavior. The theoretical and actual load models were developed in a previous study by Rakoczy and Nowak (2012). Structural analysis was performed using analytical procedures and advanced FEM programs, and was conducted on connections of a representative bridge.

1.3 Prior Investigation

The current design load model was first presented in 1889 by Theodore Cooper (Cooper 1889). Cooper's loading system was based on a standard of E10, which meant that a pair of 2-8-0 type steam locomotives could pull an infinite number of rail cars. Although rail transport has changed and steam locomotives have been replaced by electric locomotives, the standard itself did not change, but simply increased to E80. For many researchers, Cooper E Loading is recognized as a useful tool for overall bridge design in terms of determining maximum girder stress. However, the Cooper E80 loading system is not suitable for fatigue loading. Therefore, in 2011, Dick et al. presented research on the development of a unique loading, representative of current loading conditions, for the design and rating of bridges for fatigue.

Load and resistance models contain many uncertainties. For this reason, any evaluation of bridge behavior is an estimation rather than an exact formula. Therefore, probabilistic methods are the most convenient way of providing levels of safety for various design cases. The theory of structural system reliability has been studied for many years and by many researchers, such as Ang and Tang (1970), Ayyub and McCuen (1997), and Nowak and Collins (2000). Structural reliability assessments were first implemented for building code by Galambos and Ravindra (1978), and for highway bridge design code by Nowak and Lind (1979). In the field of railway bridges, the reliability approach is not very popular. In 1997, Tobias et al. presented research on a reliability-based method for railway bridge fatigue evaluation. The study involved a large-scale bridge test in addition to the fatigue resistance test database compiled at the University of Illinois at Urbana-Champaign. The fatigue model included strengths and loadings, described by probability distributions.

More recently, global FEAs of a typical riveted railway bridge in England indicated that the inner stringer-to-cross-girder connections were fatigue critical details (Imam et al. 2005). In many cases, a considerable amount of end moment may be developed at the connection due to unintentional connection stiffness. Consequently, the connection can be susceptible to fatigue damage (Fisher et al 1987; Al-Emrani 2005). Other researchers—for instance M. Al-Emrani (2005) and RK Goel (2006)—have also highlighted this issue. The topic was expanded by probabilistic fatigue life estimates for a stringer-to-cross-girder connection of a riveted railway bridge in England (Imam et al. 2008).

Previous research performed at UNL (Nowak and Rakoczy 2012) pointed out that the connections were the weakest link in the structural system. A representative steel railway bridge was analyzed in detail, and FE analysis of a typical through-plate girder railway bridge was

carried out. The analysis demonstrated that maximum stresses were concentrated in the mid-span of the stringers, floorbeams and plate girders. Furthermore, the FEM analysis showed that the connection between stringer and floorbeam acquired a certain degree of rotational stiffness and developed stresses due to bending moment. Therefore, the connection was susceptible to fatigue damage. Calculation of the maximum stresses for the various components and connections within the bridge showed that actual load caused stresses which were, on average, 0.3-0.5 of the yielding point. This was because the current design load model is based upon the heavy steam locomotive with infinite uniform load, therefore the required cross-section is overestimated. The reliability analysis of axial tension for the main components showed that reliability indices were above 5.0 for main components, and should not be a concern. This is because the design load for short bridges is conservative in comparison to current load conditions. However, further research is needed to consider the effect of corrosion and loose bolts on structural performance and the prediction of remaining life.

Thus, in the current study, to ensure safe bridge performance, connections between the stringer and floorbeams were analyzed in detail. First, the capacity of the connections was calculated, including all failure modes that could occur on the connection. Then, the damage to the connection was applied and the reduced capacity was calculated. The damage was included in FE as a lost bolt and/or modified thickens (corrosion) on the steel component.

The major contribution of this study was to develop an accurate model of steel connections, and to evaluate its capacity. The research involved the development of resistance models for double angle connections, including the load effect and capacity ratio between undamaged and damaged connections. The study provides a broad overview of the potential consequences of deteriorated steel railway bridge connections.

1.4 Organization

The current chapter included an introduction, problem statement, description of objectives, and details on the scope of the current research. Chapter 2 reviews prior investigations in the subject area, defines the specifics concerning bridge components, and provides a theoretical background. Chapter 3 describes the models of bolted connections utilized in railway bridges. The theoretical failure modes are defined and limit state functions are formulated. Calculations of load caring capacity are presented using two examples. Chapter 4 presents the definition and principles of the finite element method (FEM), along with their application. A description of the detailed models used in this study is illustrated. The FEM models for double angle connections are developed. Results of the FEM analysis with comparisons to theoretical calculations are presented. Chapter 5 provides a summary, and details the conclusions of the current study.

Chapter 2 Previous Research and Findings

2.1 Introduction

A previous study conducted by the authors (Nowak and Rakoczy 2012) on system reliability models for steel railway bridges showed that the connection between the stringer and floorbeam acquires a certain degree of rotational stiffness and develops stresses due to bending moment. The stringer-to-floorbeam connection is commonly constructed with a double angle, and considered as simple shear connections during the design stage. However, the connection is susceptible to stresses due to bending moment. Fatigue damage in stringer-to-floorbeam connections is typically associated with cracking in the connection angles or in the rivets/bolts connecting the outstanding leg to the floorbeam web, due to rotational deformation on the top of the connection angles and axial forces in the rivets/bolts resulting from restrained moment. Further research was recommended to investigate the effects of corrosion and degradation on structural performance and the prediction of remaining life. The research was demonstrated on two through plate girder bridges, which work as a series system where the failure of one component could lead to the failure of the entire system. Sensitivity analysis pointed out that the connections were the weakest link in the structural system. Therefore, the current study is focused on determining the capacity of the double angle connection under eccentric shear and combine shear and tension for different scenarios of deterioration in connections.

2.2 Bridge #1

Bridge #1 was a through-plate girder, riveted, open deck railway bridge designed according to AREA and constructed in 1894. The bridge had one simply supported span, 32 ft. 9 in. (10 m) long, with the floor system presented in figure 2.1. The main structural components included two main plate girders and a floor system of floorbeams and stringers. The girders were

spaced transversely at 10 ft. 2 in. (3.1 m) from center to center, the floorbeams were spaced 10 ft. 11 in. (3.33 m) in the longitudinal direction, and the stringers were spaced transversely at 4 ft. 11 in. (1.6 m). More detail regarding this bridge can be found in a previous study (Rakoczy 2012).

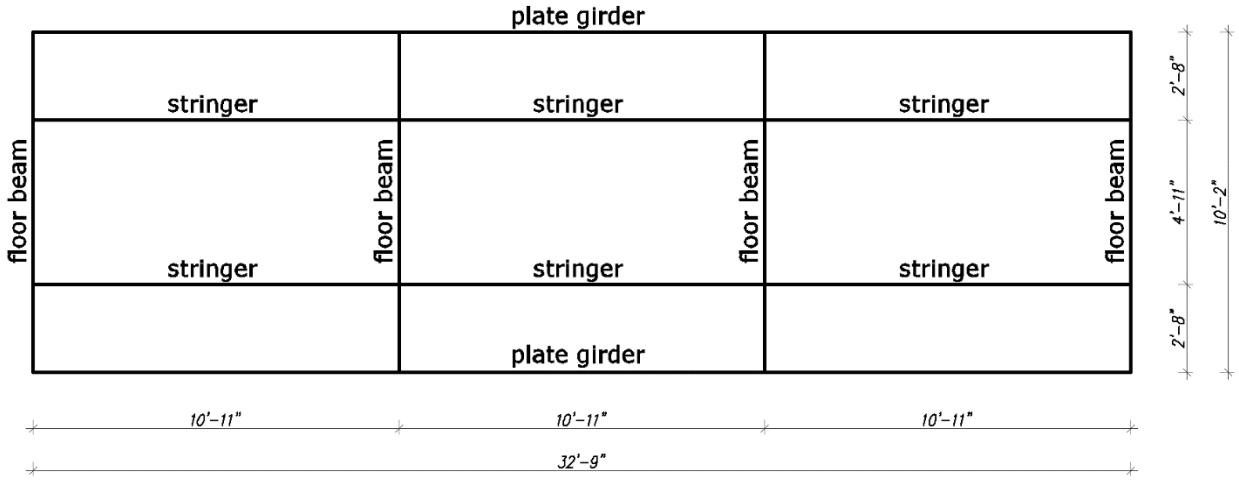

Figure 2.1 Floor system of bridge #1

All connections between members within the structure were made using rivets with a nominal diameter of 0.8 in. (20 mm). The stringer-to-floorbeam connection was made using double angles riveted to stringer and floorbeam webs. This type of connection is intended to be a simple shear connection that does not transmit the moment. The components and connections of the bridge are presented in figures 2.2 and 2.3.

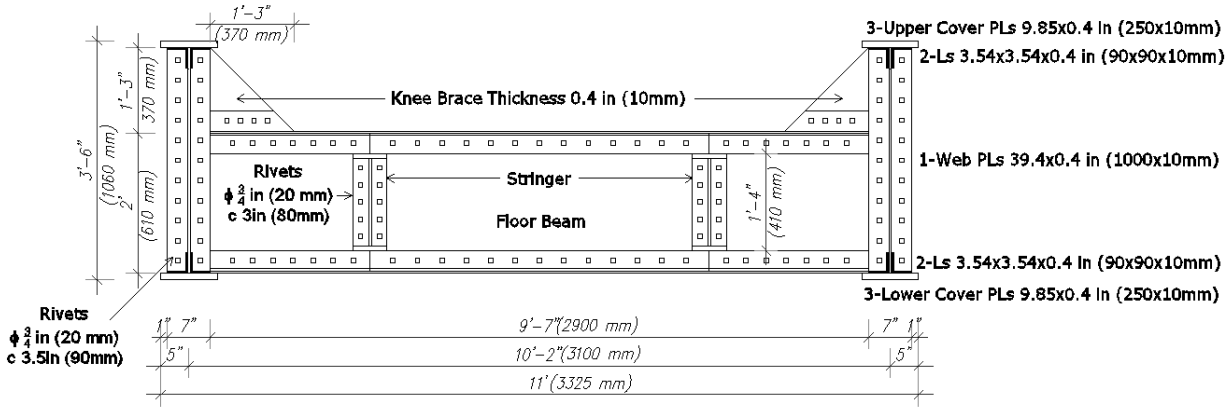

Figure 2.2 Floorbeam of bridge #1

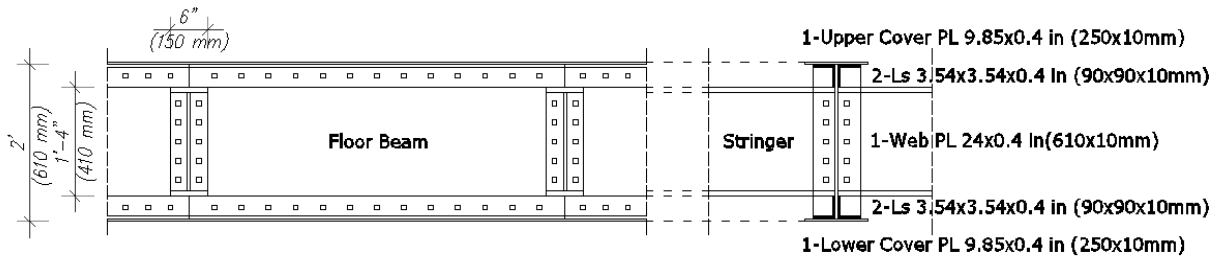

Figure 2.3 Stringer-to-floorbeam connections of bridge #1

2.3 Bridge #2

Bridge #2 was a through-plate girder, riveted, ballasted deck railway bridge. The bridge, located in New Mexico, was constructed in 1898. The bridge had three simply supported spans 64 ft. (19.5 m) long, with the floor system presented in figure 2.4. The main structural components included two main plate girders and a floor system of five floorbeams and 16 stringers. The girders were spaced transversely at 16 ft. 1 in. (4.9 m) from center to center; the floorbeams were spaced at 15 ft. 8 in. (4.8 m) in the longitudinal direction; and the stringers were spaced transversely, with 2 ft. 9 in. (2.75 m) from the exterior stringers to the interior stringer and 2 ft. 2 in. (0.66 m) between internal stringers.

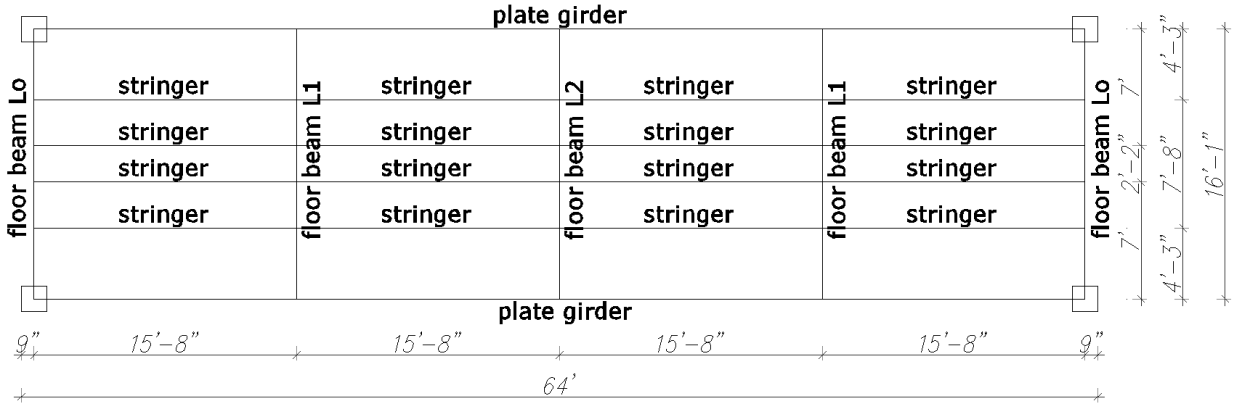

Figure 2.4 Floor system of bridge #2

The main girders were built up from 3/8 in. (9.5 mm) web plates of 6 ft. 1 in. (1.85 m) total depth, 14 in. (356 mm) upper and lower cover plates, 6 in. x 6 in. x 3/8 in. (152.4 mm x 152.4 mm x 9.5 mm) structural L shapes, and vertical web stiffeners in approximately ft. (2.1 m) intervals. The girder profile is presented in figure 2.5.

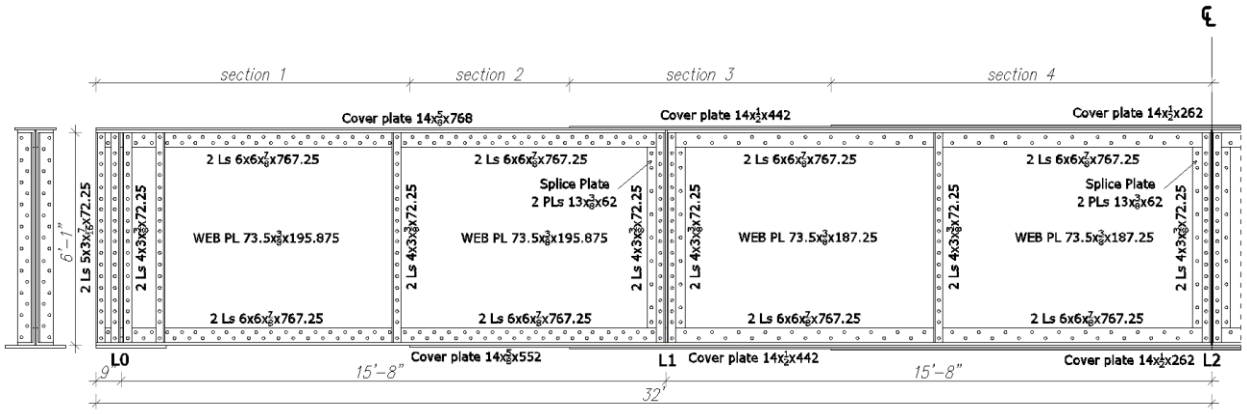

Figure 2.5 Girder profile of bridge #2

The floorbeams were also built up sections containing 42.25 in. x 0.375 in. (1073 x 9.5 mm) web plates and structural L shapes. External floorbeams L0 contained 6 in. x 6 in. x 9/16 in. (152.4 mm x 152.4 mm x 14.3 mm) double angles, while internal floorbeams L1 and L2 contained 6 in. x 6 in. x 3/4 in. (152.4 mm x 152.4 mm x 19 mm) double angles. At the

connection with the plate girder, floorbeams provided knee bracing by extending web plates up to the top of the girders. The floorbeam profile is presented in figure 2.6.

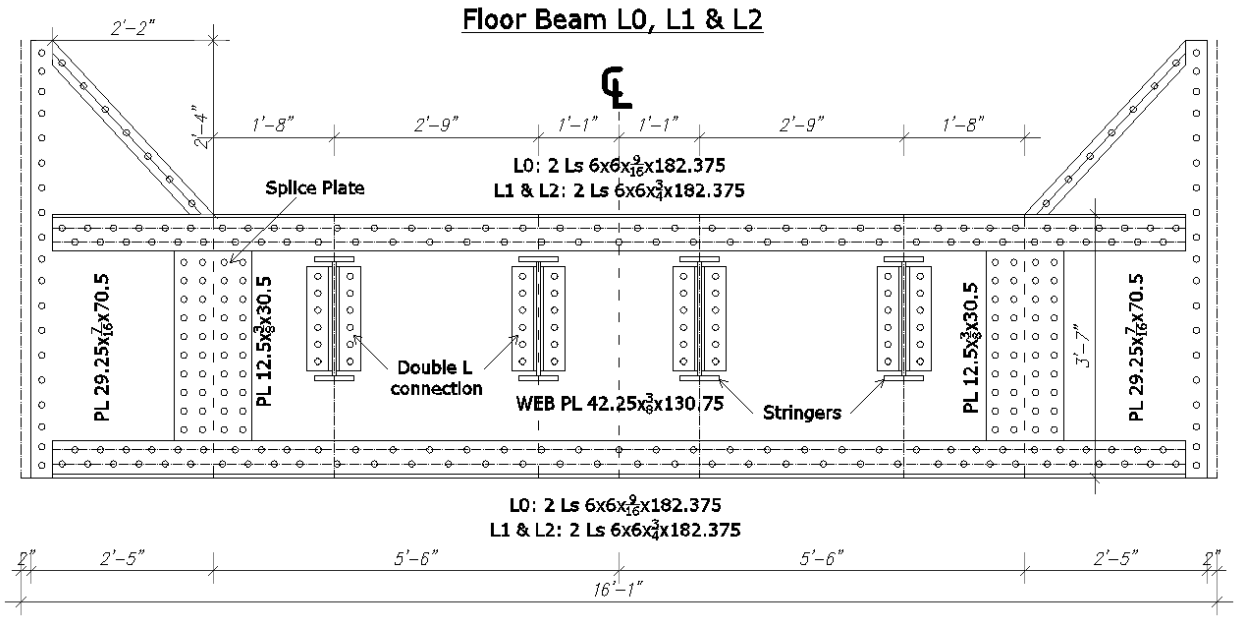

Figure 2.6 Floorbeam profile of bridge #2

The stringers were rolled S20x75 beams with 20 in. by 0.635 in. (508 x 16 mm) web and 6.39 in. by 0.795 in. (162 x 20 mm) flanges. All connections between members within the structure were made using rivets with a nominal diameter of 0.875 in. (22 mm). The stringer-to-floorbeam connection was made using double angles riveted to stringer and floorbeam webs. The components and connections of the bridge are presented in figures 2.5 and 2.6.

2.4 Double Angle Connections – Previous Findings

Previous research by the authors showed that the connection between the stringer and floorbeam acquired a certain degree of rotational stiffness and developed stresses due to bending

moment. These types of connections were considered as simple shear connections during the design stage. Therefore, the connection could be vulnerable to the failure.

The double angle connection between the floorbeam and stringer is presented in figure 2.7. Figure 2.8 presents a detailed interpretation of the double angle connection following applied load.

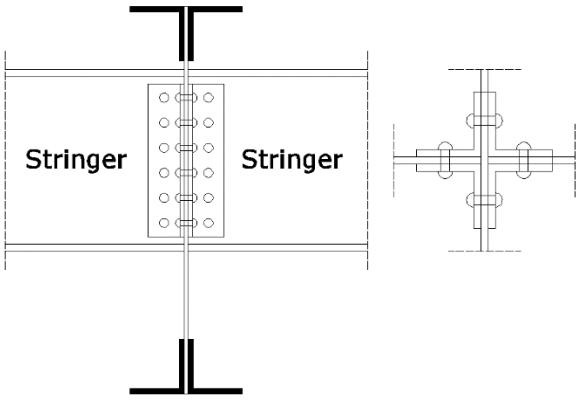

Figure 2.7 Detail of double angle connection

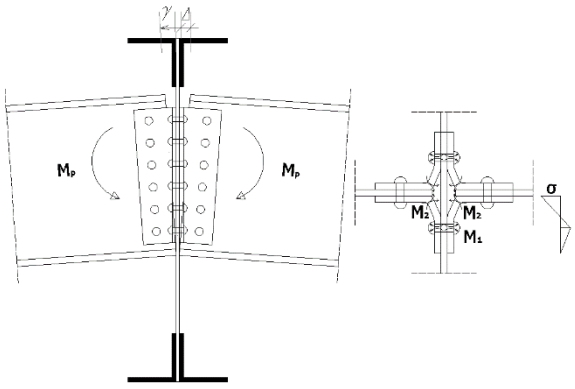

Figure 2.8 Distortion of outstanding legs of connection angles due to applied load

The connection developed plastic deformation much more quickly than did the main elements on the bridge. Therefore, connections were more critical than were the primary members, and must be considered during bridge evaluation. Additional calculations were made using ROBOT Structural Analysis for a continuous beam with and without pin connections. The stringers in the FEM model behaved as partially continuous for a four spans beam with negative moment at the interior floorbeams.

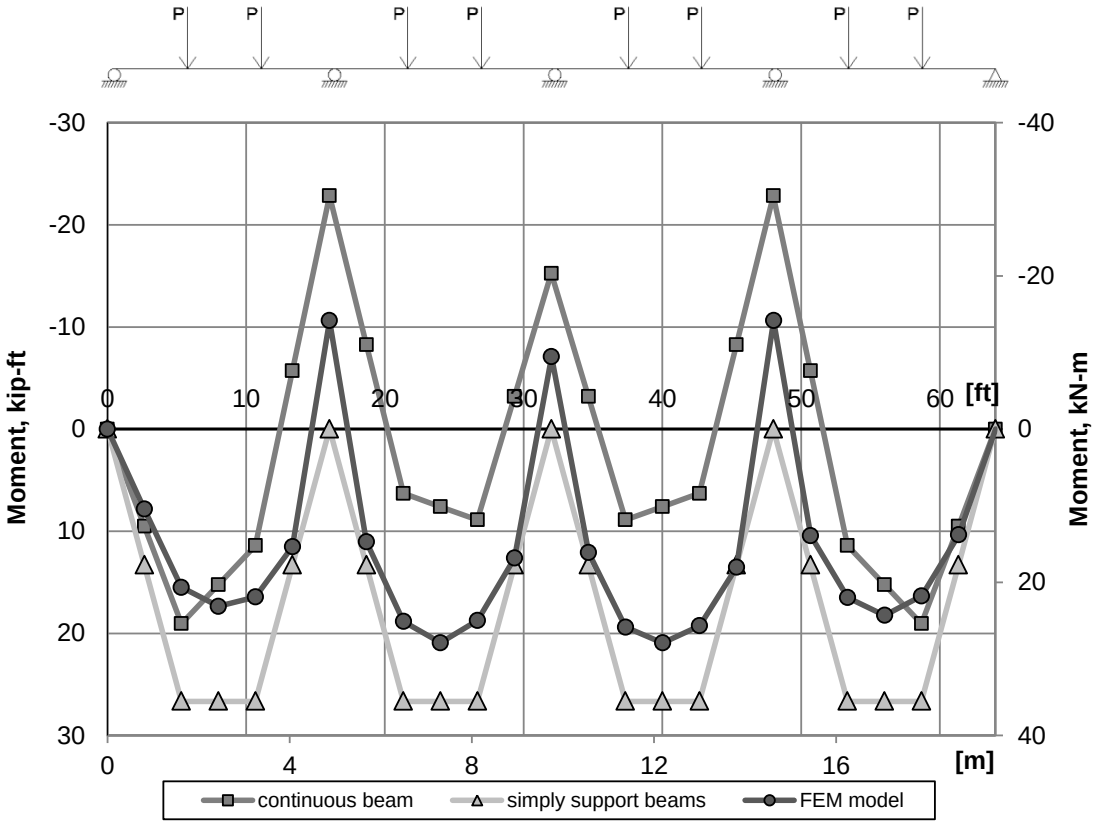

Figure 2.9 Moment diagram for continuous beam, simply supported beams and FEM model

The results presented in figure 2.9 show that the double angle connections in the FEM model were capable of developing up to 60% of the corresponding moment of a fully continuous beam. This finding has also been proven by other researchers (Al-Emrani 2006; Goerl 2006; Krajewski 2009).

2.5 Double Angle Connections – Theory Background

Steel connections are categorized as either fully restrained (FR) or partially restrained (PR) moment connections. FR connections assume the connections have sufficient stiffness to maintain the angles between intersecting members (American Institute of Steel Construction [AISC] 2011). PR connections assume connections have insufficient stiffness to maintain the angles between intersecting members (AISC 2011).

There are several "standard" types of structural steel connections. They are generally classified into three behavior categories: rigid, semi-rigid, and simple. The difference among the three can be shown through a plot of end moment versus end rotation.

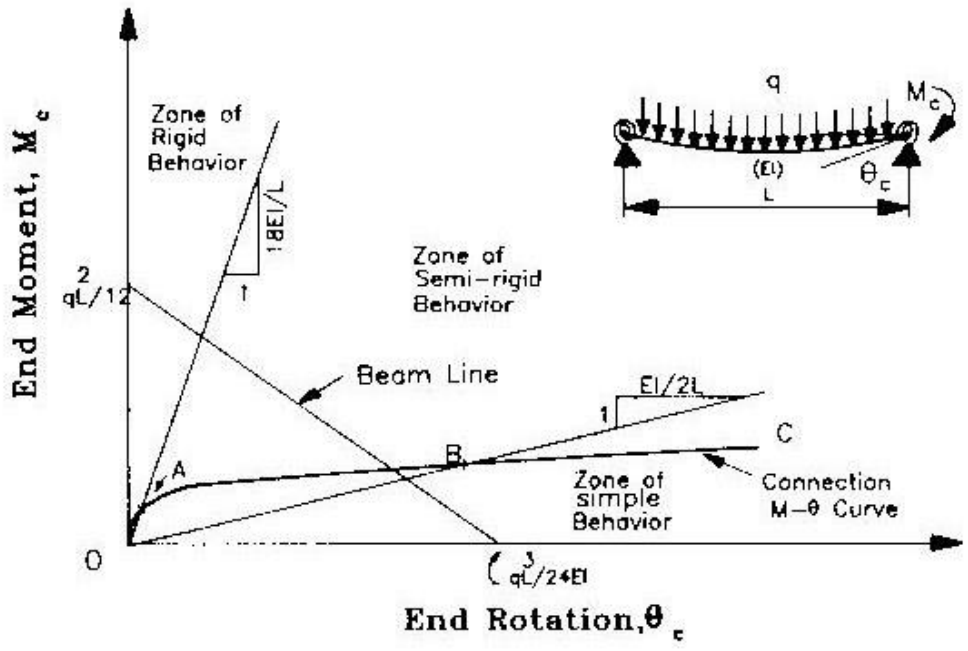

Figure 2.10 Rotational rigidity of steel connections (Astaneh 1989)

The M-θ curve OABC represents the general behavior of connections. Segment OA of the M-θ curve is the segment where connections behave as fully restrained connections. Connections in this range have an initial rotational restraint greater than or equal to L/18EI, where E is the material's elastic modulus, I is the moment of inertia of the cross-section of the beam, and L is the length of the beam. Connections with an initial rotational restraint less than or equal to L/2EI represented by segment ABC are considered to be simple connections, and do not develop any significant moment. The two initial rotational stiffness curves represent the boundaries for a partially restrained connection. As the figure shows, no connection is truly fixed or truly pinned, but these assumptions greatly simplify the design process. Most of the research in this area deals only with simple connections which assume that there is no end moment

developed in the beam and that the beam supports allow unrestrained rotations. Therefore, the current research involves connections with end moment in the beam and restrained rotations.

Chapter 3 Bolted Connections

3.1 Overview

Bolted connections became popular during the 1950s, when previous research had shown that bolts could be used to replace rivets in connections (Kulak et al. 1987). Until that time, only rivets were used in connections.

Bolted connections can be tightened to specific levels. The first are snug tight connections. The bolt is tightened using an ordinary spud wrench to bring the piles, which in this case are the angles or tees, and the web of the beam into firm contact (RCSC 2000). Alternately, a bolt can be pretensioned, in which case it is a pretensioned joint. A bolt must be tightened to its minimum pretension force, as listed in Table J3.1 of the AISC Specification (AISC 2011). There is no difference in the strength of the two types of joints, but pretensioning is usually necessary when the connection is subjected to cyclic or tension loads (Kulak et al. 1987). Slip critical connections are required to meet the provisions of Chapter J3.8 of the AISC Specification (AISC 2011). This connection is designed to prevent any slip between the faying surfaces. Early research showed that high-strength bolts can be used in a connection in the same manner as rivets (Kulak et al. 1987). This discovery led to the common use of high-strength bolts in connections. Today, bolted connections are very popular because they are relatively inexpensive in comparison to field welding, and are easy to install.

Research has shown that almost all rotation is provided in the detail material, usually either the angles or plates (Kennedy 1969). Most of the rotation in the connection occurs in the legs of the angle that are in the plane of the supporting member. This is relevant because the behavior of extended connections should be similar. The gage distance for the “in-plane” legs for extended and normal shear connections is the same.

One possible moment-rotation relationship for bolted double and single angle shear connections was quantified by Kishi and Chen (1990) using a power model relationship between moment in the connection and end rotation. The general deformation of the connection was based on the following assumptions:

1. The center of rotation of the connection was near the mid-depth of the beam during the first few increments of loading.

2. The deformation and subsequent tearing of the connection angles resulted primarily from bending moment, and the effect of shear deformation on the connection behavior was relatively small.

The final form of the moment-rotation relationship is given by equation 3.1 (Kishi and Chen 1990).

$$M = \frac{R_{ki}\Theta_r}{\left(1+\left(\Theta_r / \Theta_0\right)^n\right)^{1/n}} \tag{3.1}$$

where,

M = moment in connection (kip-in);

R_{ki} = initial connection stiffness (kip-in);

Θ_r = a rotation of connection (radians);

Θ_0 = a reference plastic rotation (radians);

N = shape factor.

The initial connection stiffness is given by equation 3.2 (Kishi and Chen 1990).

$$R_{ki} = \frac{Gt^3}{3} \frac{\alpha \cosh(\alpha\beta)}{(\alpha\beta)\cosh(\alpha\beta) - \sinh(\alpha\beta)} \tag{3.2}$$

where,

G = shear modulus of the steel (ksi);

T = thickness of angle leg (in);

α = 4.2967;

$\beta = g_l/l_p$, where g_1 = gage distance (in) and l_p = length of angle (in).

The reference plastic rotation is given by equation 3.3 (Kishi and Chen 1990).

$$\Theta_0 = \frac{M_u}{R_{ki}} \tag{3.3}$$

where,

M_u = ultimate moment capacity of connection.

The model was verified through comparison to various experimental results (Kishi and Chen 1990). The model agrees with Astaneh's recommendations for simple connections, where a simple connection is one that develops a moment at the beam end less than or equal to 20% of the fixed end moment (Astaneh 1989). Most experiments, such as those used by Kishi and Chen to verify their power model, have been performed for beam-to-column connections only, and have not been directly performed for beam-to girder connections.

3.2 Extended Double Angle Connection

Double angles or two-sided connections have certain advantages over one-sided connections. Double angle connections can resist larger end reactions because the supported member bolts are in double shear and the eccentricity perpendicular to the beam axis need not be considered for workable gages. The pin in an extended and standard double angle connection is located at the girder web, as shown in figure 3.1.

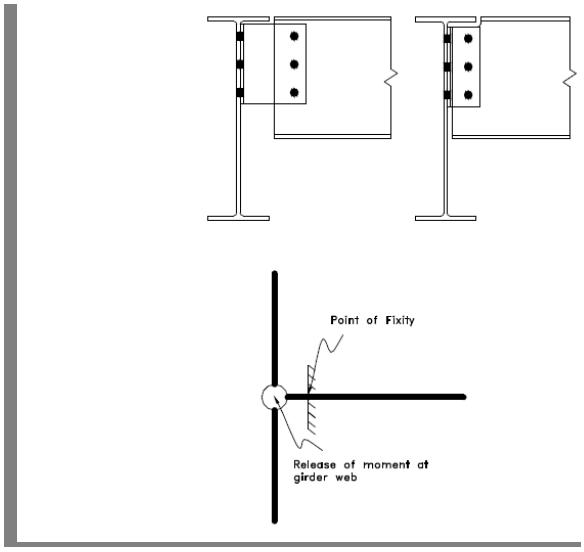

Figure 3.1 Pin and pint of fixity (Astaneh 1989)

The following limit states are considered in the design of an extended double angle connection:

1. Shear Yielding
2. Shear Rupture
3. Flexural Yielding
4. Flexural Rupture
5. Block Shear Rupture
6. Bolt Bearing
7. Bolt Slip
8. Bolt Shear

The bolt limit states include effects from the eccentricity of the loading.

3.3 Limit State Calculations

3.3.1 Shear Yielding

Shear yielding is a ductile limit state that is a function of the gross shear area of the element (Green et al. 2001). For single angles and tees, the shear area is equal to the following equation:

$$A_{gv} = h_a t_a \tag{3.4}$$

where,

h_a = the length of the angle or tee;

t_a = the thickness of the outstanding angle leg or stem thickness.

Double angles have twice the shear area of a single angle by virtue of having two legs in shear. The shear area is used to calculate the shear yielding capacity of the connection. This equation is shown below:

$$\phi R_n = \phi 0.6 A_{gv} F_y \tag{3.5}$$

where,

F_y = yield stress of the detail material;

ϕ = 1.0.

The above is Equation J4-3 from the AISC-LRFD Specification (AISC 2011). The ϕ term is a resistance factor that is dependent on the limit state. For yielding limit states, ϕ is 1.0. The yield stress, F_y, is either 36 ksi or 50 ksi for A36 or A992 steels, respectively (AISC 2011).

3.3.2 Shear Rupture

Shear rupture is also a limit state for the connection. The failure plane is located along the line of the bolts in the supported angle leg/s or tee stem; therefore, a reduced or net area is used to calculate the shear rupture strength of the connection. The net shear area is calculated using the following equation:

$$A_{nv} = \left[h_a - n\left(d_h + 1/16\right)\right] t_a \tag{3.6}$$

where,

n = the number of bolts;

d_h = the bolt hole diameter.

For the calculation of A_{nv}, the AISC-LRFD Specification requires that 1/16 of an inch be added to the nominal bolt hole diameter when calculating net areas (AISC 2011). The net shear area is the sum of both angles for double angle connections. The shear rupture capacity is provided by the equation below:

$$\phi R_n = \phi 0.6 A_{nv} F_u \tag{3.7}$$

where,

F_u = the ultimate stress of the detail material;

ϕ = 0.75.

This equation is also Equation J4-4 in the AISC-LRFD Specification. For rupture limit states, ϕ is 0.75. The ultimate stress, F_u, is either 58 ksi or 65 ksi for A36 and A992 steels, respectively (AISC 2011).

3.3.3 Flexural Yielding

Flexural yielding of the outstanding angle leg or tee stem is checked in determining the design capacity of the extended connections. In standard connections, flexural yielding need not be considered because the eccentricity of the load is within specified gage distances (AISC 2011). For most flexural limit states, the plastic section modulus, Z, is used to determine flexural design strength. The AISC-LRFD Manual (2011) allows the designer to use the elastic section modulus, S, as a conservative approximation when calculating the flexural limit states in connections. The elastic section modulus for the angles and tees is calculated using equation 3.8:

$$S = \frac{t_a h_a^2}{6} \tag{3.8}$$

The flexural design strength is provided by equation 3.9:

$$\phi M_n = \phi S F_y \tag{3.9}$$

where,

ϕ = 0.90.

In order to compare the flexural limit states to the other limit states, the moment is converted to a load that acts at an eccentricity. The eccentricity, e, varies depending upon the supported leg or stem length. The eccentricity is assumed to be the distance from the centerline of the supported bolts to the face of the supported web, as shown in figure 3.2.

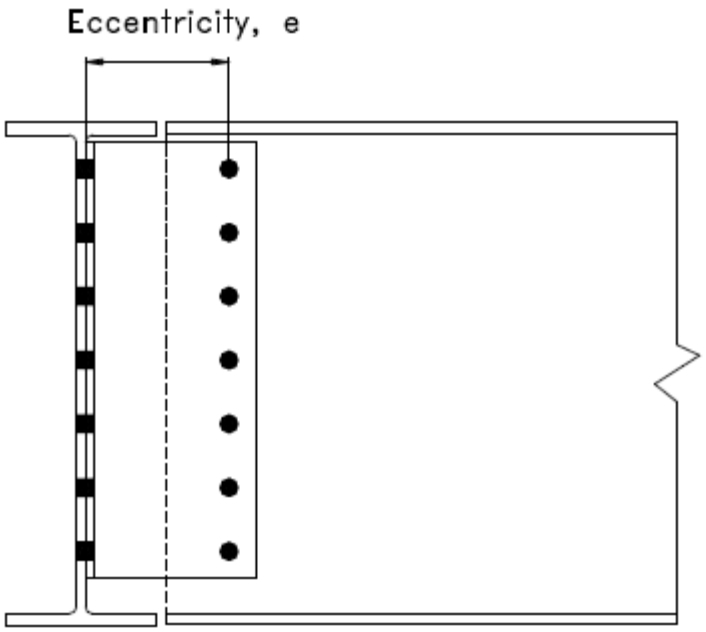

Figure 3.2 Moment eccentricity

Figure 3.2 shows the dimension that is used to determine eccentricity. The flexural capacity of the connection is dependent upon the eccentricity, unlike for shear limit states. As eccentricity increases, flexural strength decreases. The connection capacity, ϕR_n, is therefore:

$$\phi R_n = \frac{\phi M_n}{e} \tag{3.10}$$

where,

e = eccentricity.

3.3.4 Flexural Rupture

Flexural rupture is an ultimate strength limit state. The net elastic section modulus is conservatively used to determine the section capacity. In section 15 of the AISC LRFD Manual, an equation is provided for the net section modulus for bracket plates (AISC 2011). The AISC Manual permits this equation to be used to determine the net plastic section modulus for shear connections. The equation for Z_{net} is given as equation 3.11a and 3.11b.

For an odd number of bolts row:

$$Z_{net} = \frac{t_a}{4}\left(s - \left(d_h + \frac{1}{16}\right)\right)\left(n^2 s + \left(d_h + \frac{1}{16}\right)\right) \tag{3.11a}$$

For an even number of bolts row:

$$Z_{net} = \frac{t_a}{4}\left(s - \left(d_h + \frac{1}{16}\right)\right)n^2 s \qquad (3.11b)$$

where,

s = bolt spacing.

The above equations are also Equation 15-4 and 15-5 in the AISC-LRFD Specification. The equation to determine flexural rupture is:

$$\phi M_n = \phi Z_{net} F_u \qquad (3.12)$$

where,

ϕ = 0.75.

The flexural rupture strength of a connection is given in terms of a moment, so the moment, M_n, must be divided by the load eccentricity shown in figure 3.2 to calculate the end reaction. As with flexural yielding, flexural rupture follows the same trend; that is, as the eccentricity increases, the capacity decreases. Therefore the connection capacity is equal to equation 3.12.

3.3.5 Block Shear Rupture

Block shear rupture is a limit state in which the failure path includes both an area subject to shear and an area subject to tension (Green et al. 2001). In standard connections there are two possible elements that can experience block shear rupture: the connection element (angle or tee) and the net coped section. Extended connections do not require the supported member to be coped, so block shear rupture will not occur. The only element that needs to be checked for block

shear rupture is the angle or the tee. Block shear rupture also has the possibility of occurring across more than one failure plane, but there is only one possible failure plane for an extended connection. Figure 3.3 shows both the shear and tension failure planes.

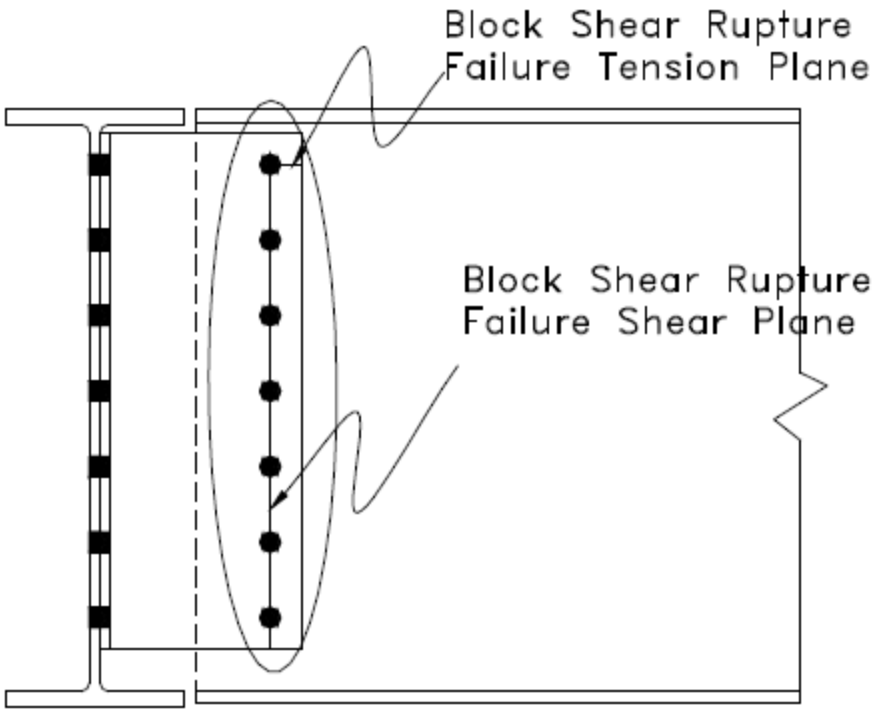

Figure 3.3 Block shear rupture failure planes

There are two equations used to determine the block shear rupture strength of a connection. The equation that controls depends on values of tension rupture and shear rupture, and which of the two is greater. All of the connections in this research project were controlled by shear rupture, therefore Equation J4-5 in the AISC-LRFD Specification was used to determine the block shear rupture strength (2011). The equation is shown below:

$$\phi R_n = \phi\left[0.6F_u A_{nv} + F_u A_{nt}\right] \leq \phi\left[0.6F_y A_{gv} + F_u A_{nt}\right] \quad (3.13)$$

where,

A_{nv} = net area subject to shear;

A_{nt} = net area subject to tension;

A_{gv} = gross area subject to shear;

ϕ = 0.75.

Block shear rupture can be conservatively approximated as the shear rupture strength of the connection. The gross area in tension, A_{gt}, is very small, and the difference between the block shear, A_{nv}, and the net area for shear rupture is the value of L_c, which is the clear distance from the outlying bolt and the connection angle or tee edge.

3.3.6 Bolt Bearing

Bolt bearing concerns the deformation of material at the loaded edge of the bolt holes (Green et al. 2001). Bearing capacity of the connection is influenced by the proximity of the bolt to the loaded edge, as well as the spacing between the bolts. The bolt edge distance is assumed to be 1-1/4 inches. This edge distance is the same as that given in the double angle tables of Part 10 in the AISC Manual. This edge distance is the minimum for connections using ¾ to 1 inch diameter bolts. This makes the connection as small as possible, which widens its range of applicability. Extended connections do not have the same carrying capacity as standard connections with an equivalent number of bolts. Therefore, an extra bolt is required in an extended connection to make up for this loss in strength, which requires more space. Lengthening the edge distance would add more capacity to an extended connection, but not enough to overcome the requirement for an additional bolt.

Bolt bearings for the beam and girder are not explicitly checked in the extended connection tables. These two limit states must be checked separately in order to verify the design strength of the connection. For both the girder and the beam, bolt hole deformation is the limiting factor, because there is no chance of the bolt tearing out. Part 10 of the AISC Manual has numbers for these limit states, provided in kips per inch of web thickness.

All bolt limit states are treated as eccentrically loaded. Eccentricity produces both a rotation and a translation of one connection element with respect to the other. The combined effect of this rotation and translation is equivalent to a rotation about a point defined as the instantaneous center of rotation (IC). In order to determine bolt bearing capacity, the instantaneous center (IC) method is utilized. This method includes the nonlinearity of the bolt deformation. Chapter 7 of the AISC-LRFD Manual (2011) contains tables with IC method coefficients. These tables are designed for a bolt group containing two to 12 bolts and eccentricities up to 36 inches. These coefficients are multiplied by the bearing capacity of a single bolt.

The bolt bearing equation given in the AISC-LRFD Specification as Equation J3-6a is given below:

$$\phi R_n = \phi 1.2 L_c t_a F_u \leq \phi 2.4 d_h t_a F_u \quad (3.14)$$

where,

ϕ = 0.75;

L_c = clear distance, in the direction of the force, between the edge of the hole and the edge of the adjacent hole or edge of the material.

Equation 3.14 considers bolt hole deformation at service loads—a conservative assumption. The equation above does not include effects from load eccentricity. The value from the equation above for one bolt is determined and multiplied by the appropriate C coefficient for the IC method:

$$\phi R_n = \phi C r_n \quad (3.15)$$

where,

ϕ = 0.75;

C = IC coefficient;

r_n = the bearing design strength for one bolt.

3.3.7 Bolt Slip

Bolt slip is considered in slip critical connections. In the design tables in the appendices of the current document, slip critical connections for three different hole types are considered. Equations for bolt slip do not include the effects of bolt eccentricity. The slip critical value for one bolt is determined and multiplied by the C coefficient from the IC method. The equation for bolt slip is given below:

$$\phi R_n = \phi \cdot 1.13 \cdot \mu \cdot h_f \cdot T_b \cdot n_s \quad (3.16)$$

where,

ϕ = resistance factor ranging from 1.0 to 0.85;

ϕ = mean slip coefficient (Class A μ = 0.33, Class B μ = 0.5);

h_f = factor for fillers from 1.0 to 0.85;

T_b = minimum fastener tension given in AISC LRFD Specification Table J3.1;

n_s = number of slip planes.

The ϕ-factor for standard holes is 1.0, while the ϕ-factor for oversized and short-slotted holes is 0.85. The minimum fastener tension is a function of bolt diameter. The slip capacity of the connection is the slip capacity of one bolt multiplied by the C coefficient.

3.3.8 Bolt Shear

Bolt shear is applicable to each bolted ply of a connection that is subjected to shear (Green et al. 2001). The shear strength of a bolt is directly proportional to the number of interfaces (shear planes) between the plies within the grip of the bolt through which a single shear force is transmitted. The outstanding legs of double angle connections have two shear planes, while the outstanding leg or stem for single angle and tee connections has one shear plane. The equation for bolt shear is shown below:

$$\phi R_n = \phi \cdot F_v \cdot A_b \cdot n_s \cdot n_b \quad (3.17)$$

where,

ϕ = 0.75;

F_v = bolt ultimate shear stress;

A_b = nominal cross-sectional area of bolt;

n_s = number of shear planes;

n_b = number of bolts.

As with the other bolt limit states, the bolt shear equation does not include the effects of load eccentricity. The shear strength of one bolt is calculated and multiplied by the C coefficient. This is equivalent to equation 3.15, except the ϕ -factor is not applied because it is applied in equation 3.17.

3.4 Case Study

3.4.1 Example #1

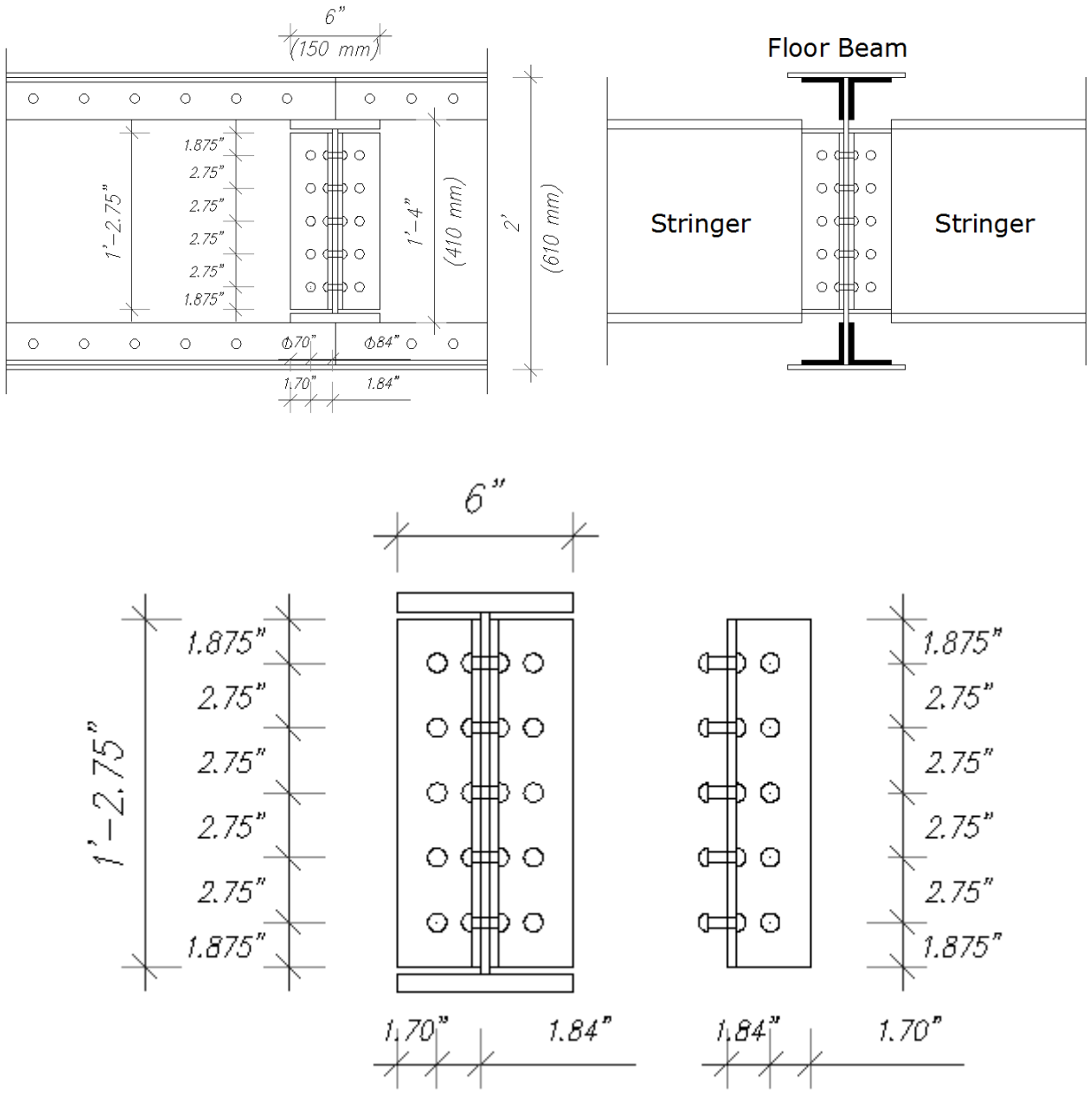

Figure 3.4 Dimensions of double angle connection – Case study, Example #1

Table 3.1 List of Dimensions and Material Properties for Detail #1

Parameter	Magnitude, US units		Magnitude, SI units		Comments
F_y	30.00	ksi	206.84	MPa	
F_u	40.00	ksi	275.79	MPa	
A_b	0.49	in^2	314.16	mm^2	
T_b	28.00	ksi	193.05	MPa	Group A
h_f	1.00	#	1.00	#	
n_b	5.00	#	5.00	#	
n_s	2.00	#	2.00	#	
h	14.75	in	374.65	mm	
L_{ev}	1.88	in	47.63	mm	
L_{eh}	1.84	in	46.74	mm	
Spacing, s	2.75	in	69.85	mm	
Bolt diameter, d_b	0.79	in	20.00	mm	
Bolt hole, d_h	0.87	in	22.00	mm	
F_{nv}	$(0.45 \cdot 120) = 54.0$	MPa	372.32	MPa	A325-N
F_{nt}	$(0.75 \cdot 120) = 90.0$	MPa	620.53	MPa	
Angle thickness, t_a	0.39	in	10.00	mm	
Floorbeam web thickness, t_{wb}	0.39	in	10.00	mm	
Stringer web thickness, t_{ws}	0.47	in	12.00	mm	

Design strength per bolt - Shear strength of the bolt

$$\phi R_n = 0.75 \cdot (0.45 \cdot F_u^b) \cdot m \cdot A_b \cdot n_v = 0.75 \cdot (0.45 \cdot 120) \cdot 1 \cdot 0.490 \cdot 1 = 19.845 kips / bolt$$

Number of bolts on the Stringer is five, and there are two shear surfaces

$$\phi R_{n\_total} = 2 \cdot 5 bolts \cdot 19.845 kip / bolt = 198.45 kip$$

Number of bolts on the floorbeam is five on each side, two columns

$$\phi R_{n\_total} = 2 \cdot 5 bolts \cdot 19.845 kip / bolt = 198.45 kip$$

Tearing and bearing – Angle thickness controls bearing and tearing:

When bearing strength is based on $2.4F_u$, LRFD-J3.10 (a) applies:

End distance $L_{e\_\min} = 1.5 \cdot d_b = 1.5 \cdot 7/8 = 1.31in < 1.875in$ OK!

Center-to-center spacing $s_{\min} = 2.67 \cdot d_b = 2.67 \cdot 7/8 = 2.34in < 2.75in$ OK!

Clear distance for exterior bolts $L_c = L_e - 0.5 \cdot d_b = 1.875 - 0.5 \cdot (0.79 + 1/16) = 1.45in$

Clear distance for interior bolts $L_c = s - d_b = 2.75 - (0.79 + 1/16) = 1.90in$

Angle thickness, $t = t_a = 0.39in$

Tearing strength exterior on the web-stringer $\phi R_n = 0.75 \cdot (1.2 \cdot L_c \cdot t \cdot F_u^p) = 0.75 \cdot (1.2) \cdot (1.45) \cdot (0.39) \cdot (40) = 20.4kips/bolt$

Tearing strength interior $\phi R_n = 0.75 \cdot (1.2 \cdot L_c \cdot t \cdot F_u^p) = 0.75 \cdot (1.2) \cdot (1.90) \cdot (0.39) \cdot (40) = 26.7kips/bolt$

Bearing strength $\phi R_n = 0.75 \cdot (2.4 \cdot d_b \cdot t \cdot F_u^p) = 0.75 \cdot (2.4) \cdot (0.79 + 1/16) \cdot (0.39) \cdot (40) = 23.9kips/bolt$

Total: $2 \cdot [2 \cdot 20.4kips + 3 \cdot 23.9kips] = 225.0kips$

Block shear strength on double-angle t = 0.39 in

$$A_{gt} = 2 \cdot L_{eh} \cdot t = 2 \cdot (1.70in) \cdot 0.39in = 1.33in^2$$

$$A_{nt} = A_{gt} - 0.5 \cdot holes \cdot t \cdot 2 = 1.33 - 0.5 \cdot (0.79 + 1/8) \cdot 0.39 \cdot 2 = 0.97in^2$$

$$A_{gv} = 2 \cdot (4 \cdot s + L_{ev}) \cdot t = 2 \cdot (4 \cdot 2.75 + 1.875) \cdot 0.39 = 10.04in^2$$

$$A_{nv} = A_{gv} - 4.5 \cdot holes \cdot t \cdot 2 = 10.04 - 4.5 \cdot (0.79 + 1/8) \cdot 0.39 \cdot 2 = 6.83in^2$$

$$F_u \cdot A_{nt} = 40ksi \cdot 0.97in^2 = 38.8kip < 0.6 \cdot F_u \cdot A_{nv} = 0.6 \cdot 40ksi \cdot 6.83in^2 = 109.28kip$$

which means shear fracture – tension yield controls.

$$\boxed{\phi \cdot R_n = \phi \cdot (0.6 \cdot F_u \cdot A_{nv} + F_u \cdot A_{nt}) = \phi \cdot (0.6 \cdot 40 \cdot 6.83 + 40 \cdot 0.97) = 0.75 \cdot 202.7 = 152.04kips}$$

$$\phi \cdot R_n = \phi \cdot (0.6 \cdot F_y \cdot A_{gv} + F_u \cdot A_{nt}) = \phi \cdot (0.6 \cdot 30 \cdot 10.04 + 40 \cdot 0.97) = 0.75 \cdot 219.5 = 164.64kips$$

Summary:

Based on bolt shear strength $T_u = 198.45kips$

Total bearing and tearing $T_u = 225.0kips$

Based on block shear (web-stringer) $T_u = 152.04kips$

Combined shear and tension

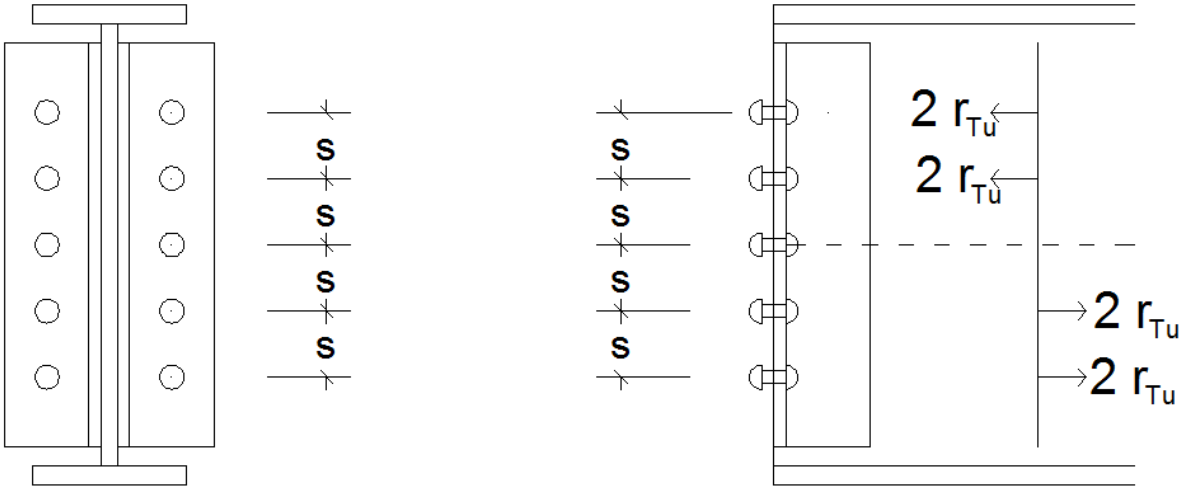

Figure 3.5 Resultant forces acting upon the double angle Connection – Case study, Example #1

Reduced tensile strength

$$\phi F_{nt}' = \phi \cdot \left[1.3 \cdot F_{nt} - \frac{F_{nt}}{\phi \cdot F_{nv}} f_v \right] \le \phi F_{nt}$$

$F_{nt} = 90ksi$ and $F_{nv} = 54ksi$ from Table J3.2

$$f_v = \frac{152.04kip}{10 \cdot 0.487in^2} = 31.2ksi$$

$$\phi F_{nt}' = 0.75 \cdot \left[1.3 \cdot 90 - \frac{90}{0.75 \cdot 54} 31.2 \right] = 35.75ksi > \phi F_{nt} = 0.75 \cdot 90ksi = 67.5ksi$$

Use $\phi F_{nt}' = 35.75ksi$

$$r_{Tn} = \phi F_{nt} \cdot A_b = 35.75 \cdot 0.487 = 18.4kip$$

Maximum Moment Capacity

$$[(2 \cdot r_{Tu}) \cdot s + (2 \cdot r_{Tu}) \cdot 2 \cdot s] \cdot 2 = 12 \cdot r_{Tu} \cdot s = M_u kip \cdot in$$

$$M_u kip \cdot in = 12 \cdot r_{Tu} \cdot 2.75in$$

$$M_u kip \cdot in = 33 \cdot r_{Tu} \cdot in$$

$$if \quad r_u = \phi F_{nt}' \cdot A_b = 18.4kip \quad then \quad M_u = 607.2kip \cdot in = 50.6kip \cdot ft$$

$$if \quad r_u = \phi F_{nt} \cdot A_b = 32.9kip \quad then \quad M_u = 1085.7kip \cdot in = 90.5kip \cdot ft$$

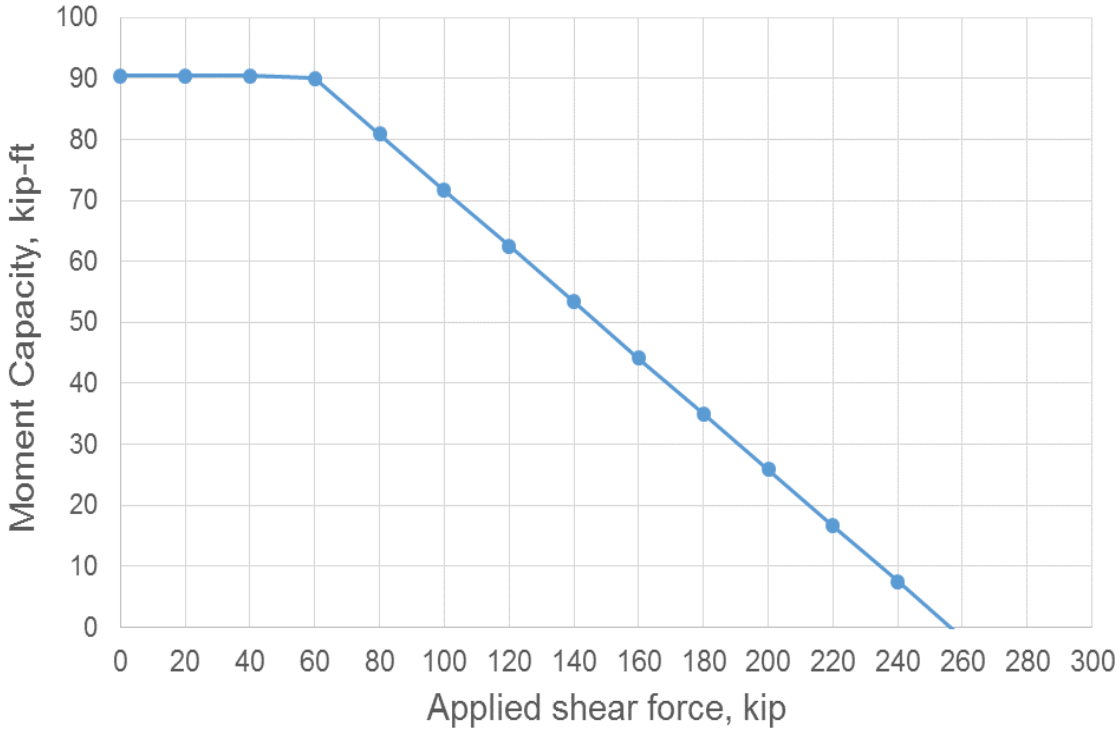

Figure 3.6 Moment capacity vs. applied shear force – Case study, Example #1

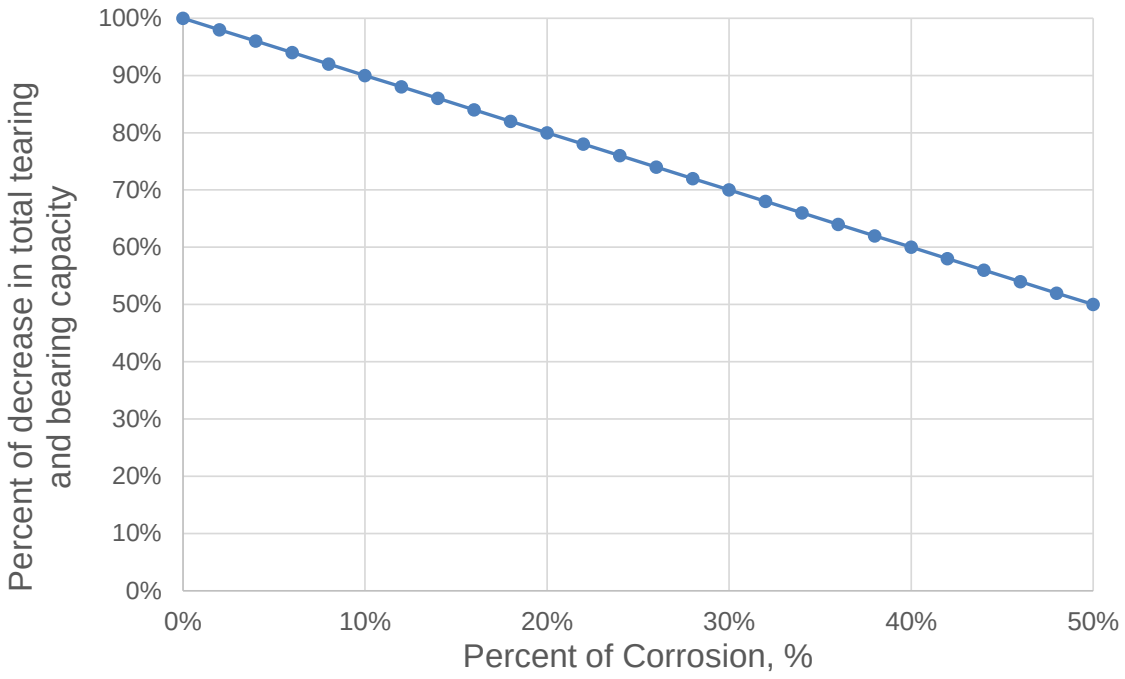

Figure 3.7 Moment capacity of double angle connection vs. percent of corrosion – Case study, Example #1

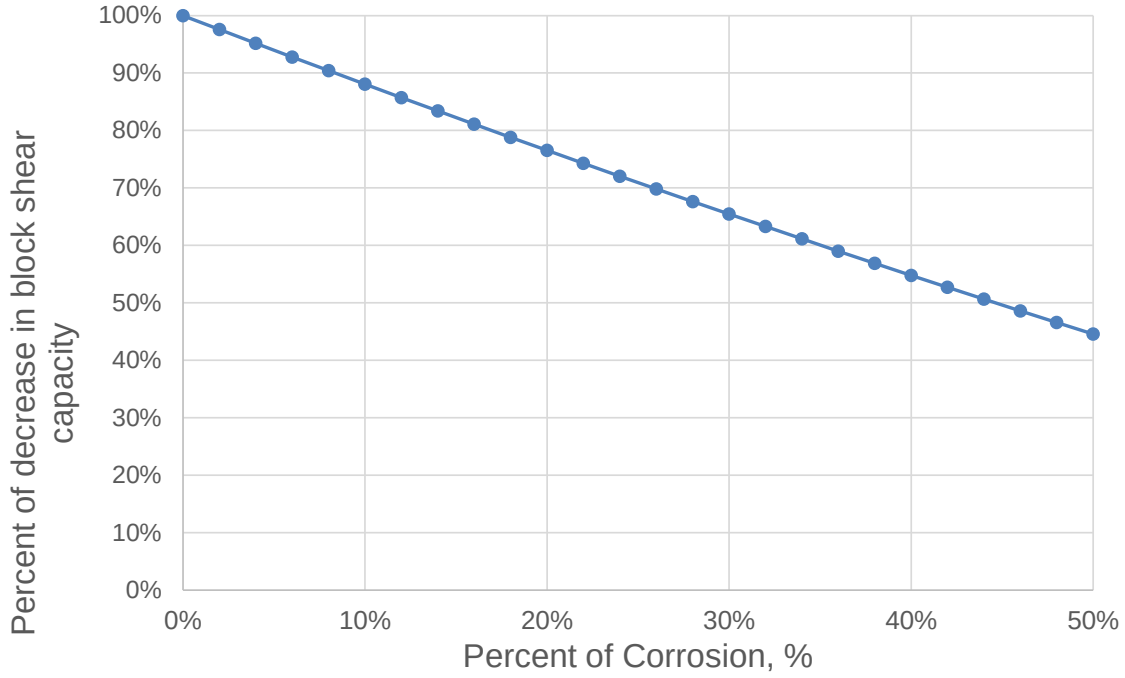

Figure 3.8 Shear capacity of double angle connection vs. percent of corrosion – Case study, Example #1

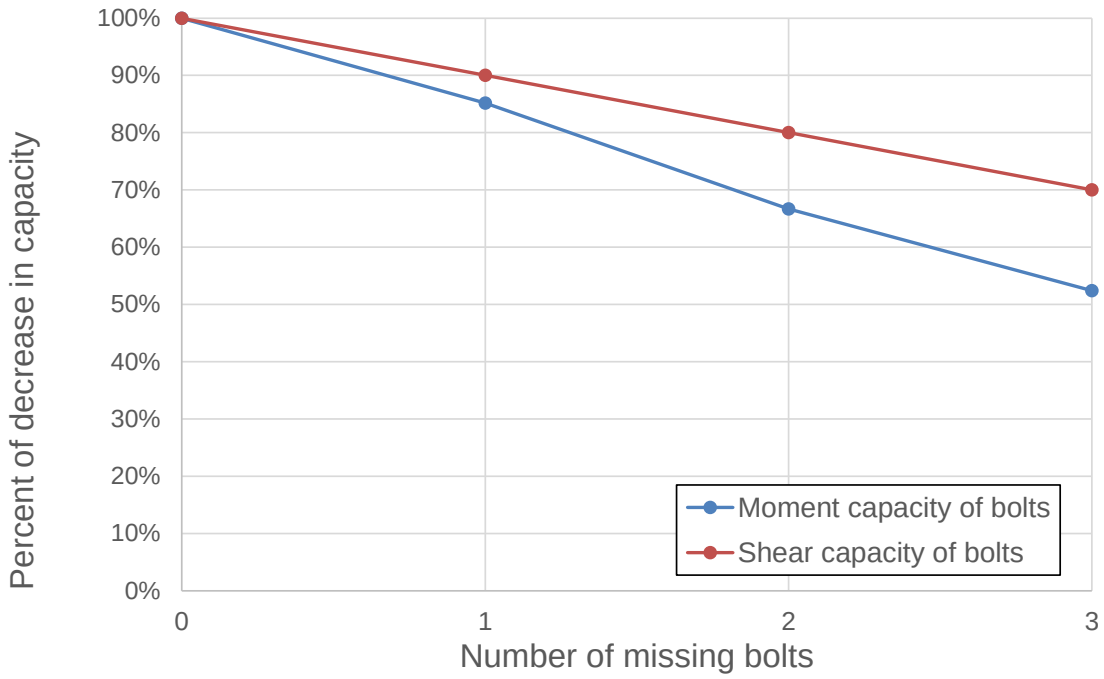

Figure 3.9 Moment capacity of double angle connection vs. number of missing bolts – Case study, Example #1

3.4.2 Example #2

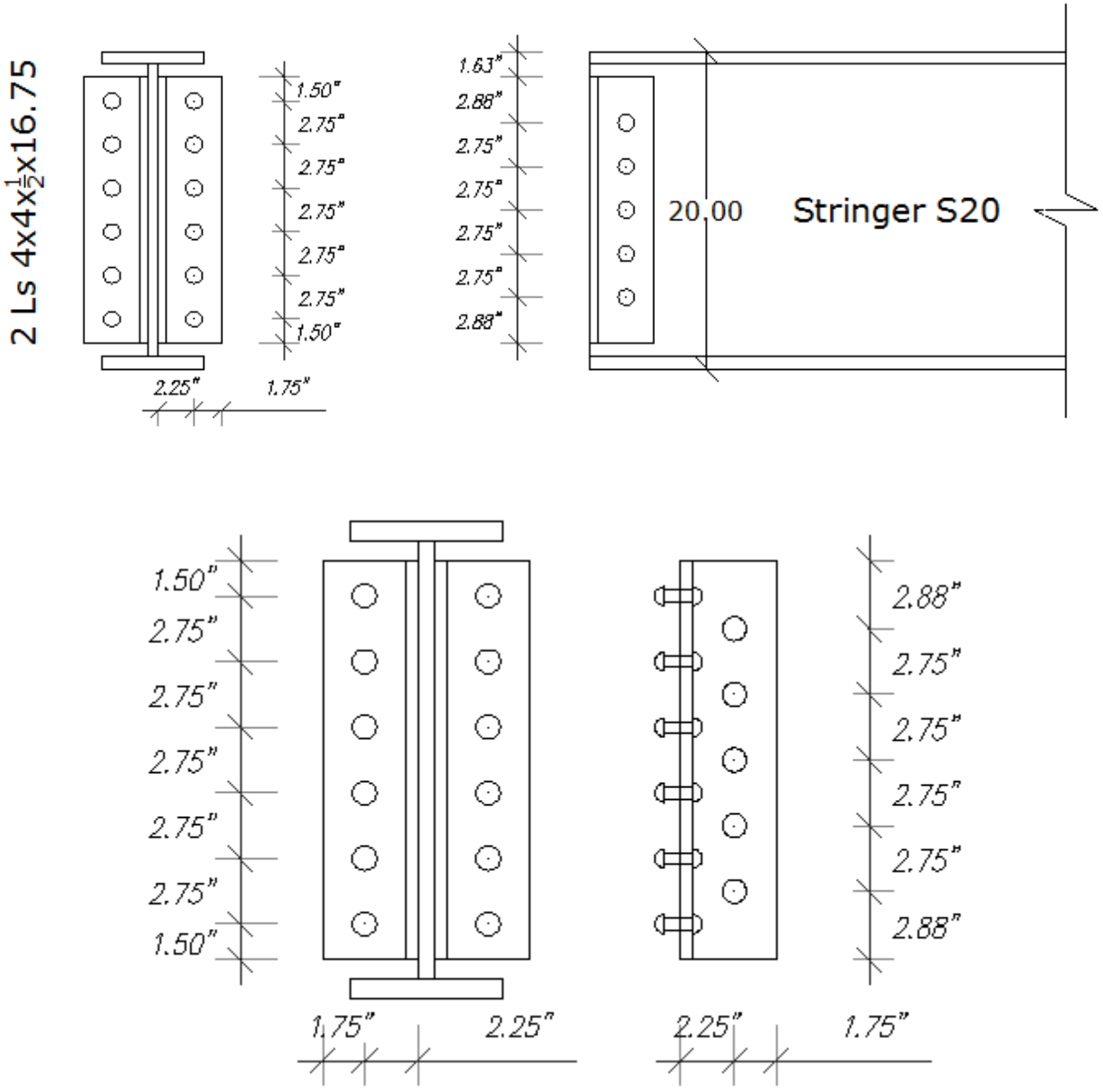

Figure 3.10 Dimensions of double angle connection – Case study, Example #2

Table 3.2 List of dimensions and material properties for detail #2

Parameter	Magnitude, US units		Magnitude, SI units		Comments
F_y	30.00	ksi	206.84	MPa	
F_u	40.00	ksi	275.79	MPa	
A_b	0.44	in^2	285.02	mm^2	
T_b	28.00	ksi	193.05	MPa	Group A
h_f	1.00	#	1.00	#	
n_b	6.00	#	6.00	#	
n_s	2.00	#	2.00	#	
h	16.75	in	425.45	mm	
L_{ev}	2.88	in	73.15	mm	
L_{eh}	1.75	in	44.45	mm	
Spacing, s	2.75	in	69.85	mm	
Bolt diameter, d_b	0.75	in	19.05	mm	
Bolt hole, d_h	0.81	in	20.64	mm	
F_{nv}	$(0.45 \cdot 120) = 54.0$	MPa	372.32	MPa	A325-N
F_{nt}	$(0.75 \cdot 120) = 90.0$	MPa	620.53	MPa	
Angle thickness, t_a	0.56	in	14.29	mm	
Floorbeam web thickness, t_{wb}	0.56	in	14.29	mm	
Stringer web thickness, t_{ws}	0.64	in	16.13	mm	

Design strength per bolt - Shear strength of the bolt

$$\phi R_n = 0.75 \cdot (0.45 \cdot F_u^b) \cdot m \cdot A_b \cdot n_v = 0.75 \cdot (0.45 \cdot 120) \cdot 1 \cdot 0.44 \cdot 1 = 17.82 kips / bolt$$

Number of bolts on the Stringer is 5, and there are 2 shear surfaces

$$\phi R_{n\_total} = 2 \cdot 5 bolts \cdot 17.82 kip / bolt = 178.2 kip$$

Number of bolts on the Floorbeam is 5 on each side - 2 columns

$$\phi R_{n\_total} = 2 \cdot 6 bolts \cdot 17.82 kip / bolt = 213.84 kip$$

Tearing and Bearing – Angle thickness controls bearing and tearing:

When bearing strength is based on $2.4F_u$, LRFD-J3.10 (a) applies:

End distance $L_{e\_\min} = 1.5 \cdot d_b = 1.5 \cdot 3/4 = 1.125in < 1.50in$ **OK!**

Center-to-center spacing $s_{\min} = 2.67 \cdot d_b = 2.67 \cdot 3/4 = 2.00in < 2.75in$ **OK!**

Clear distance for exterior bolts $L_c = L_e - 0.5 \cdot d_b = 1.50 - 0.5 \cdot (0.75 + 1/16) = 1.094in$

$L_c = L_e - 0.5 \cdot d_b = 2.88 - 0.5 \cdot (0.75 + 1/16) = 2.47in$

Clear distance for interior bolts $L_c = s - d_b = 2.75 - (0.75 + 1/16) = 1.94in$

Angle thickness, $t = t_a = 9/16 = 0.5625in$

Tearing strength exterior on the web-stringer $\phi R_n = 0.75 \cdot (1.2 \cdot L_c \cdot t \cdot F_u^p) = 0.75 \cdot (1.2) \cdot (2.47) \cdot (0.5625) \cdot (40) = 50.02kips/bolt$

Tearing strength exterior on the web-floorbeam $\phi R_n = 0.75 \cdot (1.2 \cdot L_c \cdot t \cdot F_u^p) = 0.75 \cdot (1.2) \cdot (1.094) \cdot (0.5625) \cdot (40) = 22.15kips/bolt$

Tearing strength interior $\phi R_n = 0.75 \cdot (1.2 \cdot L_c \cdot t \cdot F_u^p) = 0.75 \cdot (1.2) \cdot (1.94) \cdot (0.5625) \cdot (40) = 39.285kips/bolt$

Bearing strength $\phi R_n = 0.75 \cdot (2.4 \cdot d_b \cdot t \cdot F_u^p) = 0.75 \cdot (2.4) \cdot (0.75 + 1/16) \cdot (0.5625) \cdot (40) = 32.91kips/bolt$

Total on the web-stringer: $2 \cdot [5 \cdot 32.91kips] = 329.1kips$

Total on the web-floorbeam: $2 \cdot [2 \cdot 22.15kips + 4 \cdot 39.285kips] = 402.88kips$

Block shear strength on double-angle

$t = t_a = 9/16 = 0.5625in$

$A_{gt} = 2 \cdot L_{eh} \cdot t = 2 \cdot (1.75in) \cdot 0.5625in = 1.97in^2$

$A_{nt} = A_{gt} - 0.5 \cdot holes \cdot t \cdot 2 = 1.97 - 0.5 \cdot (0.75 + 1/8) \cdot 0.5625 \cdot 2 = 1.48in^2$

$A_{gv} = 2 \cdot (4 \cdot s + L_{ev}) \cdot t = 2 \cdot (4 \cdot 2.75 + 2.88) \cdot 0.5625 = 15.525in^2$

$A_{nv} = A_{gv} - 4.5 \cdot holes \cdot t \cdot 2 = 15.525 - 4.5 \cdot (0.75 + 1/8) \cdot 0.5625 \cdot 2 = 11.095in^2$

$F_u \cdot A_{nt} = 40ksi \cdot 1.48in^2 = 59.2kip < 0.6 \cdot F_u \cdot A_{nv} = 0.6 \cdot 40ksi \cdot 11.095in^2 = 266.3kip$

which means shear fracture – tension yield controls.

$$\boxed{\phi \cdot R_n = \phi \cdot (0.6 \cdot F_u \cdot A_{nv} + F_u \cdot A_{nt}) = \phi \cdot (0.6 \cdot 40 \cdot 11.095 + 40 \cdot 1.48) = 0.75 \cdot 325.48 = 244.11kips}$$

$$\phi \cdot R_n = \phi \cdot (0.6 \cdot F_y \cdot A_{gv} + F_u \cdot A_{nt}) = \phi \cdot (0.6 \cdot 30 \cdot 15.525 + 40 \cdot 1.48) = 0.75 \cdot 338.65 = 254.0kips$$

Summary:

Based on bolt shear strength $T_u = 178.2kips$

Total bearing and tearing $T_u = 329.1kips$

Based on block shear (web-stringer) $T_u = 244.11kips$

Combined shear and tension

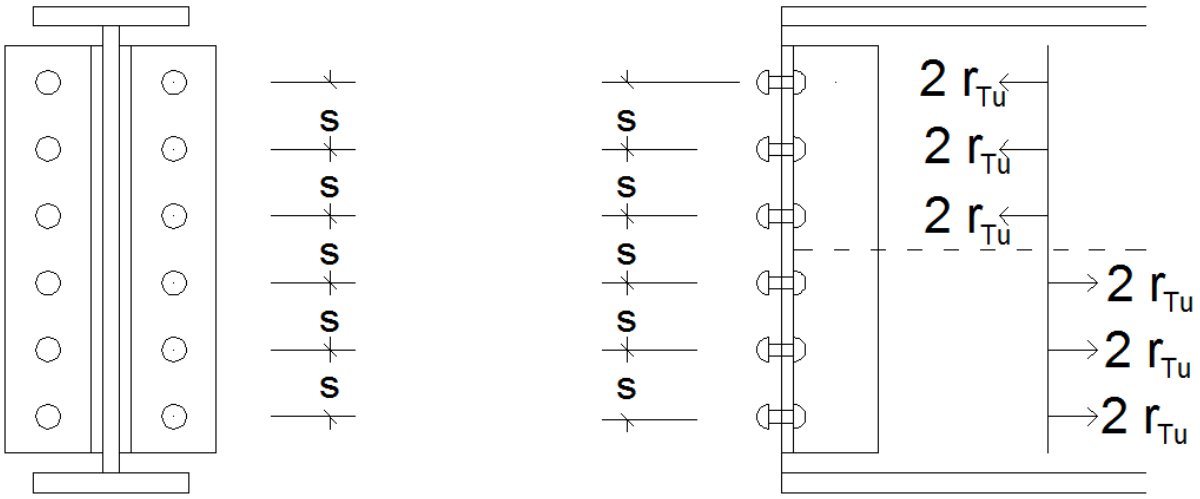

Figure 3.11 The resultant forces acting on the double angle connection – Case study, Example #2

Reduced tensile strength

$$\phi F_{nt}' = \phi \cdot \left[1.3 \cdot F_{nt} - \frac{F_{nt}}{\phi \cdot F_{nv}} f_v \right] \le \phi F_{nt}$$

$F_{nt} = 90ksi$ and $F_{nv} = 54ksi$ from Table J3.2

$$f_v = \frac{178.2kip}{12 \cdot 0.44in^2} = 33.75ksi$$

$$\phi F_{nt}' = 0.75 \cdot \left[1.3 \cdot 90 - \frac{90}{0.75 \cdot 54} 33.75 \right] = 31.5ksi > \phi F_{nt} = 0.75 \cdot 90ksi = 67.5ksi$$

Use $\phi F_{nt}' = 31.5ksi$

$$r_{Tn} = \phi F_{nt} \cdot A_b = 31.5 \cdot 0.44 = 13.86kip$$

Maximum Moment Capacity

$$[(2 \cdot r_{Tu}) \cdot 0.5 \cdot s + (2 \cdot r_{Tu}) \cdot 1.5 \cdot s + (2 \cdot r_{Tu}) \cdot 2.5 \cdot s] \cdot 2 = 18 \cdot r_{Tu} \cdot s = M_u kip \cdot in$$

$$M_u kip \cdot in = 18 \cdot r_{Tu} \cdot 2.75 in$$

$$M_u kip \cdot in = 49.5 \cdot r_{Tu} \cdot in$$

$$if \quad r_u = \phi F_{nt}' \cdot A_b = 13.86 kip \quad then \quad M_u = 686.07 kip \cdot in = 57.2 kip \cdot ft$$

$$if \quad r_u = \phi F_{nt} \cdot A_b = 32.9 kip \quad then \quad M_u = 1628.55 kip \cdot in = 135.71 kip \cdot ft$$

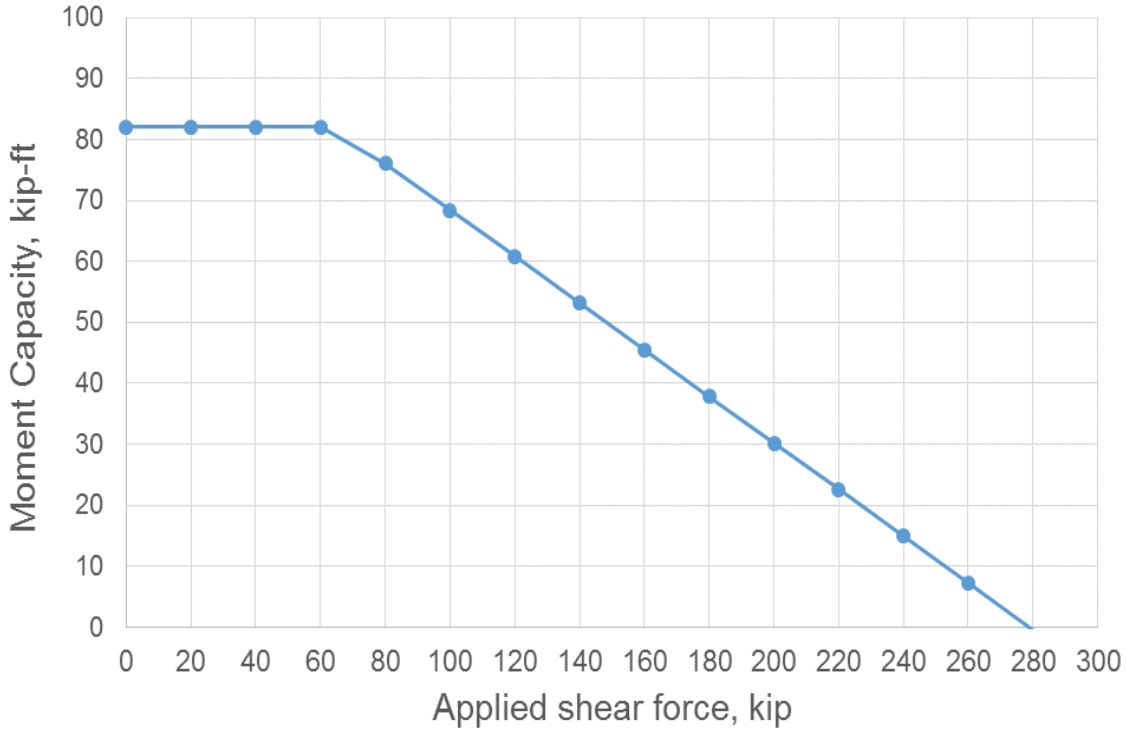

Figure 3.12 Moment capacity vs. applied shear force – Case study, Example #2

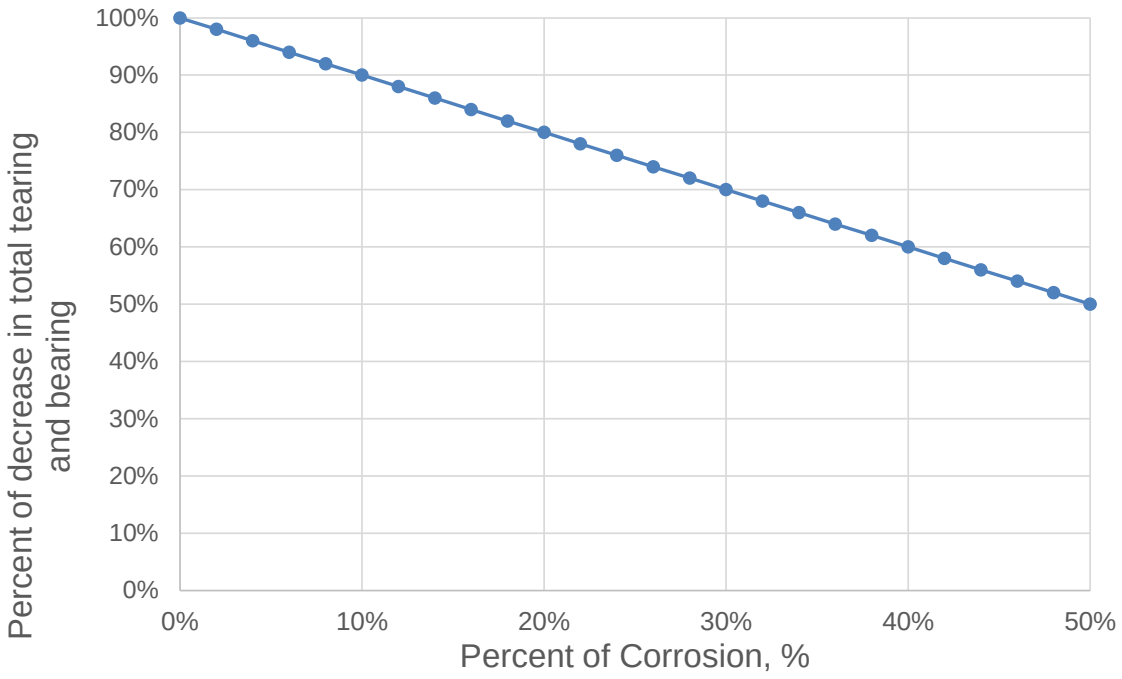

Figure 3.13 Moment capacity of double angle connection vs. percent of corrosion – Case study, Example #2

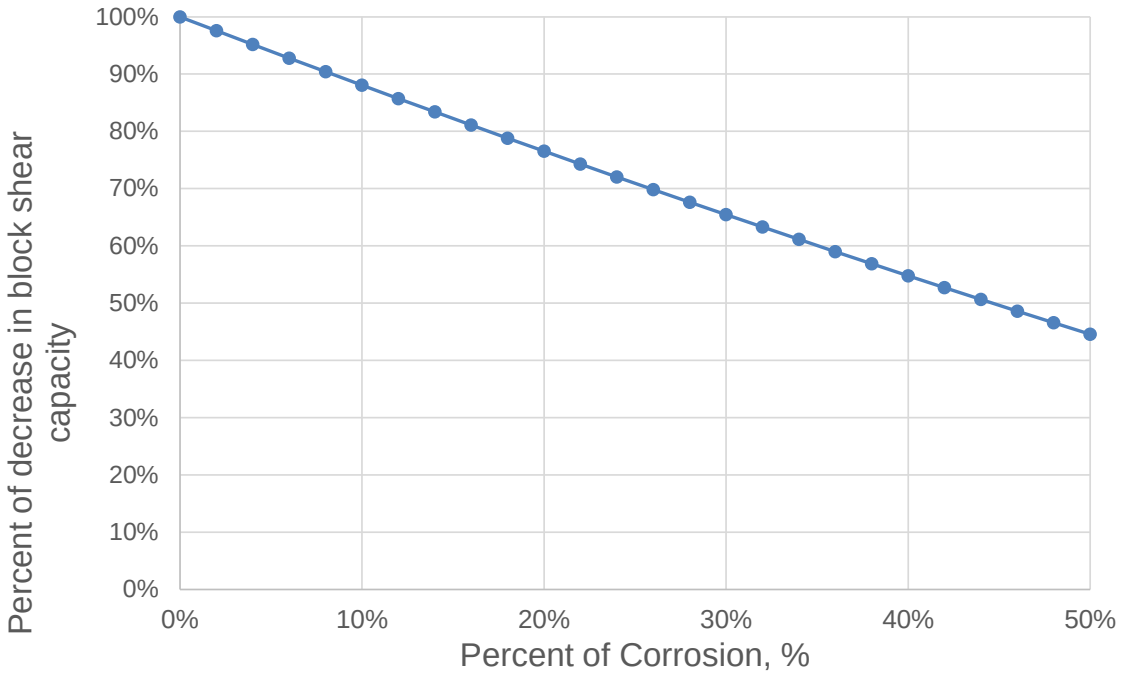

Figure 3.14 Shear capacity of double angle connection vs. percent of corrosion – Case study, Example #2

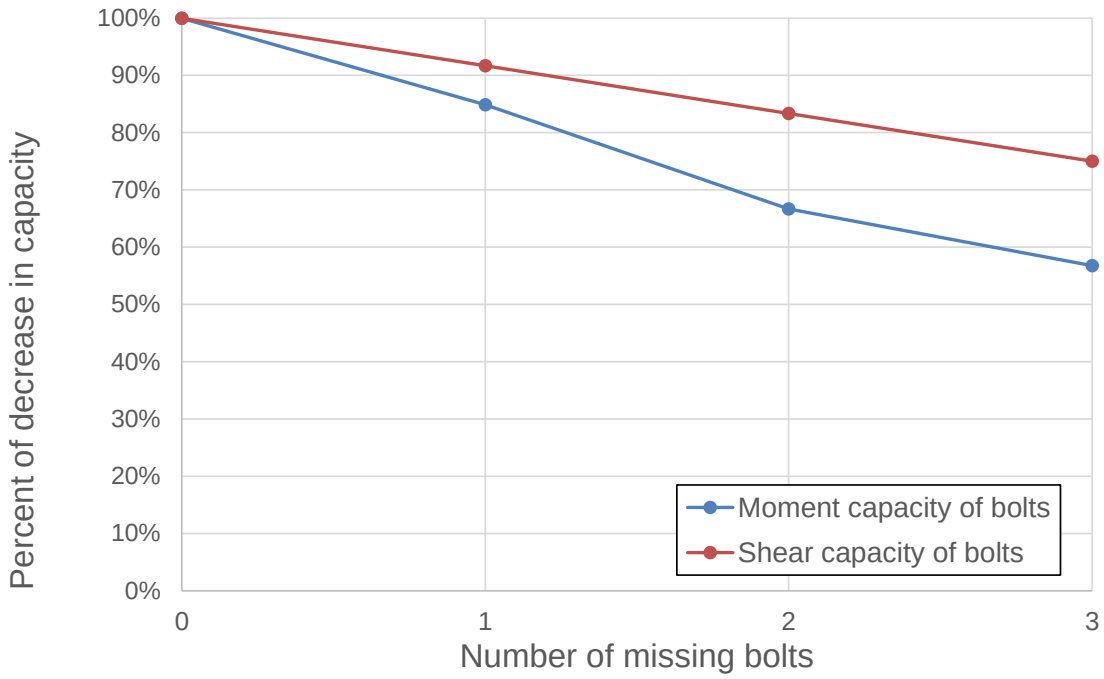

Figure 3.15 Moment capacity of double angle connection vs. number of missing bolts – Case study, Example #2

Chapter 4 Structural Analysis

4.1 Overview

The Finite Element Method (FEM) was used to investigate the behavior and performance characteristics of a typical bridge connection between stringer and crossbeam. FEM is a numerical technique for finding approximate solutions to partial differential and integral equations. “The solution approach is based either on eliminating the differential equation completely through steady state problems, or rendering the PDE into an approximating system of ordinary differential equations, which are then numerically integrated using standard techniques such as Euler's method, Runge-Kutta, and so forth (Finite Element Method 2012).

In this study, three-dimensional element models were developed using the FEM software ABAQUS/CEA. This software provides a simple, consistent interface for creating, submitting, monitoring, and evaluating results from ABAQUS/Standard and ABAQUS/Explicit simulations. ABAQUS/Standard is a general-purpose FEA that uses a traditional implicit integration scheme. ABAQUS/Explicit is a special purpose FEA that employs an explicit integration scheme to solve highly nonlinear systems with many complex contacts under transient loads (en.wikipedia.org).

ABAQUS/Standard provides both linear and nonlinear response options. The program is truly integrated, so linear analysis is always considered as linear perturbation analysis. The nonlinear procedures in ABAQUS/Standard offer two additional approaches: direct user control of increment size and automatic control approach. Automatic control approach is usually more efficient because the user cannot predict the response ahead of time. In ABAQUS/Explicit the time incrementation is controlled by the stability limit of the central difference operator. Hence, the time incrementation scheme is fully automatic and requires no user intervention.

In this study, material inelastic behavior was considered by defining elastic-plastic properties of steel based on the available models in ABAQUS. A highly detailed model was created for the double angle connection, representative of typical connections in railway bridges. The model was assembled from floorbeam, stringers, connection angles, and bolts.

4.2 Introduction to Finite Element Method

ABAQUS/Standard generally uses Newton's method as a numerical technique for solving nonlinear equilibrium equations (ABAQUS Analysis User's Manual, n.d.). The advantage of Newton's method as compared to alternate methods such as the modified Newton or quasi-Newton methods is primarily the rate of convergence of the results. However, Newton's method is not good for large finite element codes for two reasons: first, it is difficult to formulate a complete Jacobian matrix; second, formulating and solving the Jacobian for each iteration is time-consuming. In the modified Newton method, the Jacobian is recalculated only occasionally. Therefore this method can be used for mildly nonlinear problems involving softening behavior, but is not recommended for strictly nonlinear cases.

All nonlinear solutions are based on obtaining the solution by numerical methods when it is not possible to find an analytic solution. The iteration continues until a numerical solution gives a very close approximation to the true solution. During the process, series of increments are created with iterations to obtain equilibrium within each of the increments. Hence, the increment size controls the efficiency and speed of calculations. Increments that are too large require more iterations and, in some cases, the program does not manage to find a solution at all. ABAQUS provides both an "automatic" time step choice and direct user control for all classes of problems (ABAQUS Analysis User's Manual, n.d.). For nonlinear problems, automatic schemes in ABAQUS provide a reliable approach.

4.2.1 Finite Element

ABAQUS has a wide range of elements available. Each element is characterized by family, degree of freedom, number of nodes, formulation, and integration. Figure 4.1 shows the element families most commonly used in a stress analysis. One of the major distinctions between different element families is the geometry type that each family assumes.

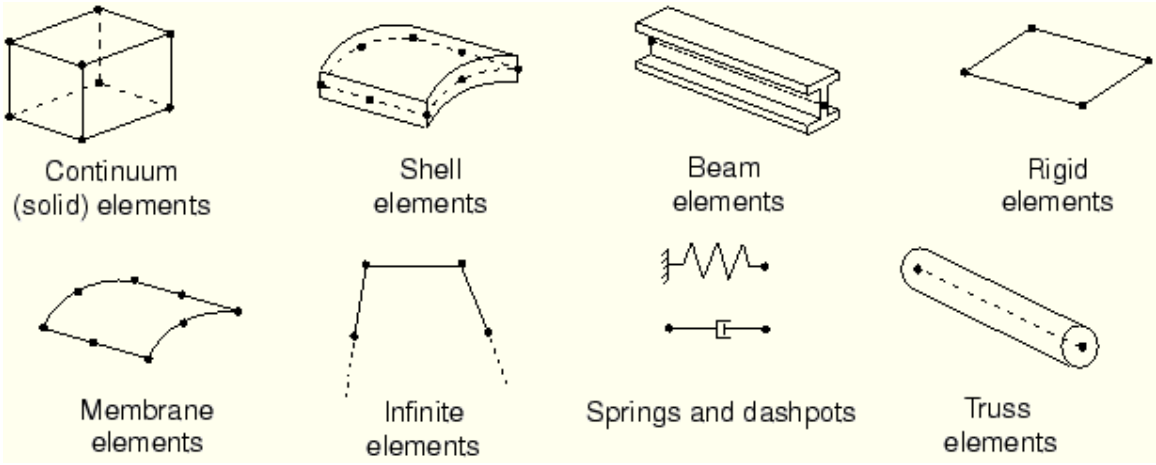

Figure 4.1 Commonly used element families (ABAQUS Analysis User's Manual)

The degrees of freedom (DOF) are the fundamental variables calculated during the analysis. For a stress/displacement simulation, the degrees of freedom are the translations at each node. Some element families, such as the beam and shell families, have rotational degrees of freedom as well. The basic DOF are presented in figure 4.2. Additional DOF include, among others, warping in open-section beam elements and temperature for continuum elements or temperature at the first point through the thickness of beams and shells.

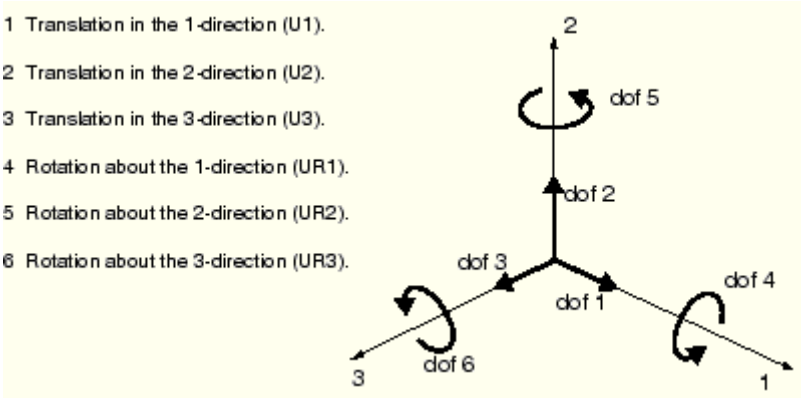

Figure 4.2 Displacement and rotational degrees of freedom (ABAQUS Analysis User's Manual)

Displacements, rotations, temperatures, and the other degrees of freedom mentioned in the previous section are calculated only at the nodes of the element. At any other point in the element, the displacements are obtained by interpolating from the nodal displacements. Usually, the interpolation order is determined by the number of nodes used in the element. Elements that have nodes only at their corners, such as the eight-node brick, use linear interpolation in each direction and are often called linear elements or first-order elements. Elements with mid-side nodes, such as the 20-node brick, use quadratic interpolation and are often called quadratic elements or second-order elements. Modified triangular or tetrahedral elements with mid-side nodes, such as the 10-node tetrahedron, use a modified second-order interpolation and are often called modified or modified second-order elements. A selection of elements is presented in figure 4.3.

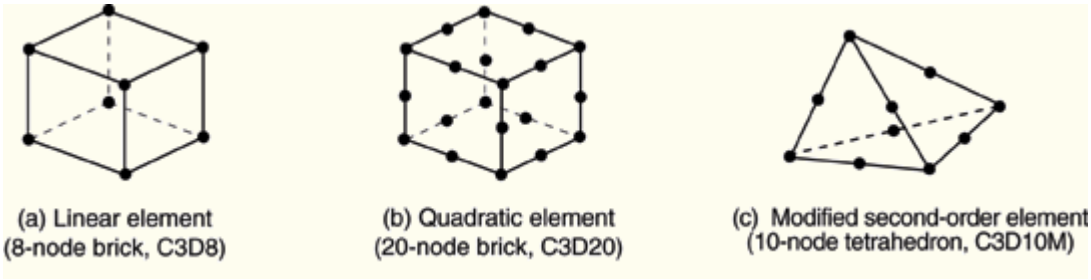

Figure 4.3 Linear brick, quadratic brick, and modified tetrahedral elements (ABAQUS Analysis User's Manual)

An element's formulation refers to the mathematical theory used to define the element's behavior. In the absence of adaptive meshing, all of the stress/displacement elements in ABAQUS are based on the Lagrangian or material description of behavior. That is, the material associated with an element remains associated with the element throughout the analysis, and material cannot flow across element boundaries. In the alternative Eulerian or spatial description, elements are fixed in space as the material flows through them. Eulerian methods are used commonly in fluid mechanics simulations.

ABAQUS uses numerical techniques to integrate various quantities over the volume of each element. Using Gaussian quadrature for most elements, ABAQUS evaluates the material response at each integration point in each element. Some continuum elements in ABAQUS can use full or reduced integration - a choice that can have a significant effect on the accuracy of the element for a given problem.

In this study, continuum elements, along with an eight-node brick, were used to model the bolts, angles, stringers, and crossbeam.

4.2.2 Connections and Constraints

In ABAQUS, many types of kinematic constrains can be defined. Two surfaces can be tied together using surface-based tie constraints. In this type of connection each node on the first, or, slave surface has the same values for its degrees of freedom as the point on the second, or, master surface to which it is closest. A surface-based tie constraint can be used to make the translational and rotational motion, as well as all other active degrees of freedom, equal for a pair of surfaces. The offset distances between the surfaces' elements can be defined in the constraints or can be taken as a default; the simulation takes the initial thickness and offset of shell elements underlying the surface into account. The surface-to-surface formulation generally avoids stress noise at tied interfaces. Only a few surface restrictions apply to the surface-to-surface formulation.

ABAQUS can use one of two approaches to generate coefficients: the "surface-to-surface" approach or the "node-to-surface" approach. The true surface-to-surface approach optimizes the stress accuracy for a given surface pairing. The improved stress accuracy with the surface-to-surface approach is realized only if neither surface of the tie pairing is node-based. The surface-to-surface method for establishing the tie coefficients involves a more complex algorithm than the node-to-node method, because it generally uses more master nodes per constraint.

In this study, the surface-to-surface approach in tie constrains was used to create a bond between bolt heads and the web of modeled parts in the analyzed connection, as pictured in figure 4.4. Also, as a general mechanical constraint, the displacement and rotation were assigned for boundary conditions on both ends of the crossbeam.

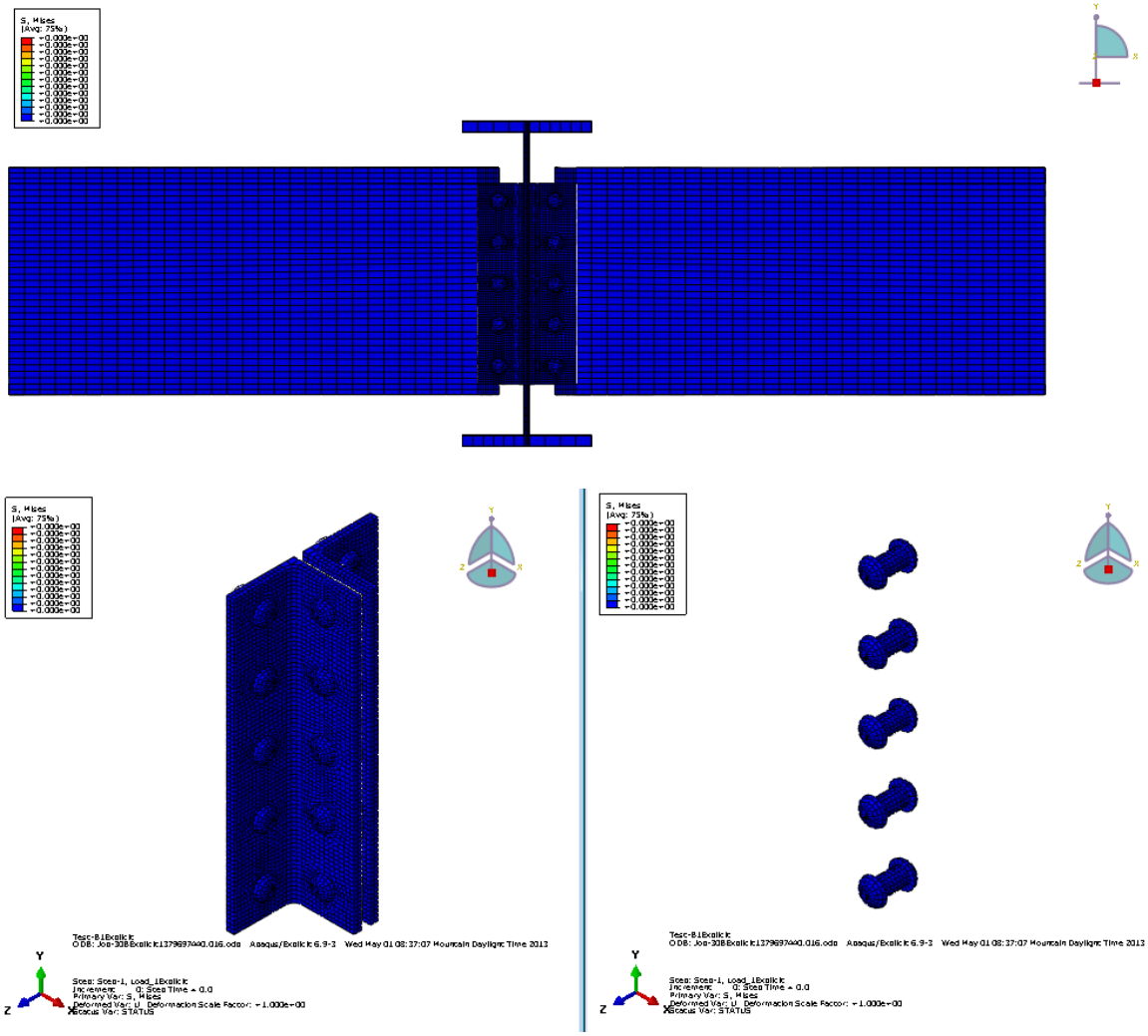

Figure 4.4 The bolted connection model used in the analysis

The applied load was assigned as a pressure on the end of one stringer to simulate eccentric force on the connection. The pressure was gradually increased and the results were recorded on each time step. For each case, the time history was developed and further analyzed.

4.2.3 Material Models

The constitutive library provided in ABAQUS contains a range of linear and nonlinear material models for all categories of materials. It includes simple models such as isotropic, linear elastic without temperature dependence, and very sophisticated material models which include much more detail on the material's response under failure. For a routine design of a component that is not in a critical situation, the simple model is sufficient. However, if the component is subjected to a severe overload, it is important to determine how it might deform under that load and whether it has sufficient ductility to withstand the overload without catastrophic failure. From a numerical viewpoint, the implementation of a constitutive model involves the integration of the state of the material at an integration point over a time increment during a nonlinear analysis. In the inelastic response models that are provided in ABAQUS, elastic and inelastic responses are distinguished by separating the deformation into recoverable (elastic) and non-recoverable (inelastic) parts.

In this study, an isotropic, nonlinear elastic-plastic without temperature dependence model was used, and general properties were assigned concerning density, i.e., Young's Modulus, and Poisson's Ratio. This approach allowed for the proper computation of self-weight and adequate load distribution in a complex model. In ABAQUS, a few models define plastic behavior. One of these is user-defined data, where the yield stress is defined as a function of plastic strain. Figure 4.5 shows a typical tensile stress-strain curve with characteristic points for standard steel. The characteristic points are proportional limit, yield point, ultimate stress, and failure point. Bellow, the proportional limit stress-strain relation is linear, and is referred to as the Young's Modulus.

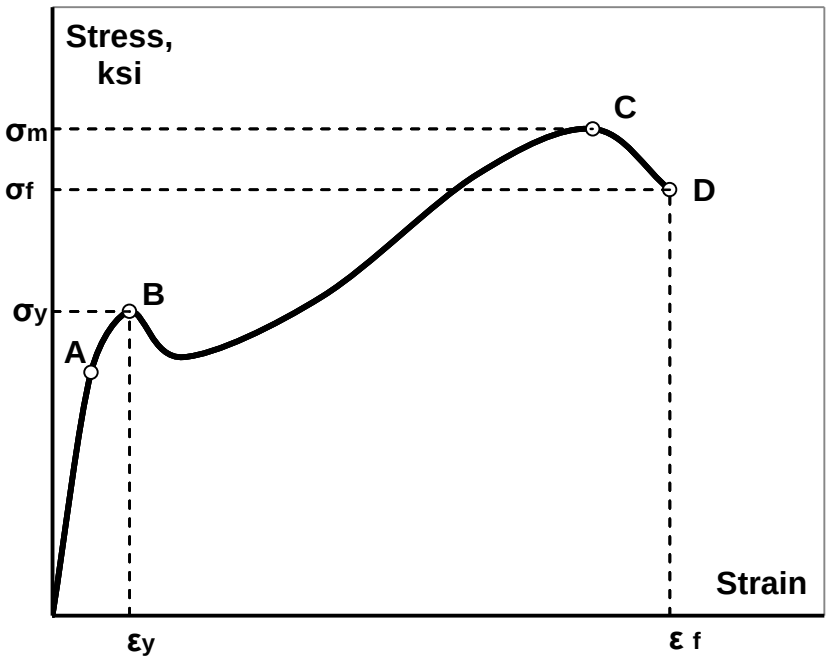

Figure 4.5 Tensile stress-strain curve for steel (a = elastic limit, b = upper yield stress, c = ultimate stress, d = breaking stress)

Yield stress is the maximum stress for which the material shows an elastic behavior, and it means that the deformations are reversible. Figure 4.6 shows the stress-strain path for elastic material under loading and unloading.

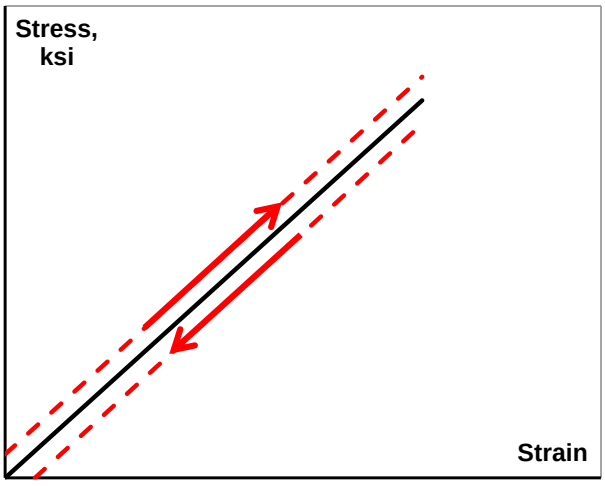

Figure 4.6 Elastic behavior

When the yield point is reached and the load continues to grow, then plastic deformation occurs. Plastic deformation is not reversible, so after releasing the load strain it does not return to zero. The stress-strain path for plastic behavior is presented in figure 4.7. The left side of the figure demonstrates that after the first loading and complete unloading, deformation is maintained; the right side shows both the previous unloading path and new path after reloading takes place.

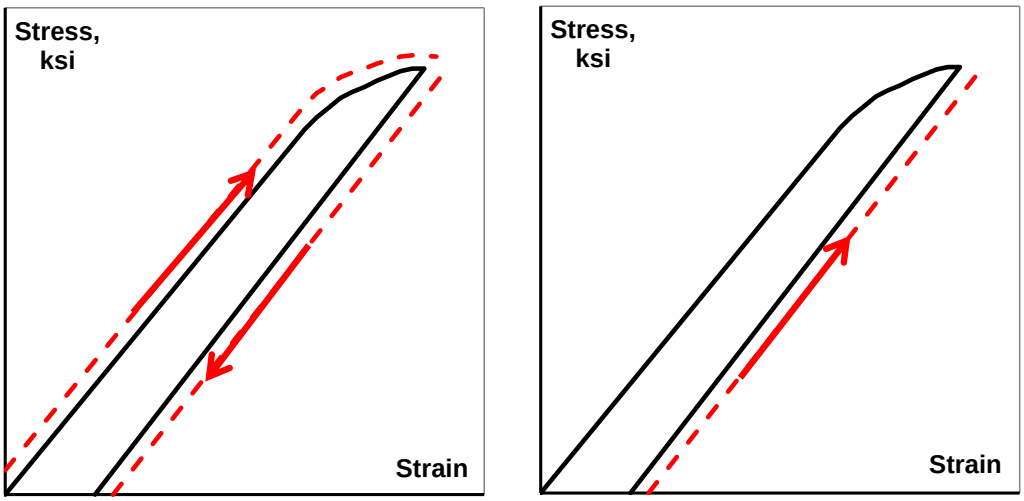

Figure 4.7 Plastic behavior

In addition to the tensile stress-strain relation, other characteristics of steel are important. When a material is stretched in one direction, it usually tends to shrink in the other two directions perpendicular to the direction of stretching. The Poisson's ratio is a ratio of transverse and longitudinal strain.

4.3 Description of FE Model for Double Angle Connection

The FE analysis was performed on a typical double angle connection, used wildly between crossbeams and stringers. The main structural components included a crossbeam, two

stringers, two pairs of angles, and group of bolts. Five bolts were used to connect angles to a stinger, and two columns of five bolts were used to connect angles to a crossbeam. All parts were created using solid elements.

The original model was modified by removing bolts to represent deterioration in the bolted connection. Four conditions of connection were considered. Connection #1 was an untouched connection, with all bolts in place. Connection #2 was modified by removing the first upper bolt on the stringer. Connection #3 was missing one upper bolt on the crossbeam (left side). Connection #4 was missing two upper bolts on the crossbeam, on each side. For all cases, the load and boundary conditions remained the same. For case #1 only, the maximum applied load was larger, but the records and time histories were created for the same load range as for the other cases.

The typical load acting on the connection was a wheel force from a railcar or locomotive. The axial load can be simulated as a concentrated load or as a pressure on a small area of upper flange. To insure a good stress distribution, pressure was used instead of a concentrated force. Load was applied on one end of a stringer. Eccentric force acting upon the connection generated complex stresses in the bolts and in the angle. The connection had to carry tensile stresses combined with shear stresses. To calculate the theoretical capacity of the connection, two groups of bolts needed to be distinguished. One group of bolt was working under combined shear and tension, and the other carried eccentric shear, as presented in figure 4.8.

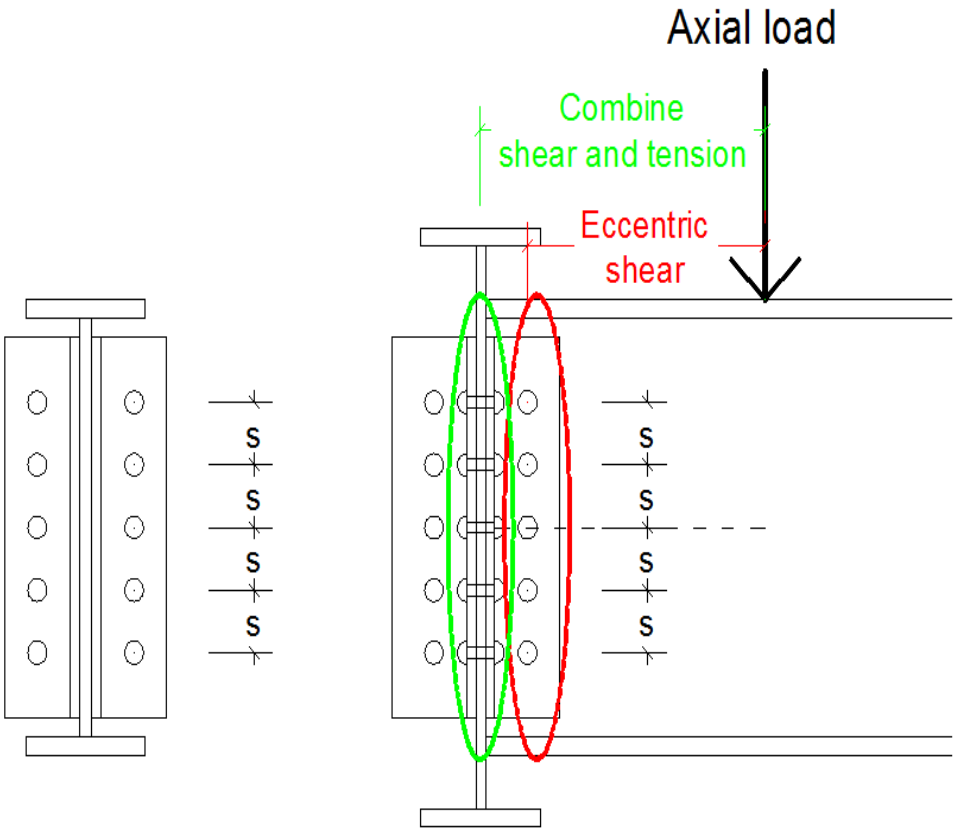

Figure 4.8 Forces acting on the double angle connection

The pressure was gradually increased to produce a shear force from 0 kN to 425 kN. The load was acting on the 1.0 m arm. Therefore, the maximum applied moment on the connection was 425 kNm. For each time-step, the stresses and displacement on bolts and the angle were recorded. Time histories were developed and further analyzed. The results are presented in figures 4.10-4.15 for connection #1, figures 4.16-4.21 for connection #2, 4.22-4.27 for connection #3, and figures 4.28-4.33 for connection #4.

4.4 Results of FEA for Double Angle Connection

4.4.1 Connection #1 - Undamaged Connection

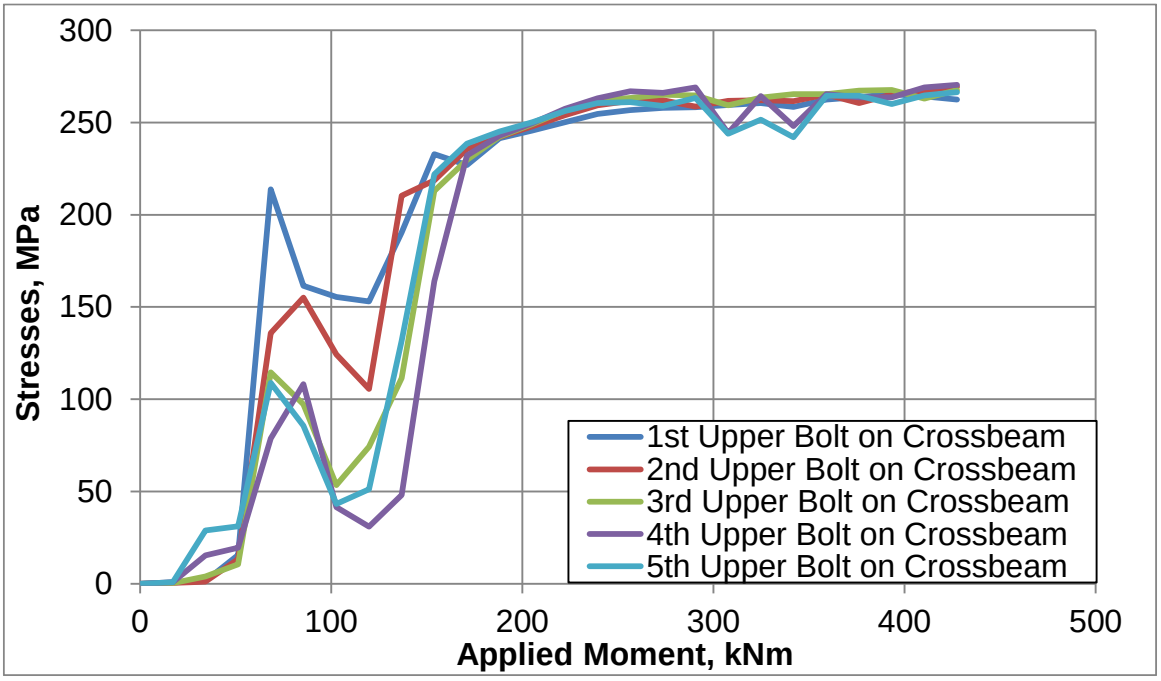

Figure 4.9 Stress histories for bolts on crossbeam - undamaged connection

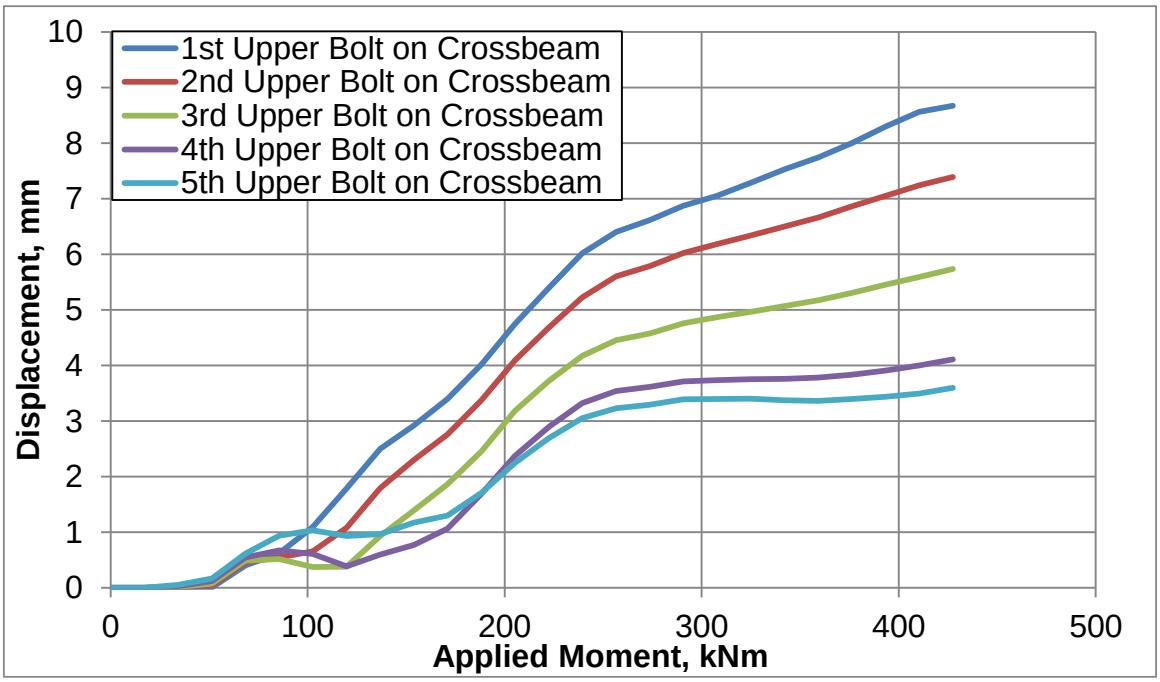

Figure 4.10 Displacement histories for bolts on crossbeam - undamaged connection

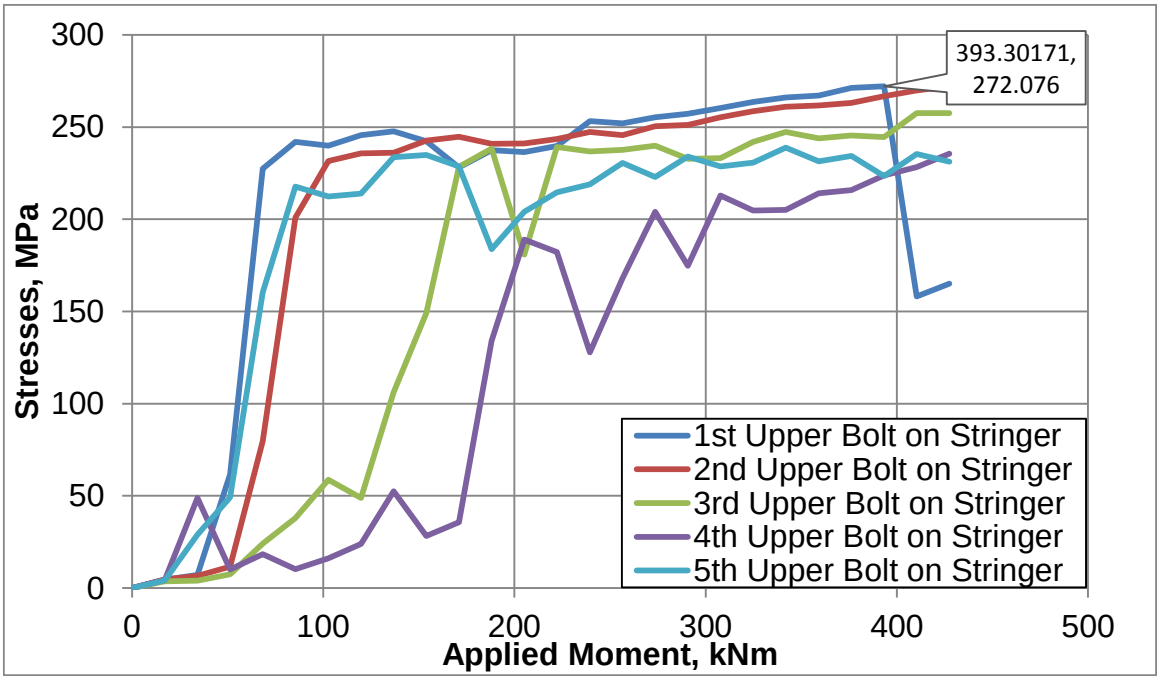

Figure 4.11 Stress histories for bolts on stringer - undamaged connection

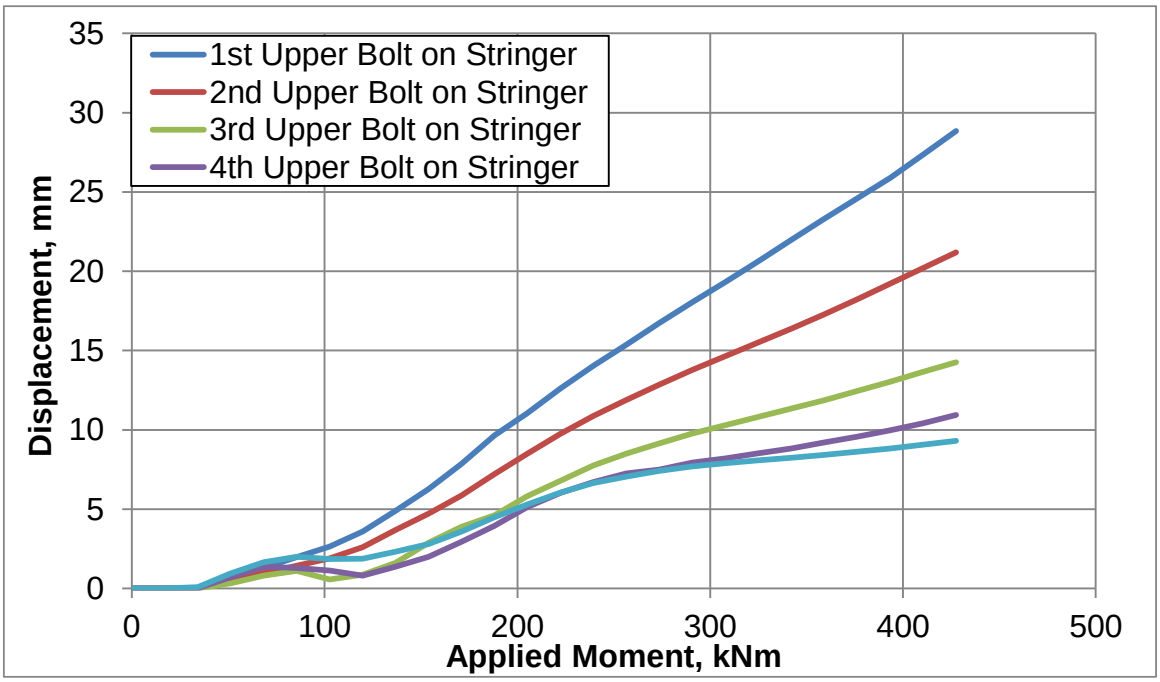

Figure 4.12 Displacement histories for bolts on stringer - undamaged connection

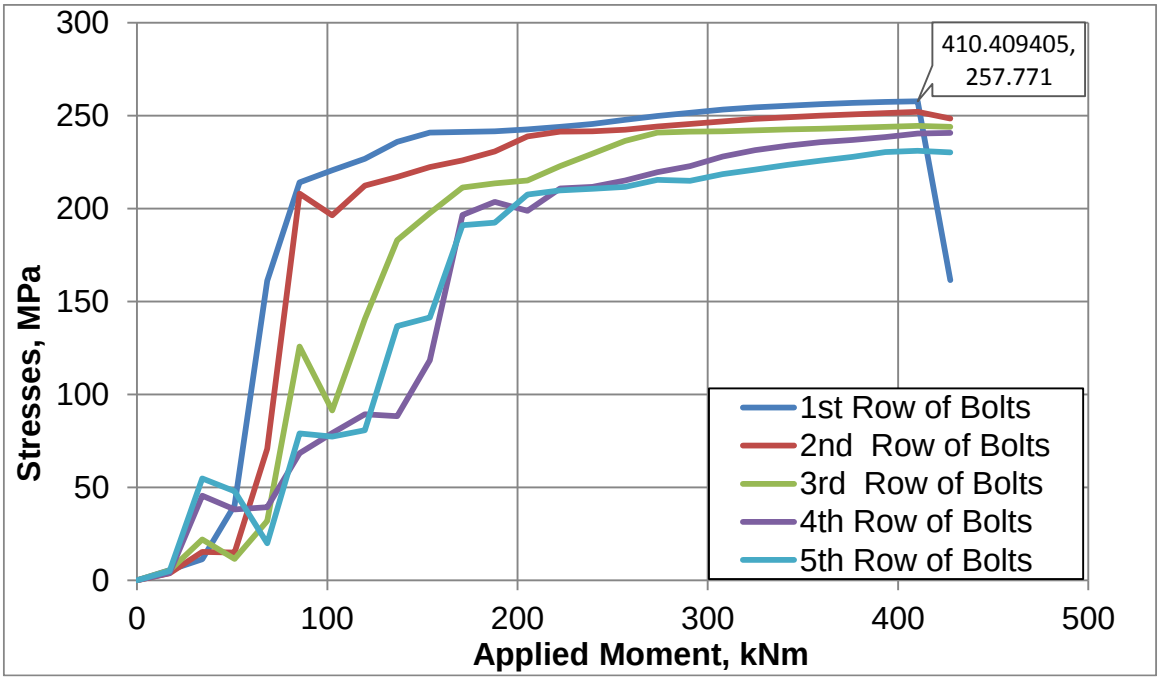

Figure 4.13 Stress histories for an angle - undamaged connection

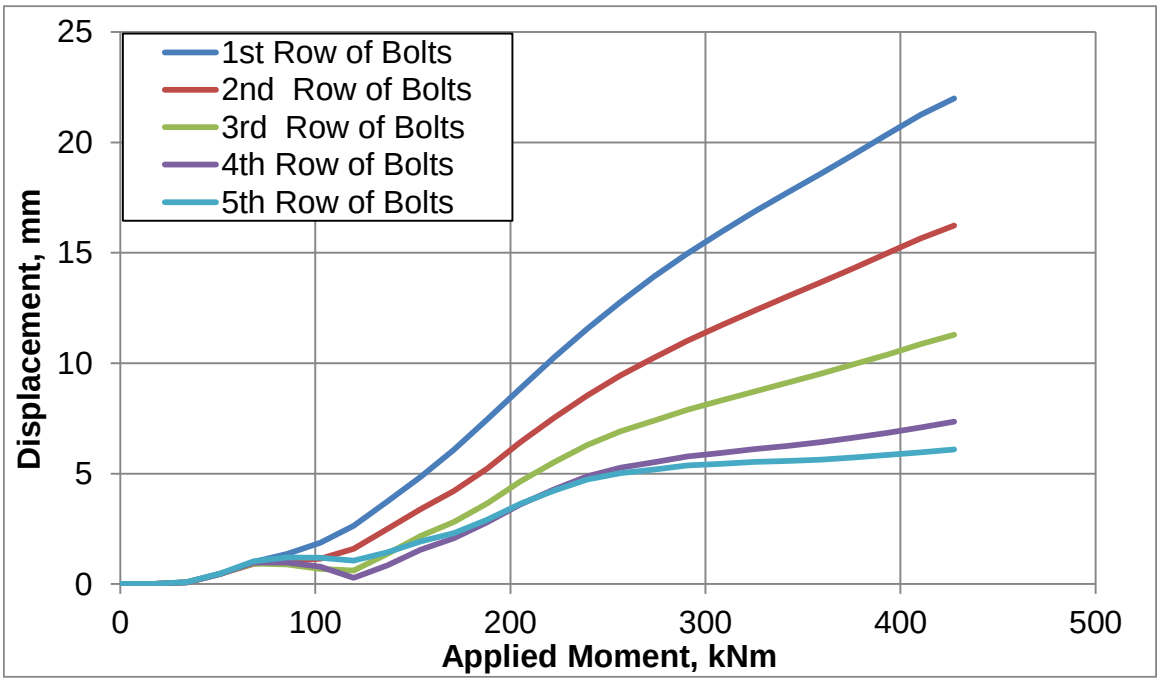

Figure 4.14 Displacement histories for an angle - undamaged connection

4.4.2 Connection #2 - One Missing Bolt on Stringer

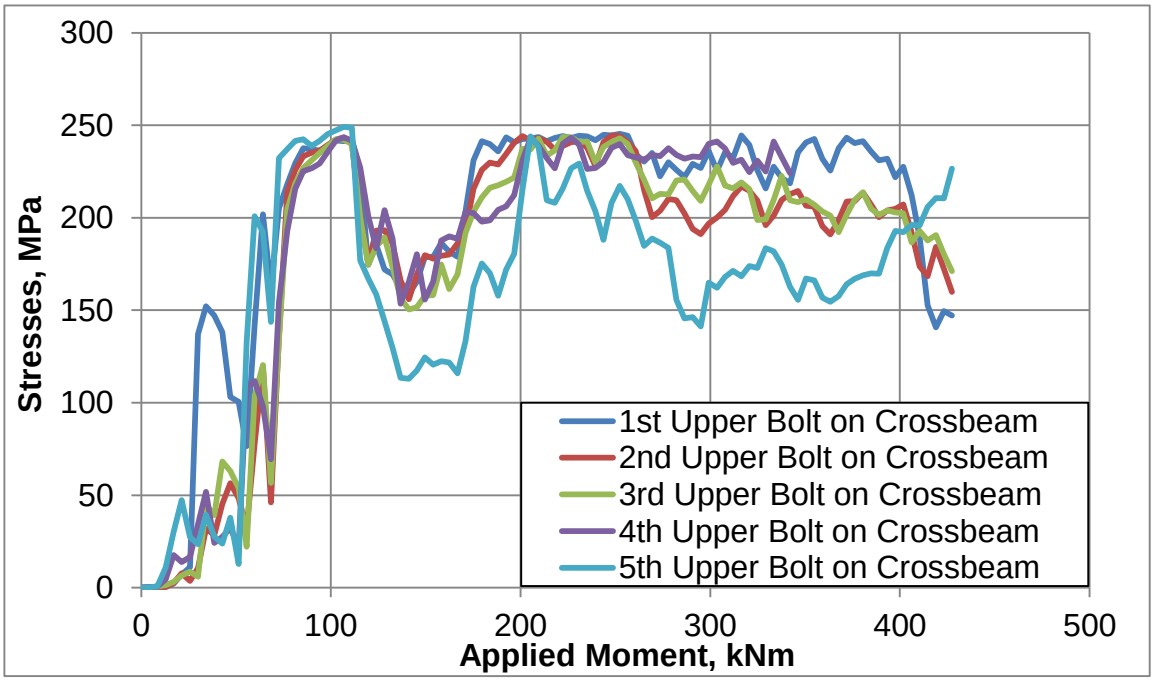

Figure 4.15 Stress histories for bolts on crossbeam - one missing bolt on stringer

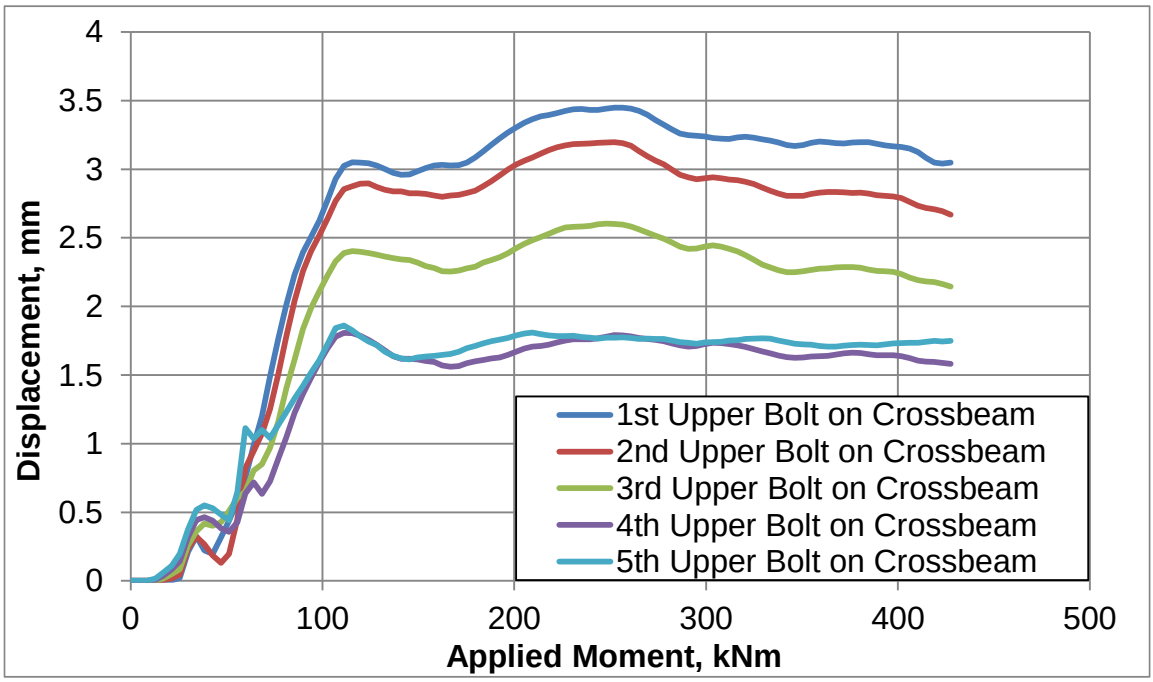

Figure 4.16 Displacement histories for bolts on crossbeam - one missing bolt on stringer

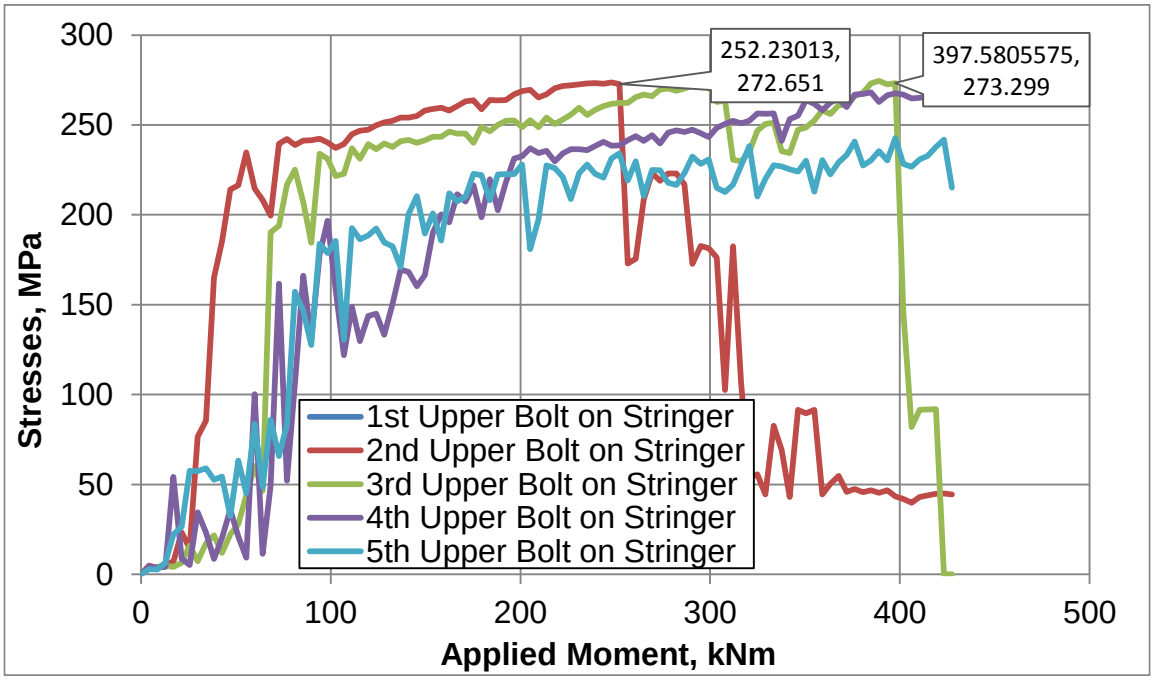

Figure 4.17 Stress histories for bolts on stringer - one missing bolt on stringer

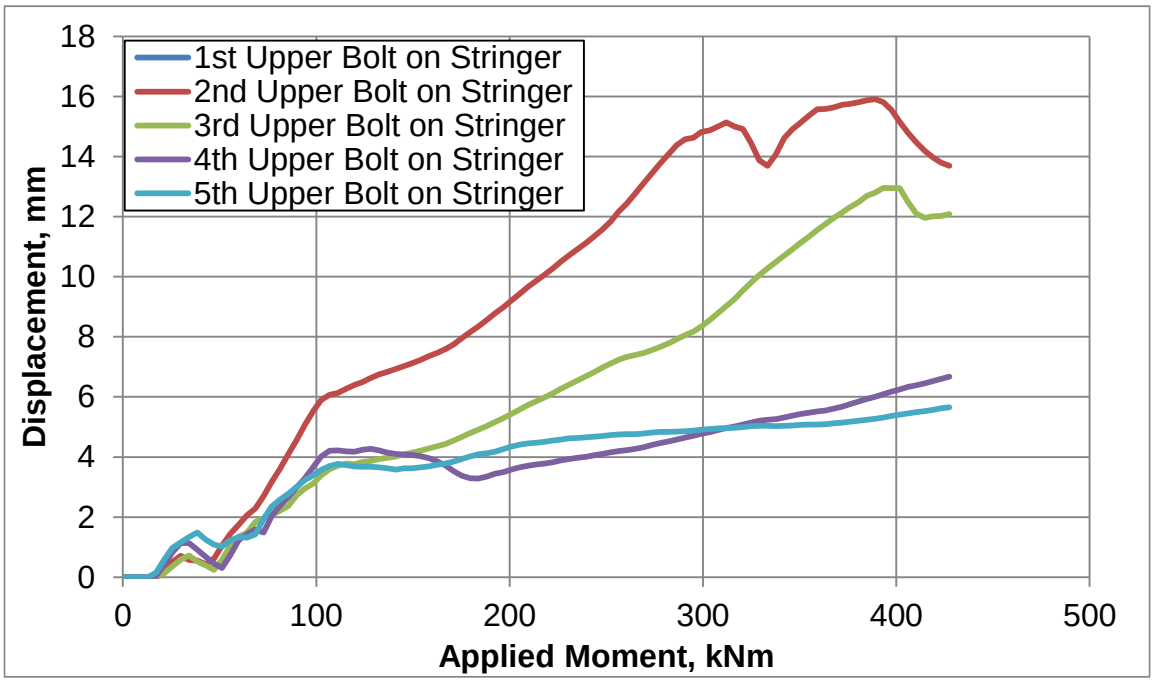

Figure 4.18 Displacement histories for bolts on stringer - one missing bolt on stringer

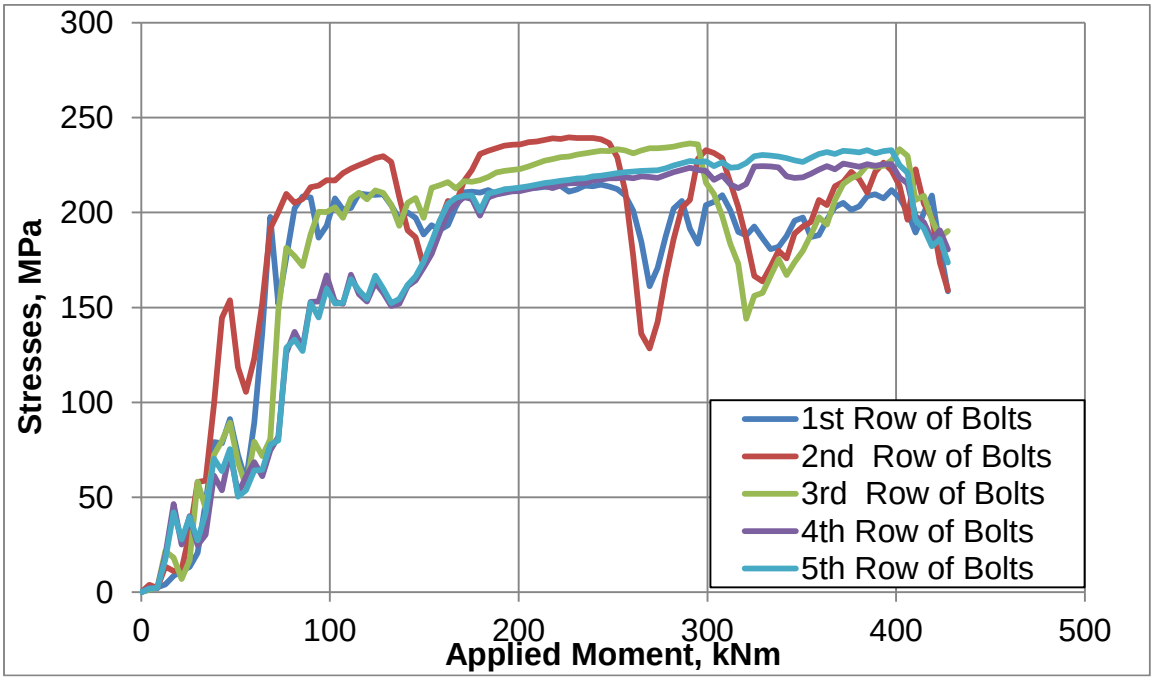

Figure 4.19 Stress histories for an angle - one missing bolt on stringer

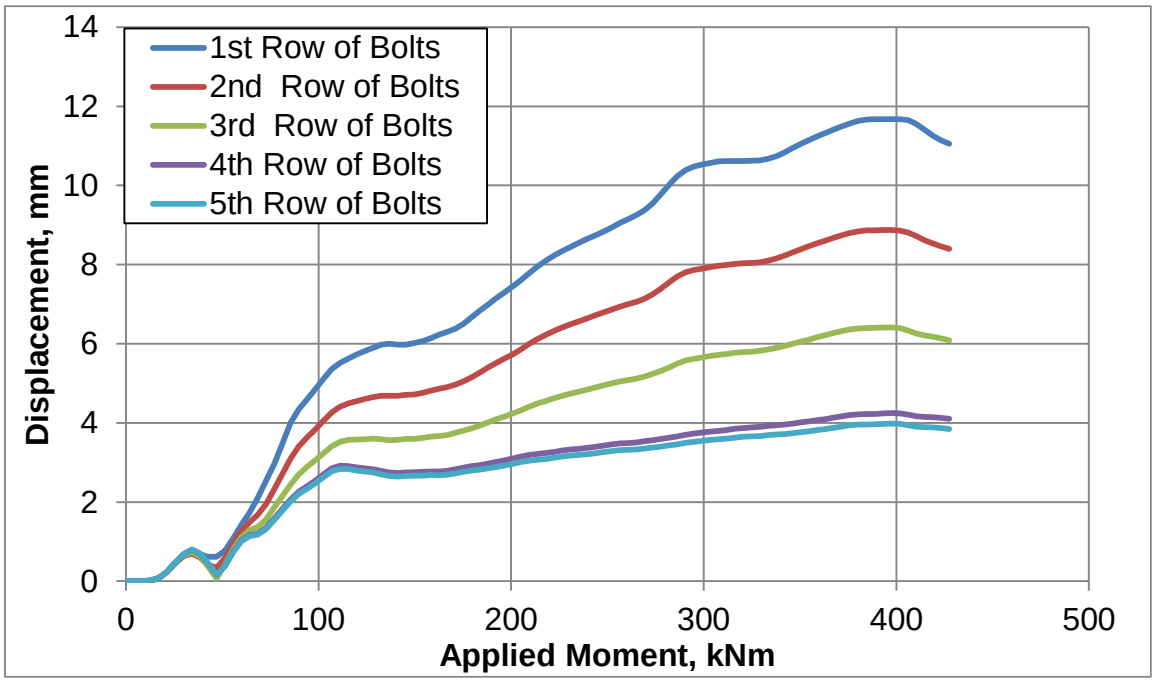

Figure 4.20 Displacement histories for an angle - one missing bolt on stringer

4.4.3 Connection #3 - One Missing Bolt on Crossbeam

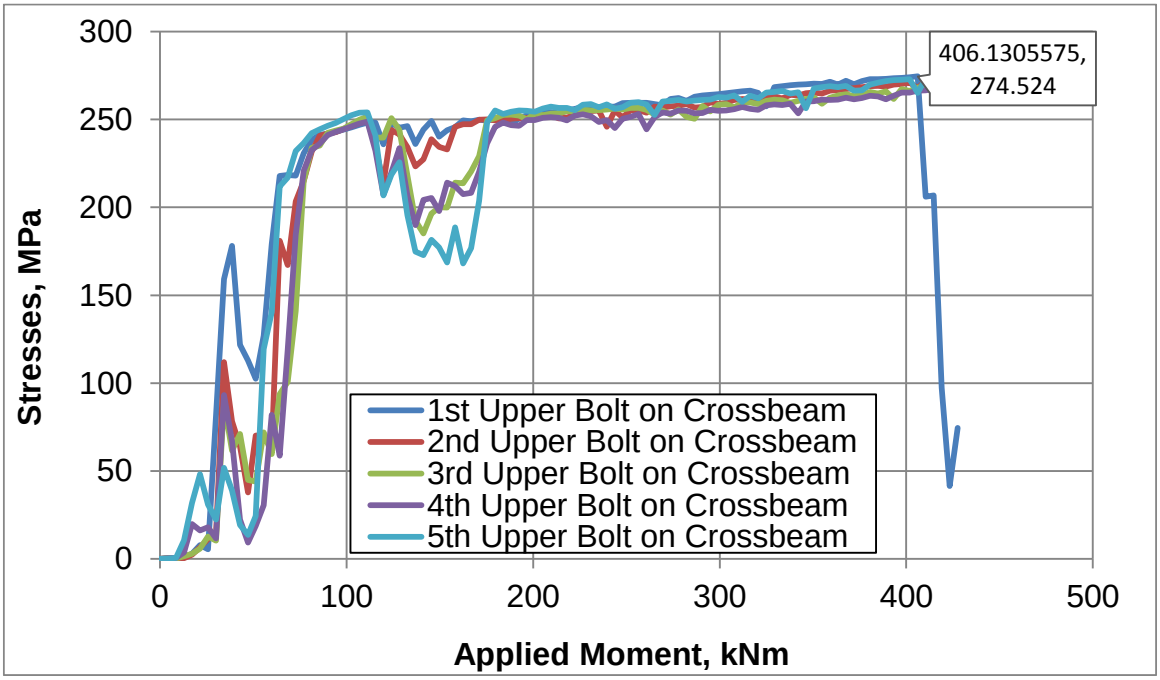

Figure 4.21 Stress histories for bolts on crossbeam - one missing bolt on crossbeam

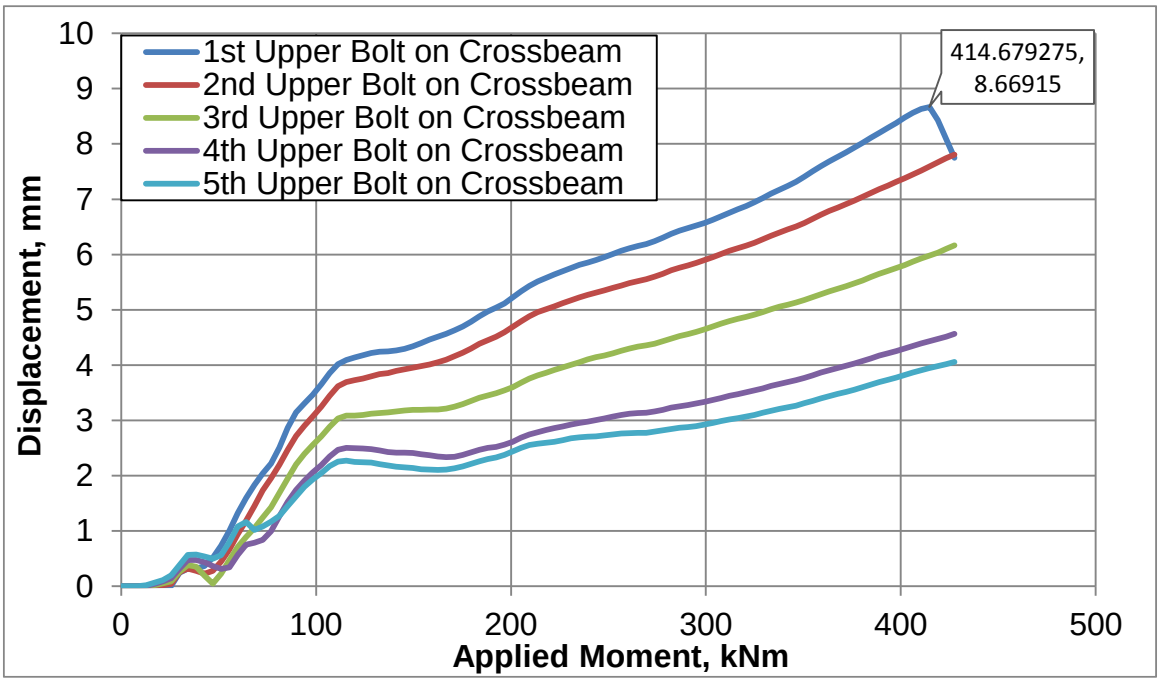

Figure 4.22 Displacement histories for bolts on crossbeam - one missing bolt on crossbeam

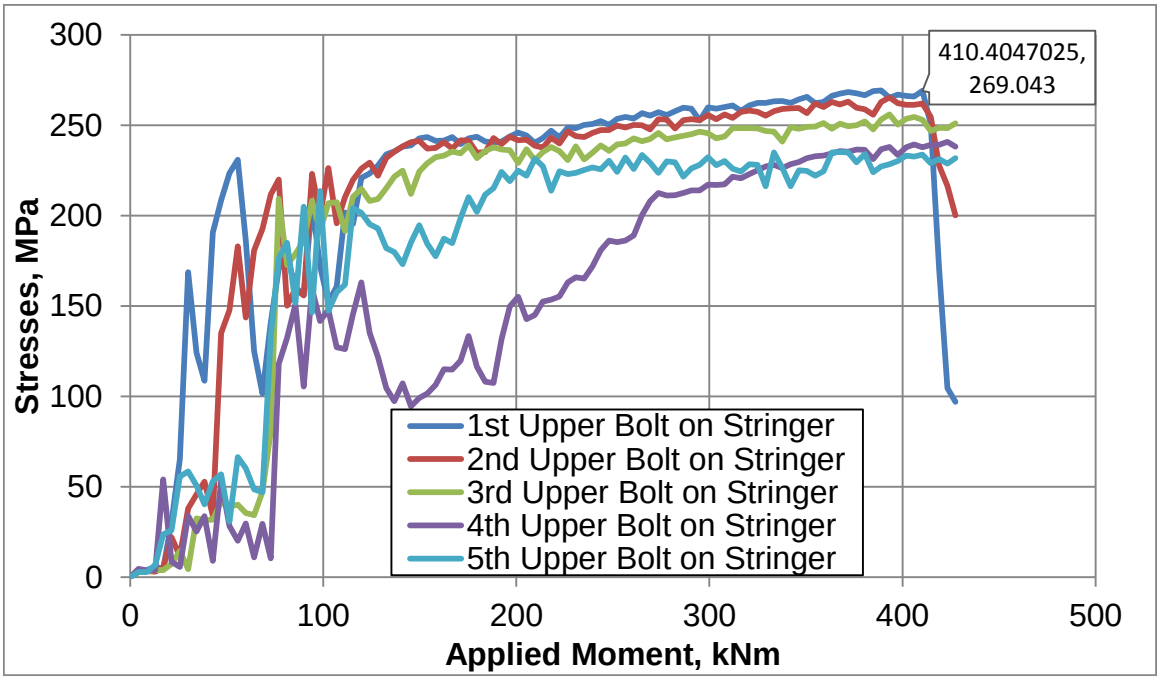

Figure 4.23 Stress histories for bolts on stringer - one missing bolt on crossbeam

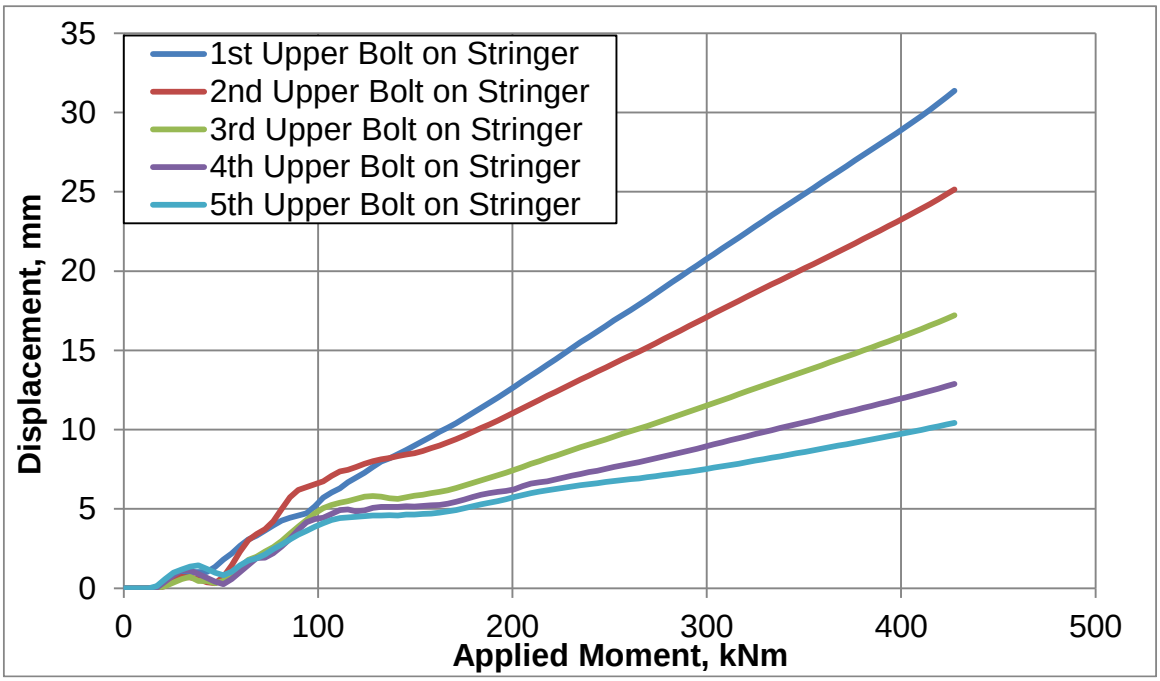

Figure 4.24 Displacement histories for bolts on stringer - one missing bolt on crossbeam

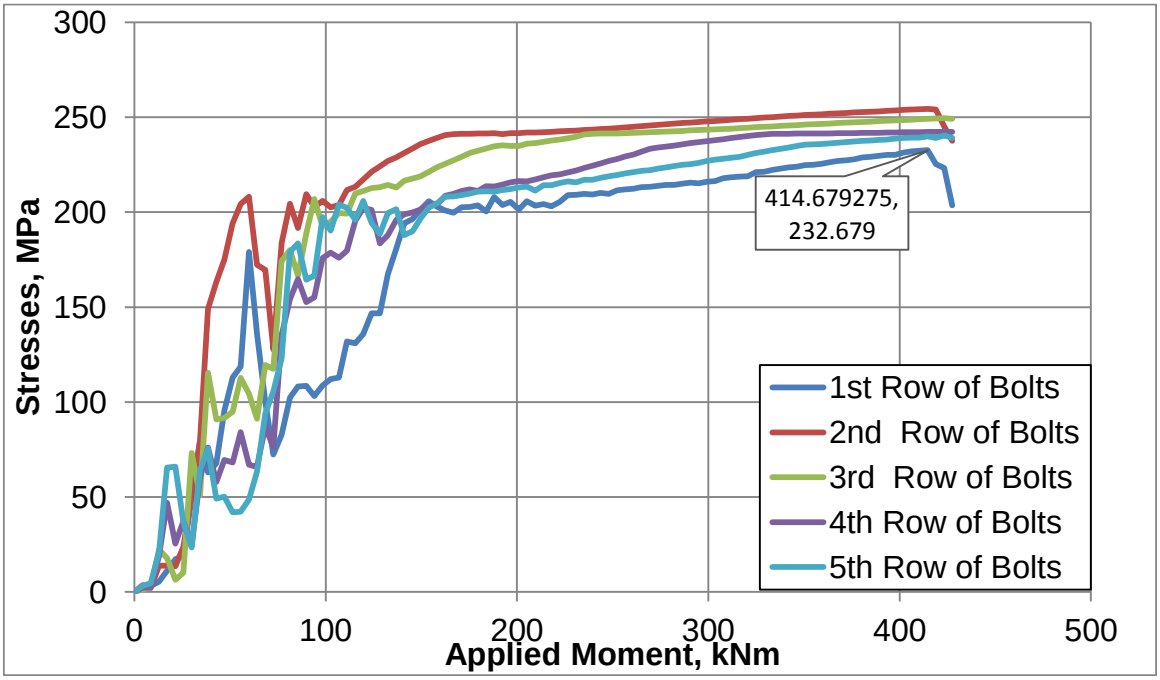

Figure 4.25 Stress histories for an angle - one missing bolt on crossbeam

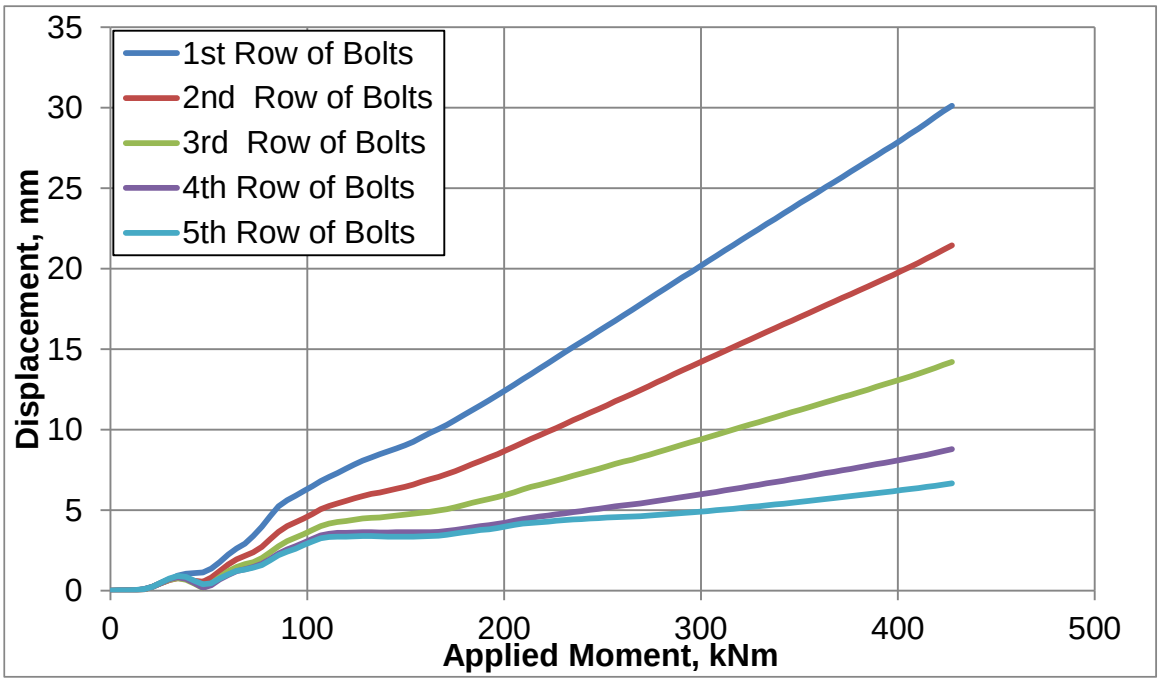

Figure 4.26 Displacement histories for an angle - one missing bolt on crossbeam

4.4.4 Connection #4 - Two Missing Bolts on Crossbeam

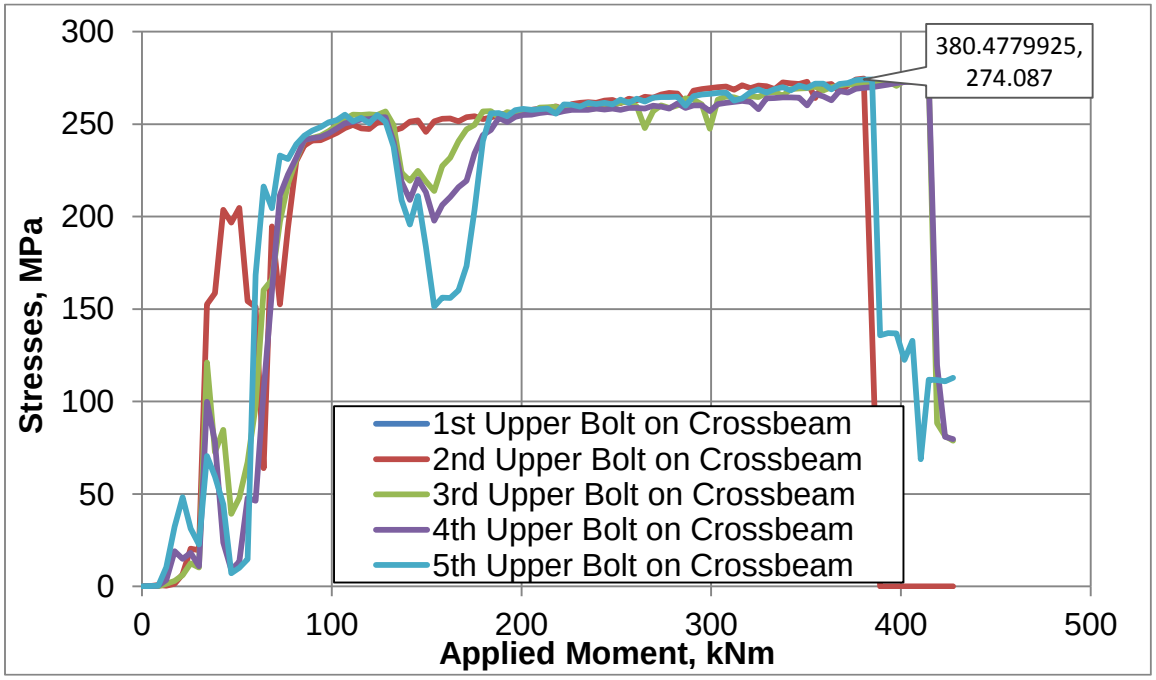

Figure 4.27 Stress histories for bolts on crossbeam - one missing bolt on crossbeam

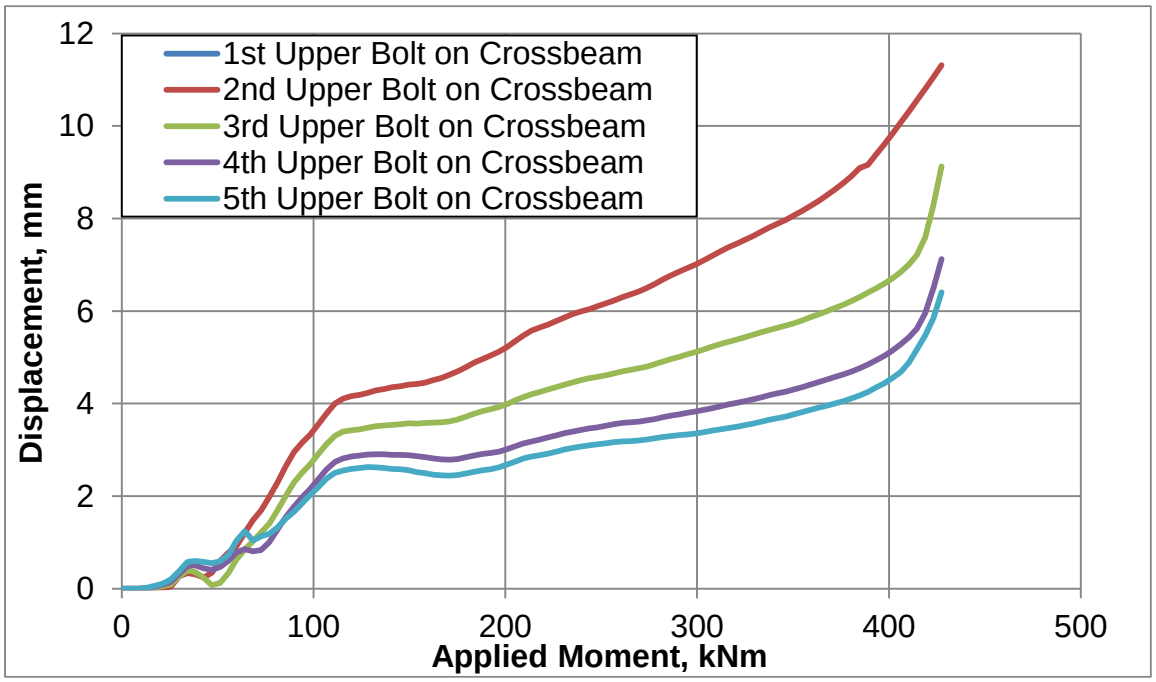

Figure 4.28 Displacement histories for bolts on crossbeam - one missing bolt on crossbeam

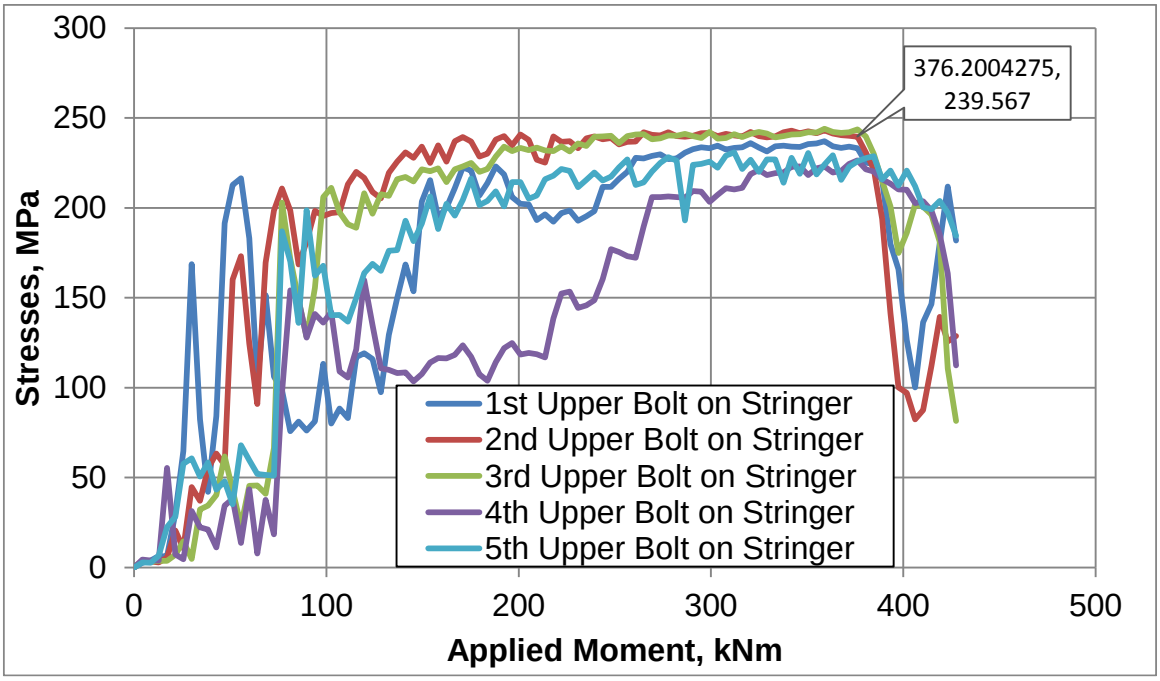

Figure 4.29 Stress histories for bolts on stringer - one missing bolt on crossbeam

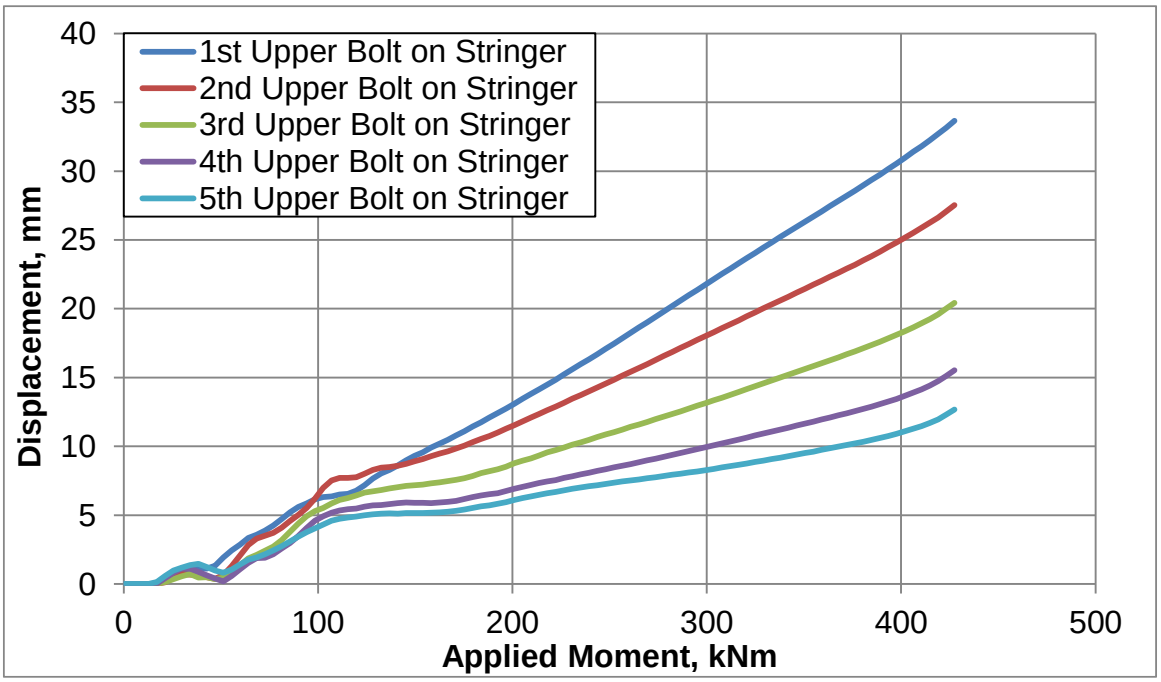

Figure 4.30 Displacement histories for bolts on stringer - one missing bolt on crossbeam

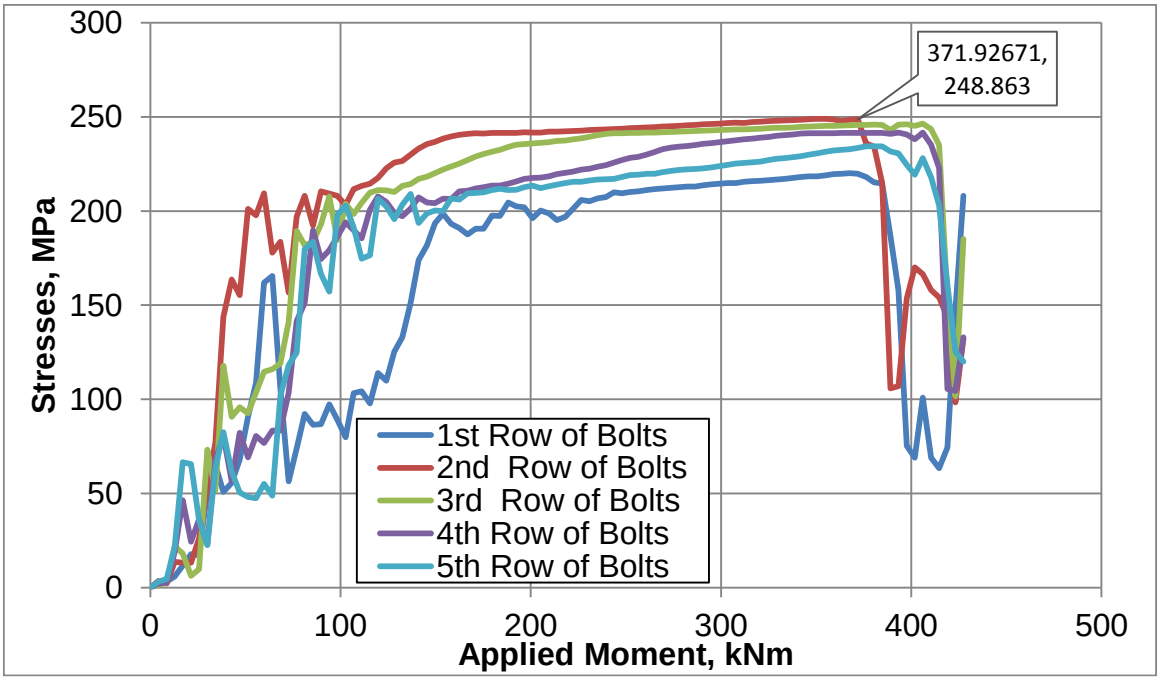

Figure 4.31 Stress histories for an angle - one missing bolt on crossbeam

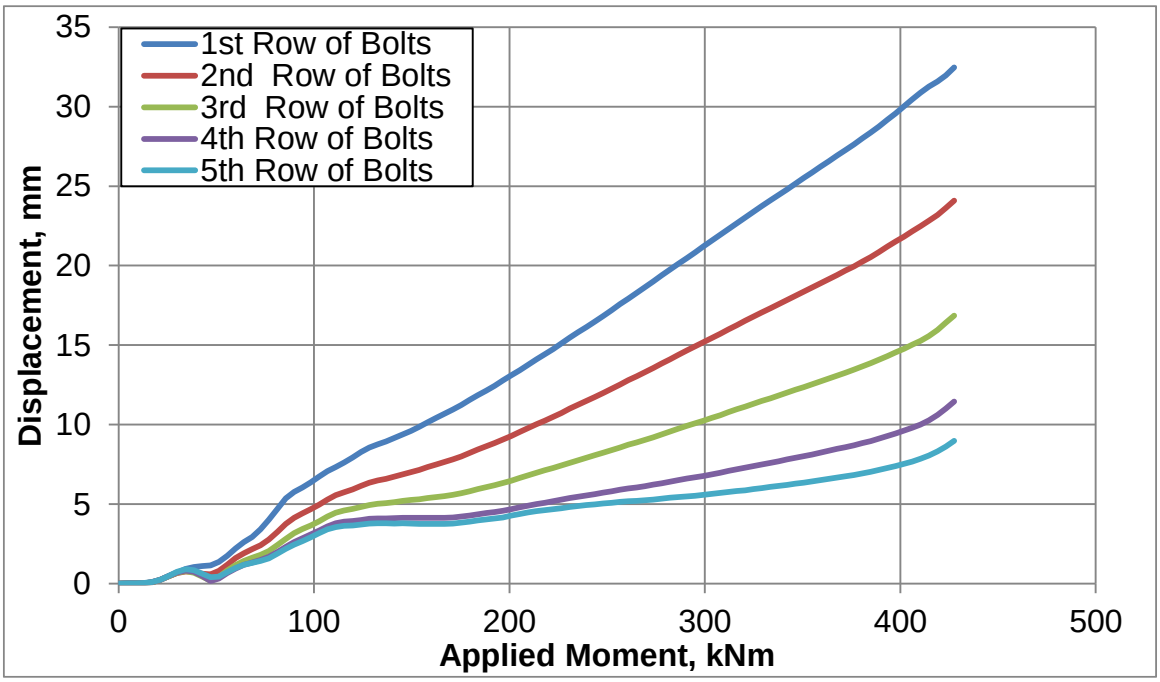

Figure 4.32 Displacement histories for an angle - one missing bolt on crossbeam

The FE analysis revealed that connections between the stringer and crossbeam developed a certain degree of rotational stiffness. The distortion of outstanding legs of connection angles was visible in each considered case. The displacement in the angle caused tension in the bolts on the crossbeam and shear in the bolts on the stringer. All phenomena occurred simultaneously. It was difficult to distinguish which were most critical. The final failure was assumed to be on the fracture of the element—when the stresses dropped dramatically.

During the FE analysis, no visible fracture occurred on the angle; however, in Case #4, stresses fell in the angle before the upper bolt on the stringer was broken. In other cases, upper bolts on the stringer or on the crossbeam failed first. The results are summarized and compared to theoretical calculations in table 4.1. More detailed drawings of stress distribution and displacement of the members due to applied load are presented in appendices A, B, C, and D.

Table 4.1 Summary of FEA results and analytical calculations

	Theoretical Shear Capacity, kN	Theoretical Moment Capacity, kNm	FEA Moment Capacity, kNm	
Undamaged Connection	877.3	122.6	393.3	1st Upper Bolt on Crossbeam
One Missing Bolt on Stringer	789.5	122.6	252.2	2nd Upper Bolt on Stringer
One Missing Bolt on Crossbeam	789.5	104..4	406.1	1st Upper Bolt on Crossbeam
Two Missing Bolts on Crossbeam	701.8	81.7	371.9	Angle on the first Row of Bolt

Chapter 5 Summary and Conclusions

This report provided a detailed evaluation of critical connections used frequently in through-plate railway bridges. A previous study showed that "the most fatigue-critical components were the stringer-to-floorbeam connections" (Rakoczy and Nowak, 2012). Therefore, the current research focused on a review and analysis of the major factors that influence the capacity of double angle connections.

Theoretical capacities of two typical connections were calculated based on the limit state function in the design codes. The following limit states were considered: shear yielding, shear rupture, flexural yielding, flexural rupture, block shear rupture, bolt bearing, bolt slip, and bolt shear. The smallest capacity for shear was developed based on the block shear. The overall capacity of the connection was limited to the combined shear and tension due to bending moment. That means that connections usually failed due to bending moment, not due to shear. After the maximum capacity was calculated, the connection was studied under different conditions. The deterioration was simulated by decreasing the thickness of members (corrosion), and by removing bolts from the connection. Sensitivity analysis was performed, and it was found that bearing and shear capacity were proportional to the degree of corrosion: there was a 50% decreased capacity due to 50% corrosion. Missing bolts were reflected in decreasing shear capacity and decreasing moment capacity. However, moment capacity dropped more dramatically due to lost bolts than did shear capacity.

In addition, nonlinear FE analysis of a representative connection was carried out. Four cases were considered that included both undamaged and damaged connections. Connection #1 was an untouched connection with all bolts in place. Connection #2 was modified by removing the first upper bolt on the stringer. Connection #3 was missing one upper bolt on the crossbeam

(left side). Connection #4 was missing two upper bolts on the crossbeam, on each side. The FEM analysis confirmed the partial fixity of those connections regardless of condition.

Failure in the connections was determined under eccentric force, which represented the axial load from freight and passenger trains. The displacement and stresses were recorded in each time step, and time histories were developed. All connections demonstrated the ability to carry greater bending moment than predicted theoretically. Connection #2 had the lowest capacity, when the upper bolt between the angle and stringer was missing. Unexpectedly, missing one bolt on the crossbeam did not affect overall bending capacity. Even if two bolts on the crossbeam were missing (Connection #4), the connection could carry larger moment than Connection #2. Missing bolts on the crossbeam resulted in increased distortion in the angles, but the connection was capable of carrying relatively large moment.

The double angle connection can be recognized as a hybrid system of many elements. In this study, the contribution of a component failure to system failure was presented. Depending on the level of redundancy in the system, the failure can occur suddenly or over time. The statistical correlation among failure modes and component failure can have a large effect on the reliability of the system; however, is very difficult to assess this correlation. Therefore, testing is recommended in the area of beam-to-girder connections. Almost all tests are oriented toward beam-to-column connections. The behavior of a beam-to-girder connection varied from that of a beam-to-column connection. Beam-to-girder connections are made to the web of the girder and the web of the beam, while beam-to column connections connect the column flange to the girder web. The stiffness between the girder web and the column flange varies. This undoubtedly affects overall connection behavior. Further research in this area is recommended.

References

AASHTO LRFD Bridge Design Specifications, American Association of State Highway and Transportation Officials, Washington D.C., 2012.

AASHTO, Guide Specifications for Fatigue Evaluation of Existing Steel Bridges, American Association of State Highway and Transportation Officials, 1990.

ABAQUS Analysis User's Manual.

American Institute of Steel Construction (AISC), Manual of Steel Construction LRFD 3rd Edition, AISC, Chicago, Ill, 2011.

Al-Emrani, M., "Fatigue Performance of Stringer-to-Floor-Beam connections in Riveted Railway Bridges", Journal of Bridge Engineering, Vol. 10, No. 2, pp. 179-185, 2005.

American Railway Engineering and Maintenance of Way Association (AREMA), Manual for Railway Engineering, Chapter 15, Washington, D.C., 2005.

Ang, A. H-S., Bases for Reliability Approach to Structural Fatigue, Proceedings, ICOSSAR'77, Munich, Germany, 1970.

Ang, A. H-S., and Tang W. H., "Probability Concepts in Engineering, Emphasis on Application to Civil Engineering and Environmental Engineering", John Wiley & Sons Inc., USA, 2007.

Astaneh, A., "Demand and Supply of Ductility in Steel Shear Connections."
Journal of Constructional Steel Research. 14, 1-19. 1989.

Ayyub, B. M., and McCuen, R. H., "Probability, Statistics and Reliability for Engineers, CRC Press, New York, 1997.

Chotickai, P., and Kanchanalai, T., "Field Testing and Performance Evaluation of a Through-Plate Girder Railway Bridge", TRB, No 2172, Transportation Research Board of the National Academies, Washington, D.C., 2010, pp.132-141.

Coopers Loading System, Wikipedia, the free encyclopedia, en.wikipedia.org, 2012.

Dick, S. M., Otter, D. E., and Connor, R. J., "Comparison of Railcar and Bridge Design Loadings for Development of a Railroad Bridge Fatigue Loading", AREMA 2011 Annual Conference, Minneapolis, MN, September 20, 2011.

Finite element method, Wikipedia, the free encyclopedia, en.wikipedia.org, 2012.

Fisher, J. W., Yen, B. T., Wang, D., and Mann J. E., "NCHRP Report 302: Fatigue and Fracture Evaluation for Rating Riveted Bridges", TRB, National Research Council, Washington D.C., pp. 25-35, 1987.

Foutch, D. A., Tobias, D. H., and Choros, J., "Bridge loads under current operating conditions." Struct. Res. Ser. Rep., Department of Civil Engineering, University of Illinois at Urbana-Champaign, Urbana, IL, Manual for railway engineering. American Railway Engineering Association, Washington, D.C., 1996.

Federal Railroad Administration, 49 CFR Parts 213 and 237, Bridge Safety Standards, 2010

Galambos, T. V., and Ravindra, M. K., "Load and Resistance Factor Design", Journal of Structural Division, ASCE, ST9, Proc. Paper 14008, 1978.

Goerl, R. K., "Study of Behavior of Stringer to Floor Beam Connection in Riveted Railway Open Web Girder Bridges", Journal of IPWE, April, 2006.

Green, P.S., Sputo, T., and Veltri, P. "Connections Teaching Toolkit: A Teaching Guide for Structural Steel Connections", Chicago, Ill, 2003.

Green, P.S., and Sputo, T., "Design of All-Bolted Extended Double Angle, Single Angle, and Tee Shear Connections", PhD Dissertation, University of Florida, 2005.

Imam, B., Righiniotis, T. D., and Chryssanthopoulos, M.K., "Connection Fixity Effects on Stress Histories in Riveted Rail Bridges" Proceedings of the 2nd International Conference on Bridge Maintenance, Safety and Management: Kyoto, 2004.

Imam, B., Righiniotis, T. D., and Chryssanthopoulos, M.K., "Remaining Fatigue Life Estimates for Riveted Railway Bridges", Proceedings of the 5th International Conference on Bridge Management, Thomas Telford, UK, 2005.

Imam, B., Righiniotis, T. D., and Chryssanthopoulos, M. K., Bell, B., "Probabilistic Fatigue Life Estimates for Riveted Railway Bridges", Proceedings of the 3rd International Conference of Bridge Maintenance, Safety and Management, 2008.

Kennedy, D. J. L., "Moment-Rotation Characteristics of Shear Connections", AISC Engineering Journal. AISC, 6(4), 105-115, 1996.

Kishi, N. and Chen, W. F., "Moment-Rotation Relations of Semi rigid Connections with Angles." Journal of Structural Engineering. 111(7), 1813-1834, 1990.

Kulak, G., Fisher, J., and Struik, J. "Guide to Design Criteria for Bolted and Riveted Joints", John Wiley & Sons, Inc., New York, New York, 1987.

Krajewski, J., "Repair of Fatigue Damaged Stringer to Floor-Beam Connections", ODOT Bridge Design Conference, Oregon 2009.

Nowak, A.S. and Collins, K.R., “Reliability of Structures”, McGraw Hill, New York, 2000.
Nowak, A. S. and Lind, N. D., “Practical Bridge Code Calibration”, Journal of Structural Division, ASCE, pp. 2497-2510, December 1979.

Nowak, A. S. and Rakoczy, A. M., "Development of System Reliability Models for Railway Bridges", MATC – UNL: 426, December 2012.

Rakoczy, A. M., "Development of System Reliability Models for Railway Bridges", PhD Dissertation, University of Nebraska-Lincoln, August 2012.

Rakoczy, A. M. and Nowak, A. S., “Reliability-Based Strength Limit State for Steel Railway Bridge,” Structure and Infrastructure Engineering, published online, Pages 1–14, September 2013.

Research Council on Steel Connections (RCSC) “Specification for Structural Joints Using”, ASTM A325 or A490 Bolts. AISC, Chicago, Ill, 2000.

Tobias D. H., Foutch D. A., and Choros J., “Loading Spectra for Railway Bridges under Current Operating Conditions”, Journal of Bridge Engineering (ASCE), pp. 127-134, 1996.

Tobias, D. H., and Foutch, D.A., “Reliability-Based Method for Fatigue Evaluation of Railway Bridges”, Journal of Bridge Engineering 2(2), pp.53-60, 1997.

Unsworth, J. F., “Design of Modern Steel Railway Bridges”, CRC Press, Boca Raton, FL, 2010.

Appendix A Results of FEA for Undamaged Connection

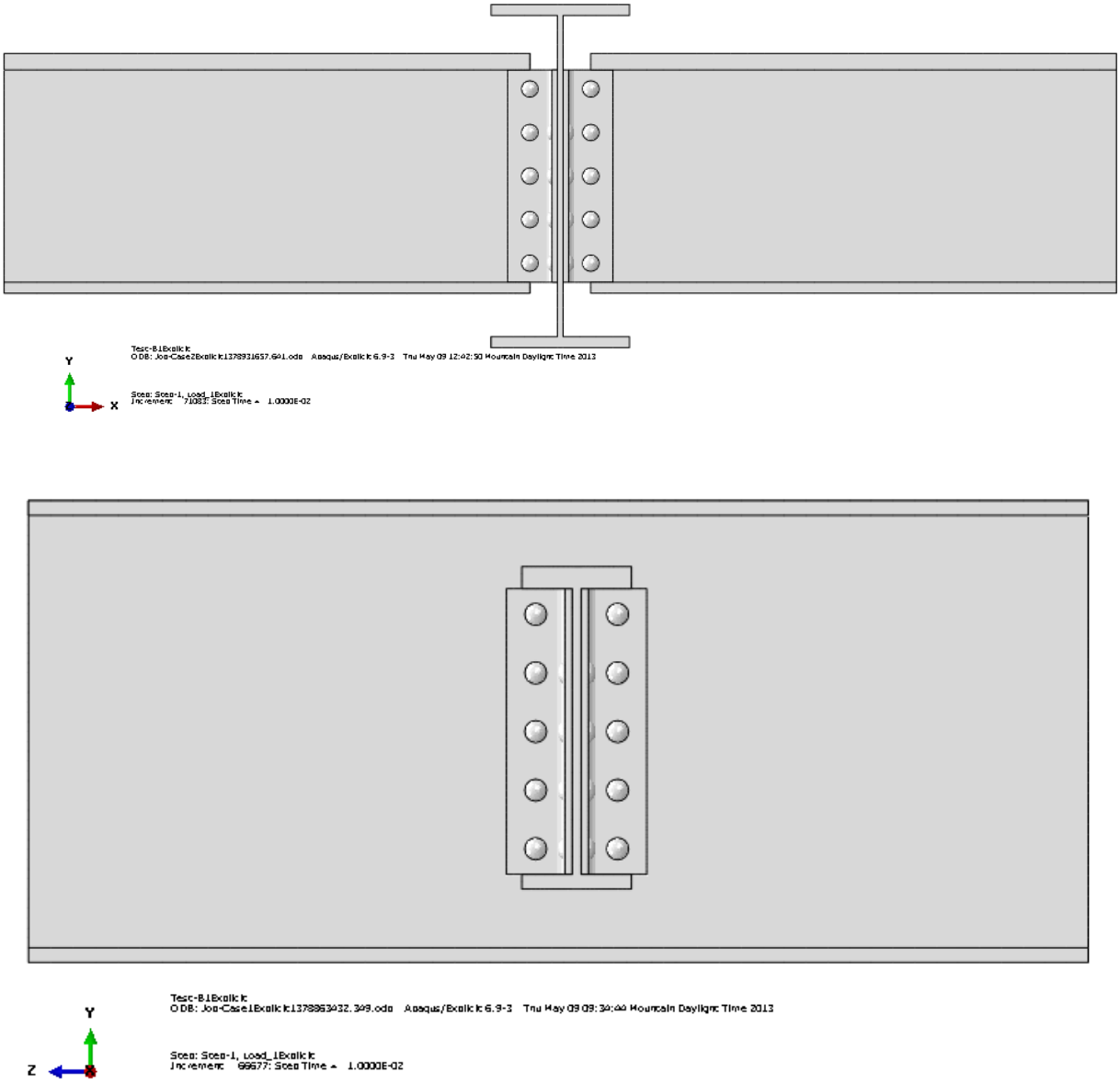

Figure A.1 Detailed View of Undamaged Connection

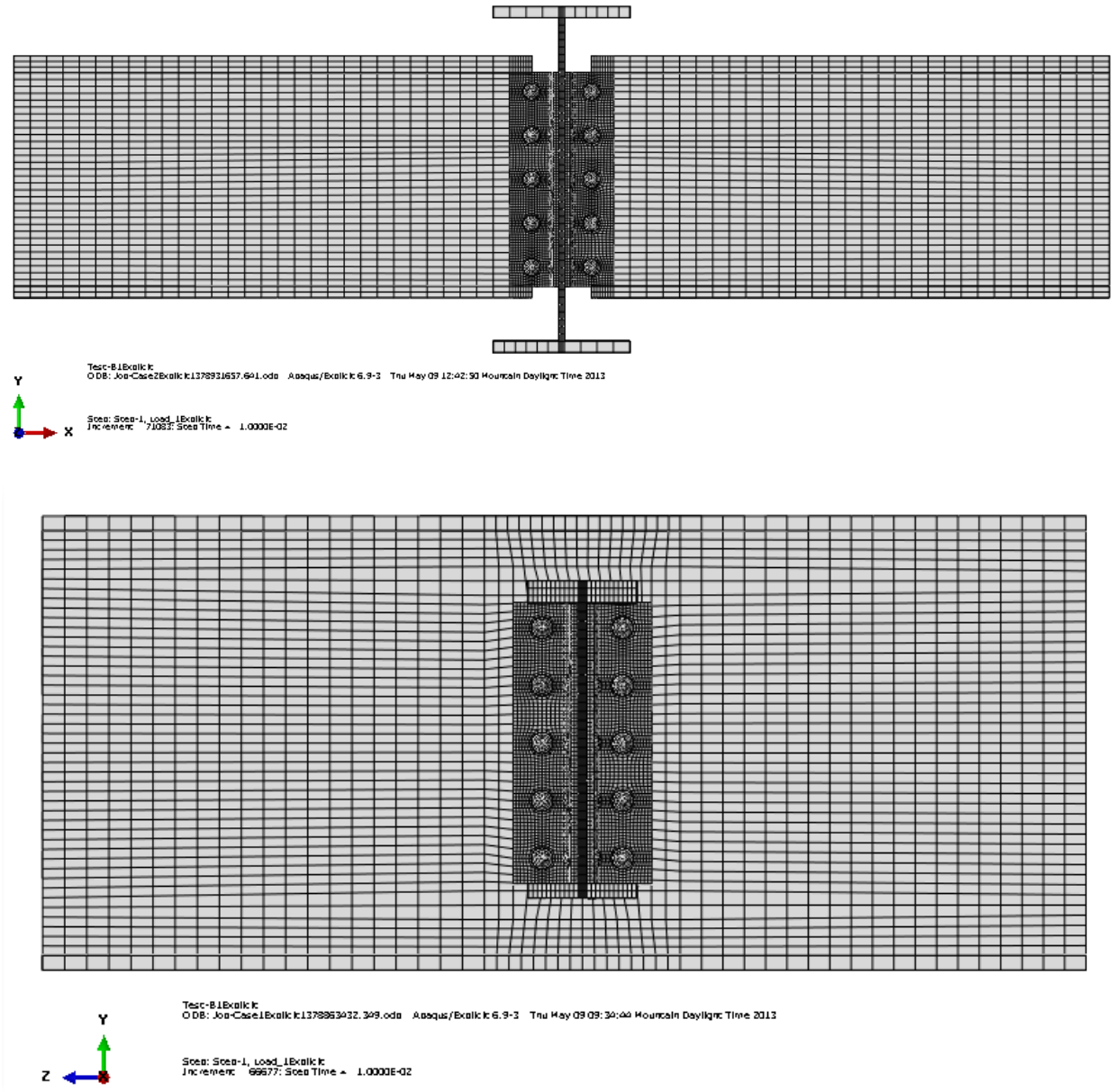

Figure A.2 Mesh of Undamaged Connection

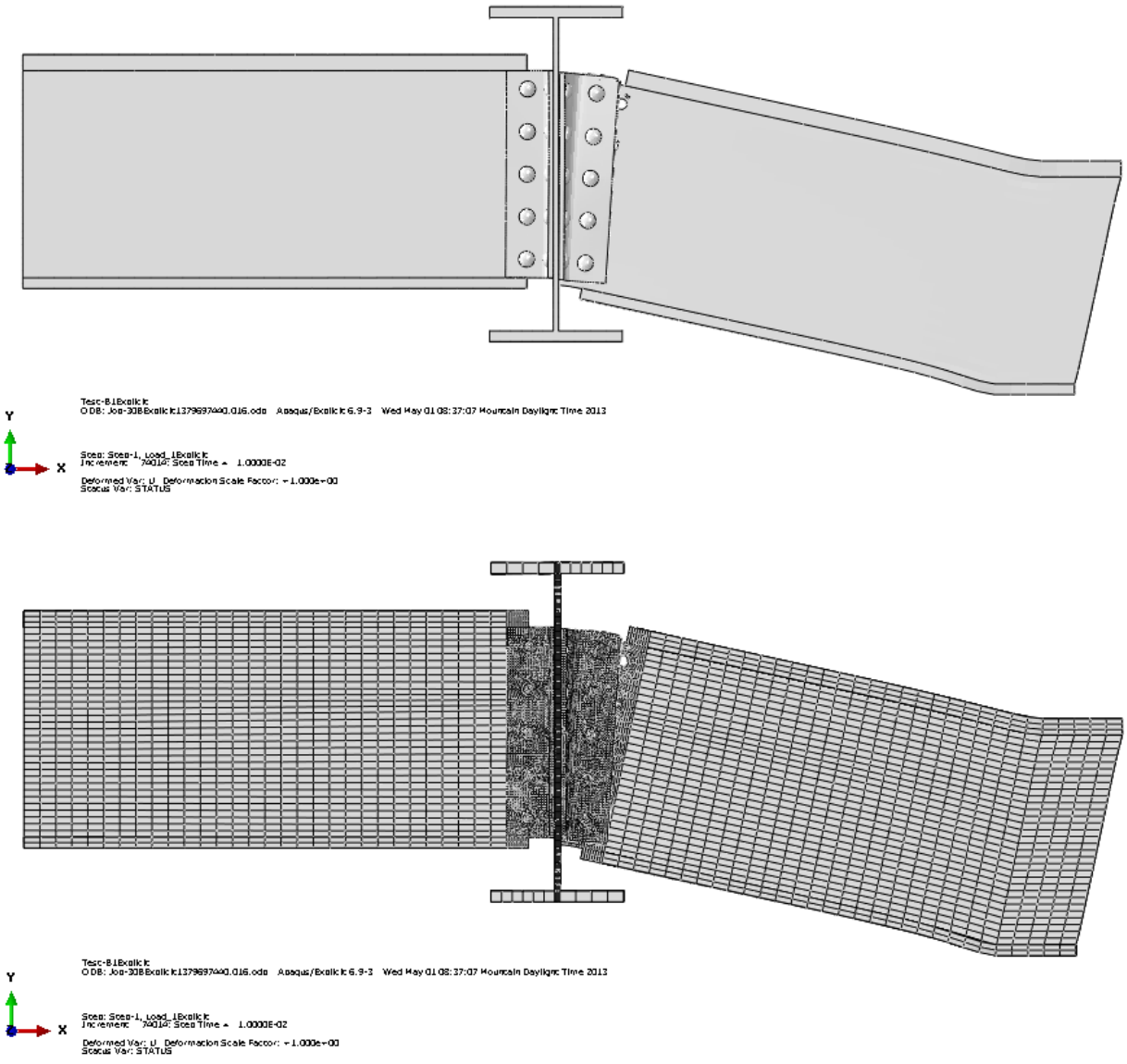

Figure A.3 Deformation after Applied Load – View from Side

.

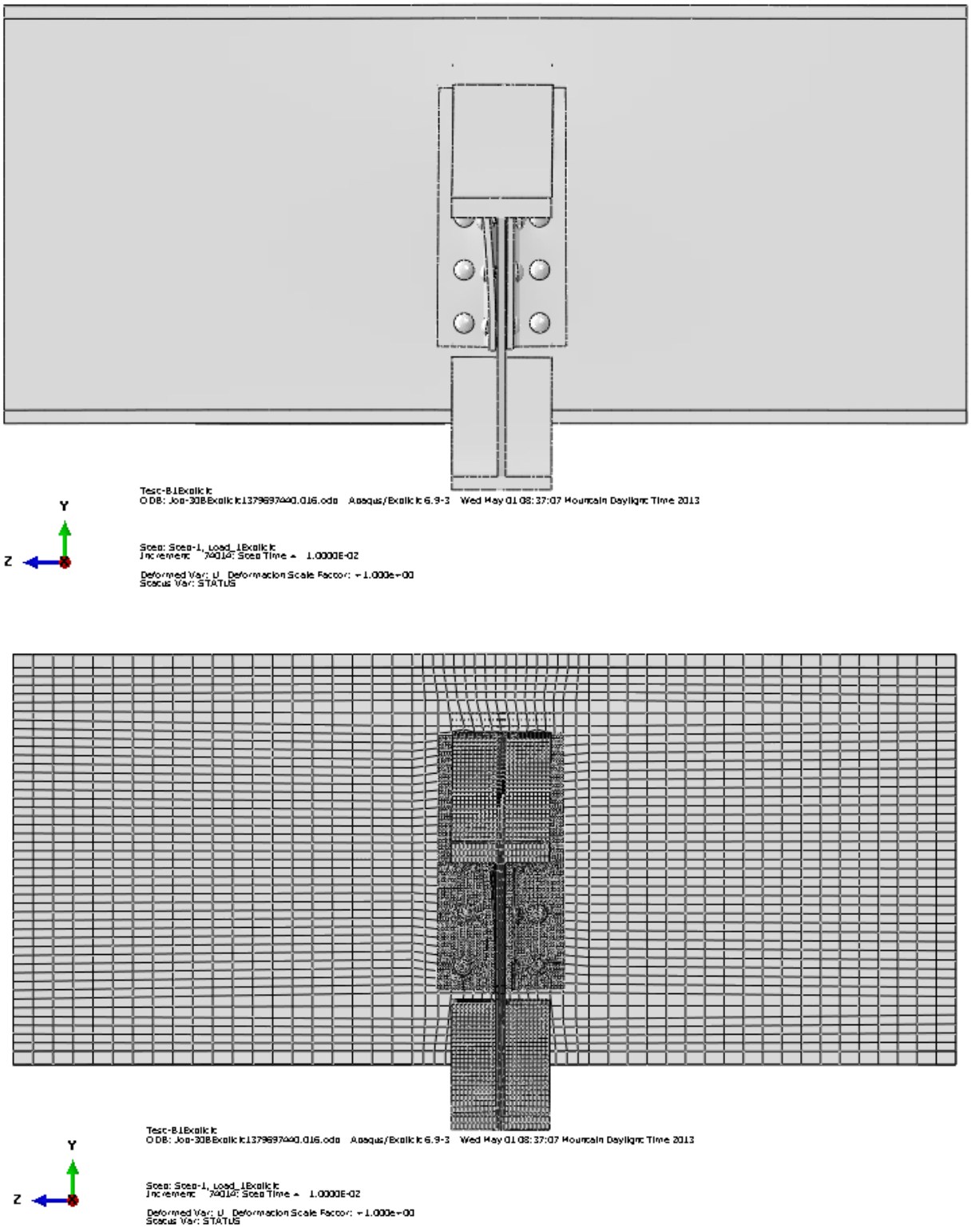

Figure A.4 Deformation after Applied Load – View from Front

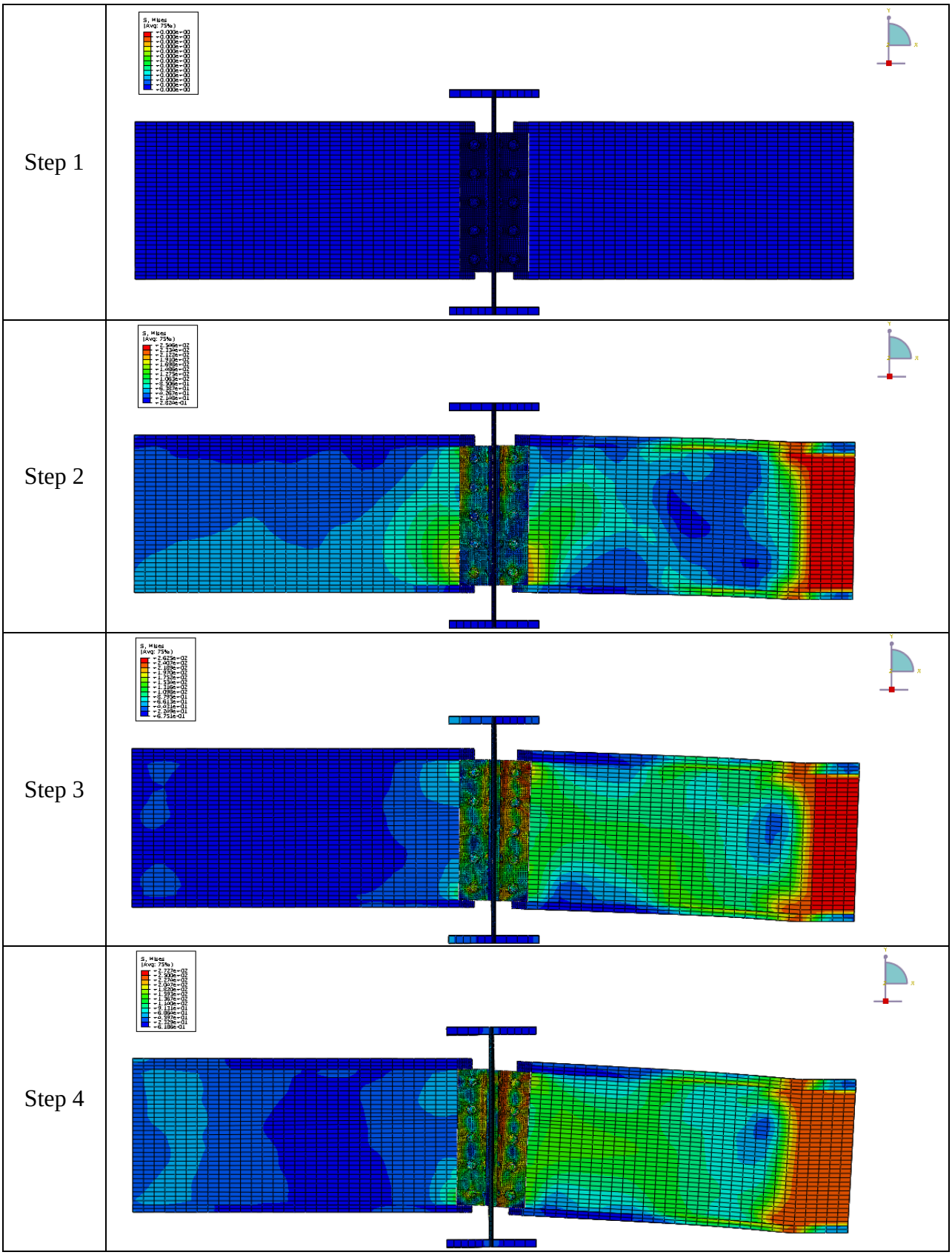

Figure A.5 Stress Distribution on the Connection under Applied Load – General View

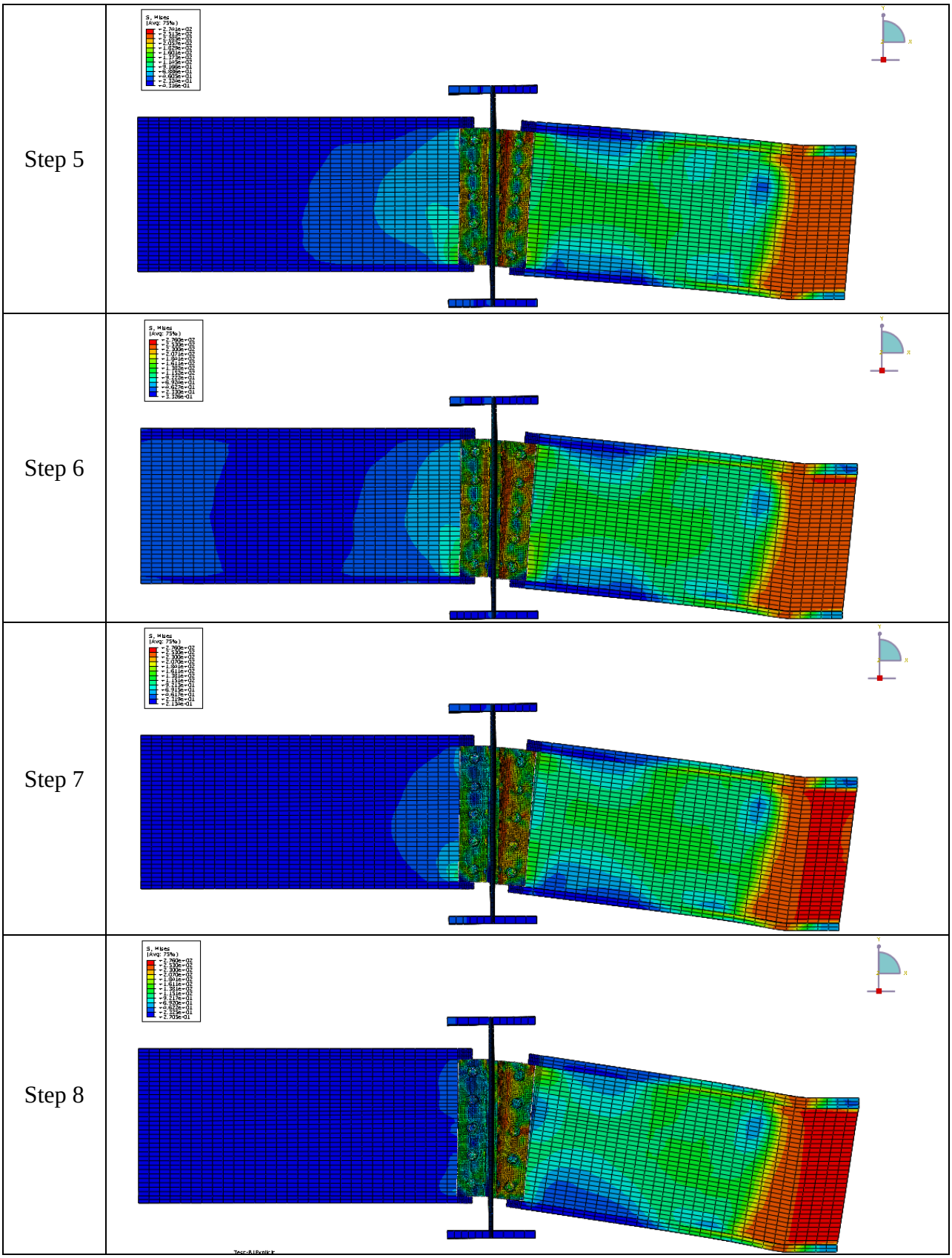

Figure A.5 cont. Stress Distribution on the Connection under Applied Load – General View

Step 9	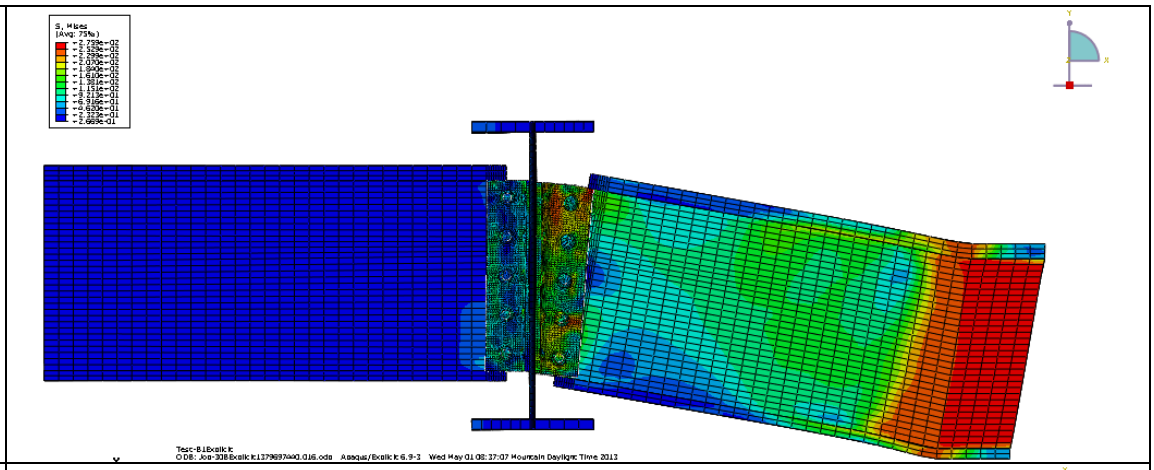
Step 10	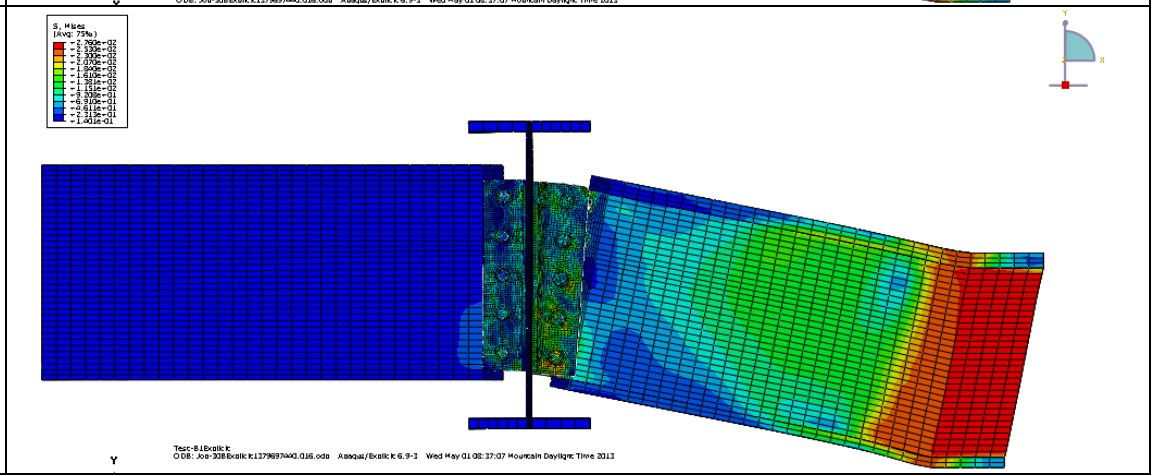
Step 11	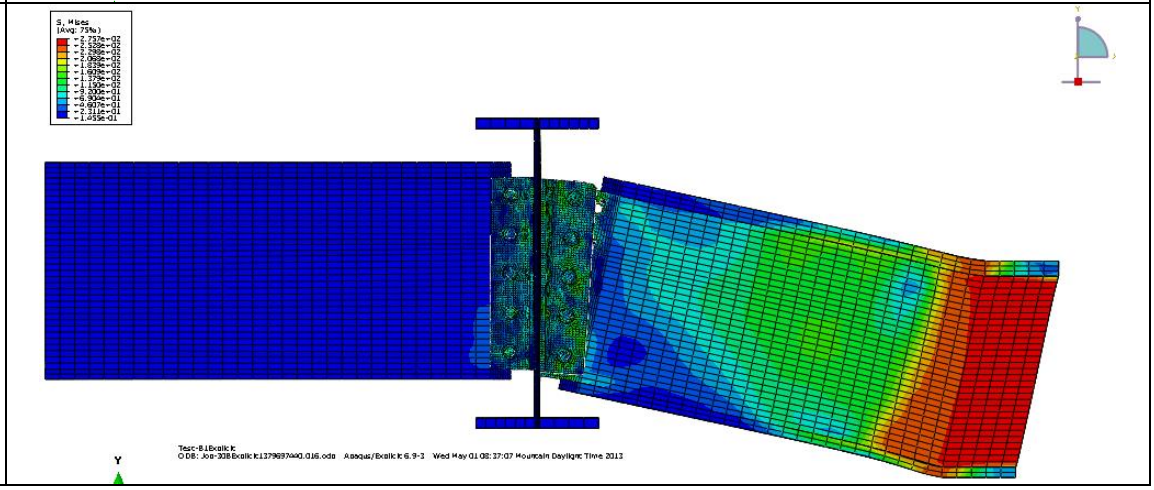

Figure A.5 cont. Stress Distribution on the Connection under Applied Load – General View

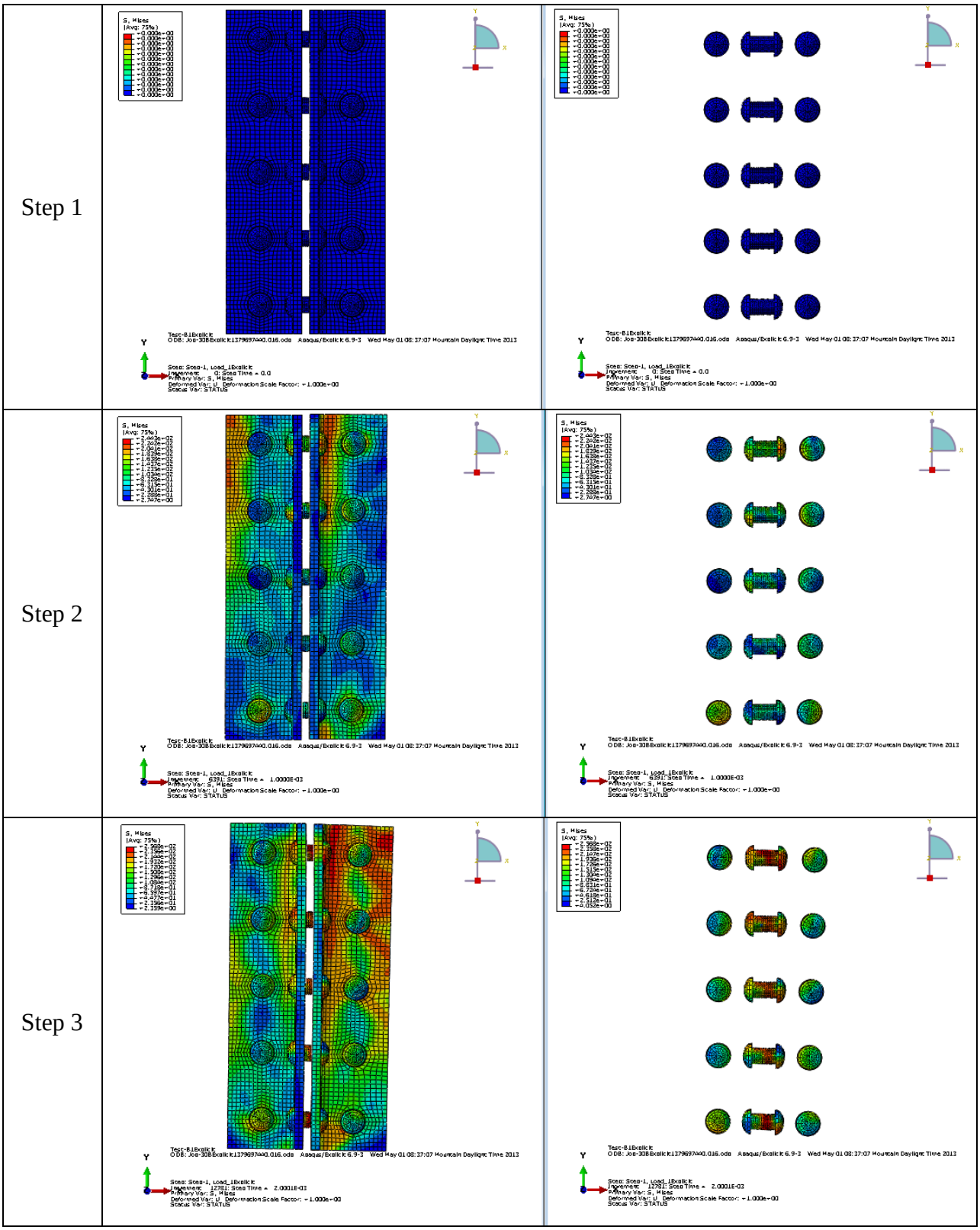

Figure A.6 Stress Distribution on the Connection under Applied Load – Side View

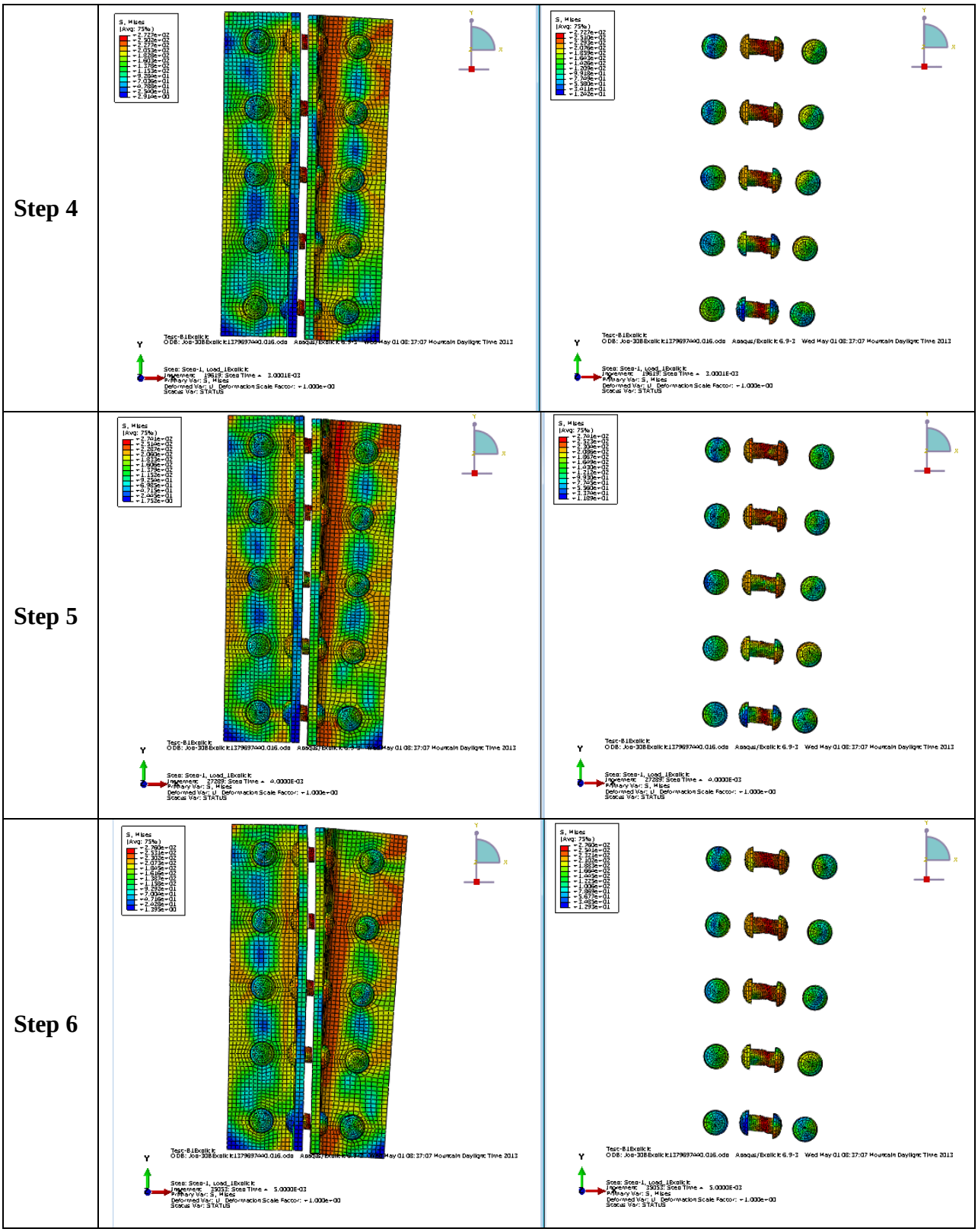

Figure A.6 cont. Stress Distribution on the Connection under Applied Load – Side View

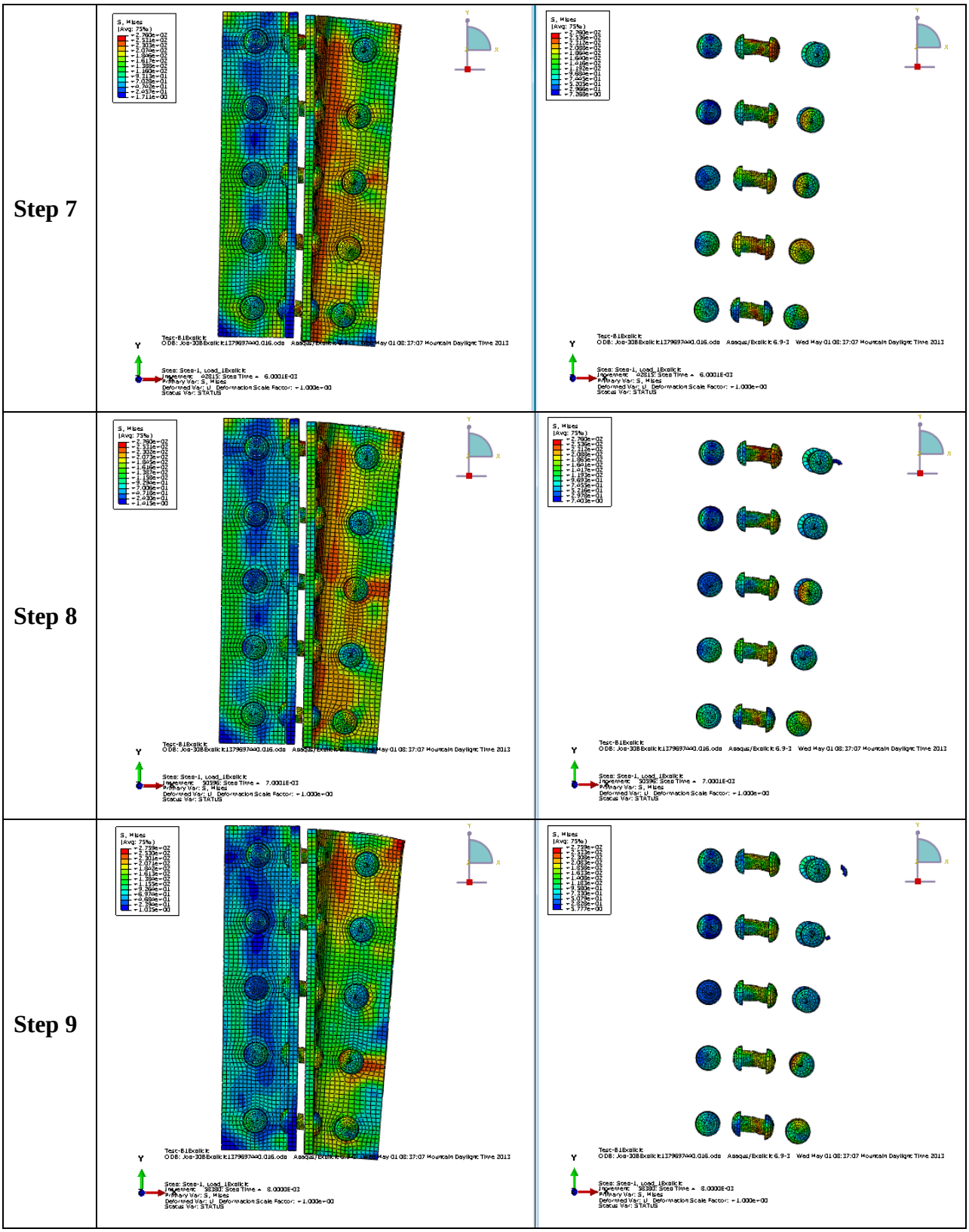

Figure A.6 cont. Stress Distribution on the Connection under Applied Load – Side View

Step 10	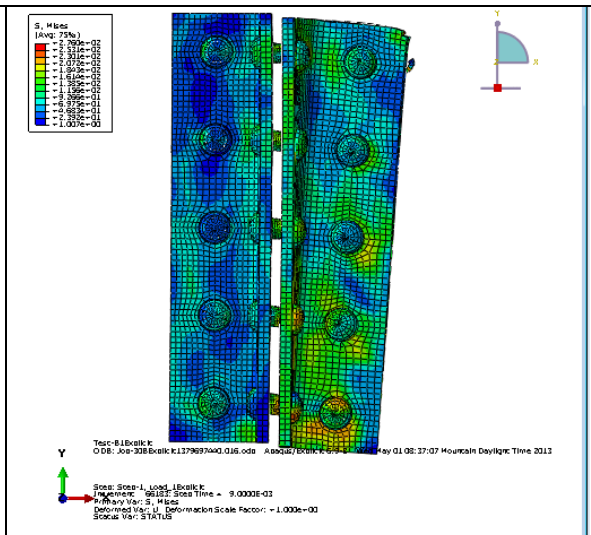	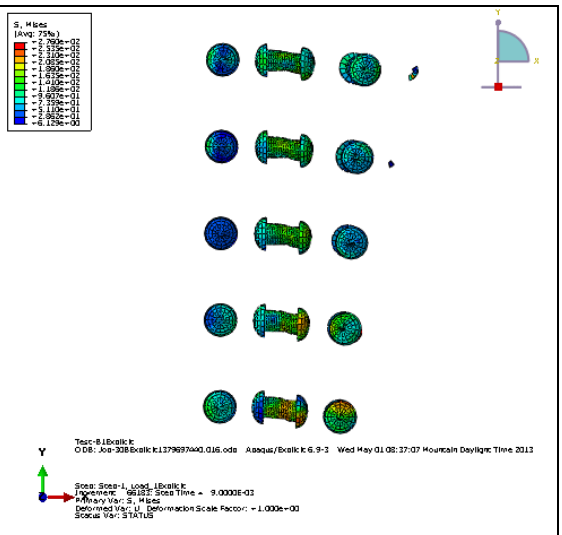
Step 11	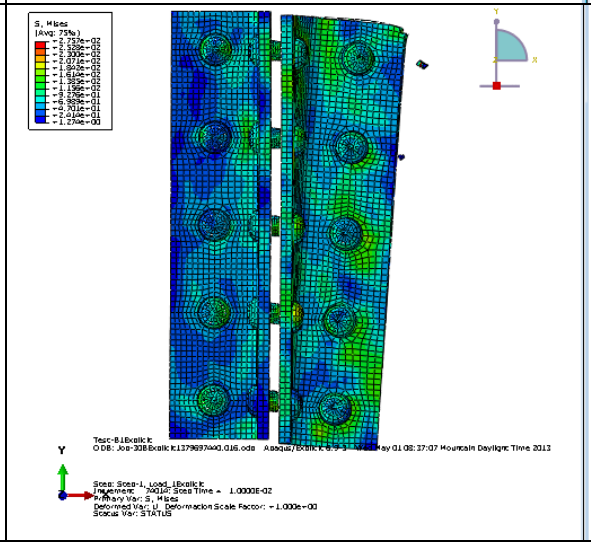	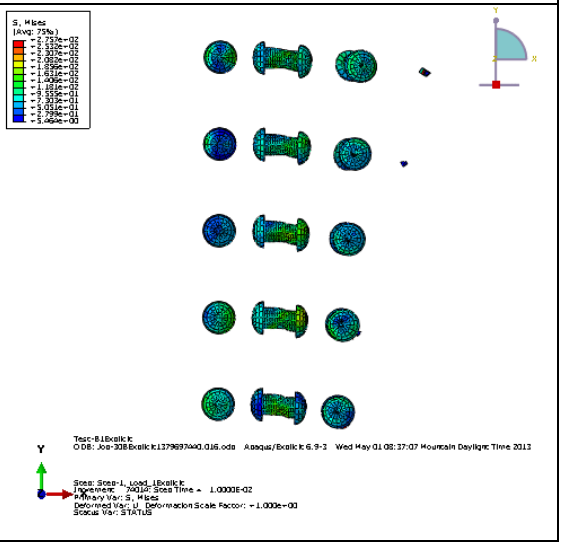

Figure A.6 cont. Stress Distribution on the Connection under Applied Load – Side View

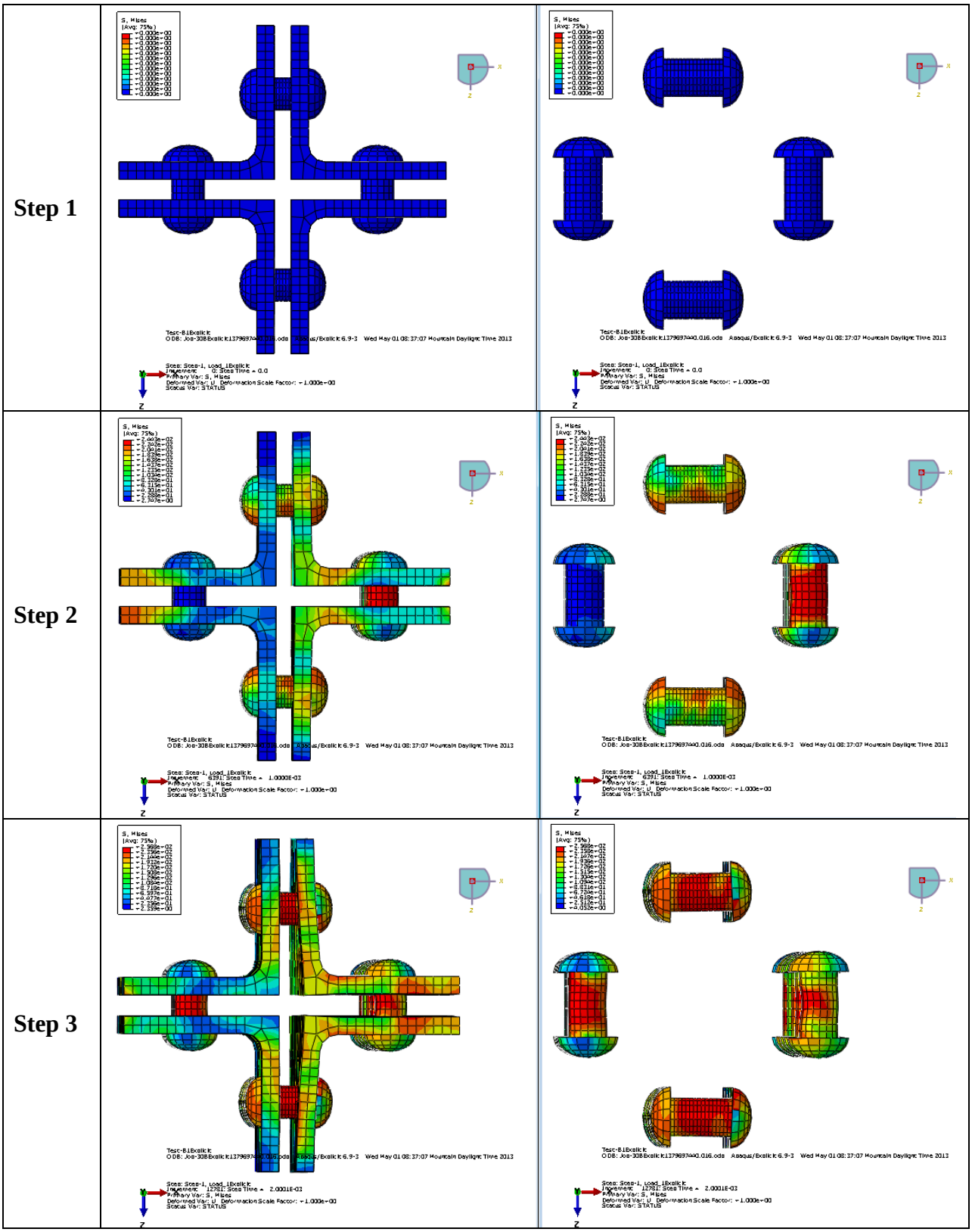

Figure A.7 Stress Distribution on the Connection under Applied Load – Top View

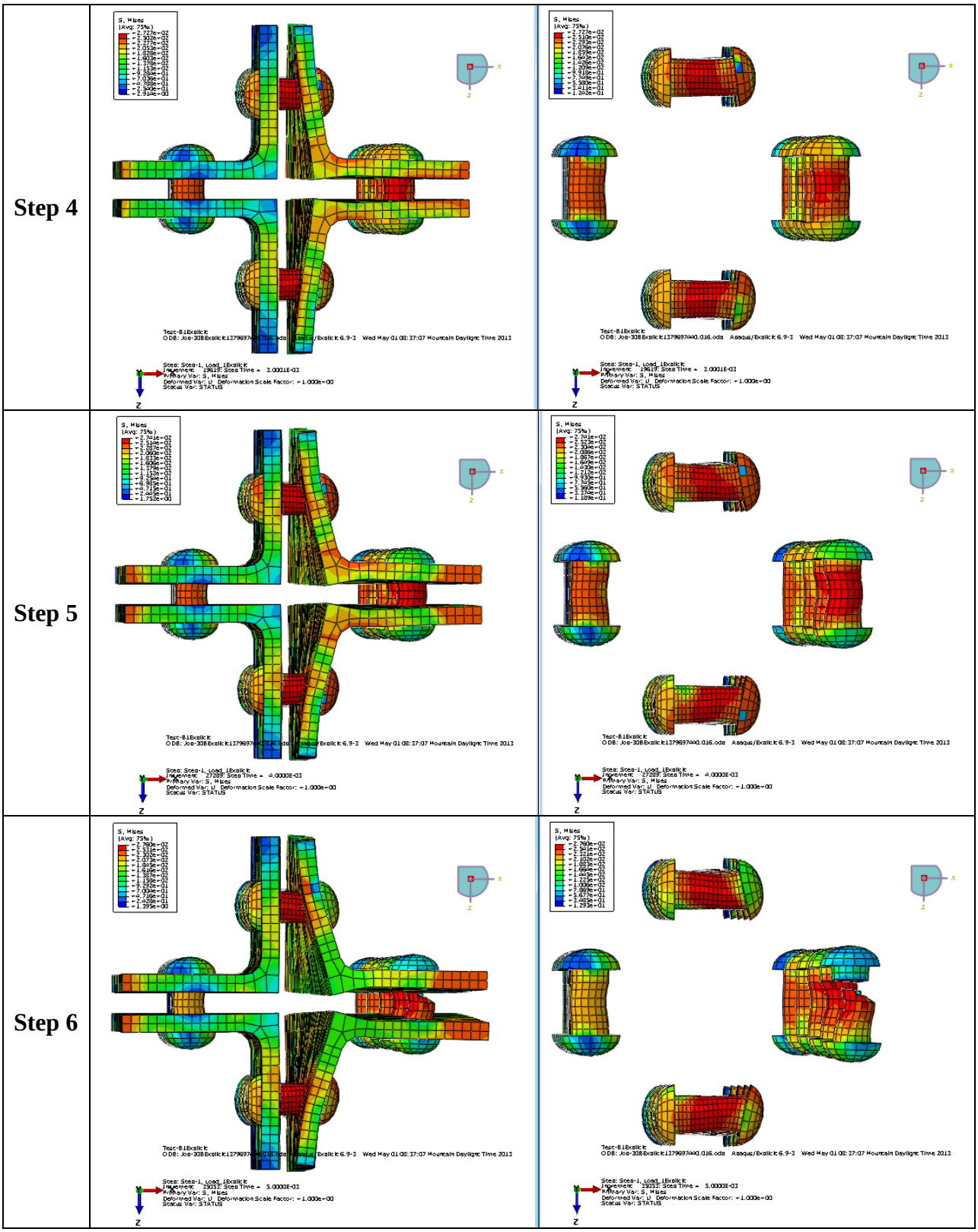

Figure A.7 cont. Stress Distribution on the Connection under Applied Load – Top View

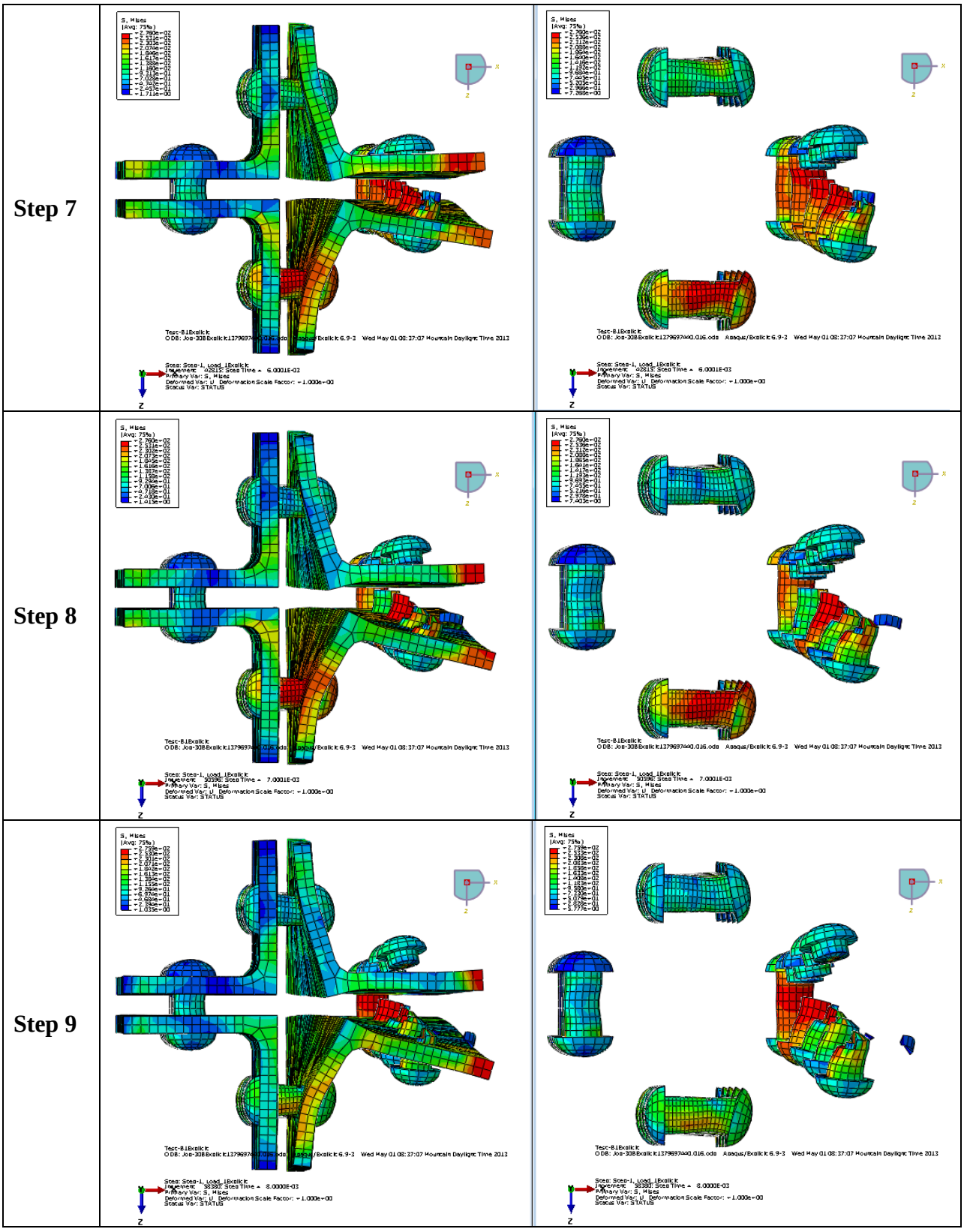

Figure A.7 cont. Stress Distribution on the Connection under Applied Load – Top View

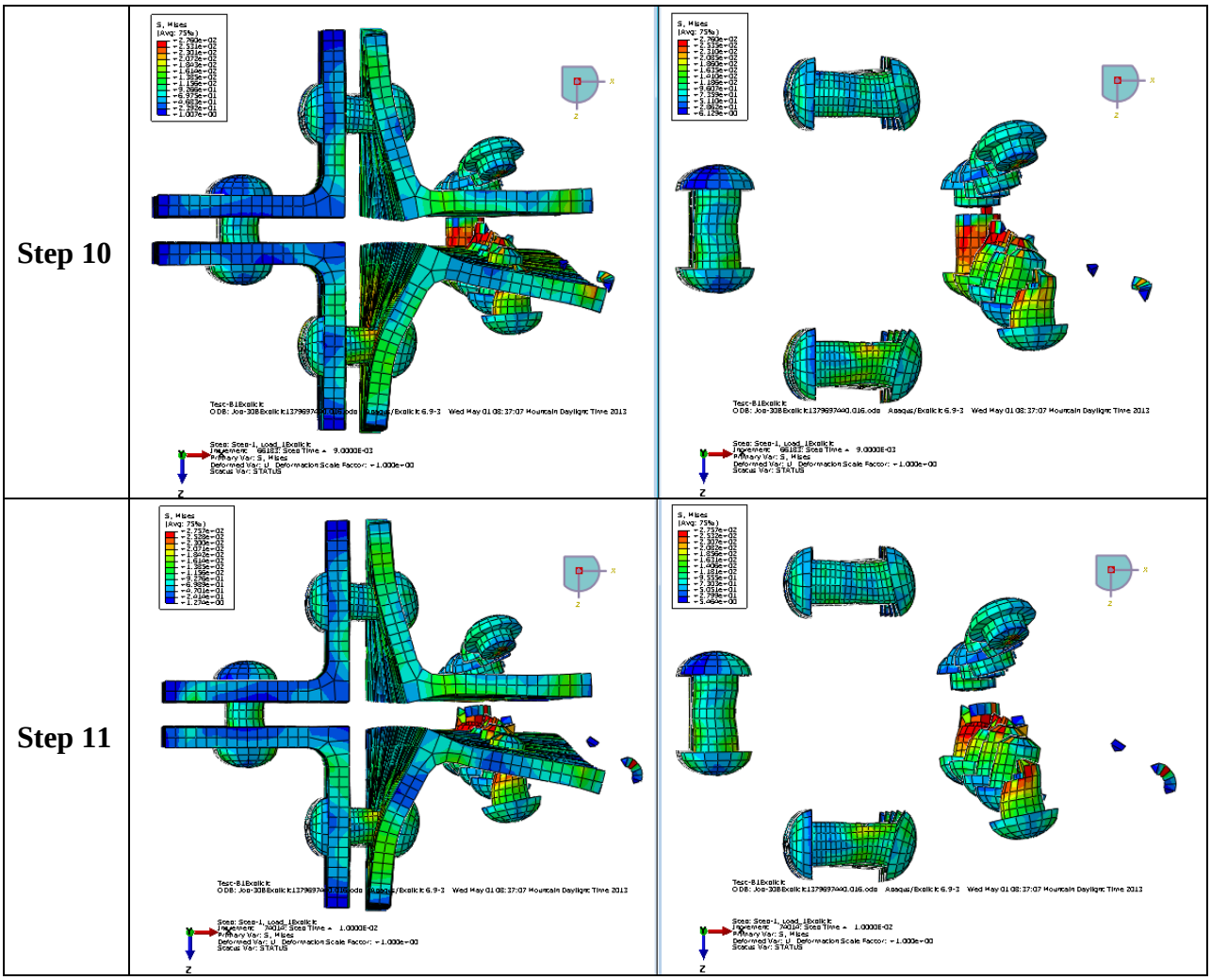

Figure A.7 cont. Stress Distribution on the Connection under Applied Load – Top View

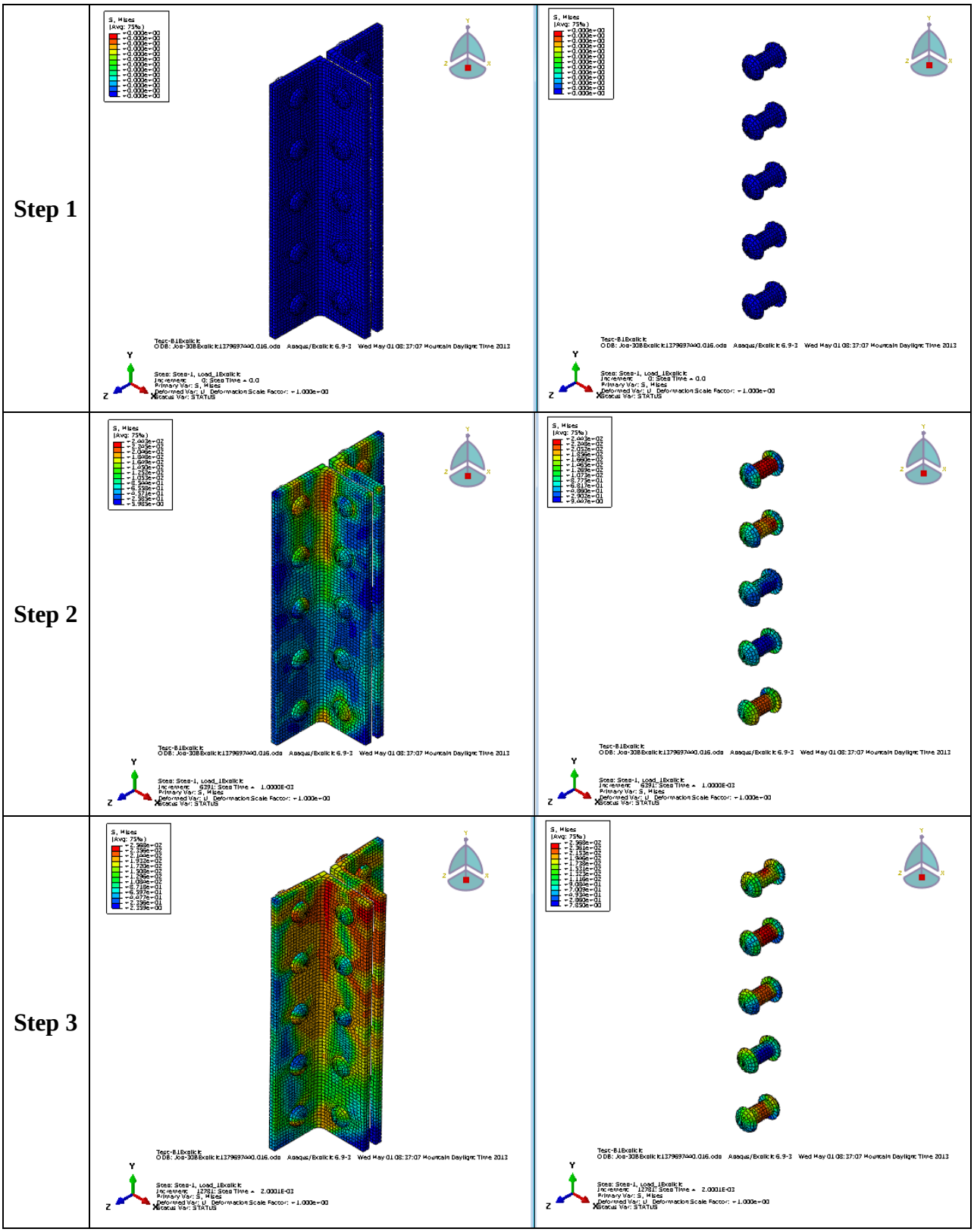

Figure A.8 Stress Distribution on the Connection under Applied Load – Isometric View

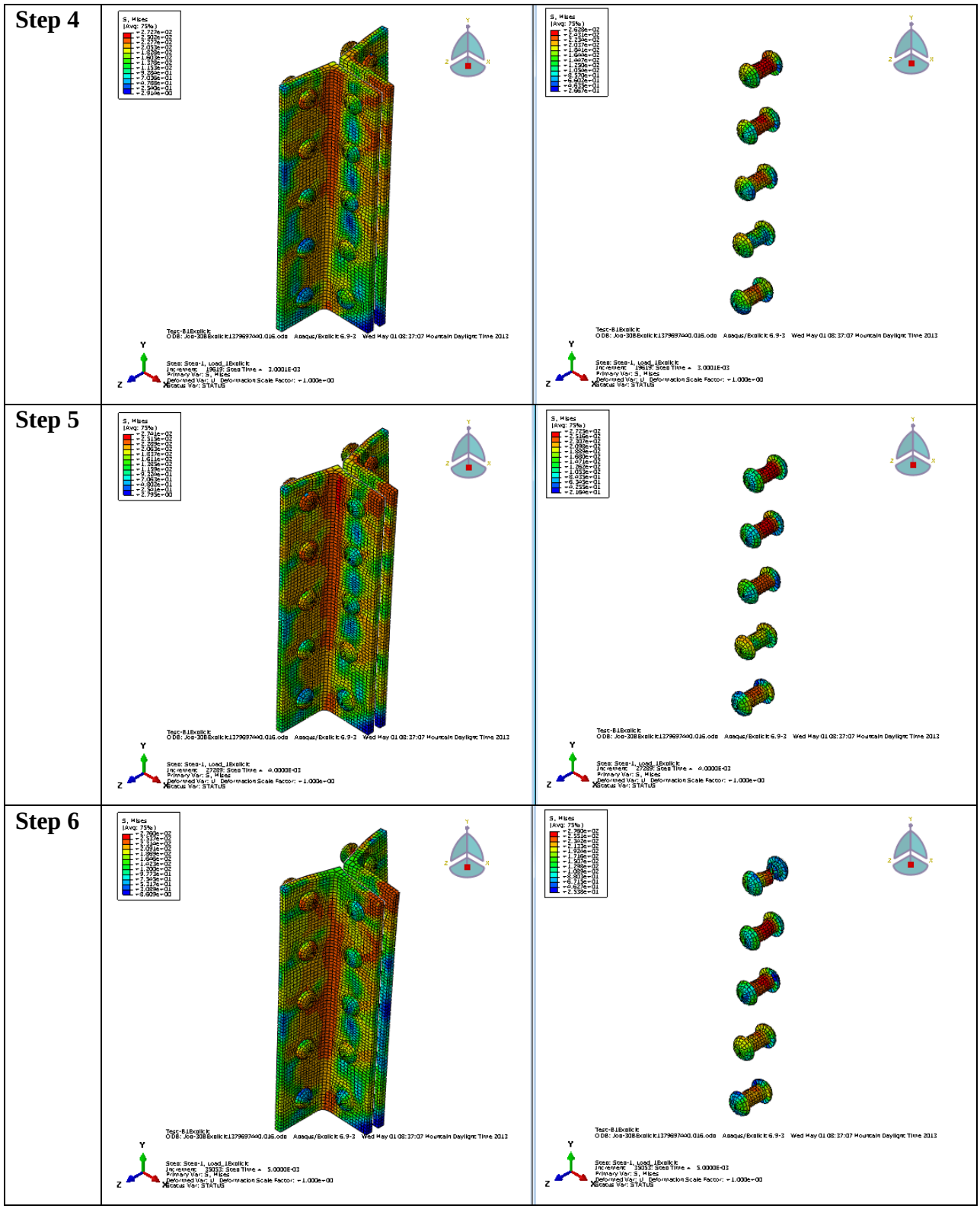

Figure A.8 cont. Stress Distribution on the Connection under Applied Load – Isometric View

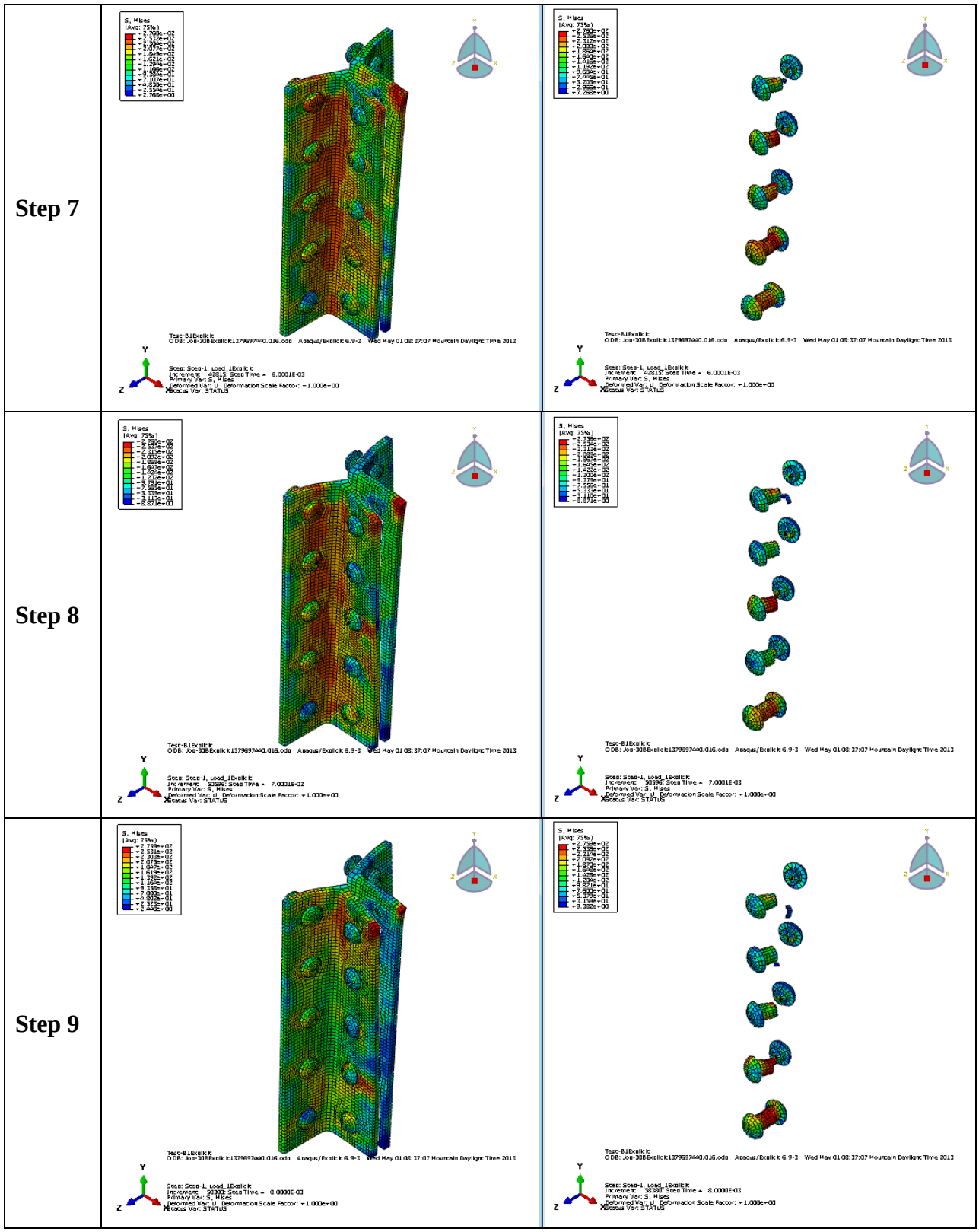

Figure A.8 cont. Stress Distribution on the Connection under Applied Load – Isometric View

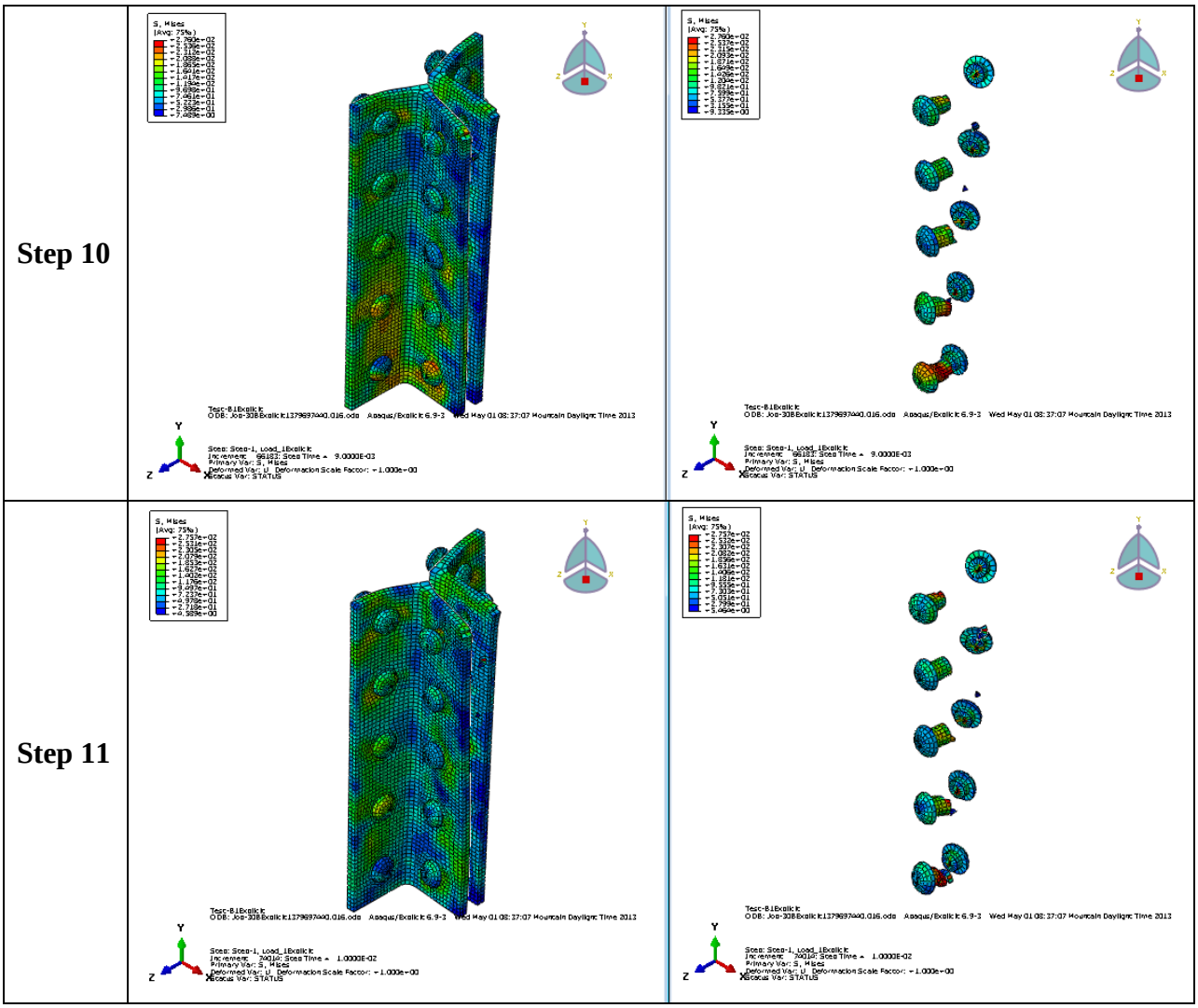

Figure A.8 cont. Stress Distribution on the Connection under Applied Load – Isometric View

Appendix B Results of FEA for Connection with Missing Upper Bolt on the Stringer

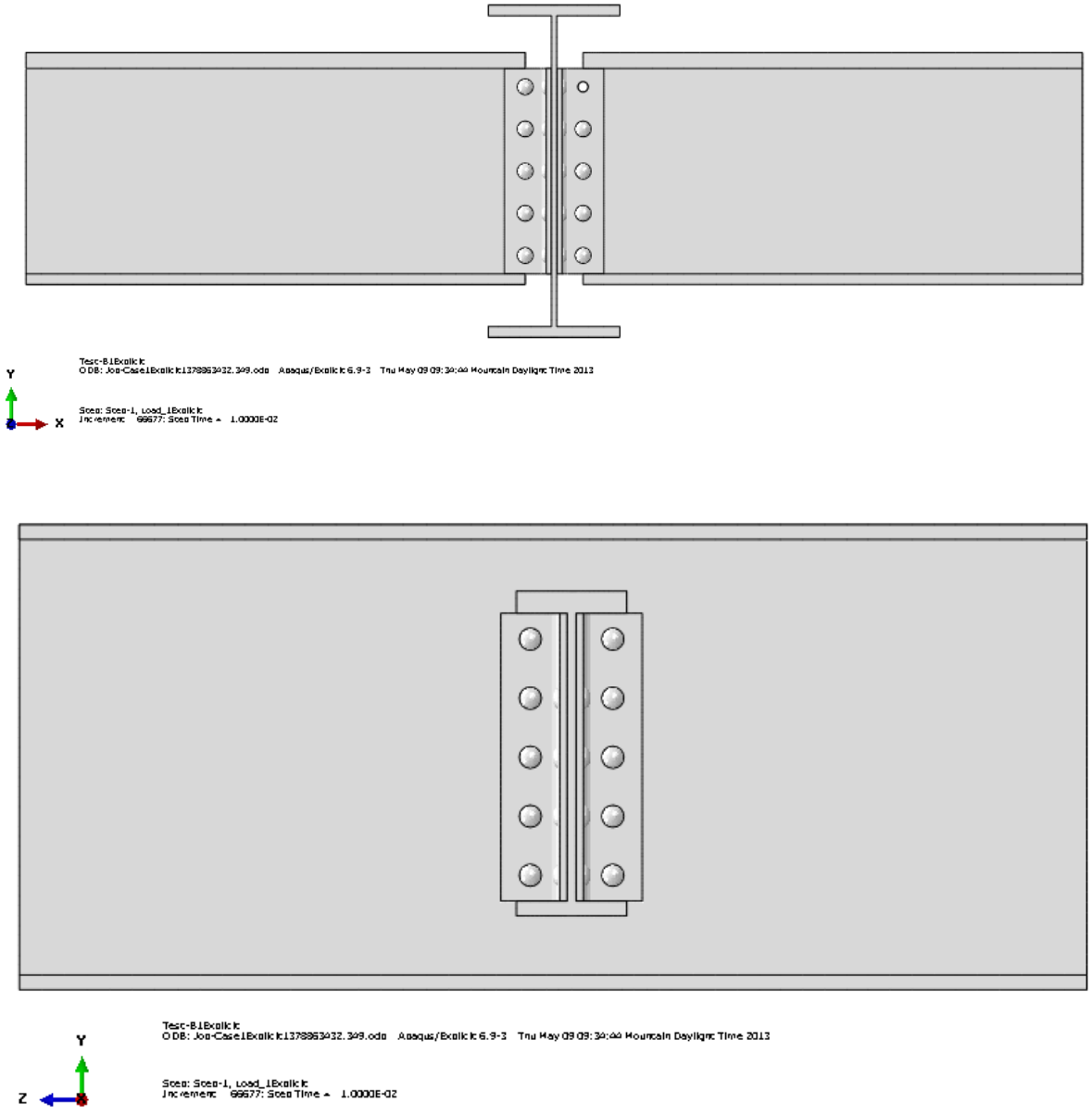

Figure B.1 Detailed View of Undamaged Connection

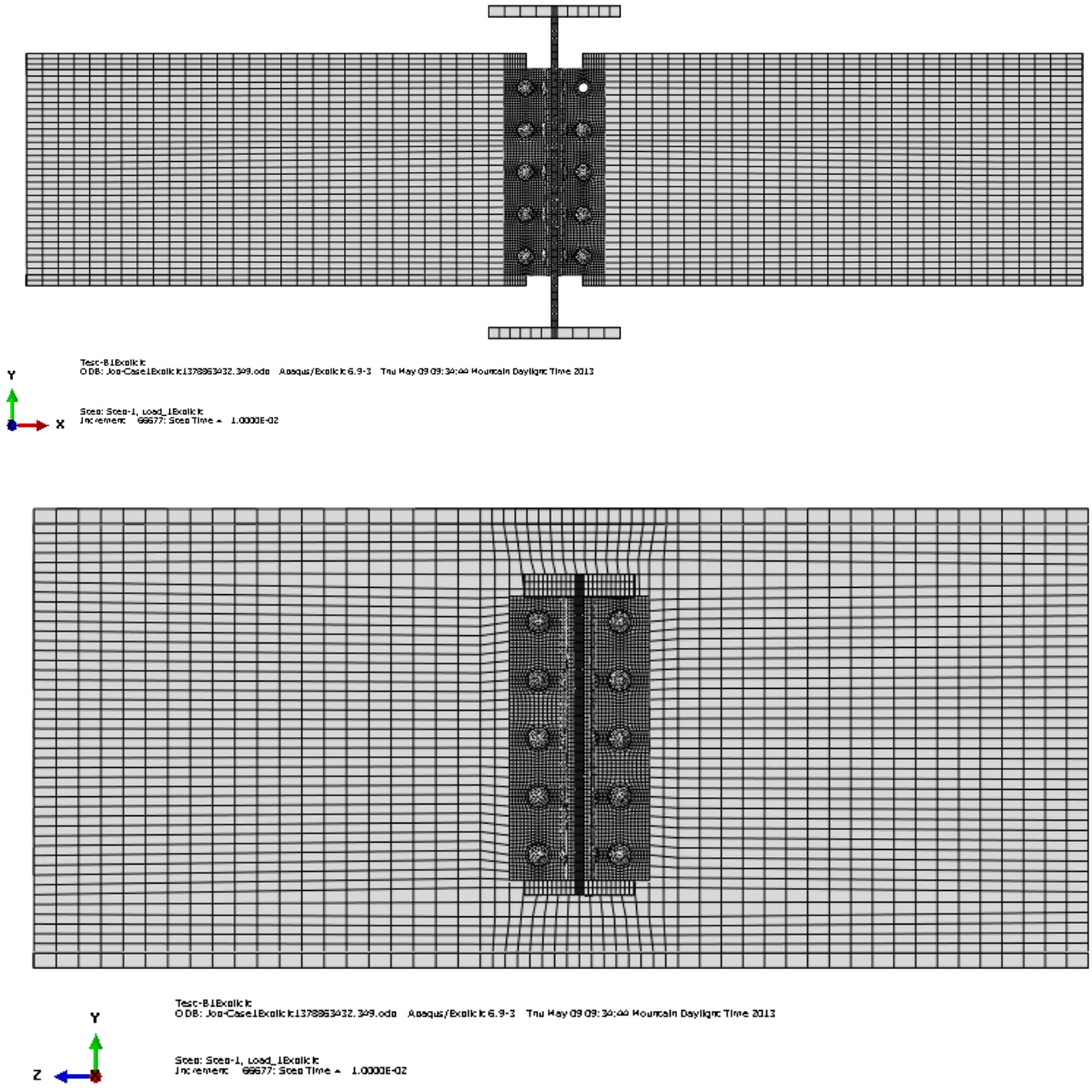

Figure B.2 Mesh of Undamaged Connection

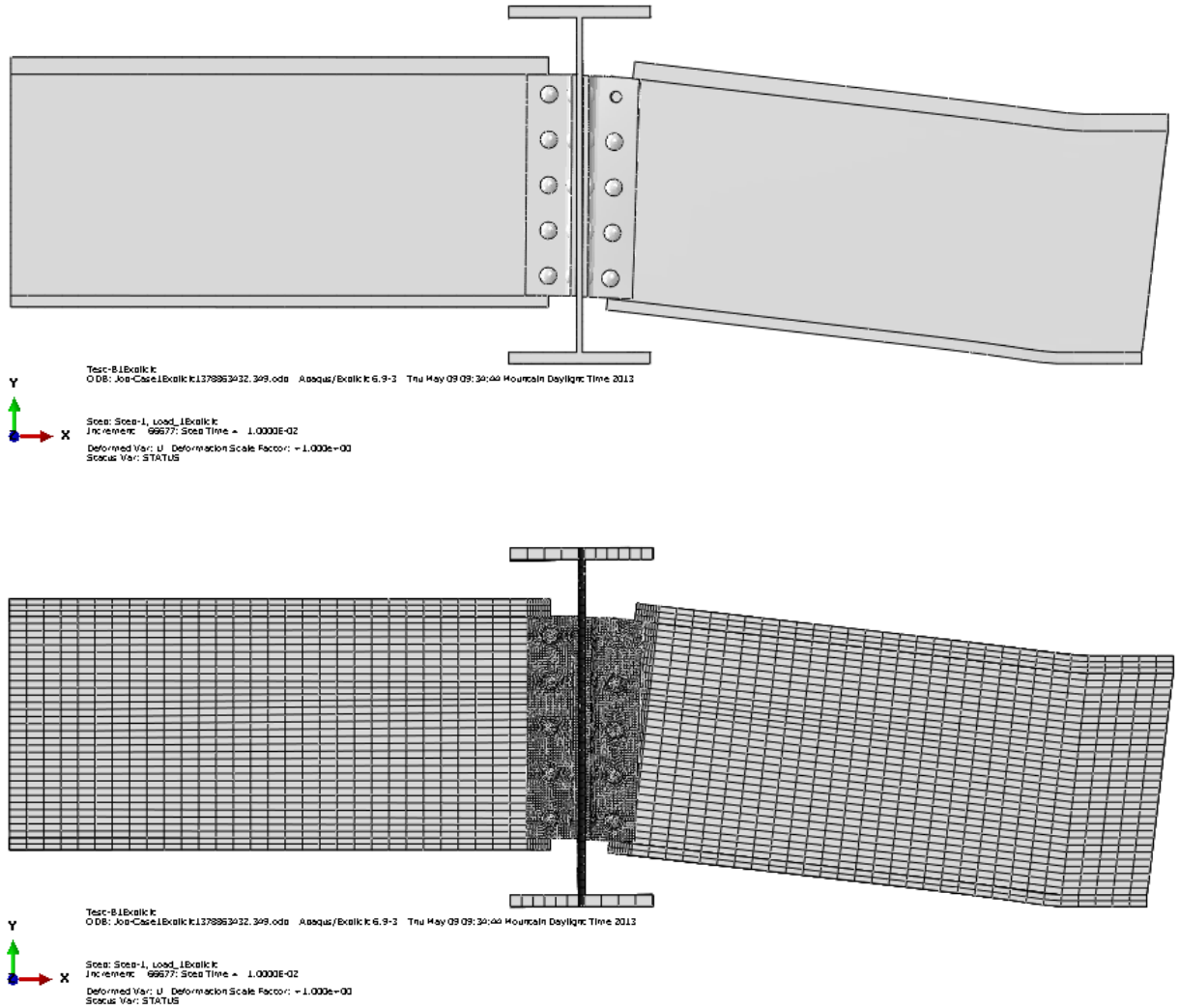

Figure B.3 Deformation after Applied Load – Side View

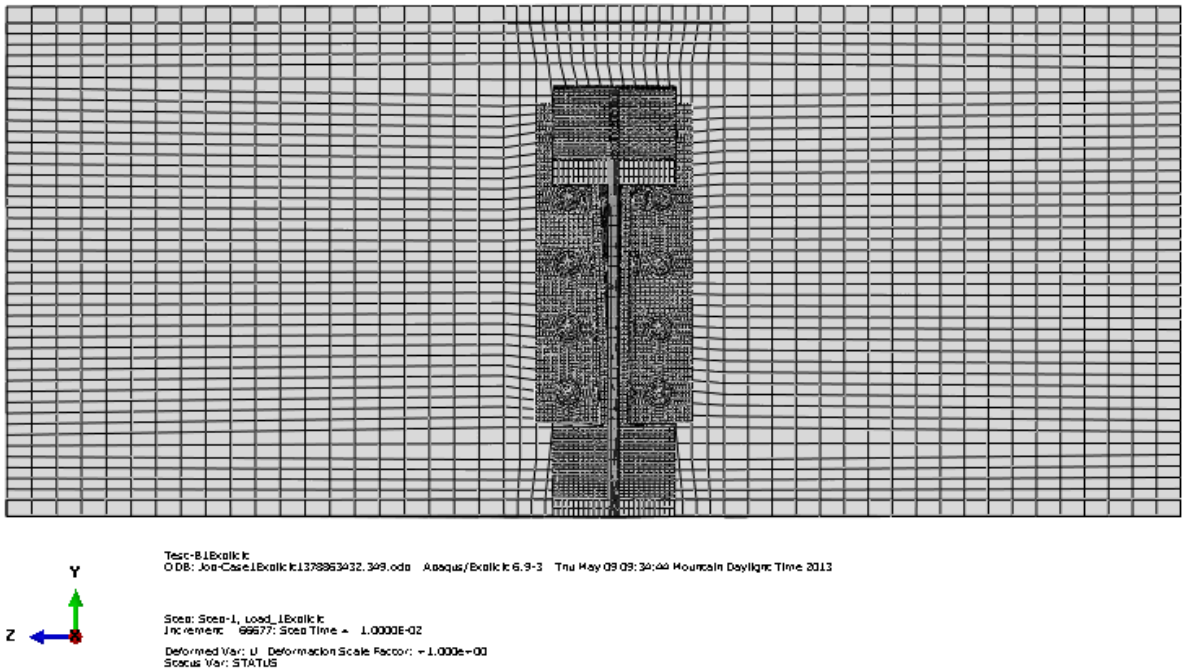

Figure B.4 Deformation after Applied Load – Front View

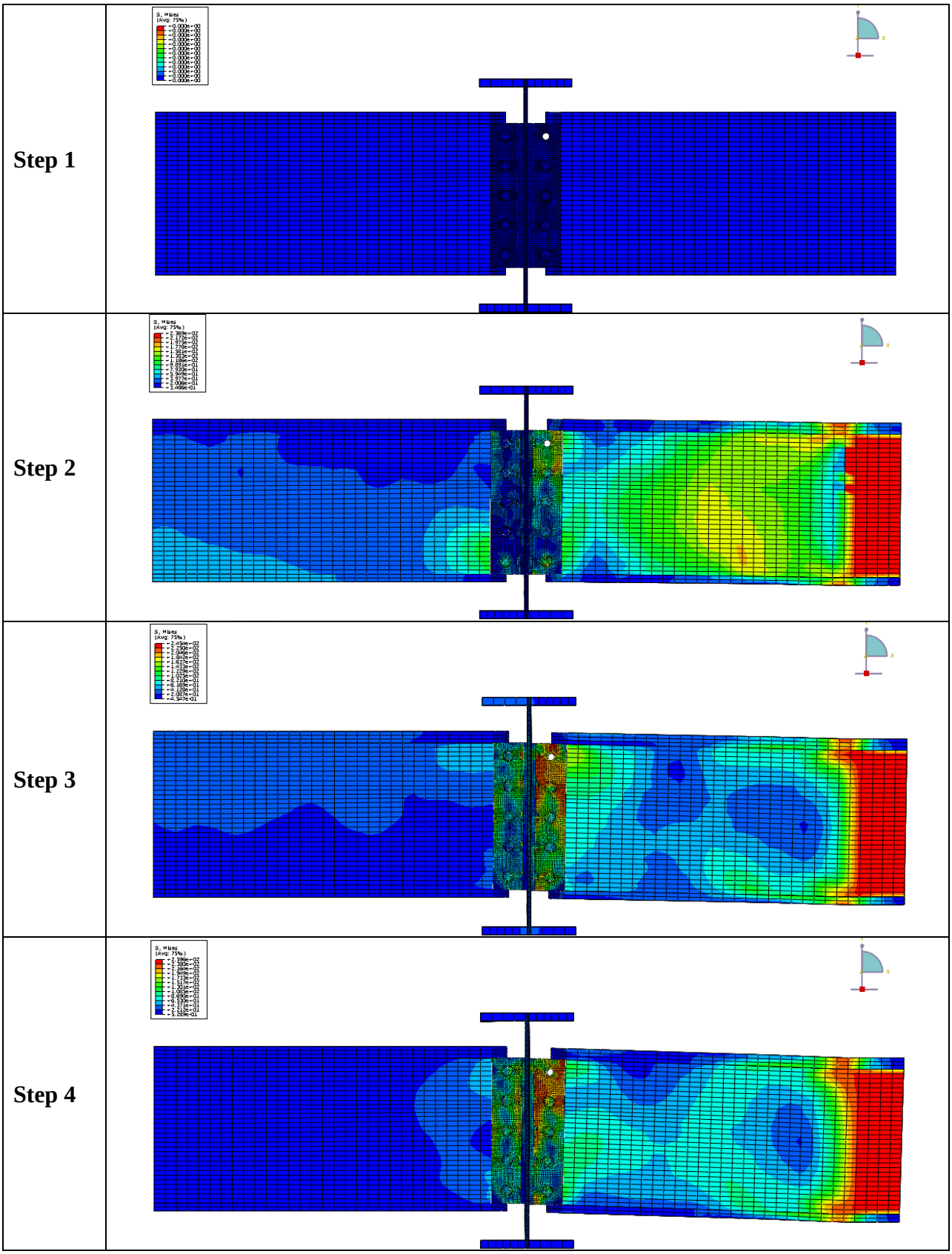

Figure B.5 Stress Distribution on the Connection under Applied Load – General View

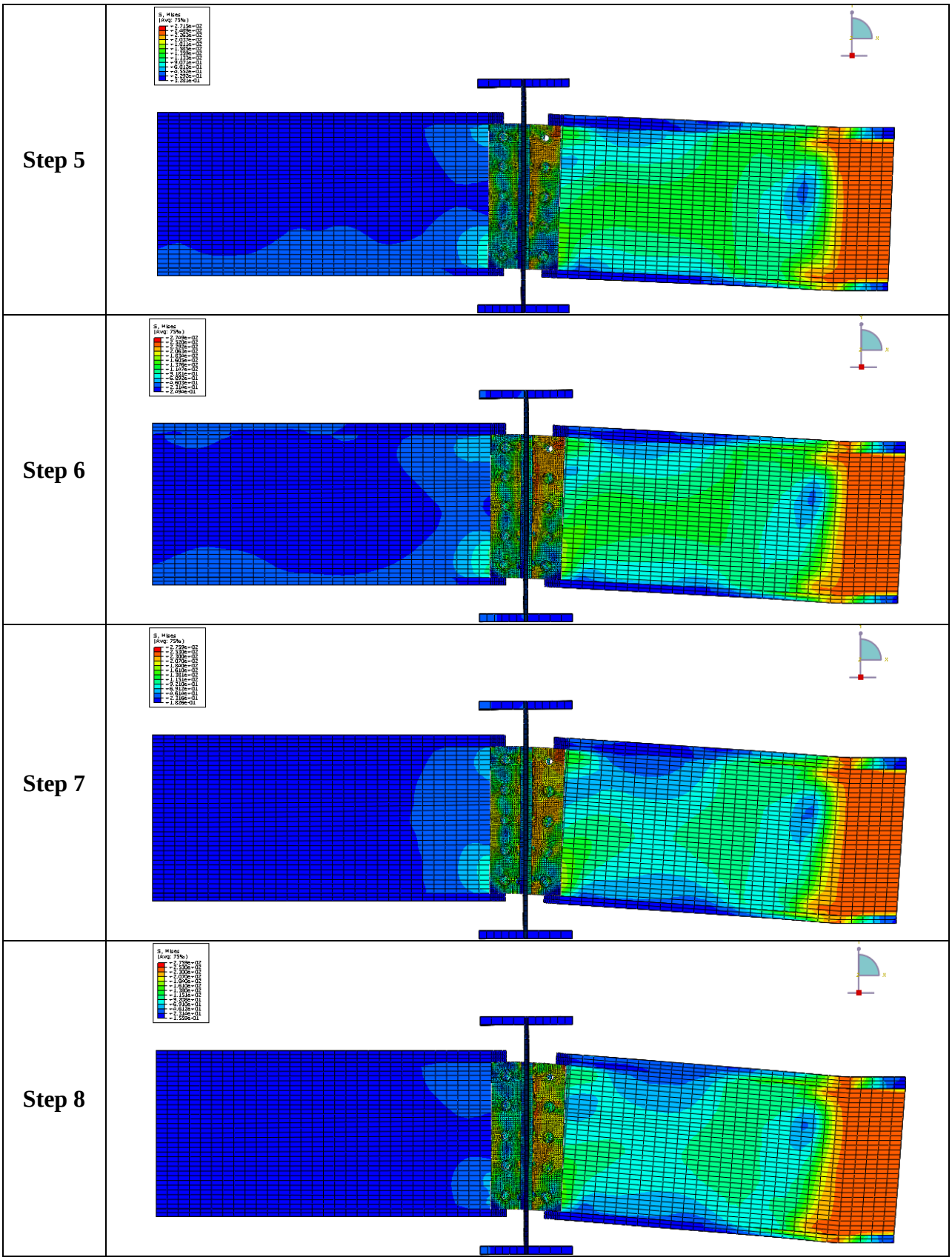

Figure B.5 cont. Stress Distribution on the Connection under Applied Load – General View

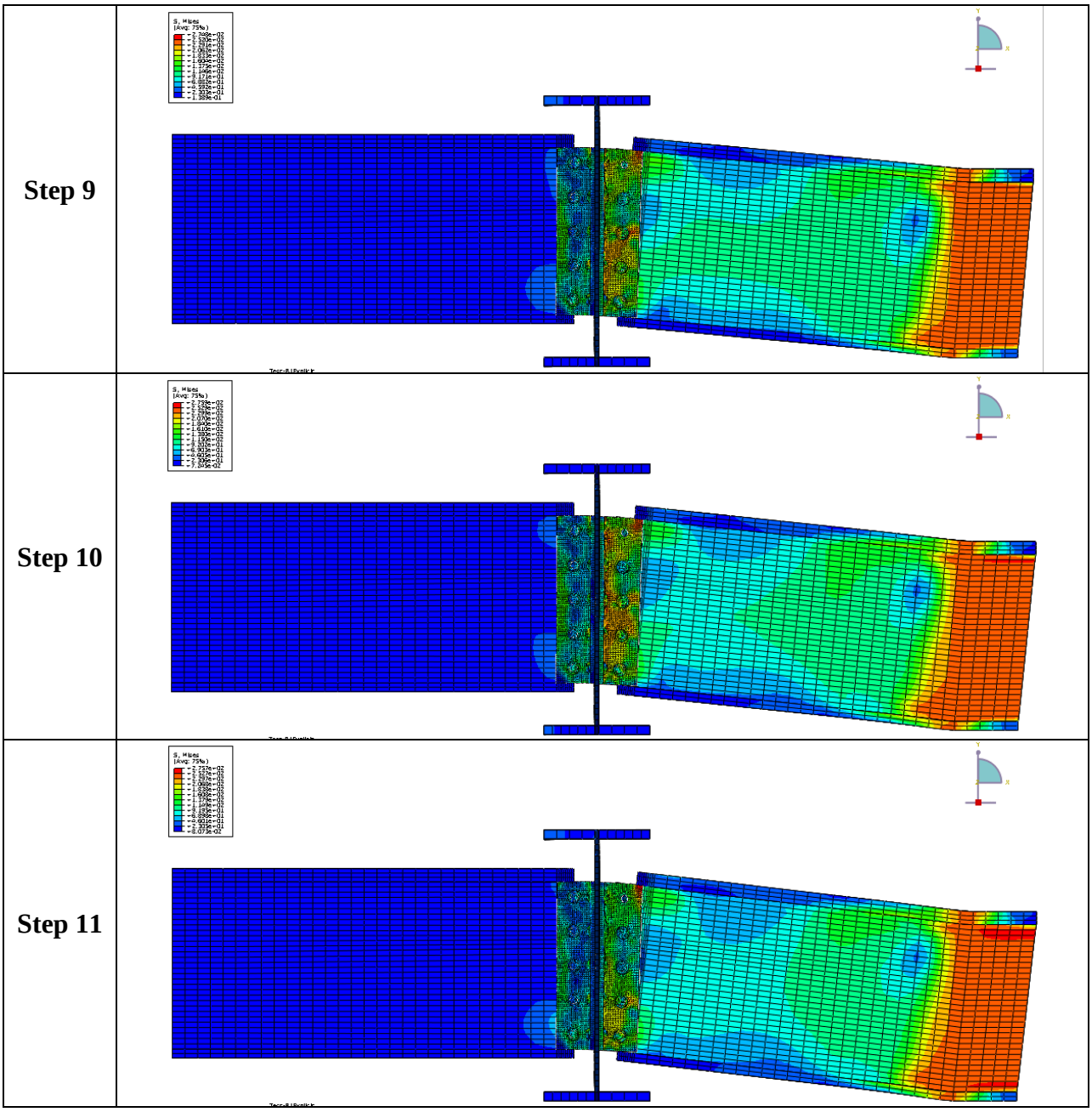

Figure B.5 cont. Stress Distribution on the Connection under Applied Load – General View

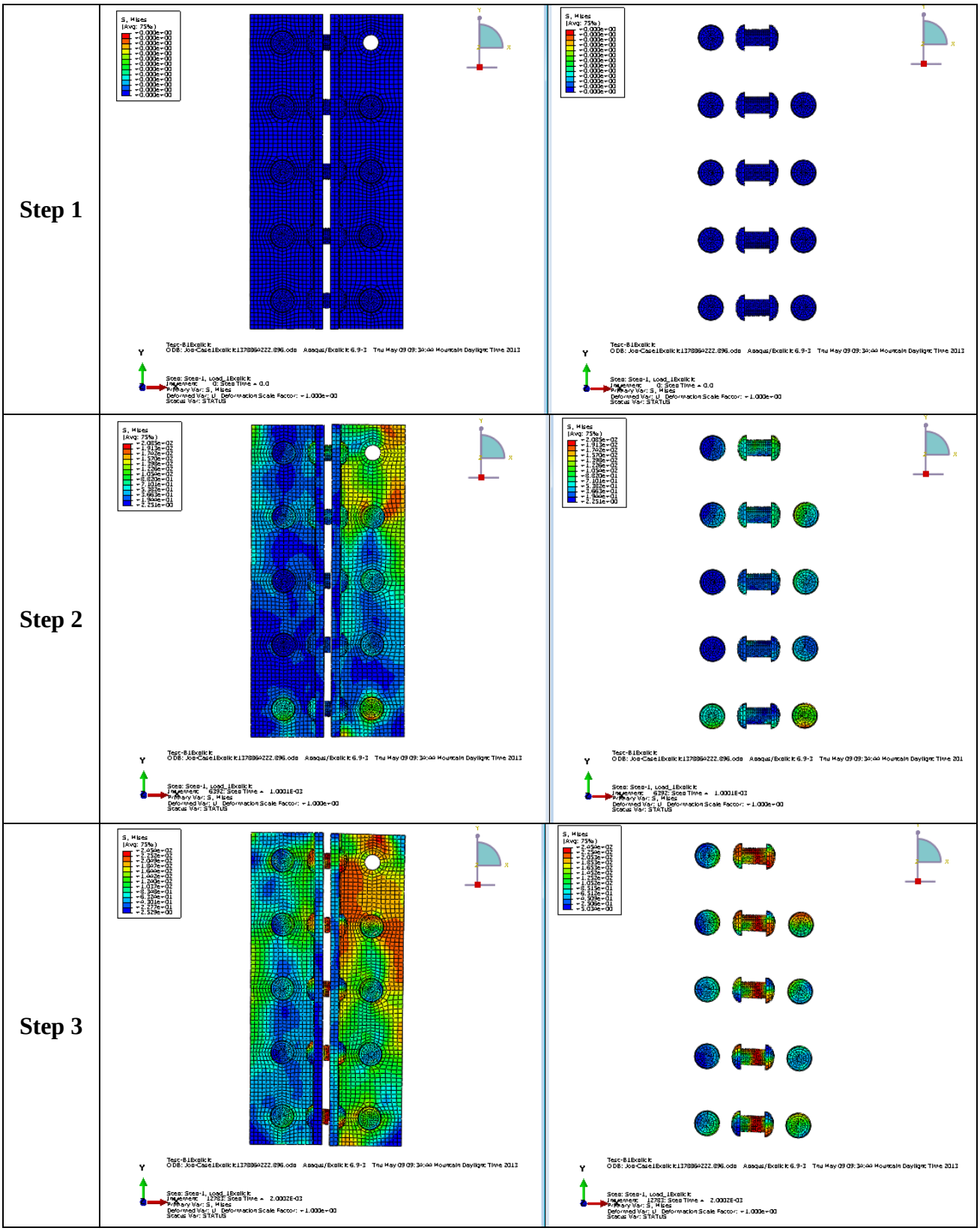

Figure B.6 Stress Distribution on the Connection under Applied Load – Side View

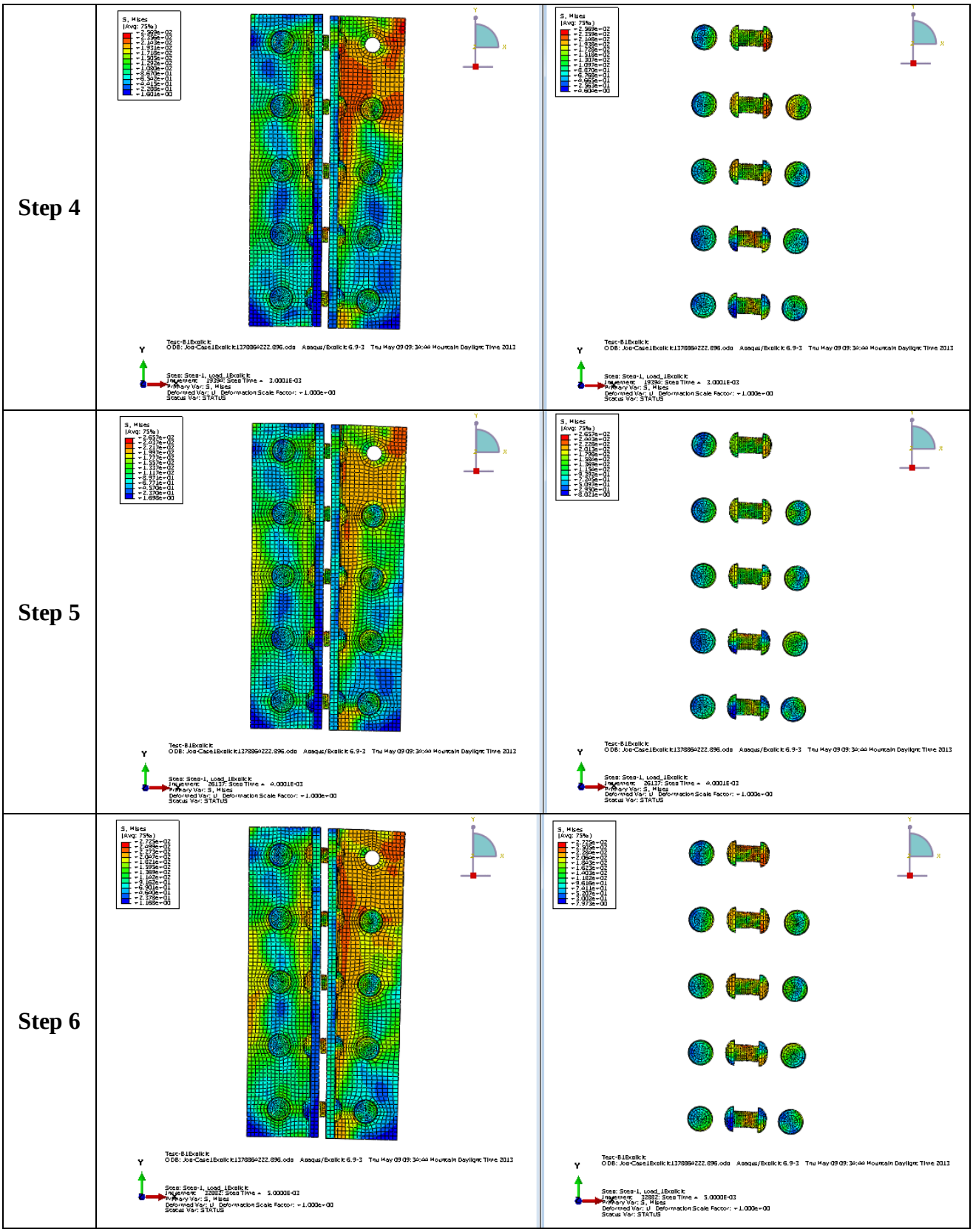

Figure B.6 cont. Stress Distribution on the Connection under Applied Load – Side View

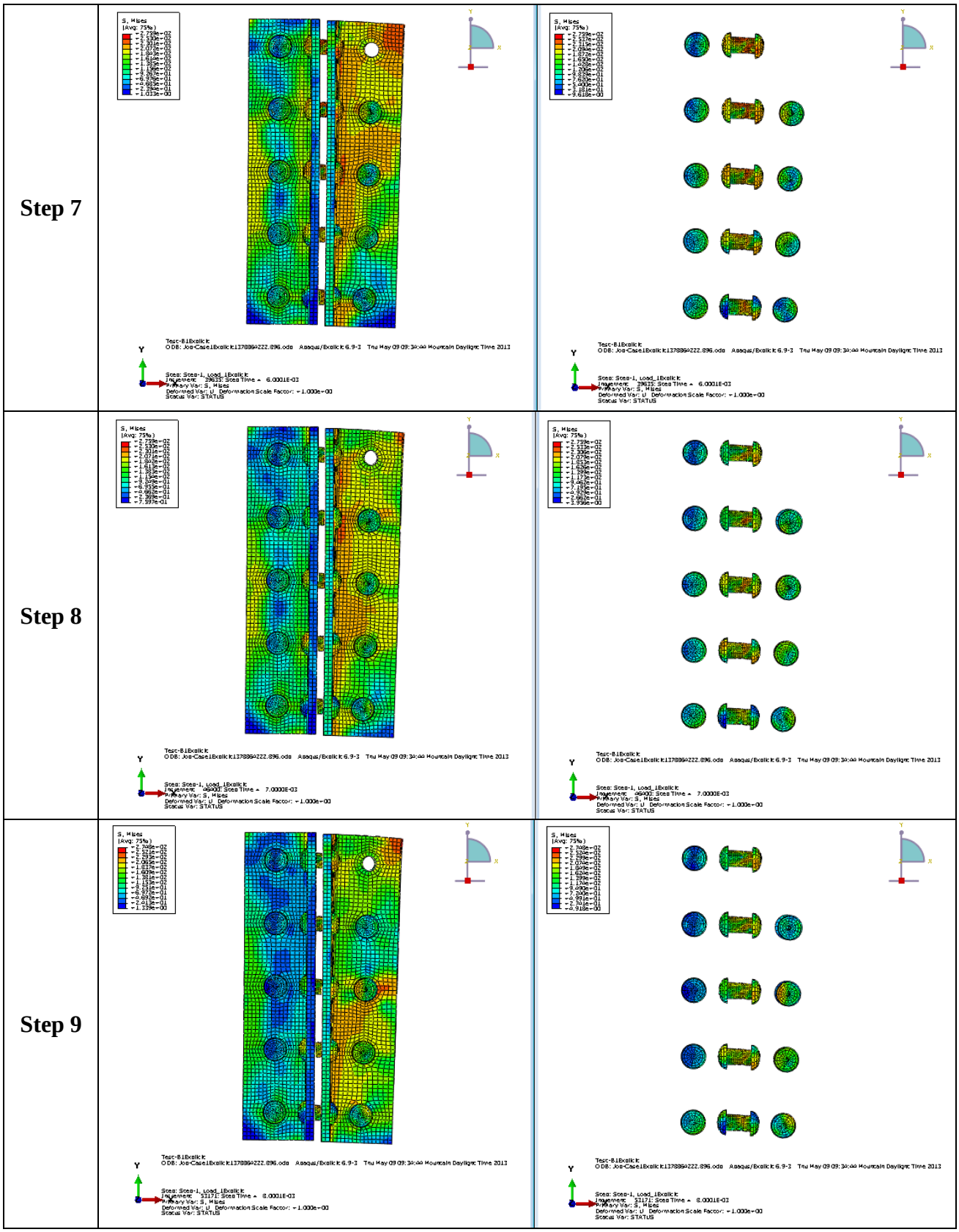

Figure B.6 cont. Stress Distribution on the Connection under Applied Load – Side View

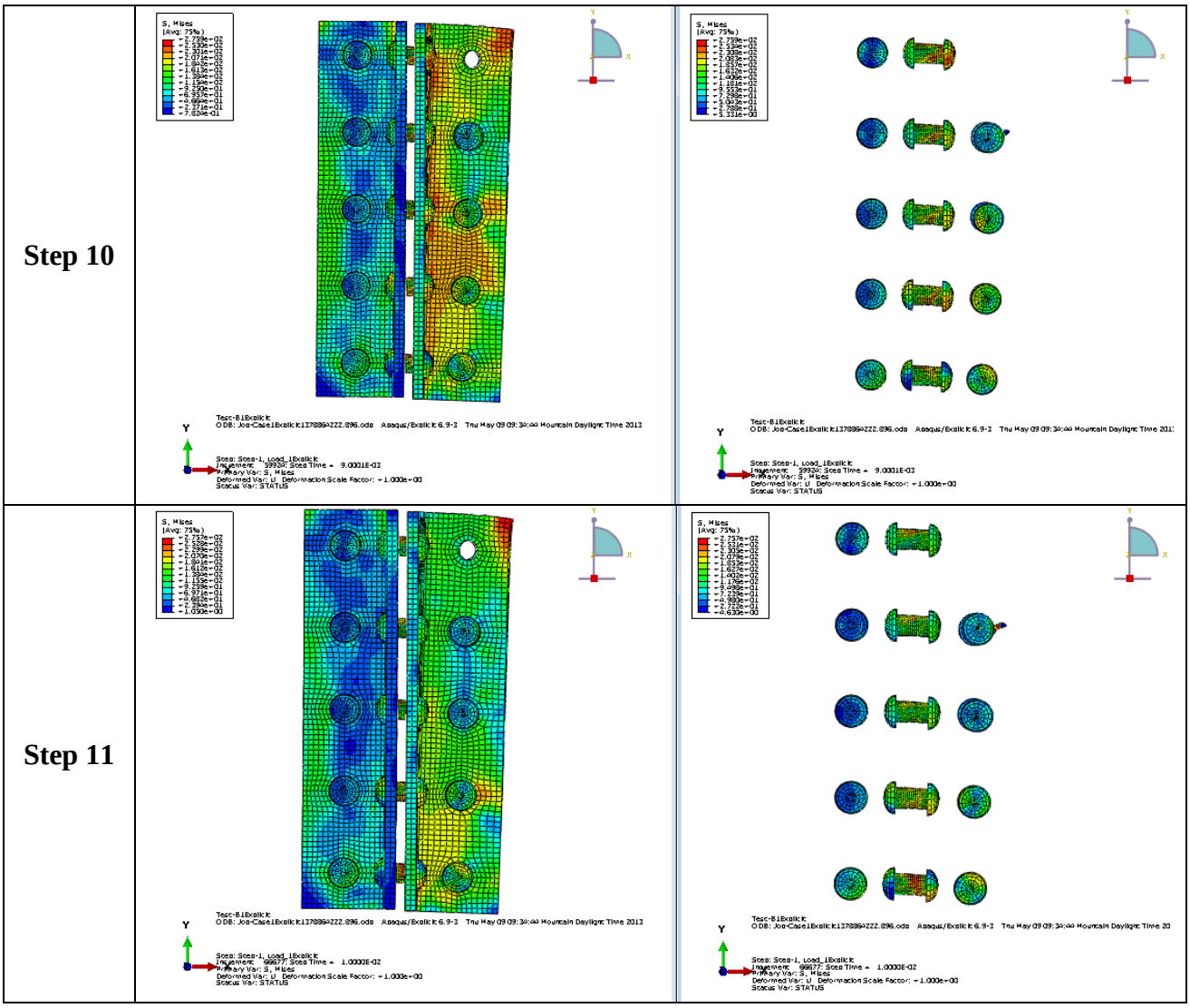

Figure B.6 cont. Stress Distribution on the Connection under Applied Load – Side View

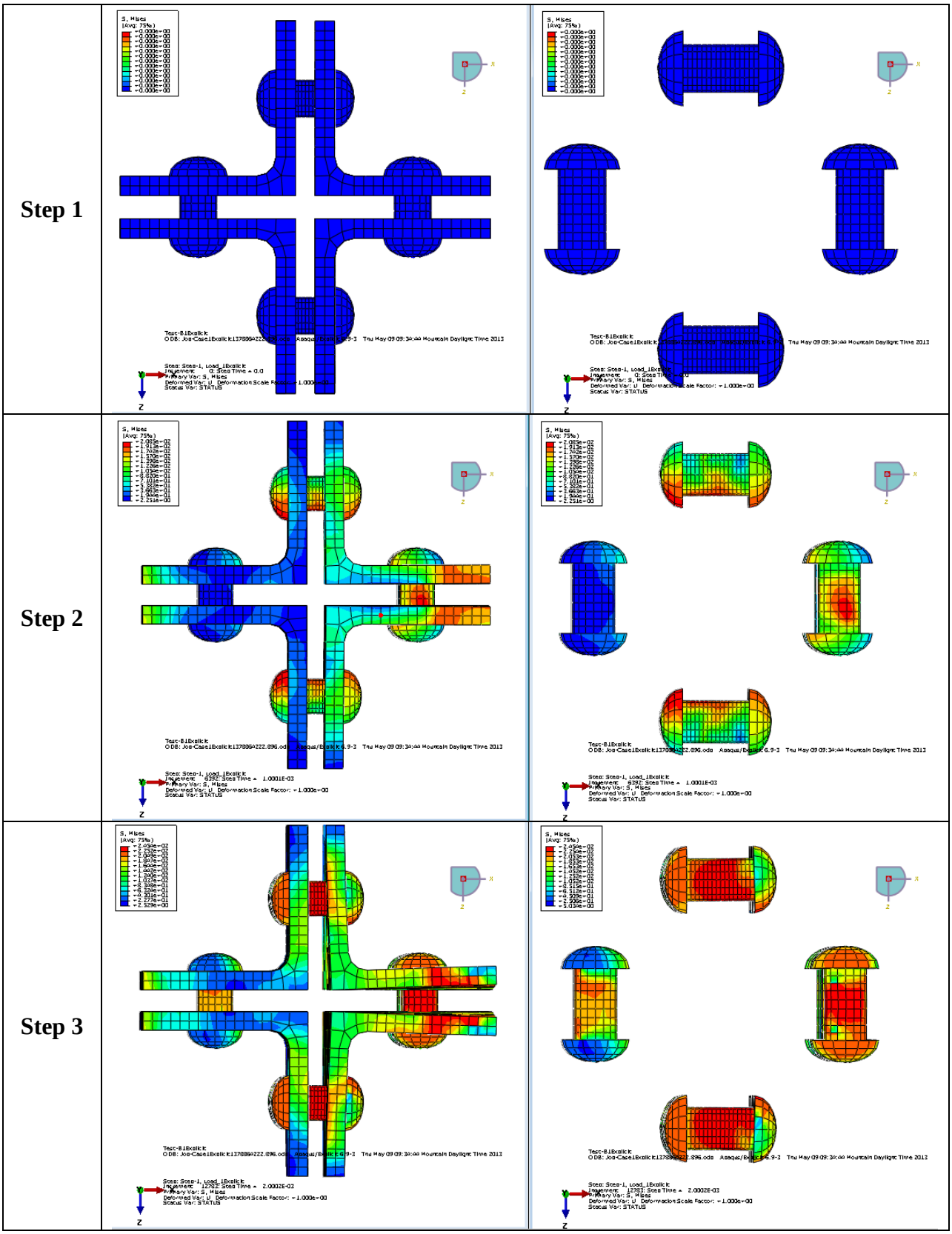

Figure B.7 Stress Distribution on the Connection under Applied Load – Top View

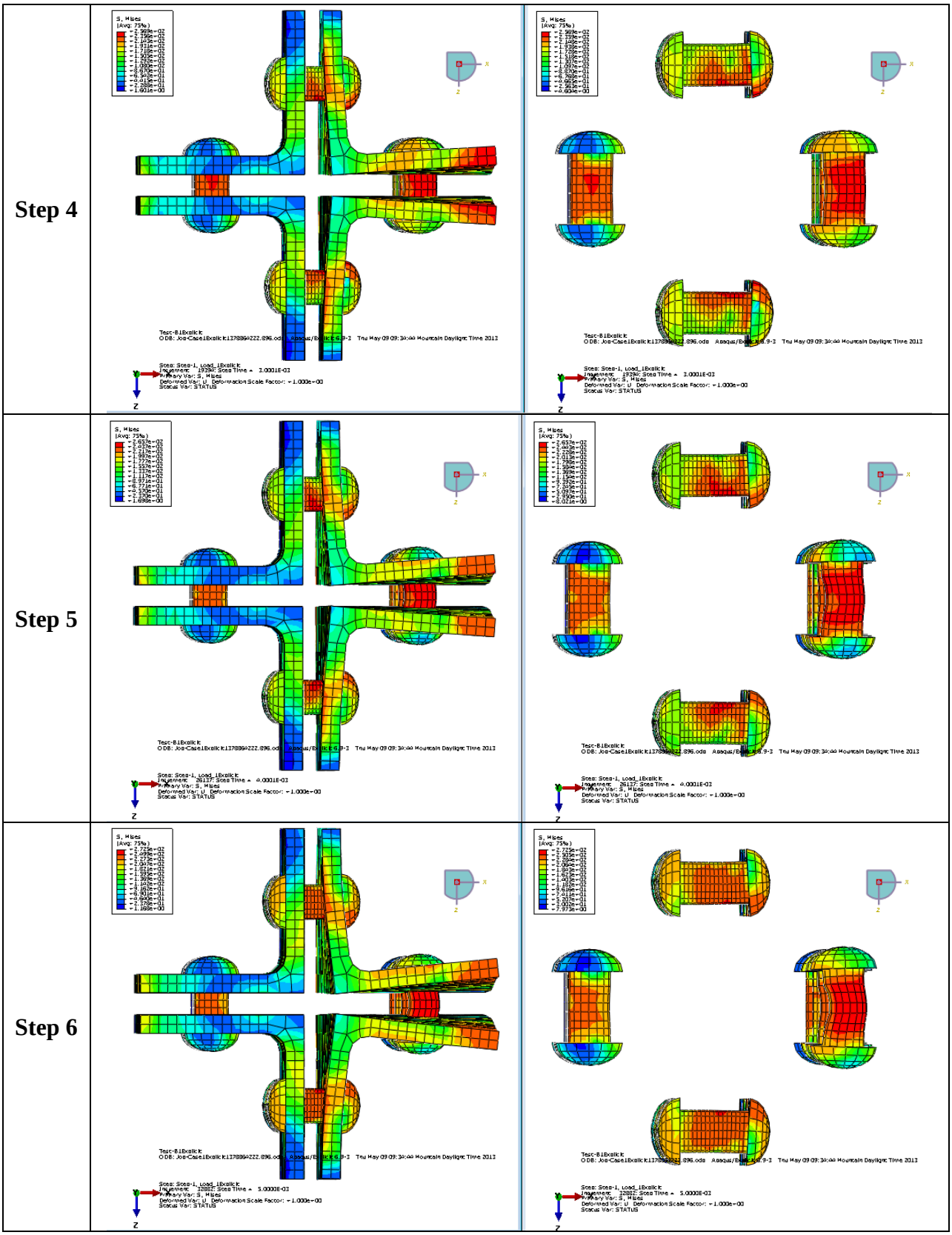

Figure B.7 cont. Stress Distribution on the Connection under Applied Load – Top View

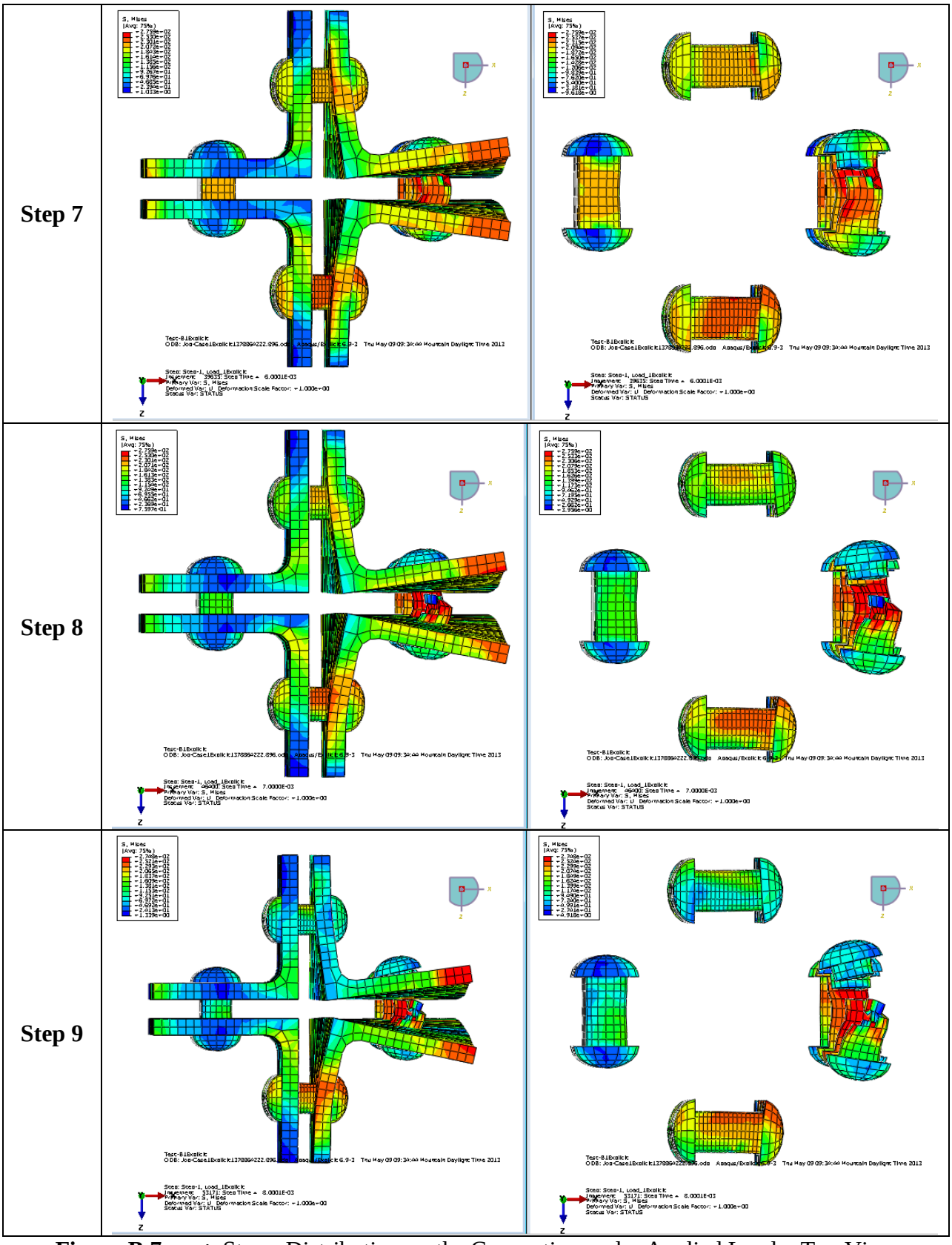

Figure B.7 cont. Stress Distribution on the Connection under Applied Load – Top View

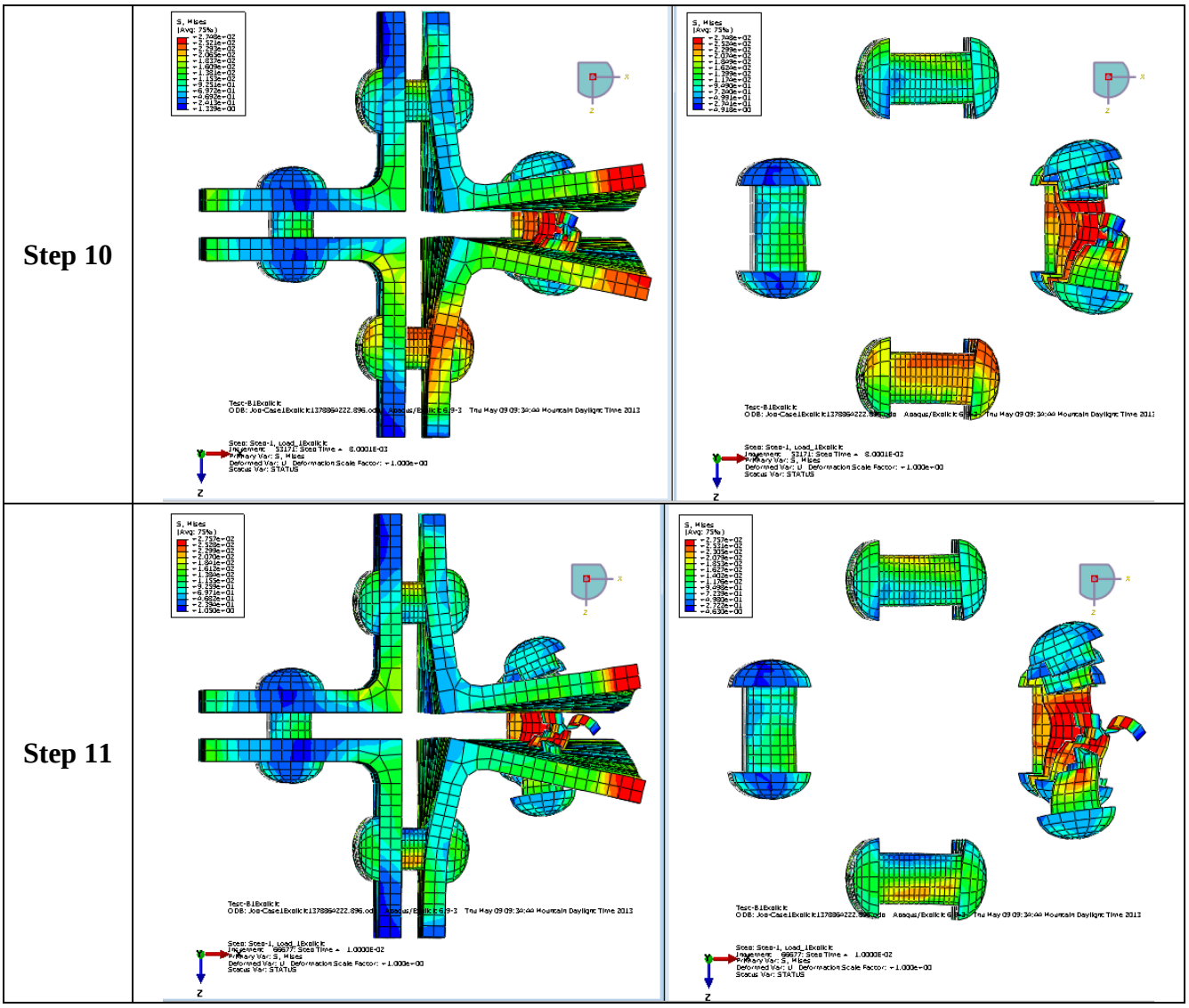

Figure B.7 cont. Stress Distribution on the Connection under Applied Load – Top View

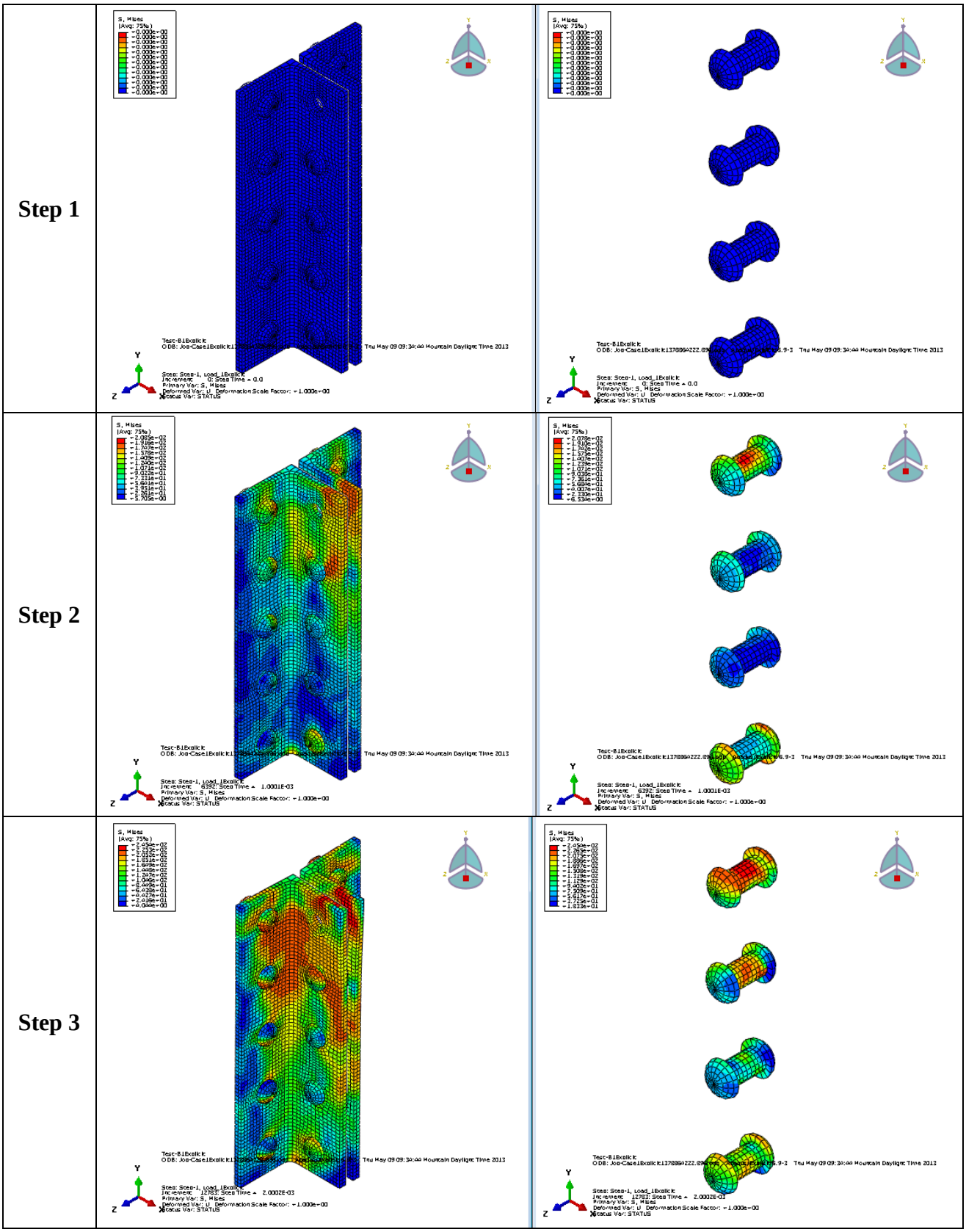

Figure B.8 Stress Distribution on the Connection under Applied Load – Isometric View

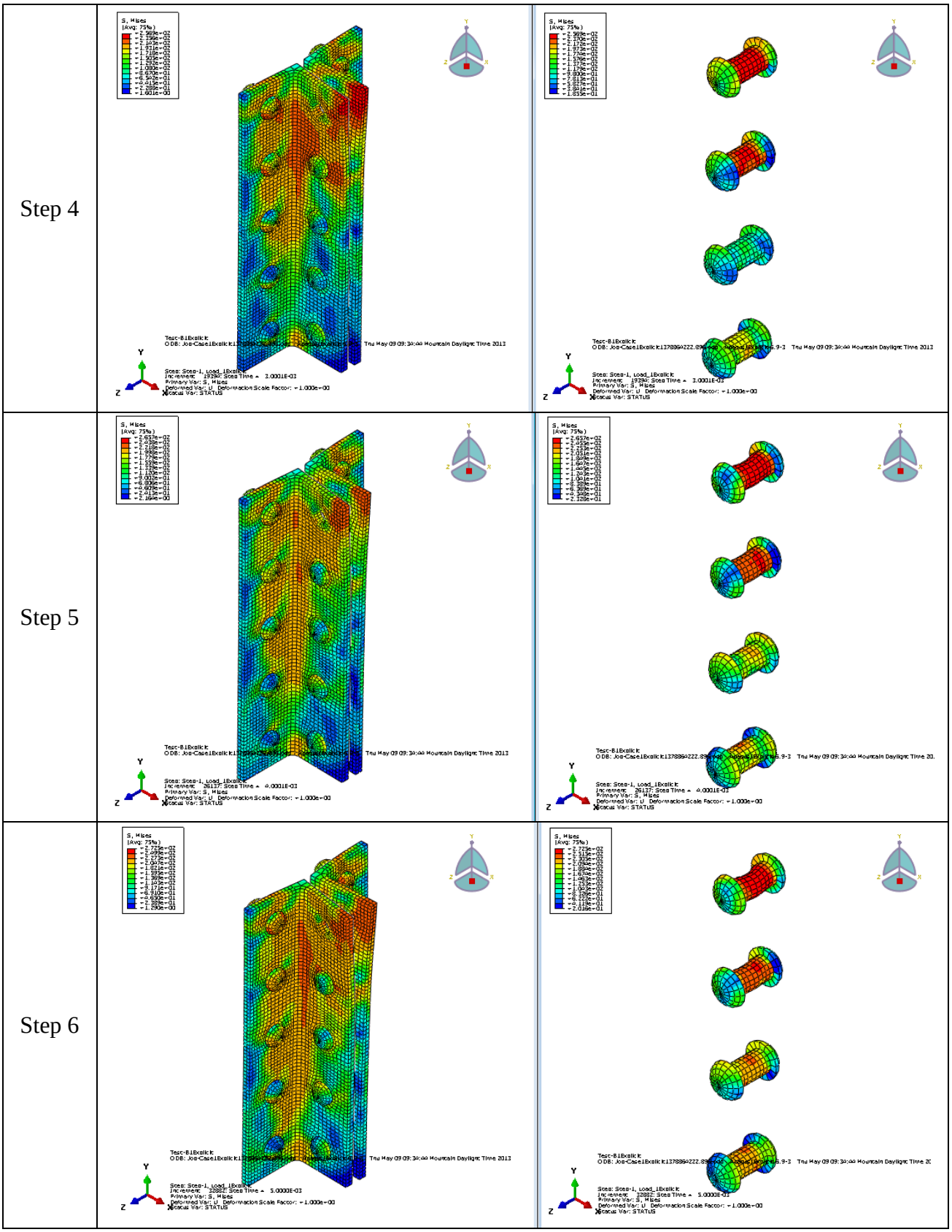

Figure B.8 cont. Stress Distribution on the Connection under Applied Load – Isometric View

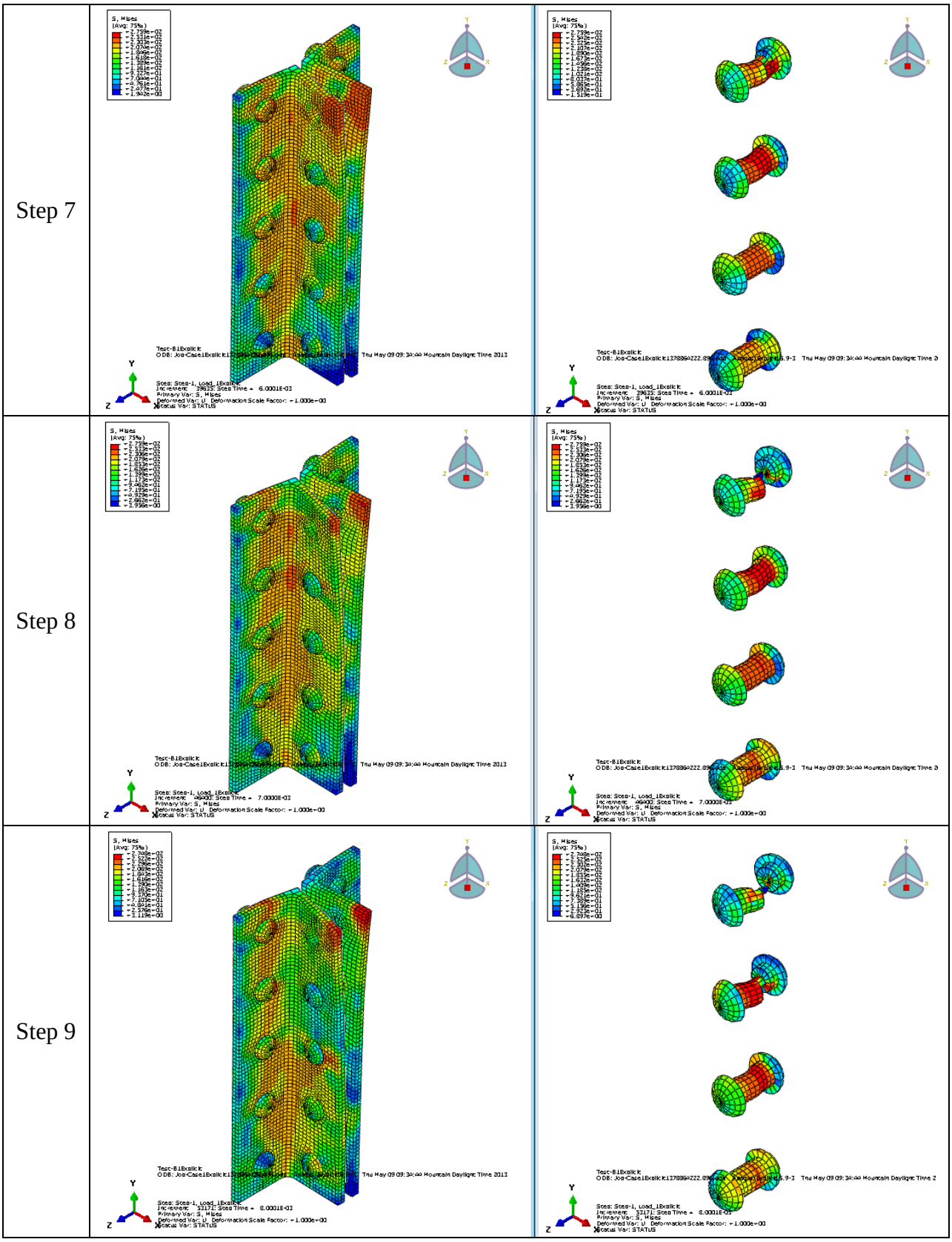

Figure B.8 cont. Stress Distribution on the Connection under Applied Load – Isometric View

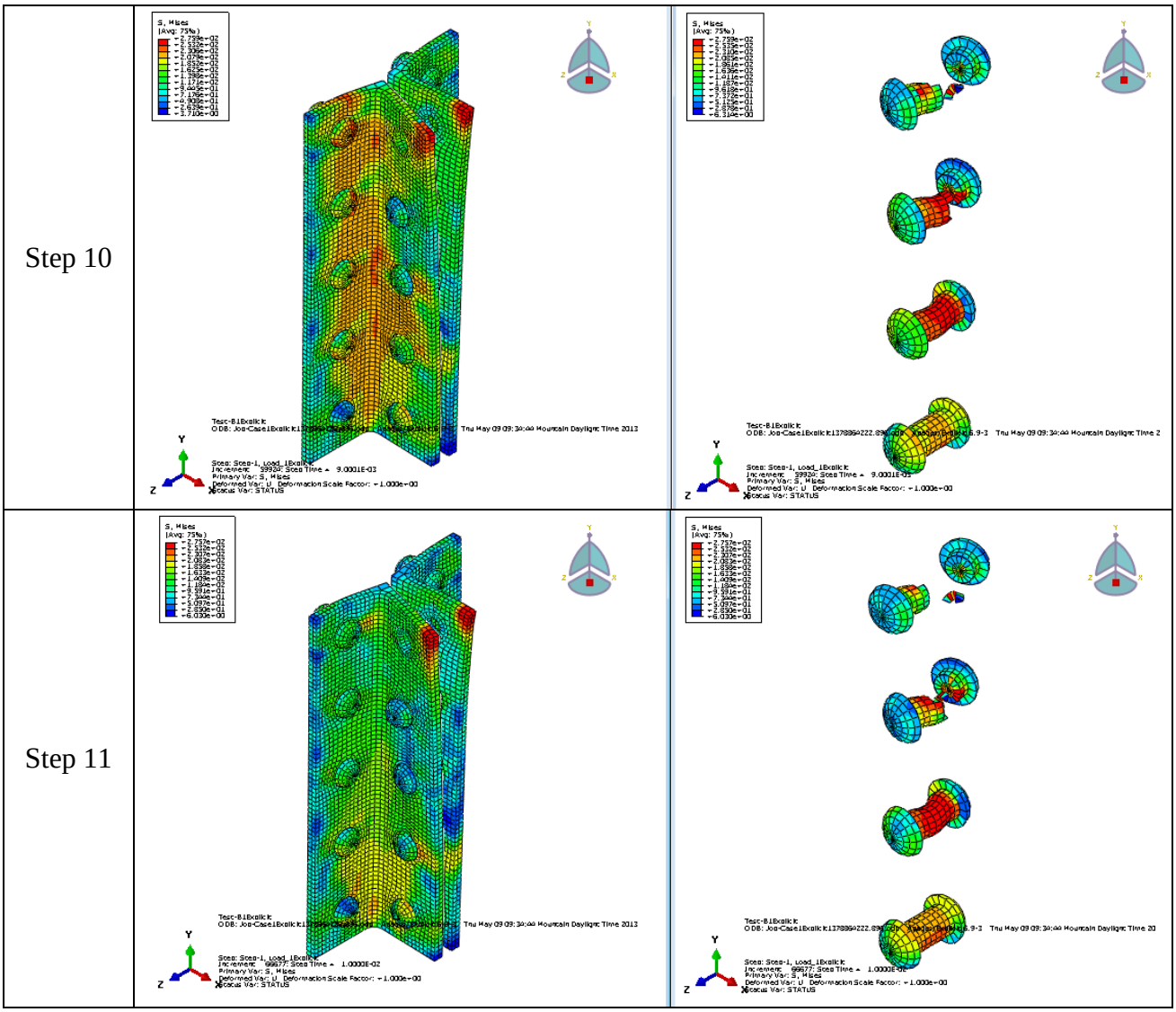

Figure B.8 cont. Stress Distribution on the Connection under Applied Load – Isometric View

Appendix C Results of FEA for Connection with Missing Upper Bolt on the Crossbeam

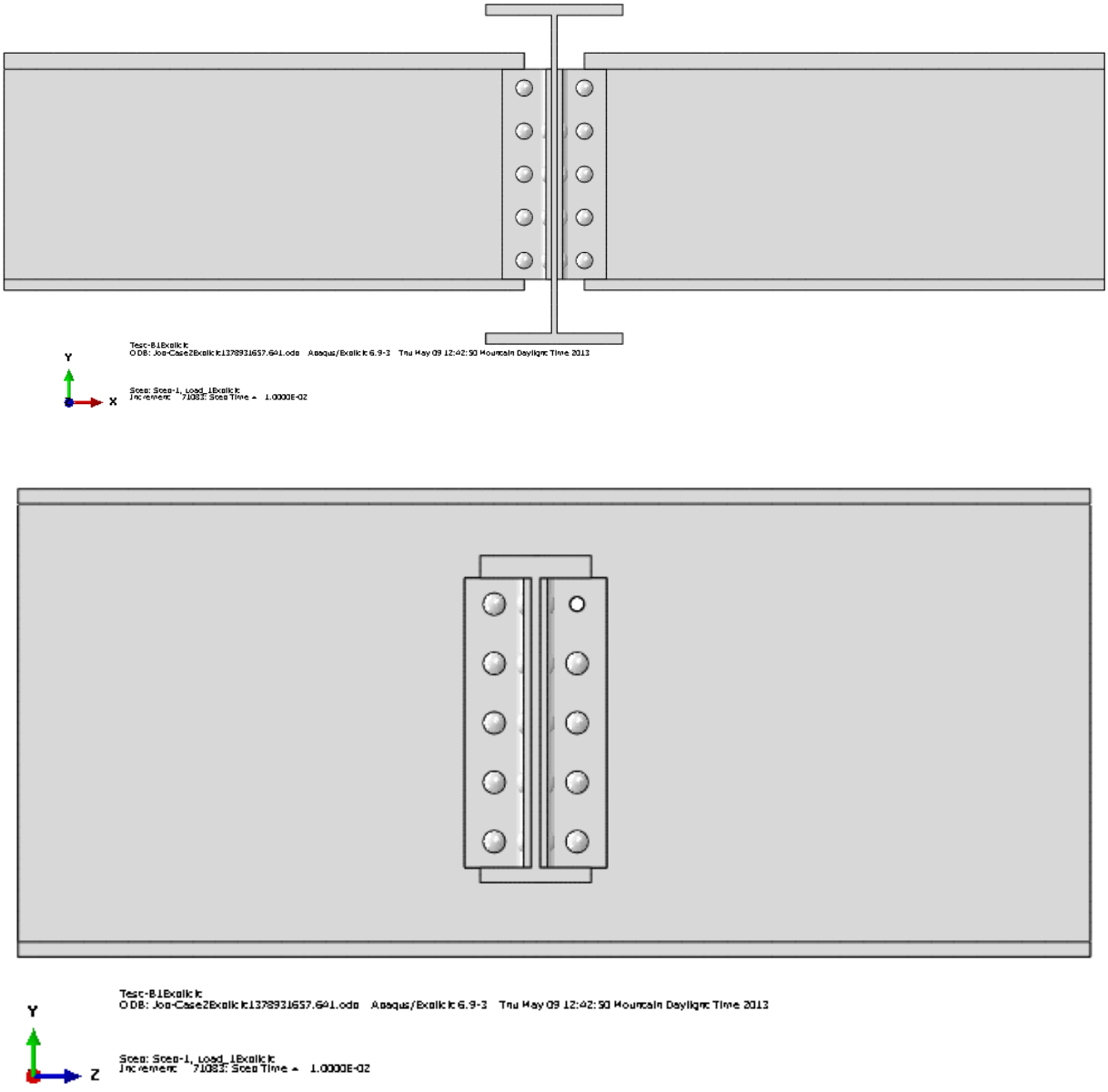

Figure C.1 Detailed View of Undamaged Connection

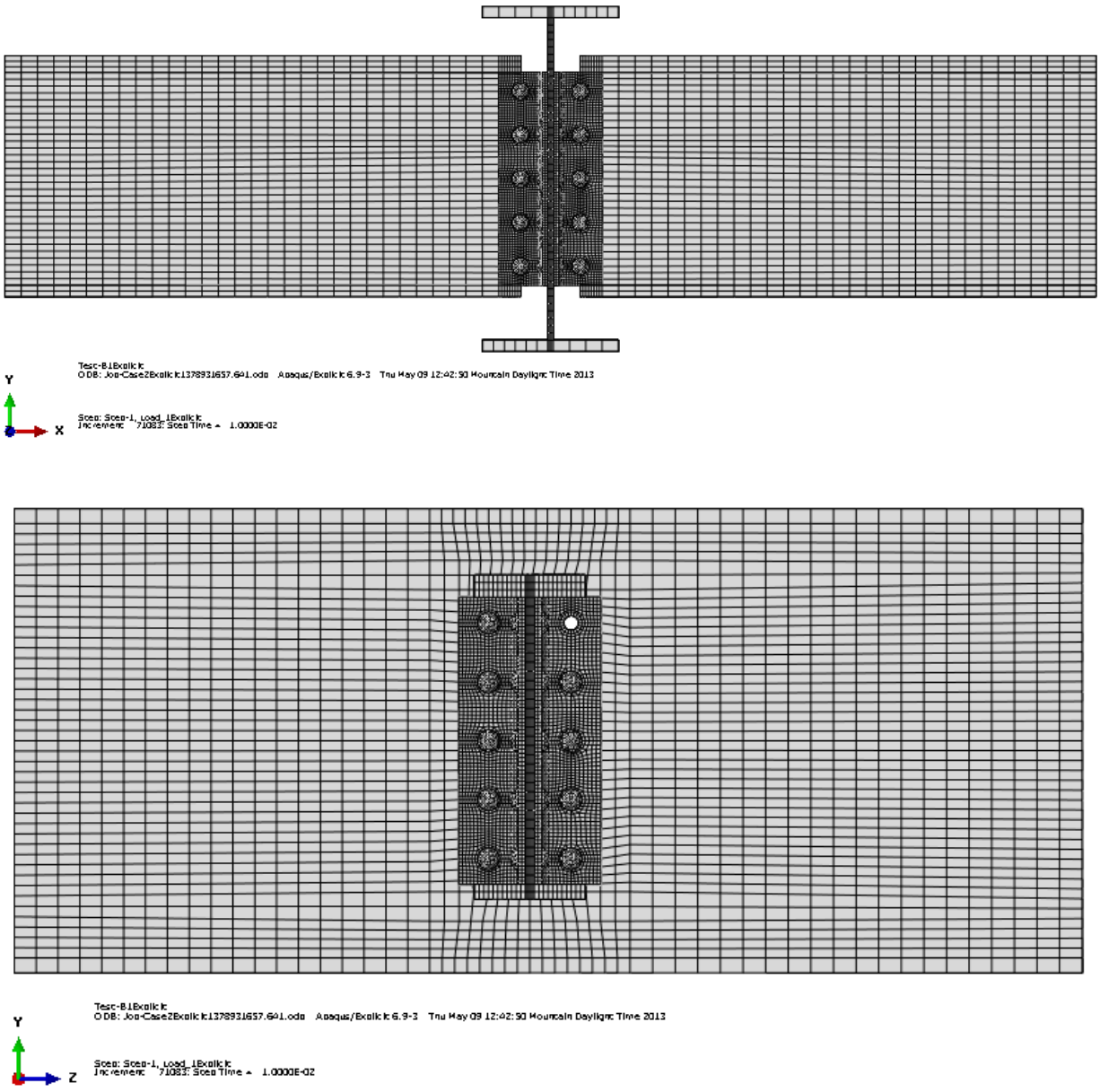

Figure C.2 Mesh of Undamaged Connection

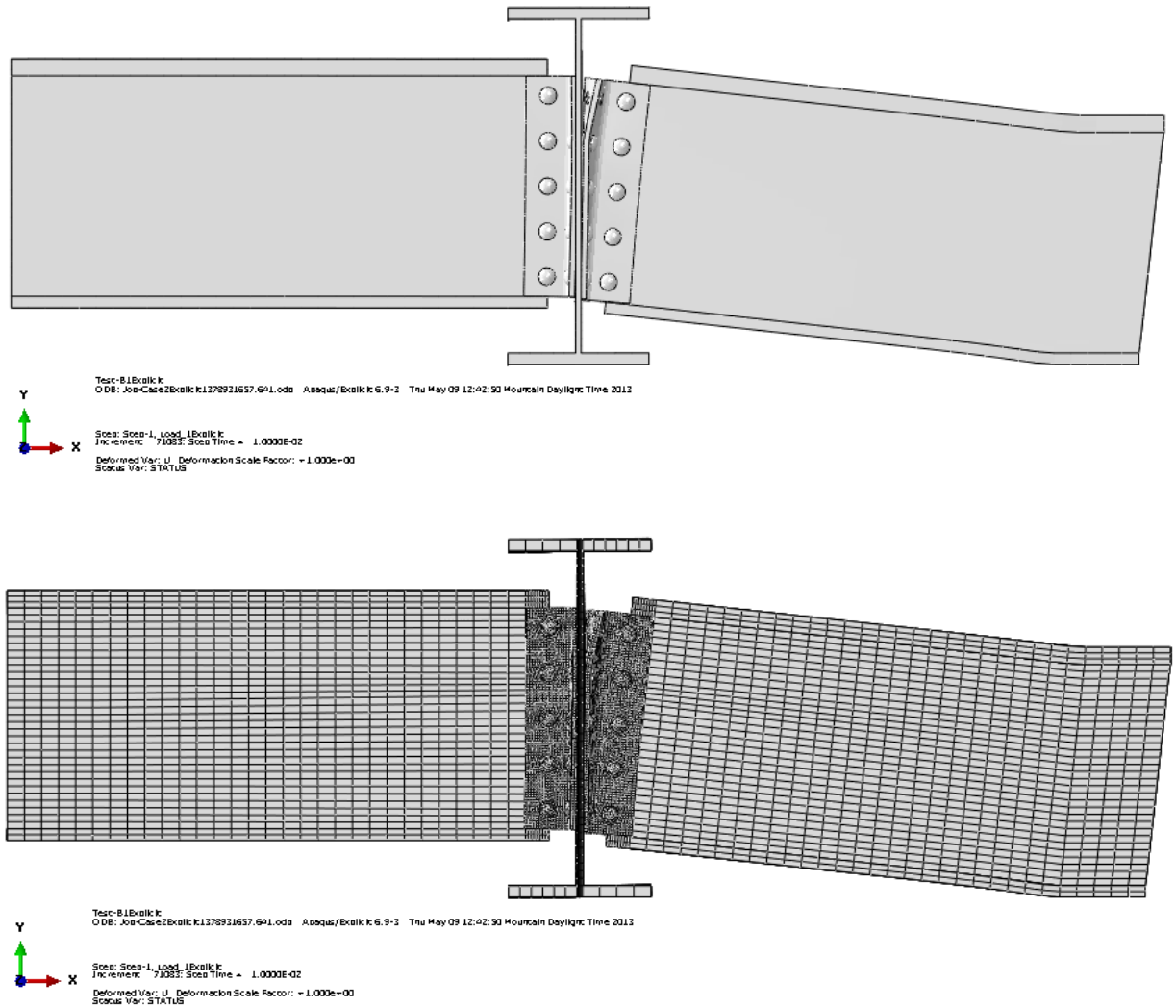

Figure C.3 Deformation after Applied Load – Side View

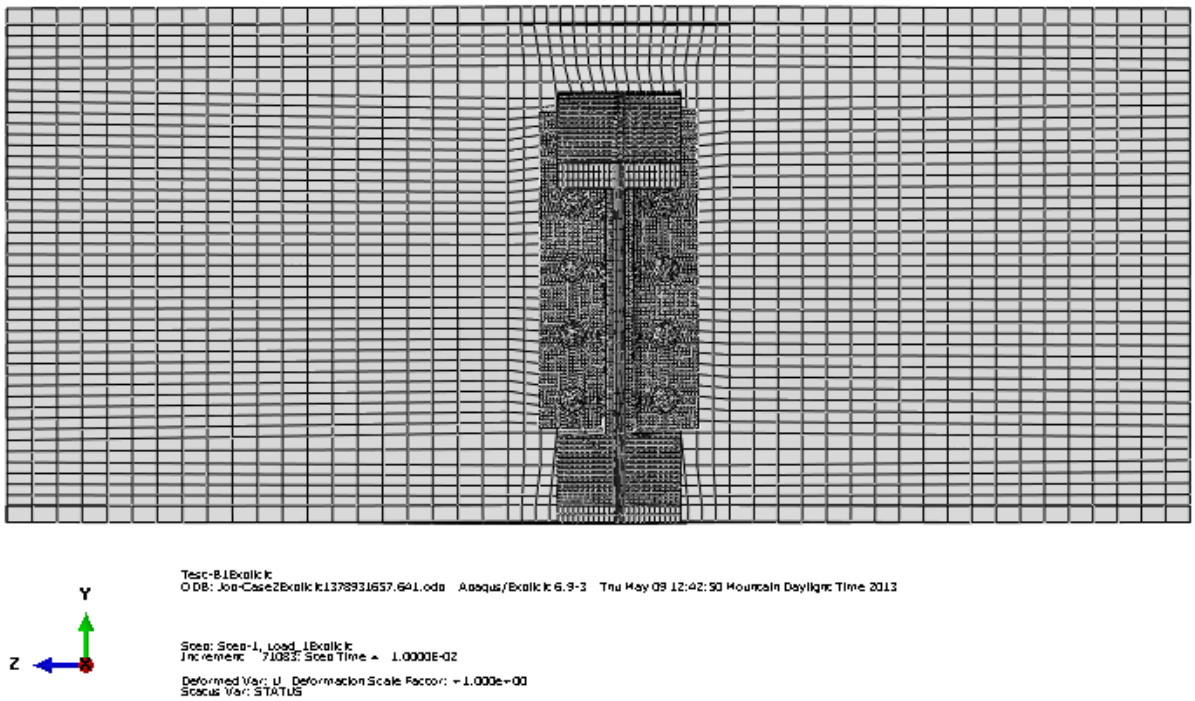

Figure C.4 Deformation after Applied Load – Front View

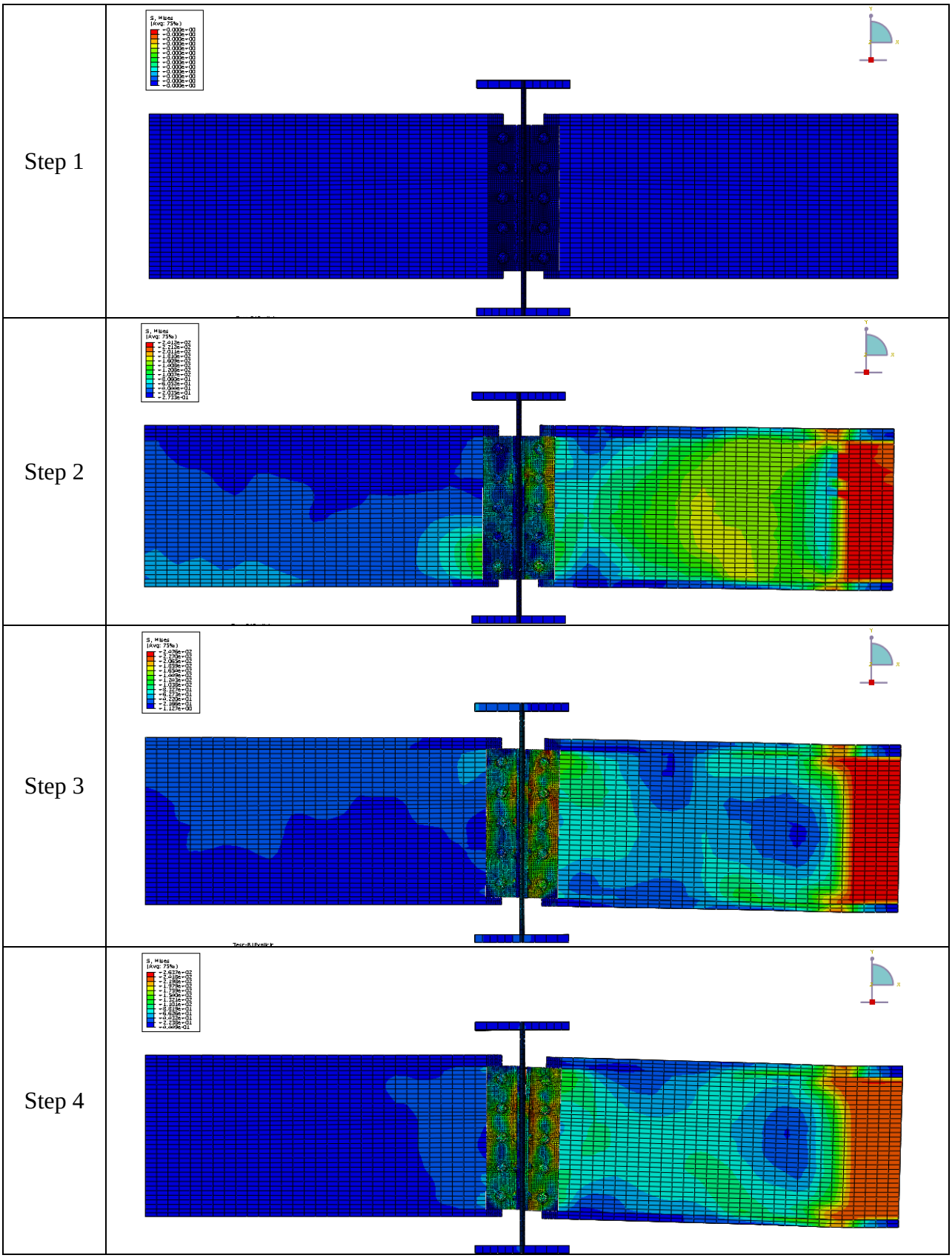

Figure C.5 Stress Distribution on the Connection under Applied Load – General View

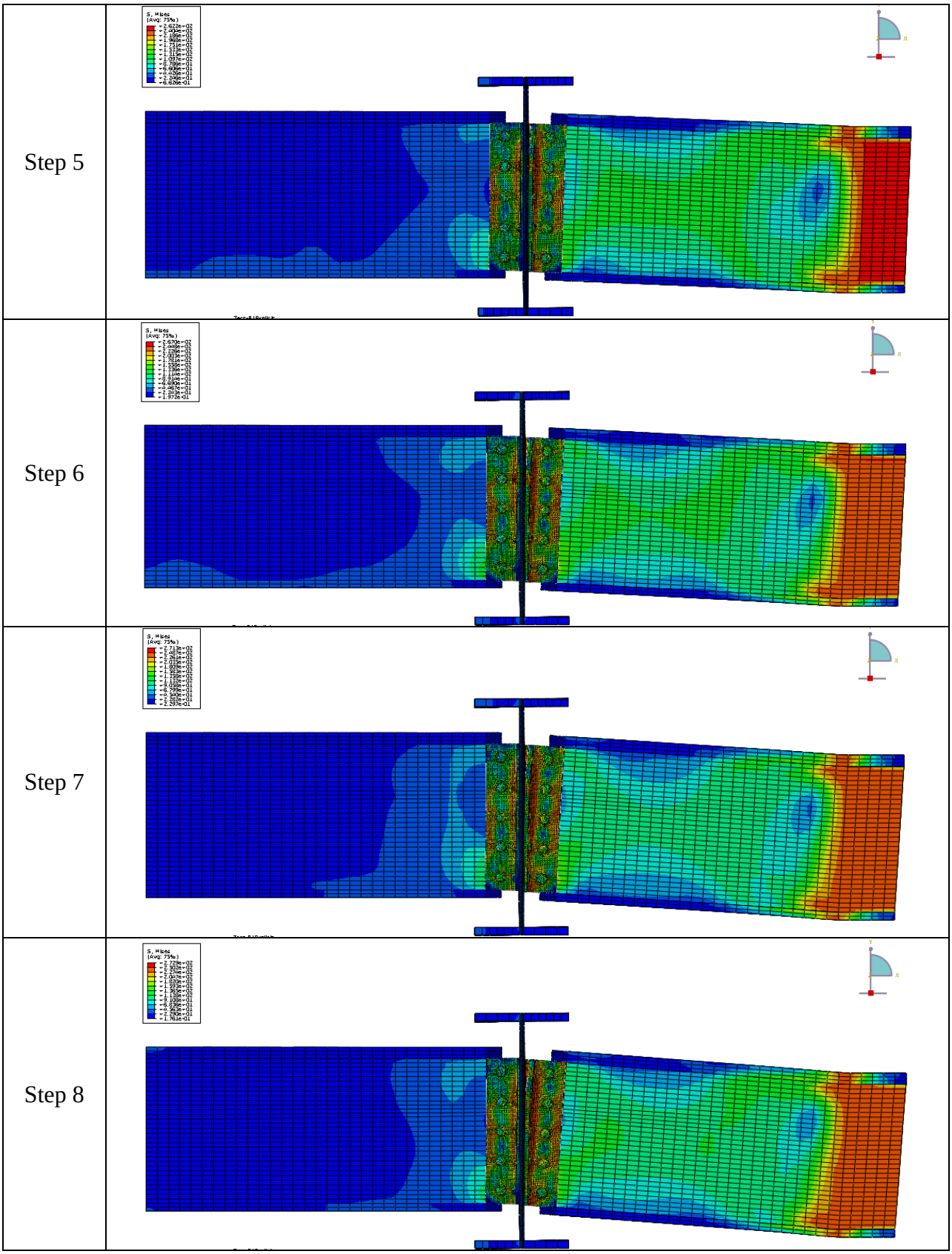

Figure C.5 cont. Stress Distribution on the Connection under Applied Load – General View

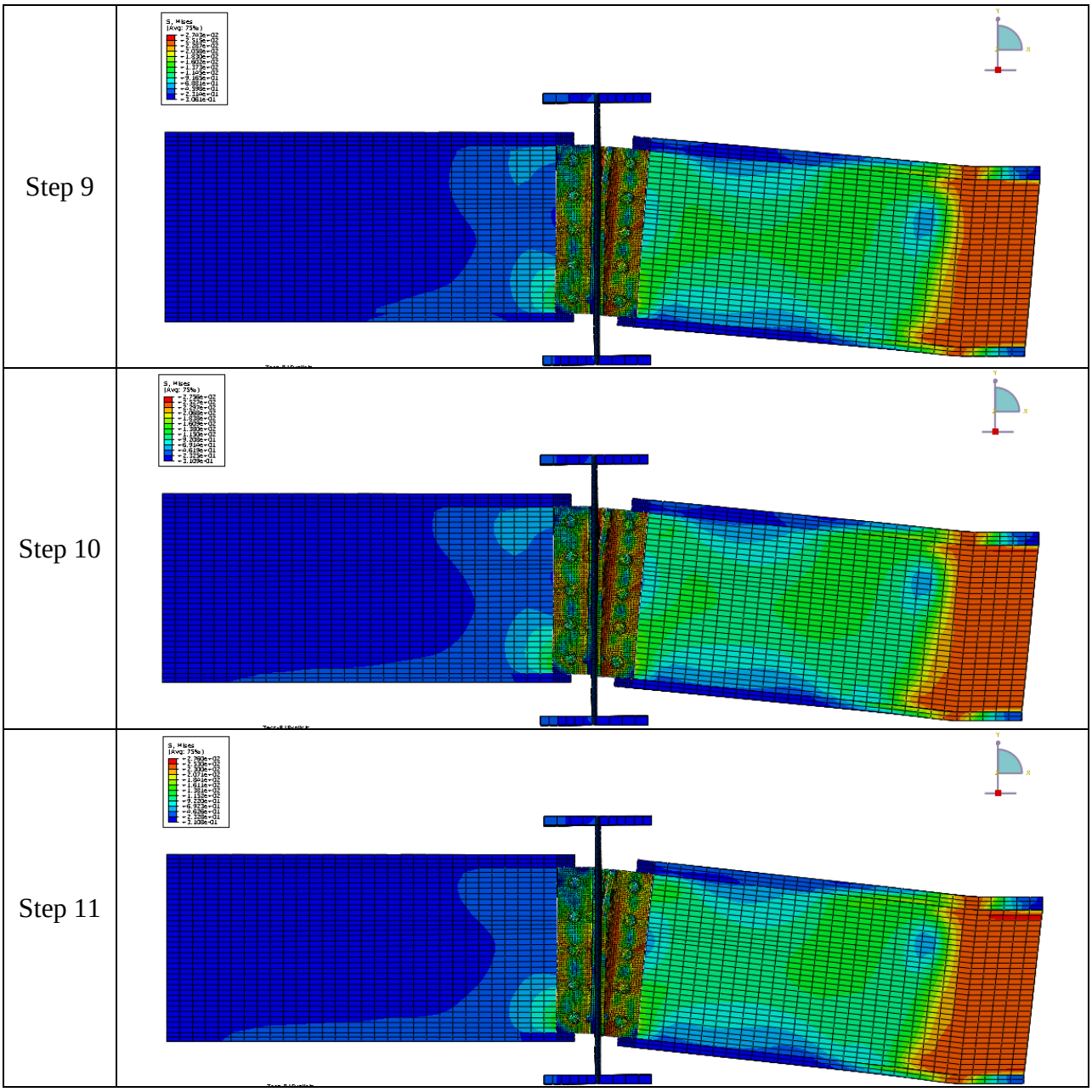

Figure C.5 cont. Stress Distribution on the Connection under Applied Load – General View

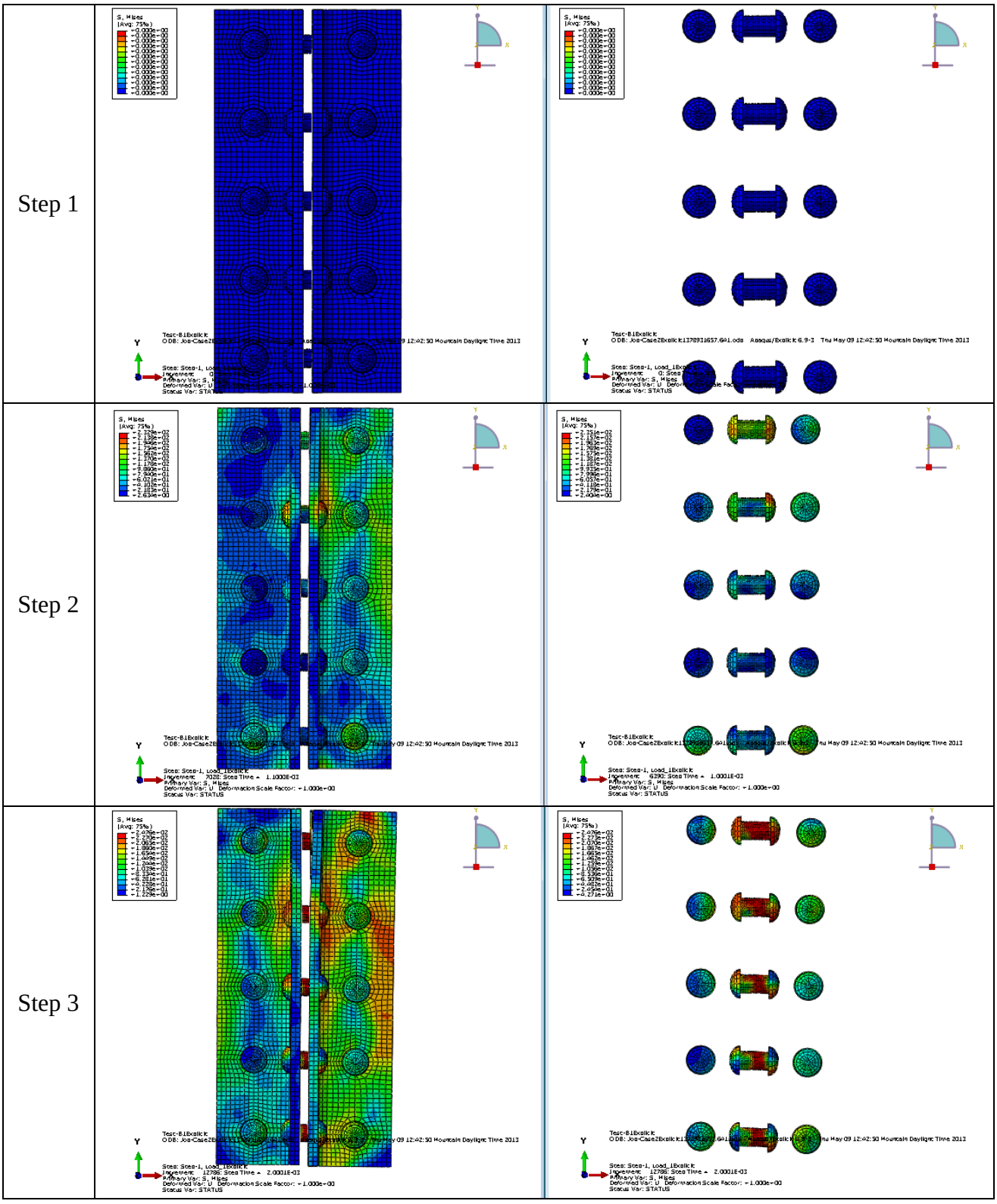

Figure C.6 Stress Distribution on the Connection under Applied Load – Side View

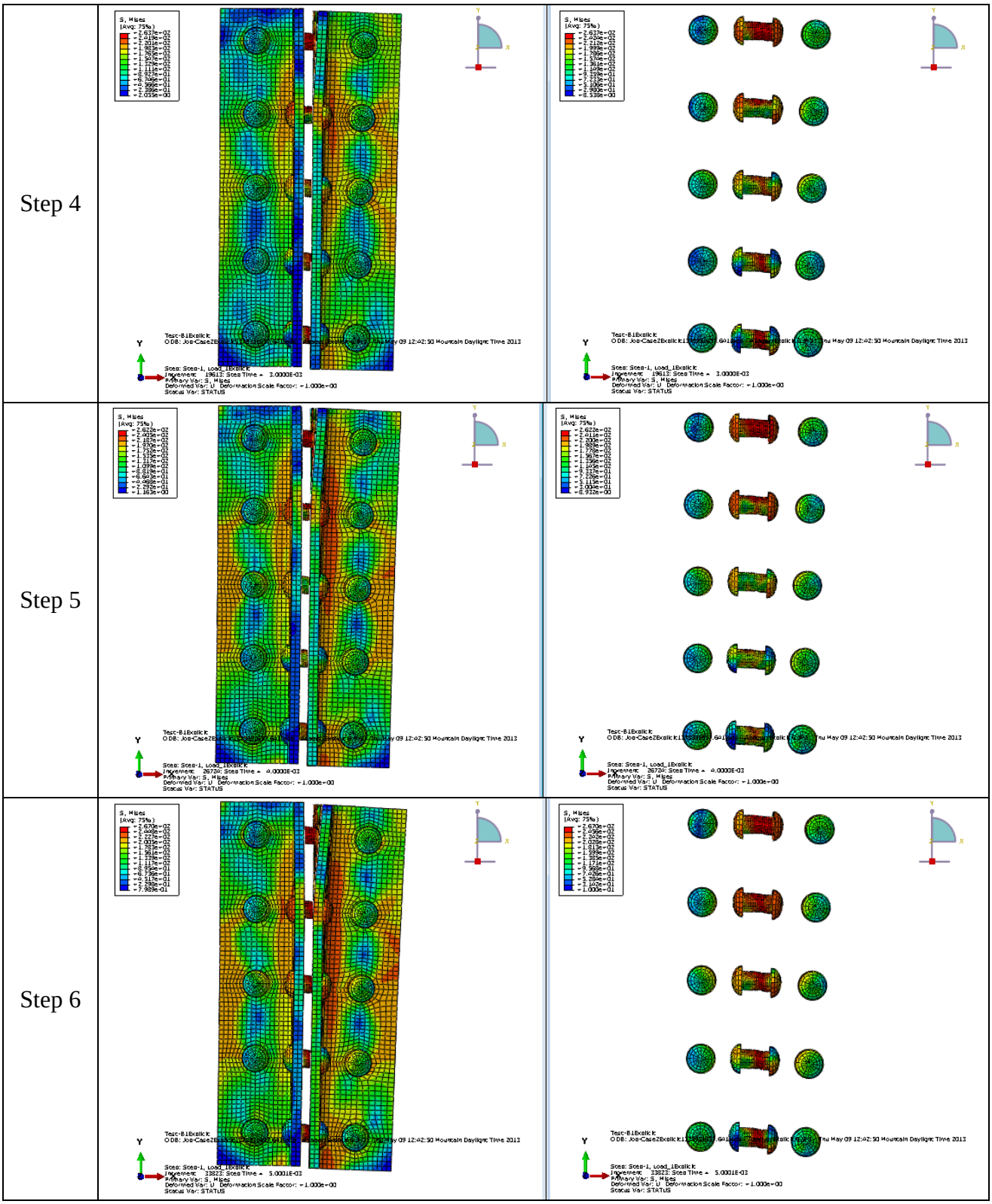

Figure C.6 cont. Stress Distribution on the Connection under Applied Load – Side View

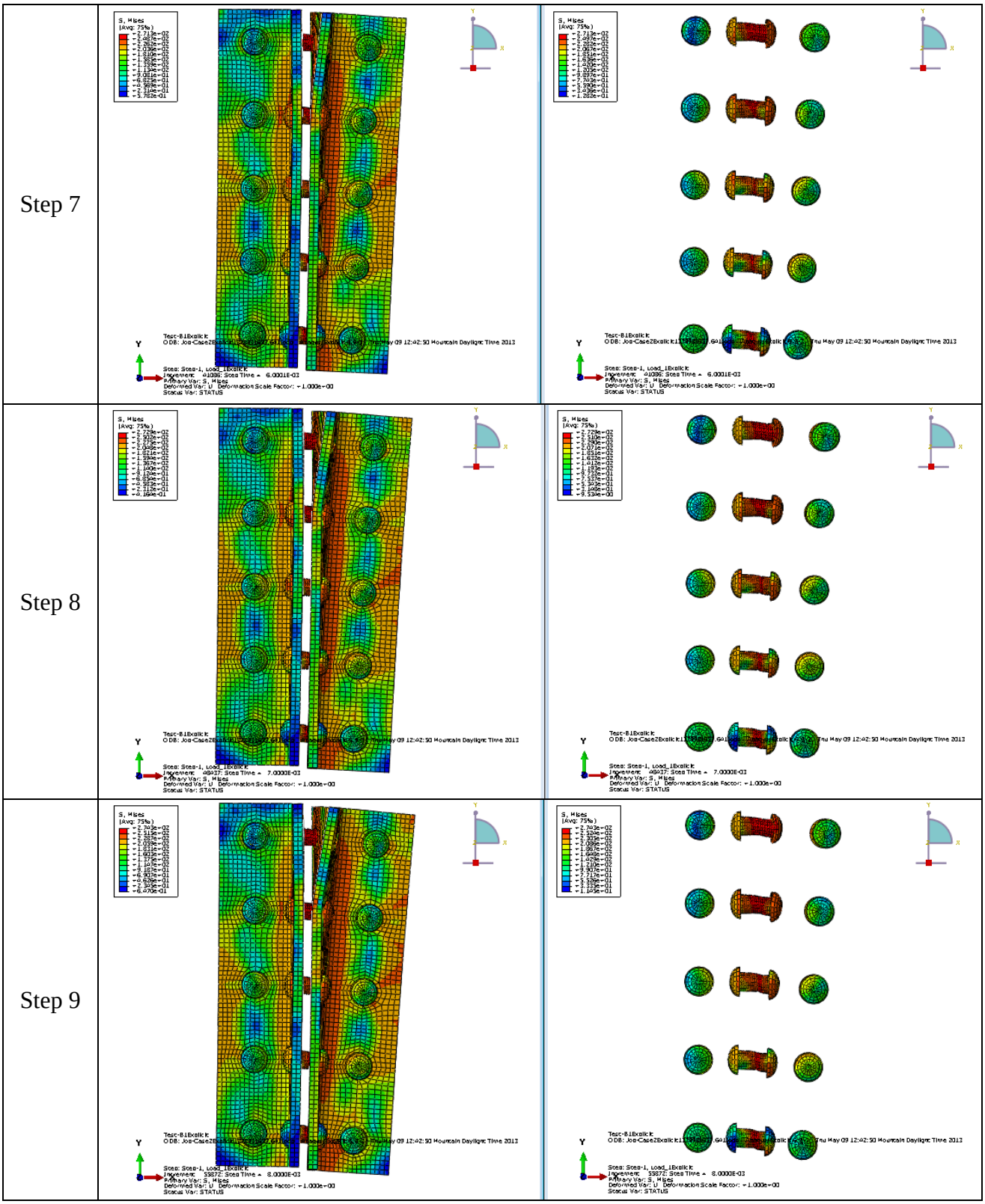

Figure C.6 cont. Stress Distribution on the Connection under Applied Load – Side View

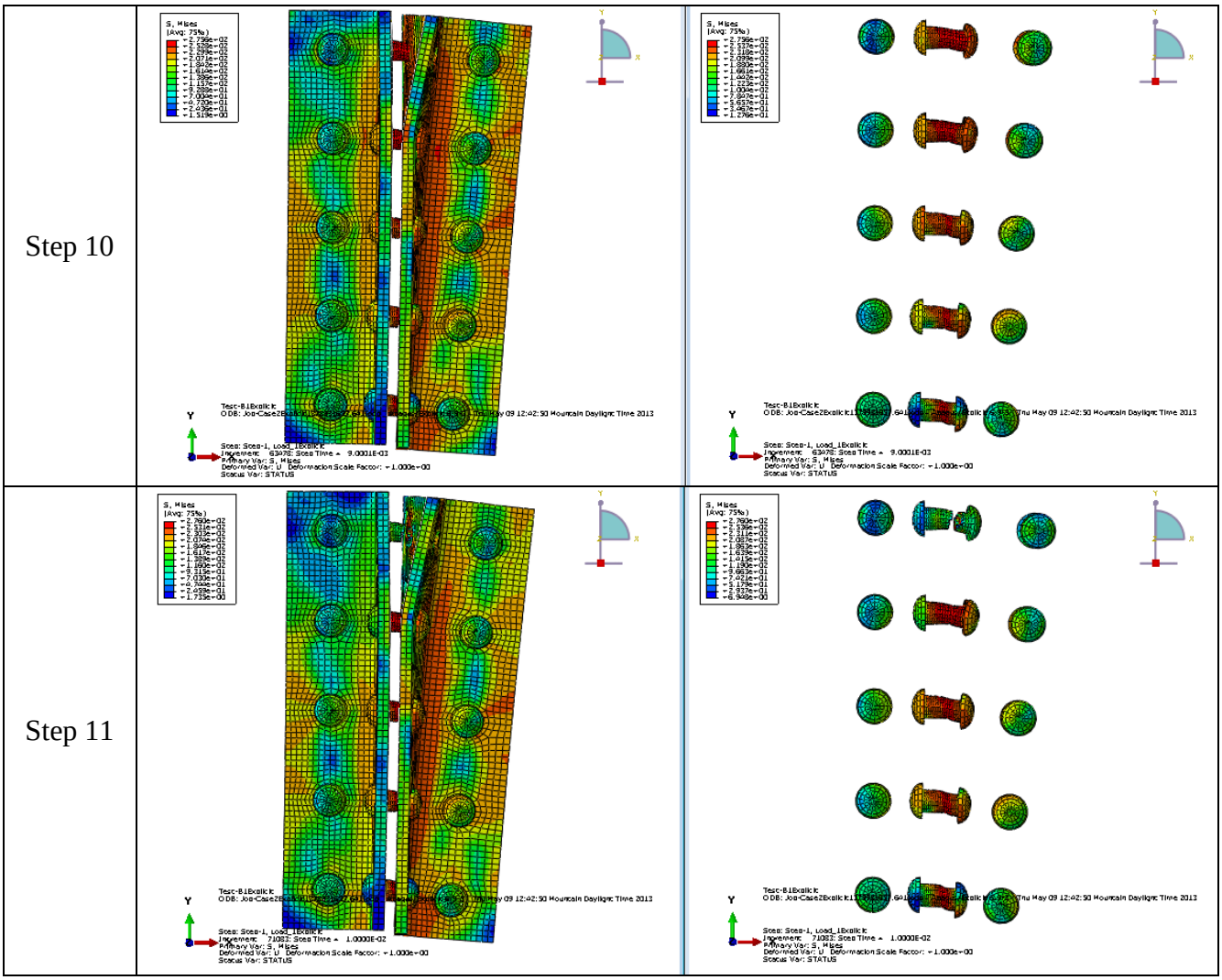

Figure C.6 cont. Stress Distribution on the Connection under Applied Load – Side View

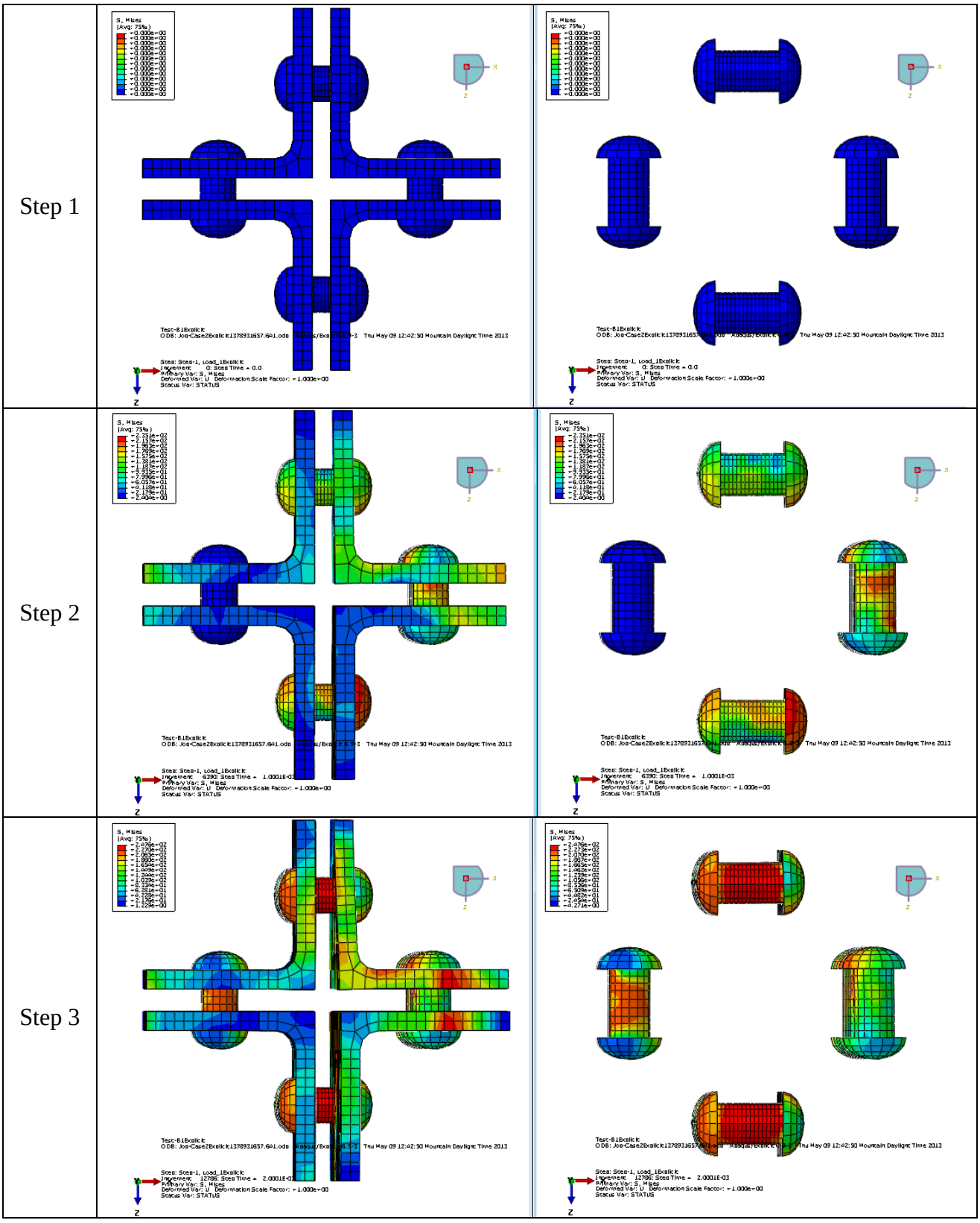

Figure C.7 Stress Distribution on the Connection under Applied Load – Top View

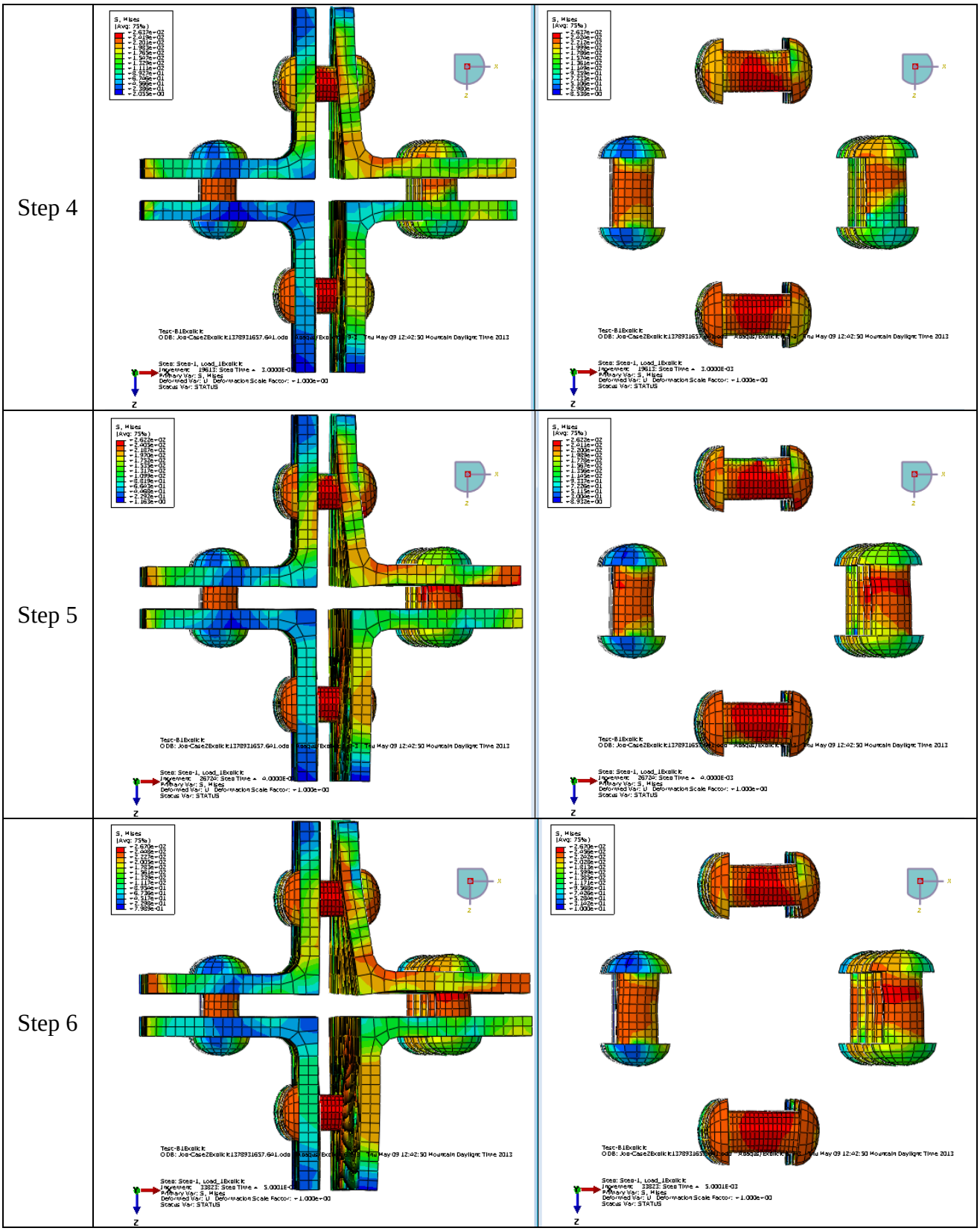

Figure C.7 cont. Stress Distribution on the Connection under Applied Load – Top View

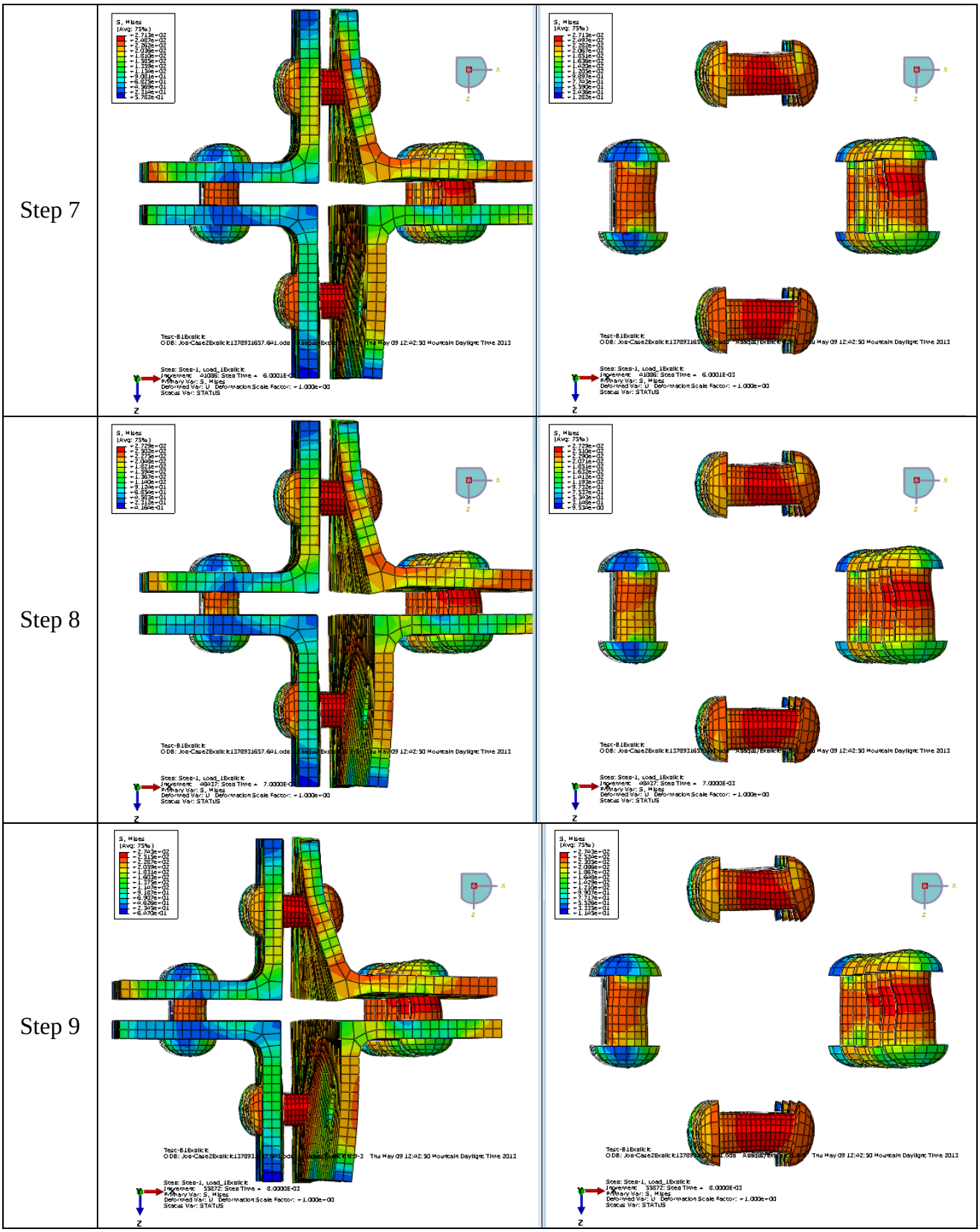

Figure C.7 cont. Stress Distribution on the Connection under Applied Load – Top View

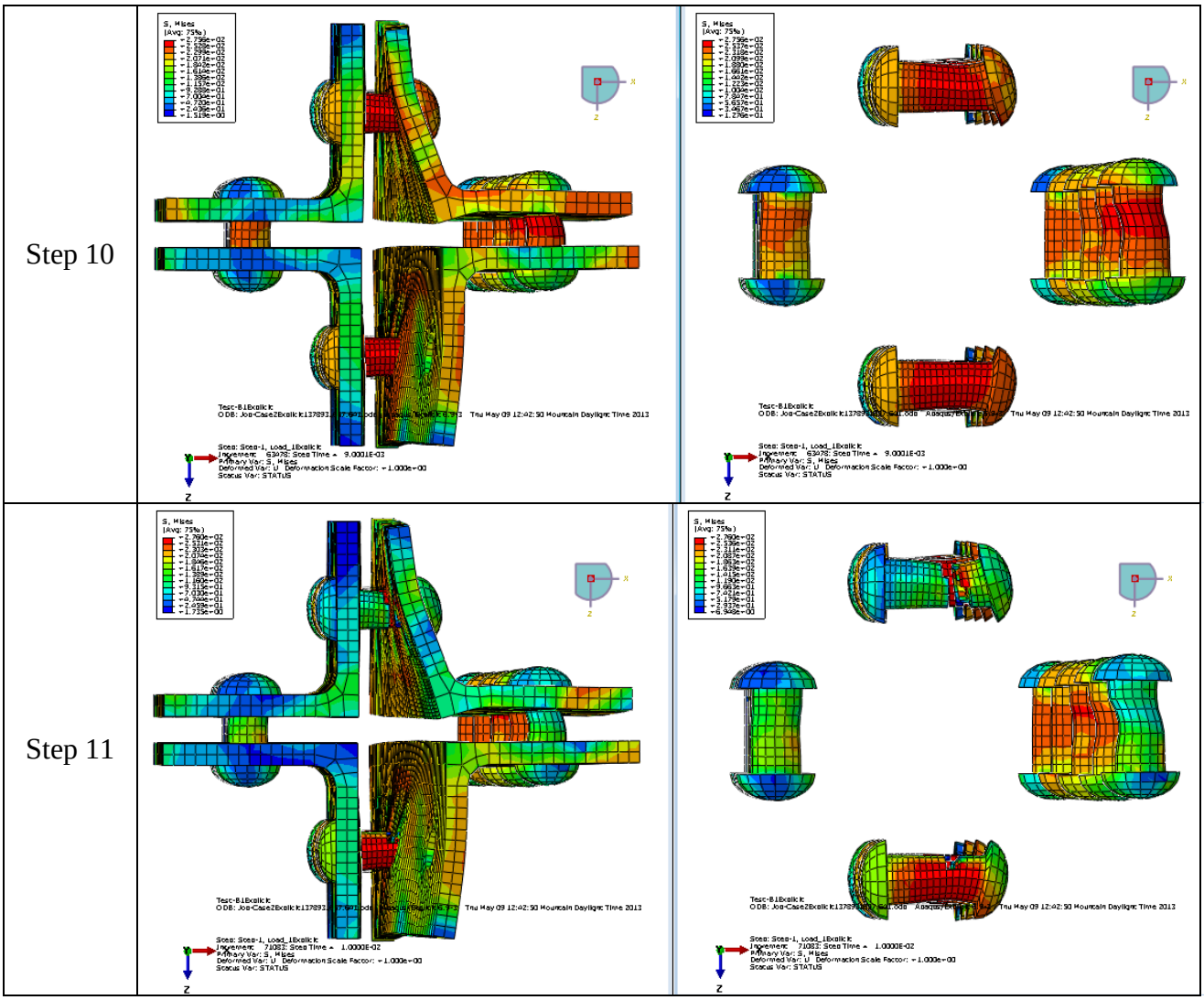

Figure C.7 cont. Stress Distribution on the Connection under Applied Load – Top View

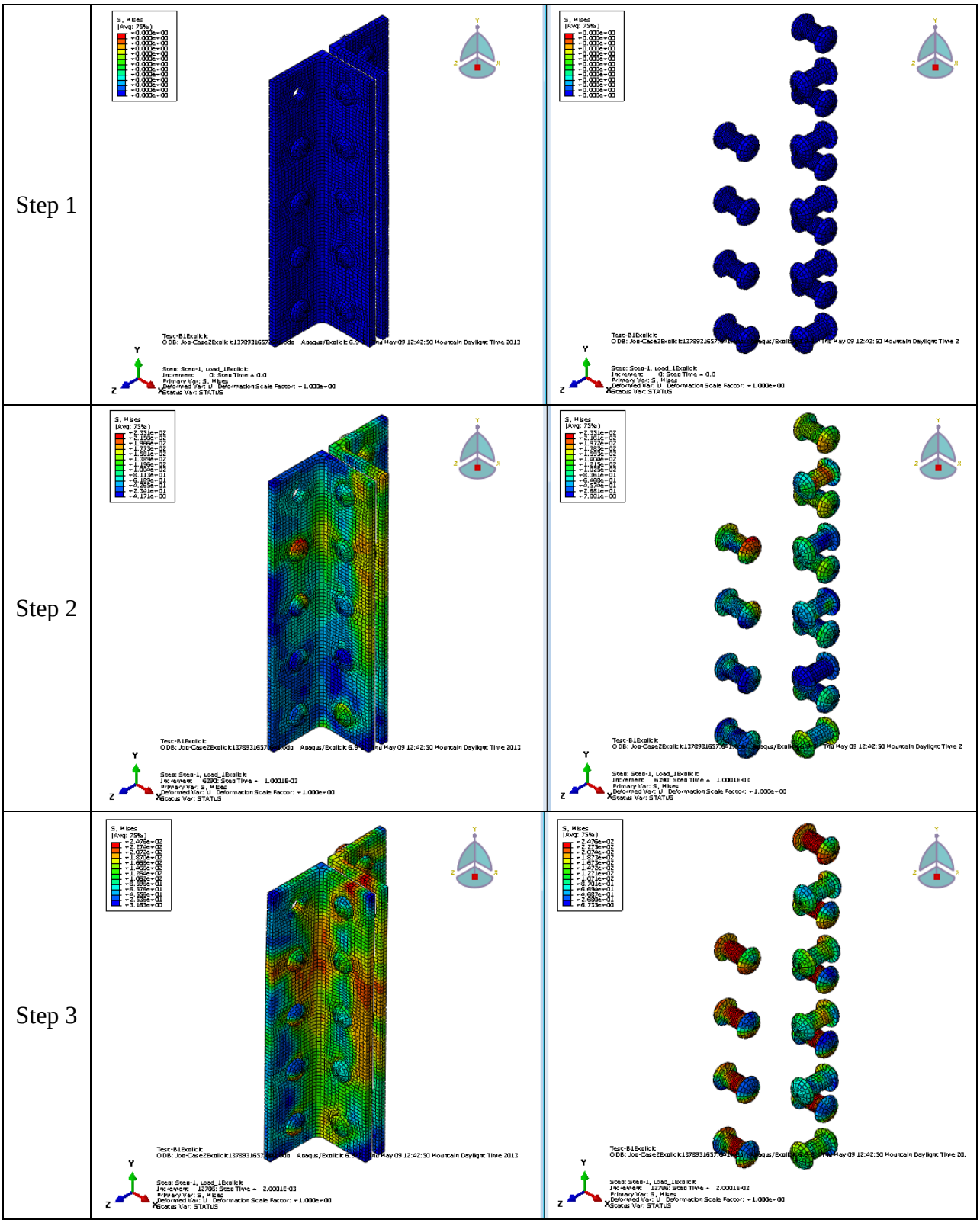

Figure C.8 Stress Distribution on the Connection under Applied Load – Isometric View

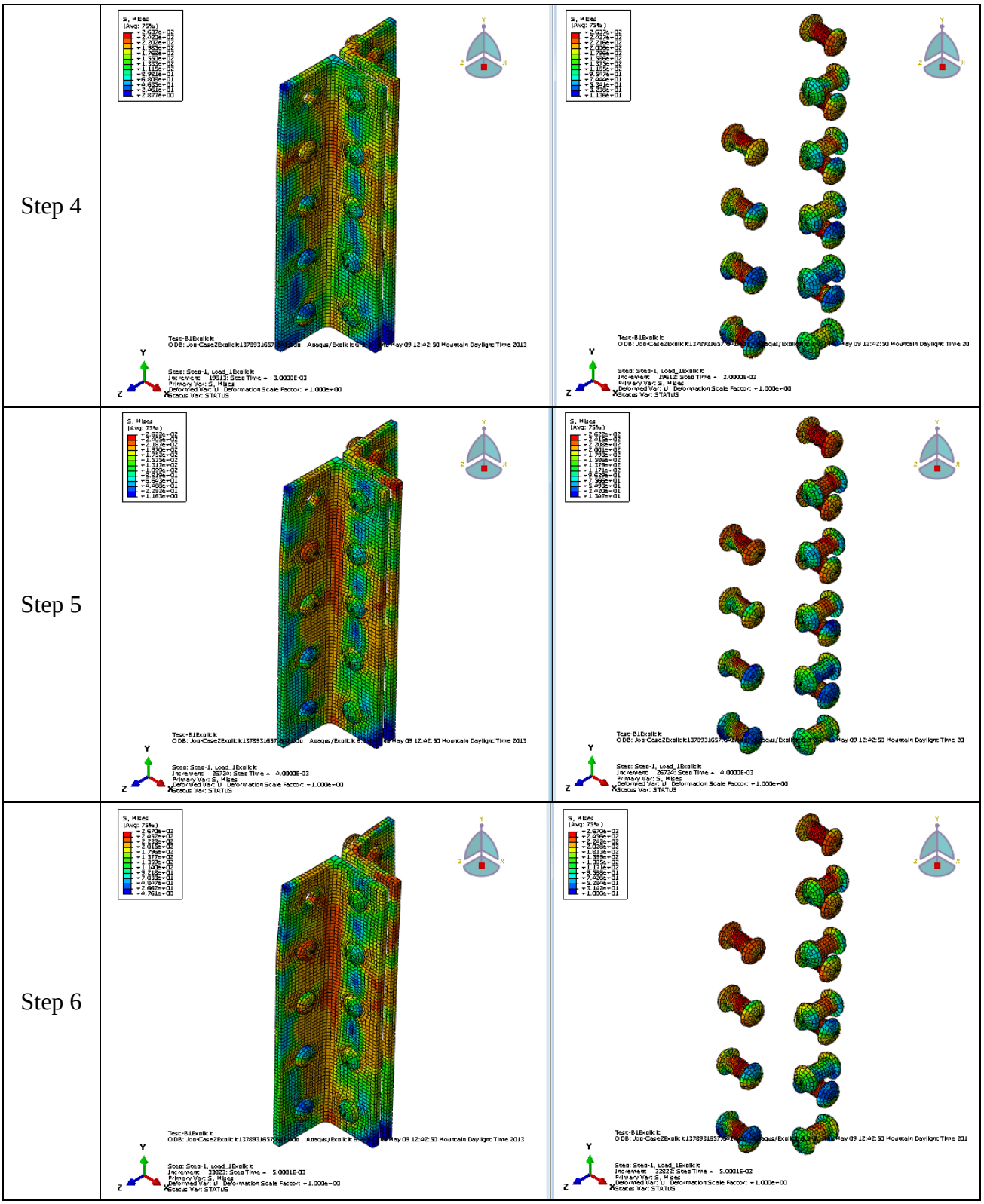

Figure C.8 cont. Stress Distribution on the Connection under Applied Load – Isometric View

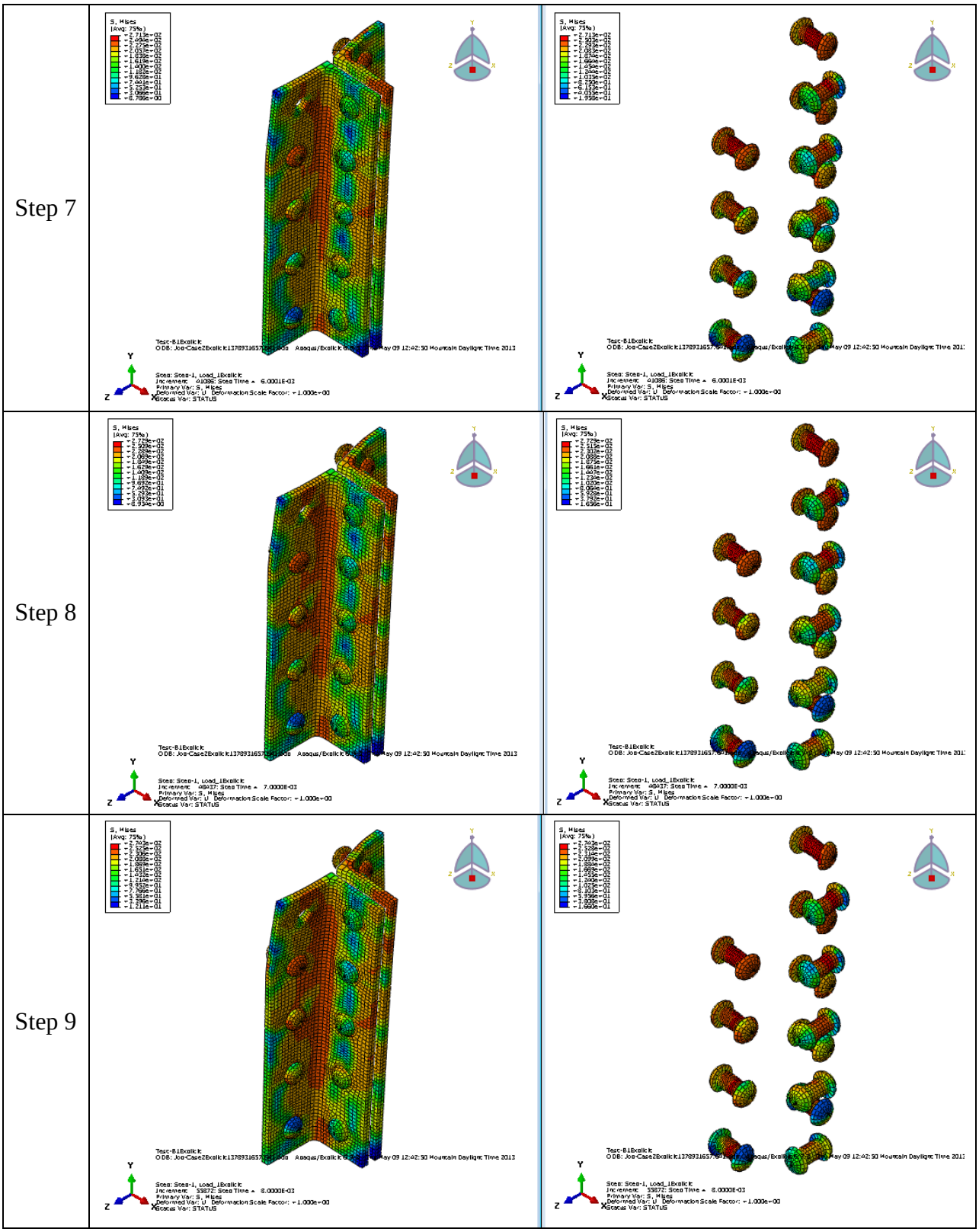

Figure C.8 cont. Stress Distribution on the Connection under Applied Load – Isometric View

Step 10	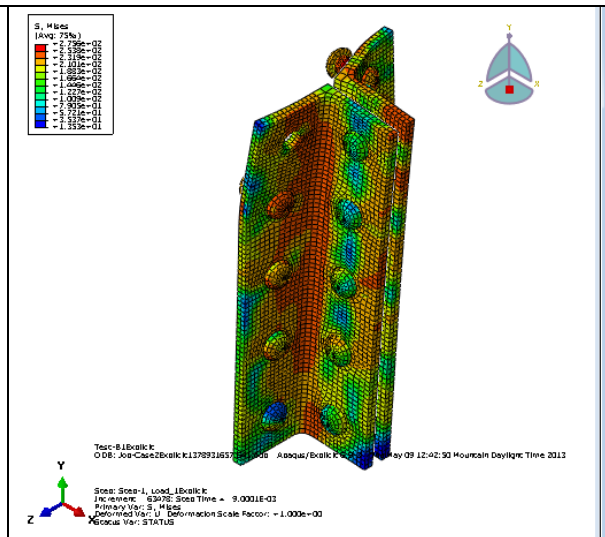	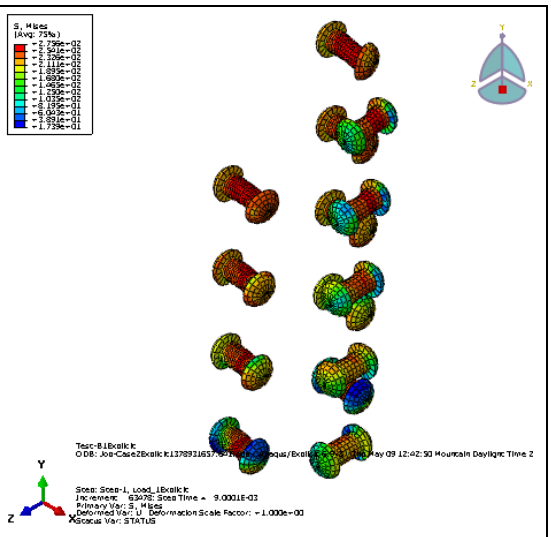
Step 11	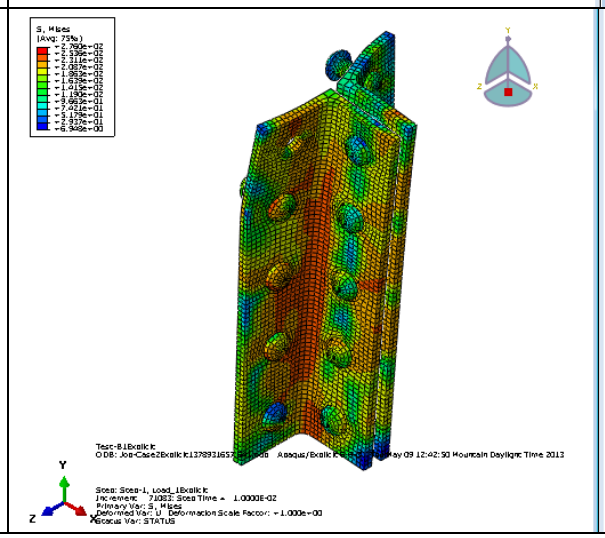	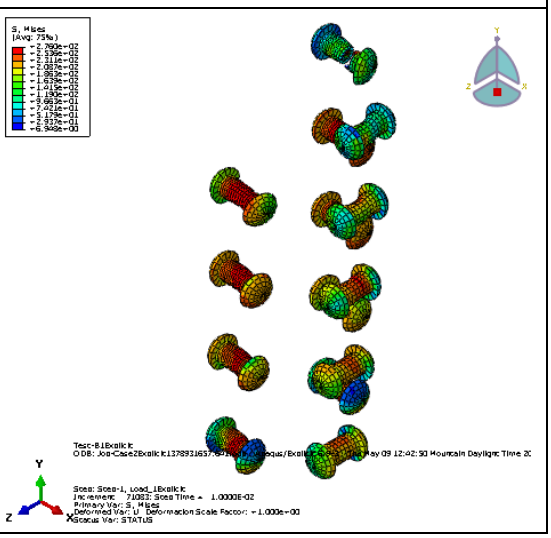

Figure C.8 cont. Stress Distribution on the Connection under Applied Load – Isometric View

Appendix D Results of FEA for Connection with Two Missing Upper Bolts on the Crossbeam

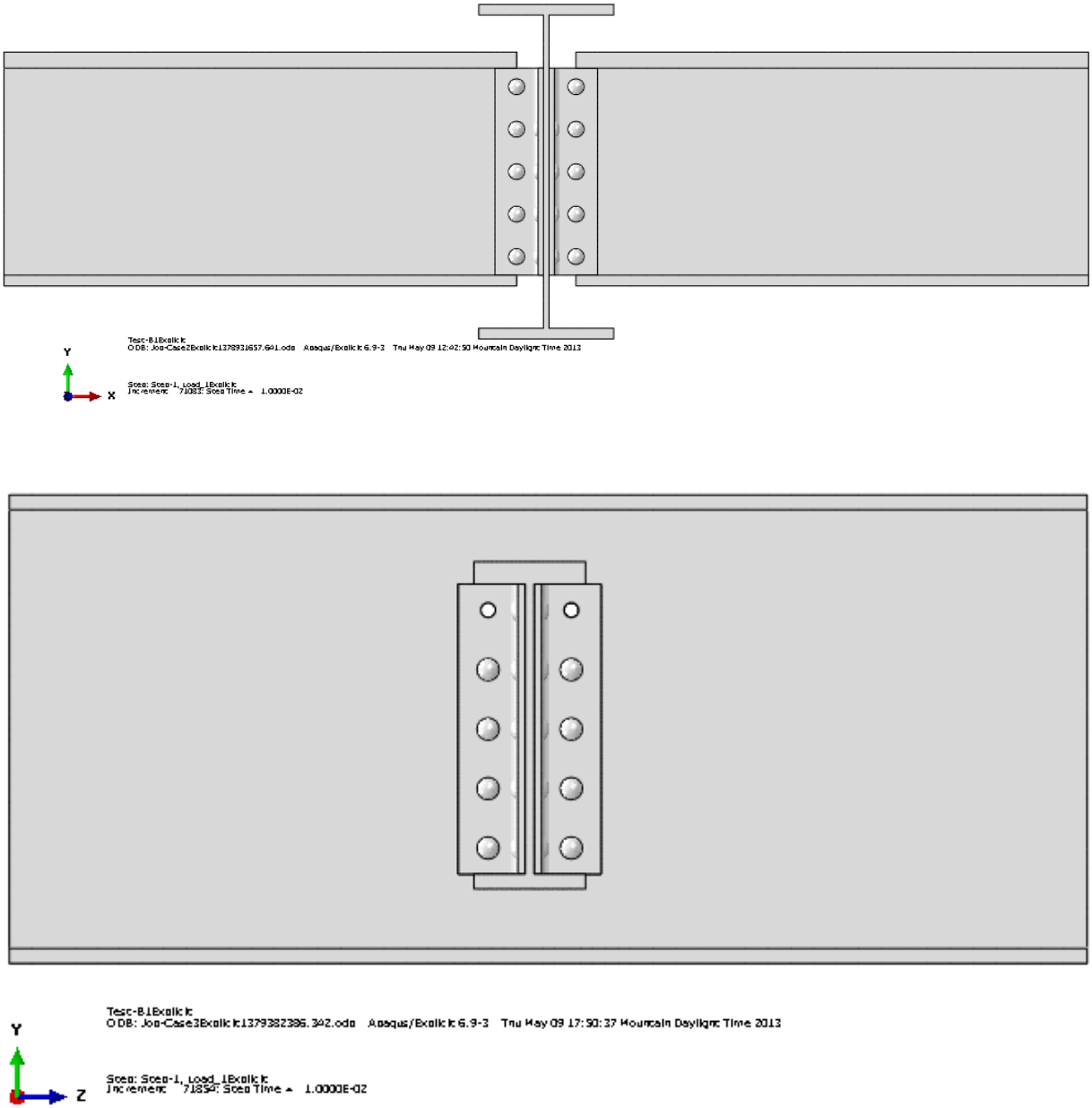

Figure D.1 Detailed View of Undamaged Connection

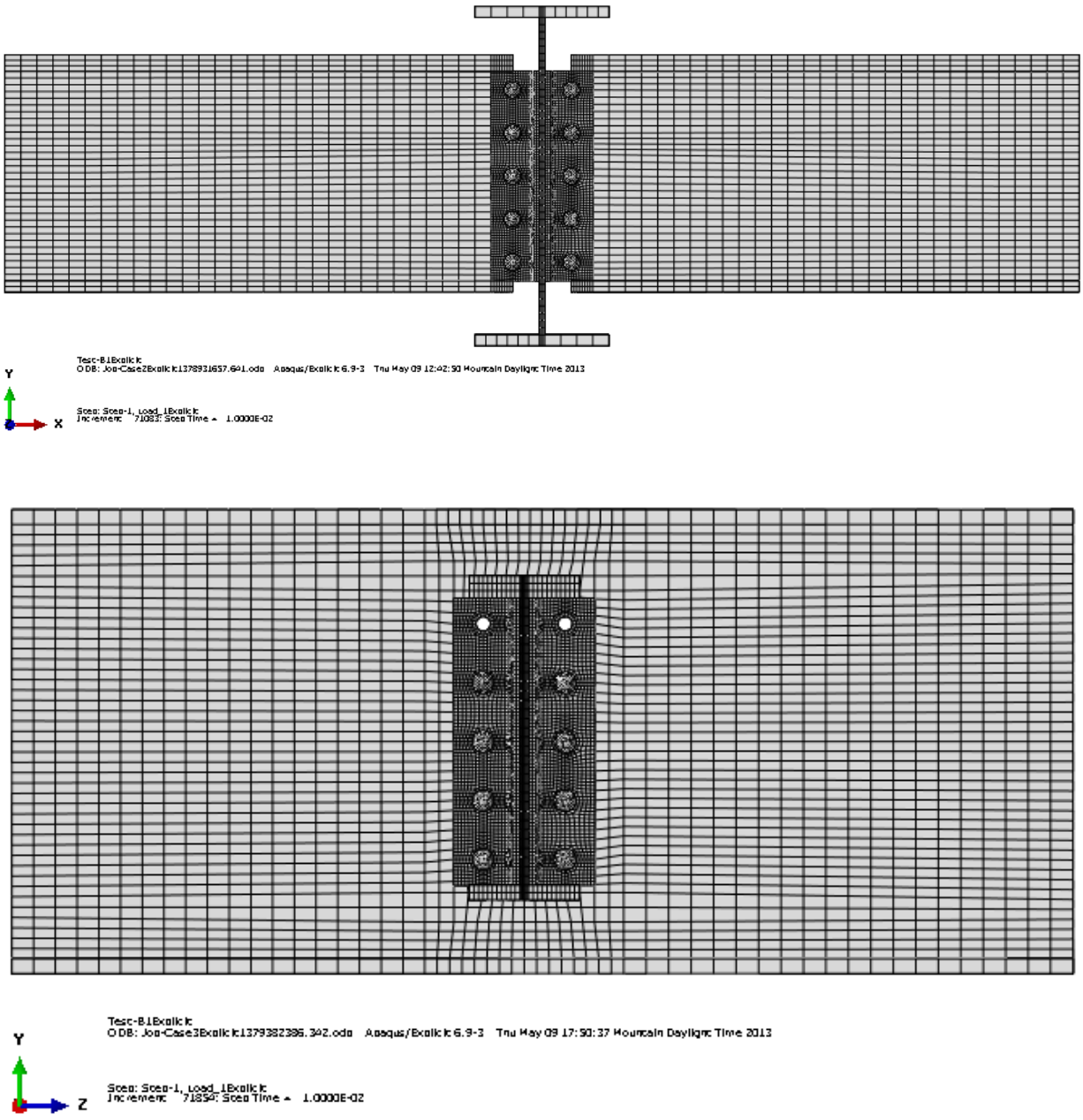

Figure D.2 Mesh of Undamaged Connection

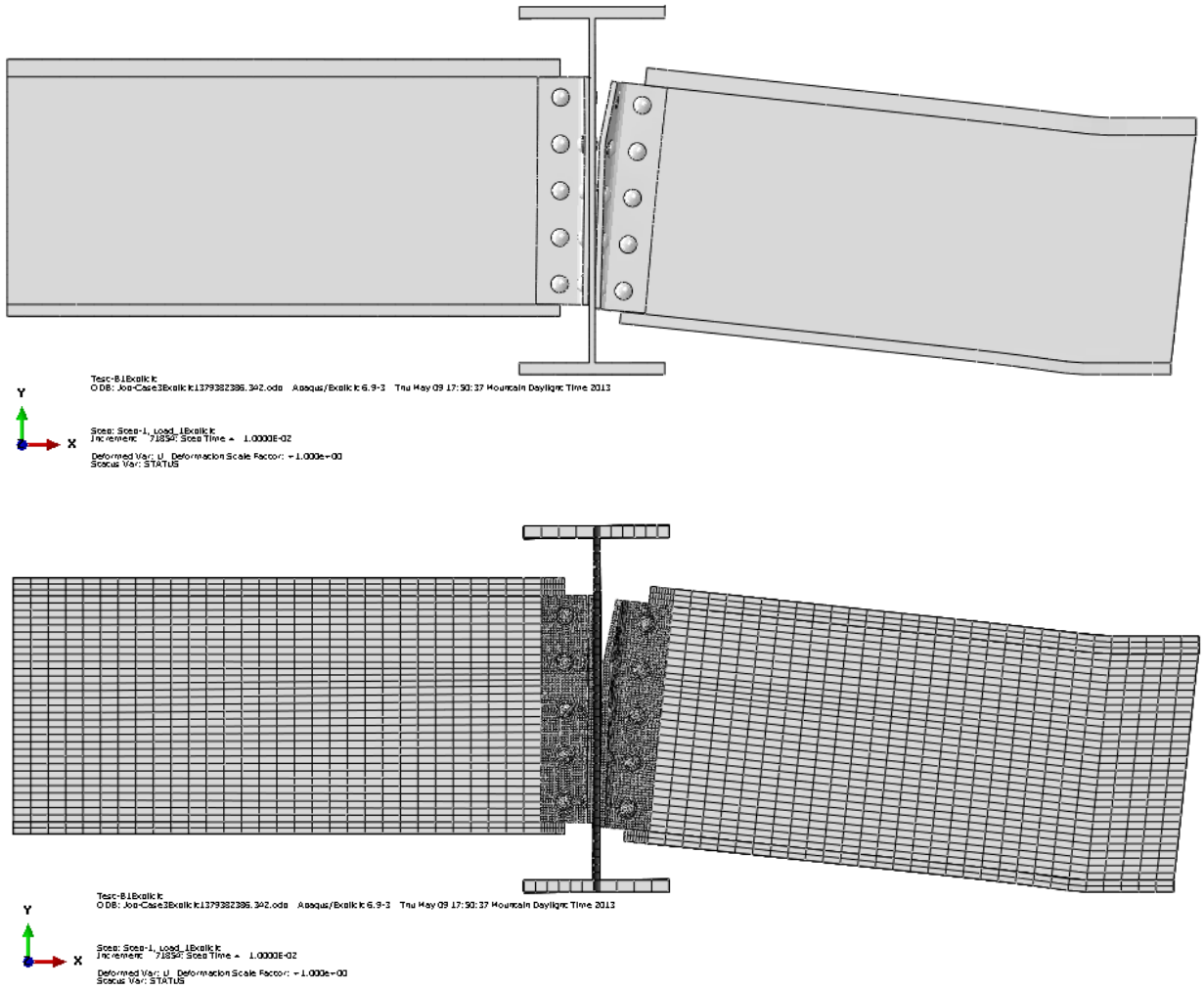

Figure D.3 Deformation after Applied Load – Side View

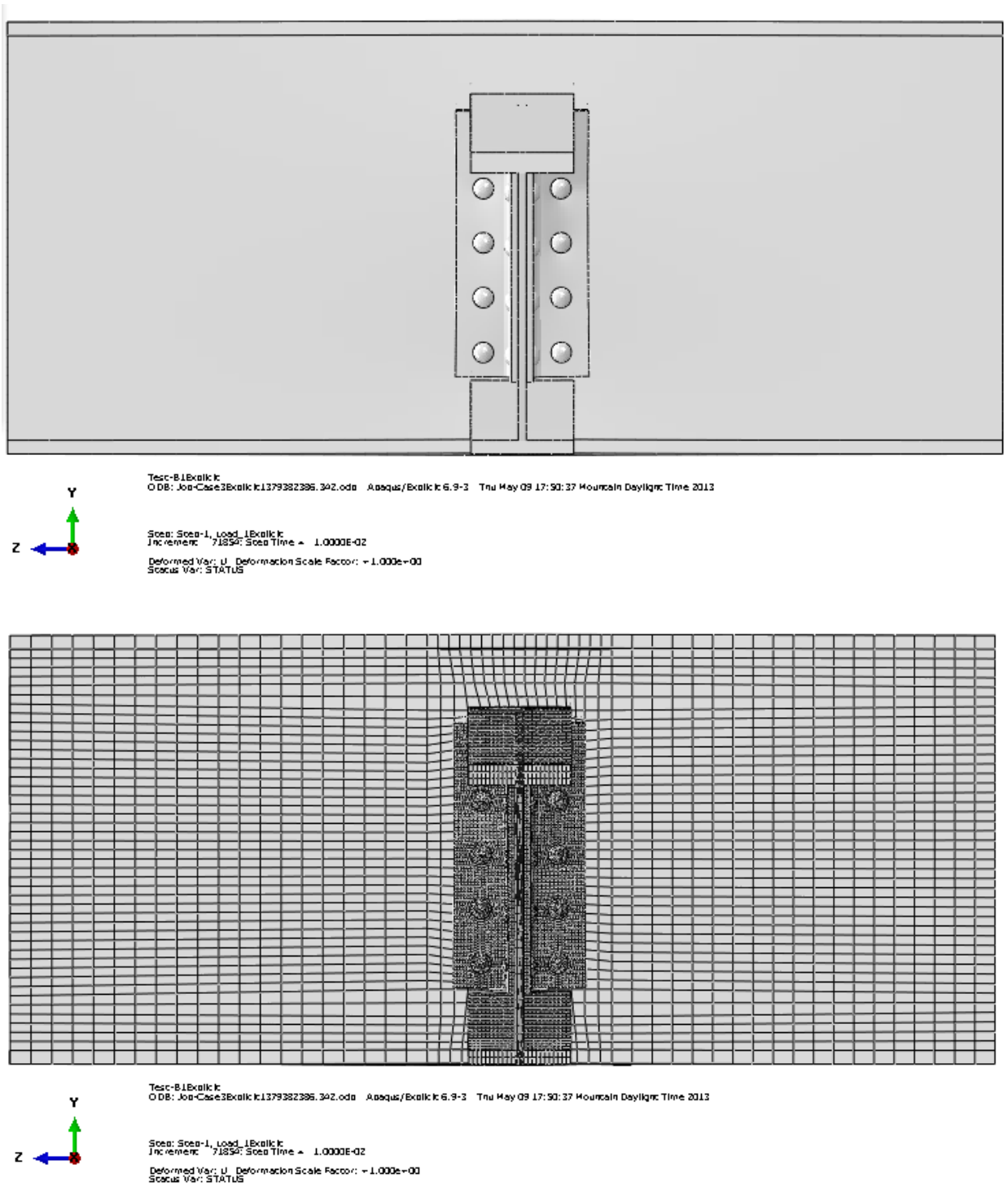

Figure D.4 Deformation after Applied Load – Front View

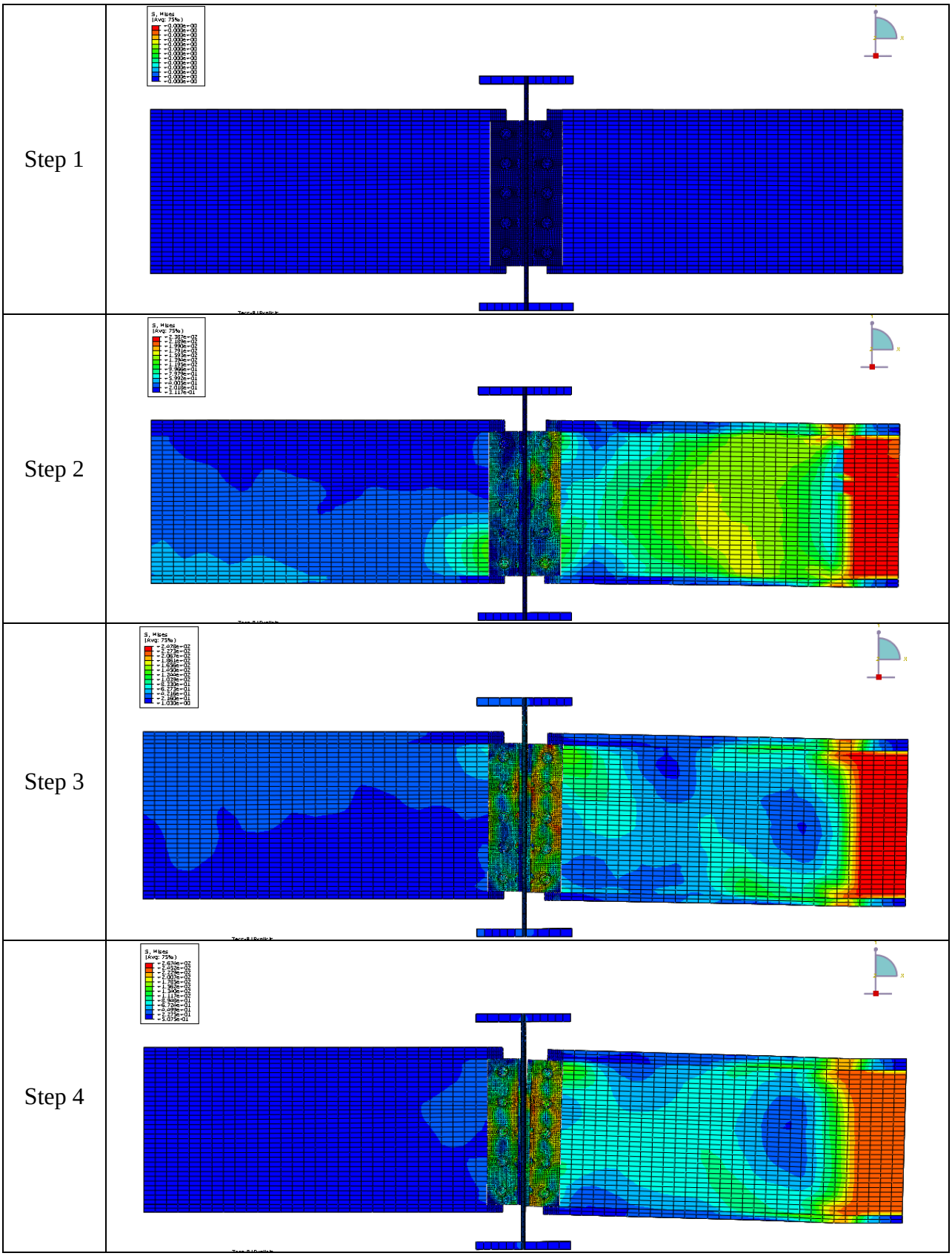

Figure D.5 Stress Distribution on the Connection under Applied Load – General View

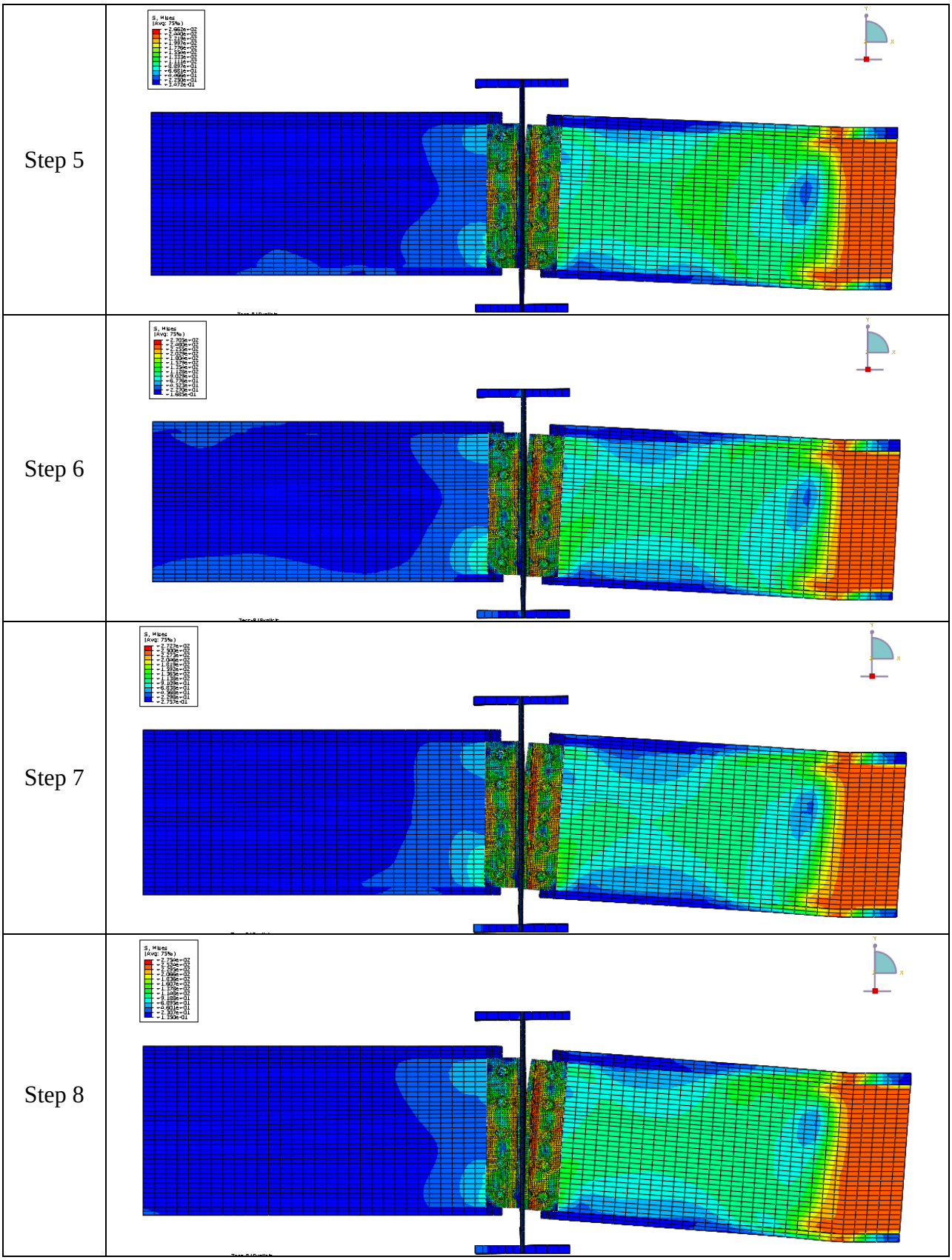

Figure D.5 cont. Stress Distribution on the Connection under Applied Load – General View

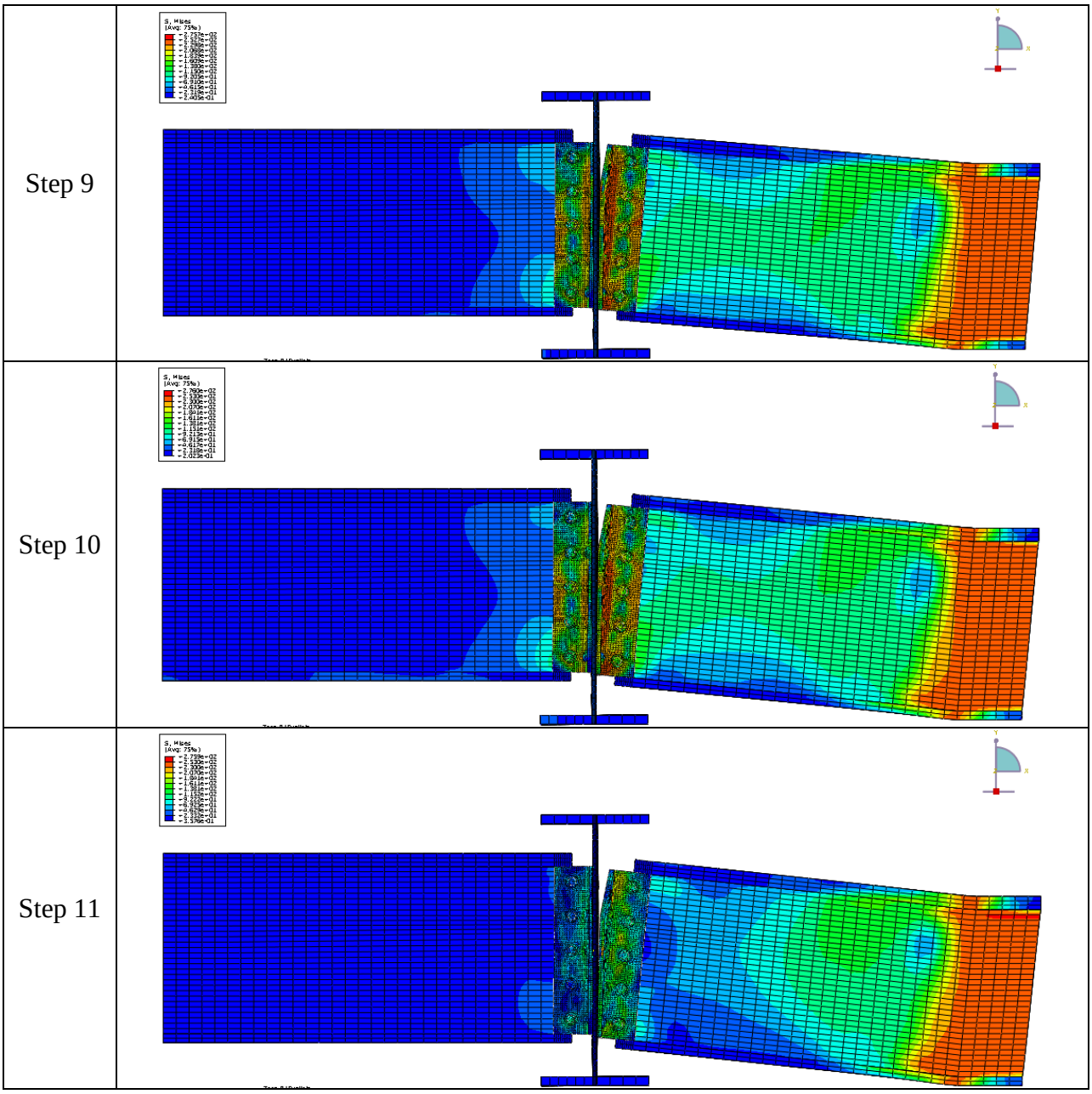

Figure D.5 cont. Stress Distribution on the Connection under Applied Load – General View

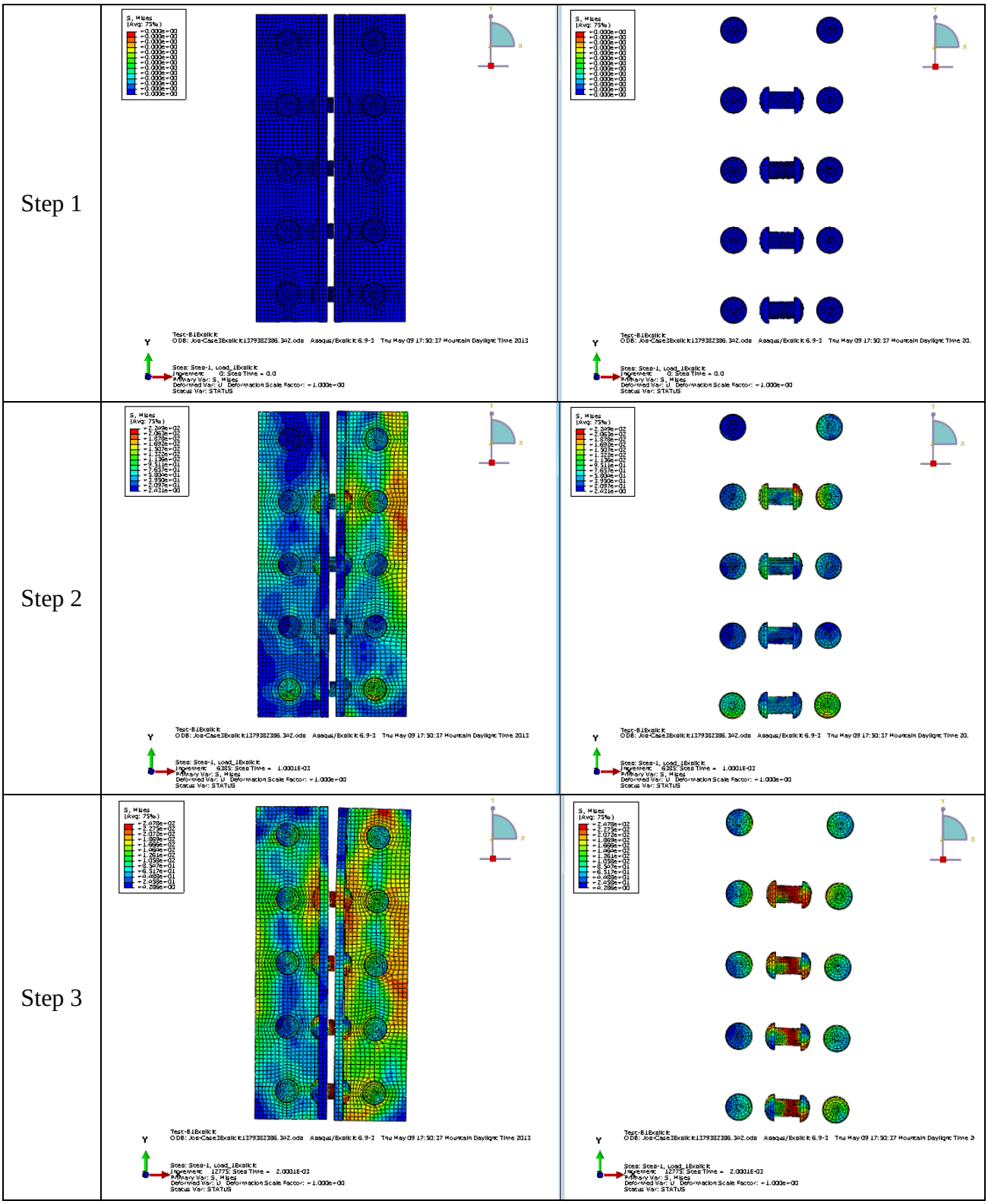

Figure D.6 Stress Distribution on the Connection under Applied Load – Side View

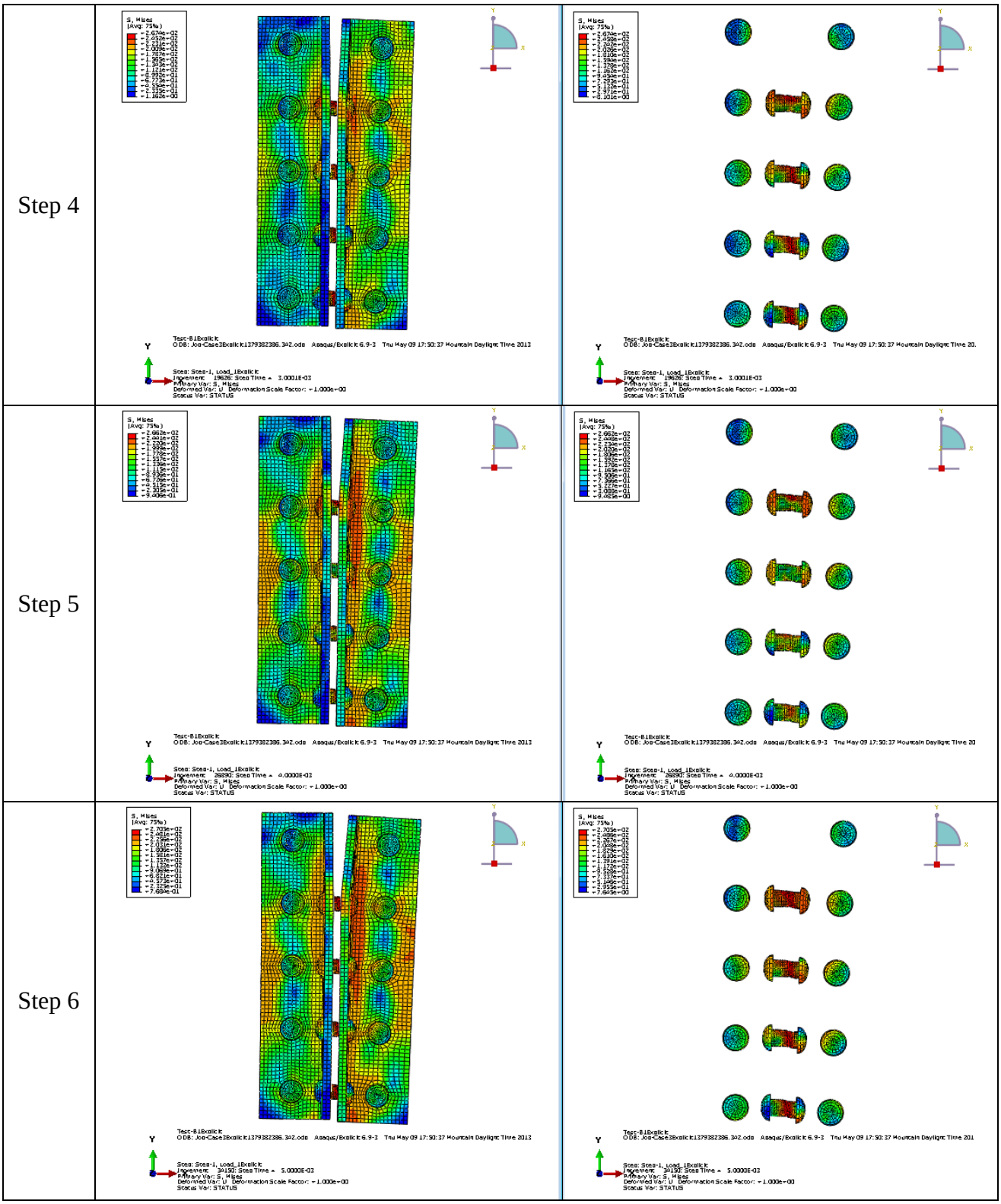

Figure C.6 cont. Stress Distribution on the Connection under Applied Load – Side View

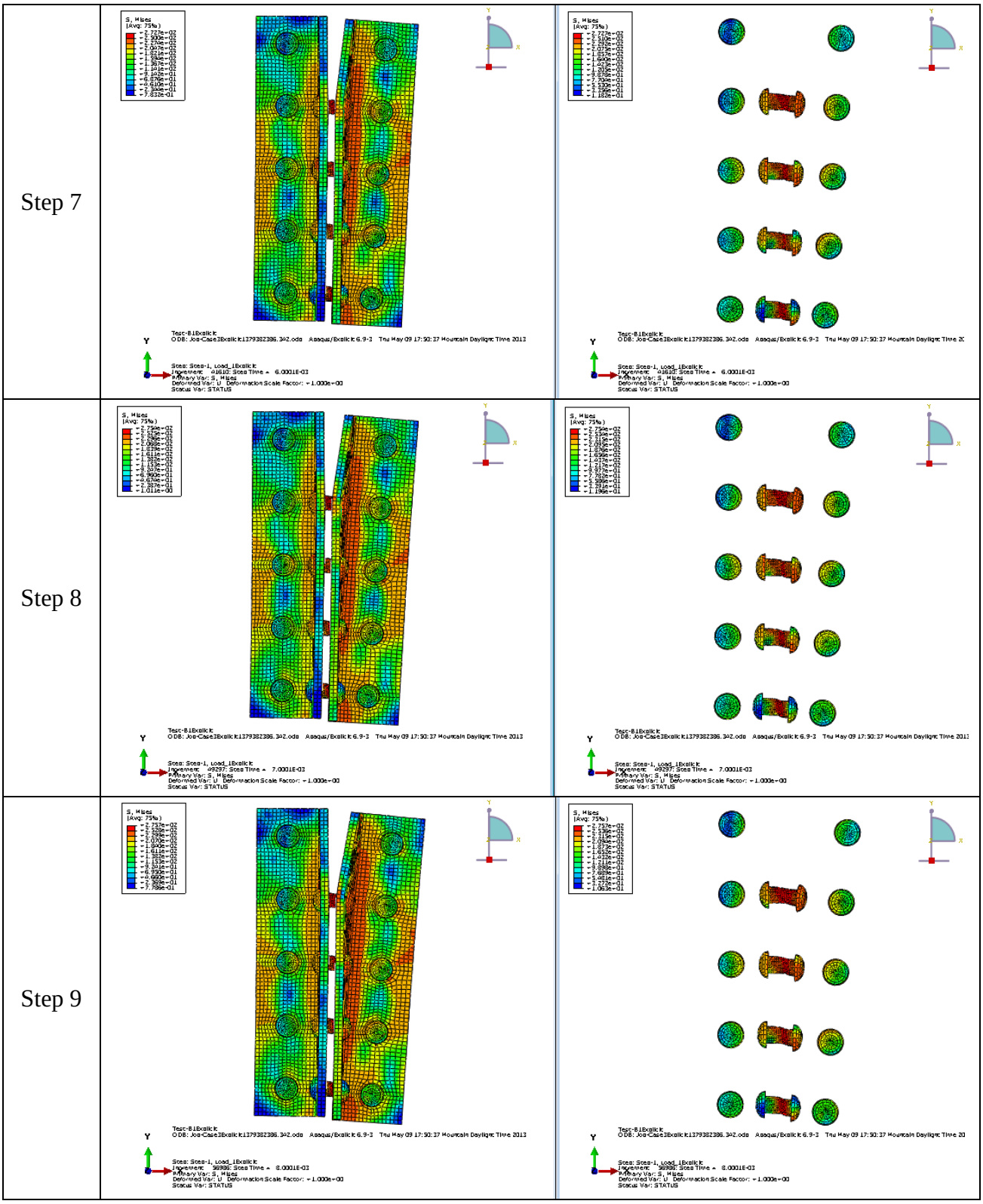

Figure D.6 cont. Stress Distribution on the Connection under Applied Load – Side View

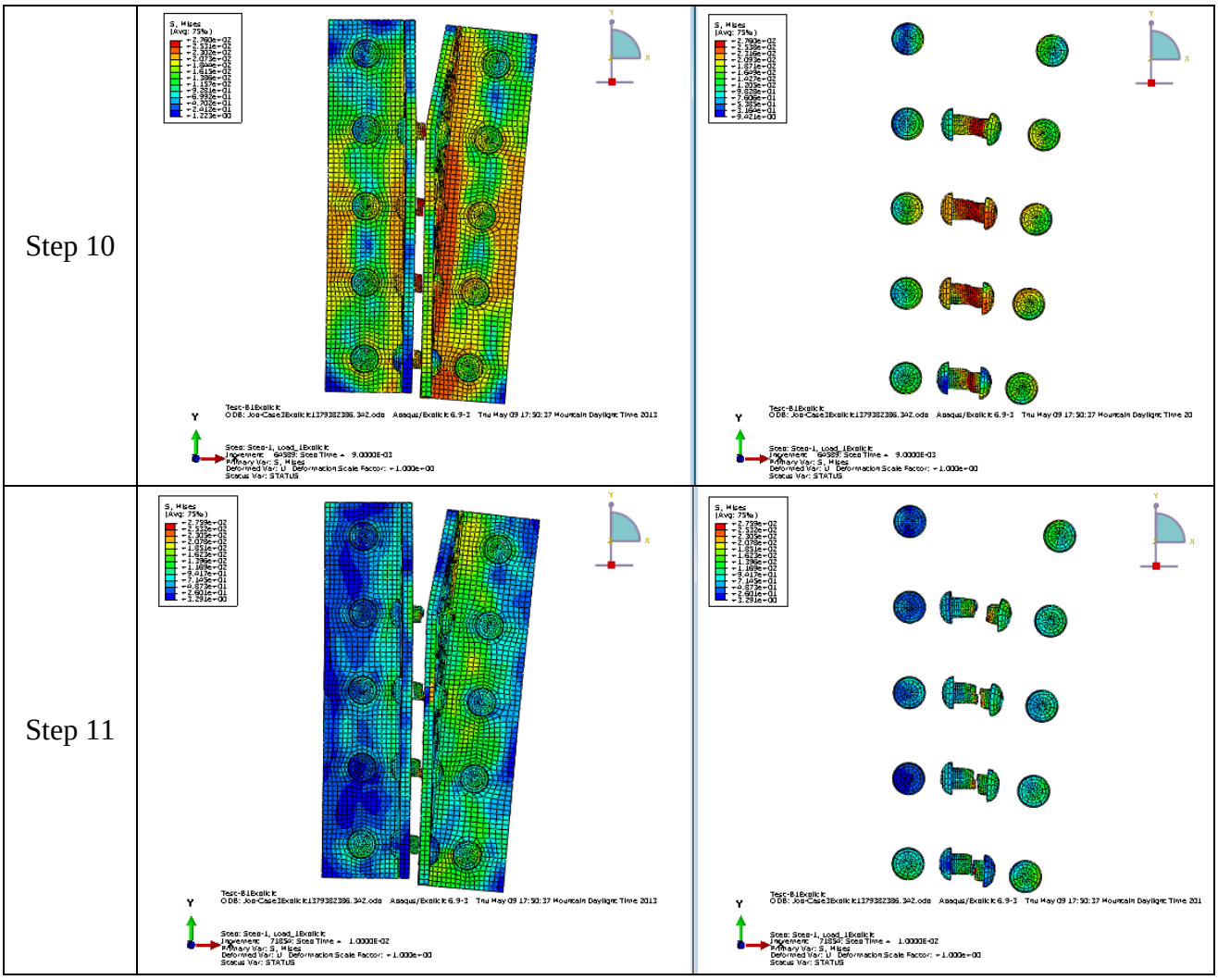

Figure D.6 cont. Stress Distribution on the Connection under Applied Load – Side View

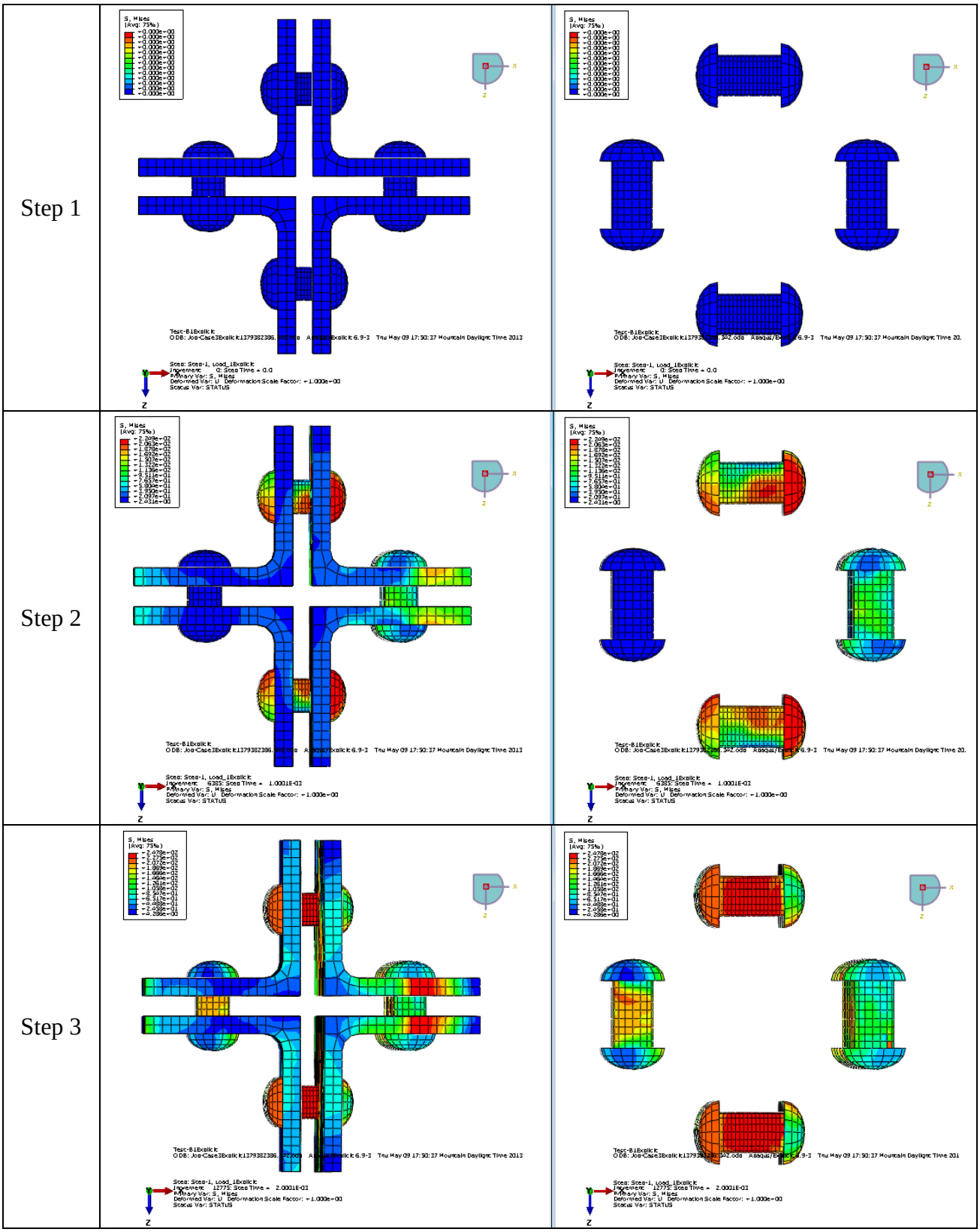

Figure D.7 Stress Distribution on the Connection under Applied Load – Top View

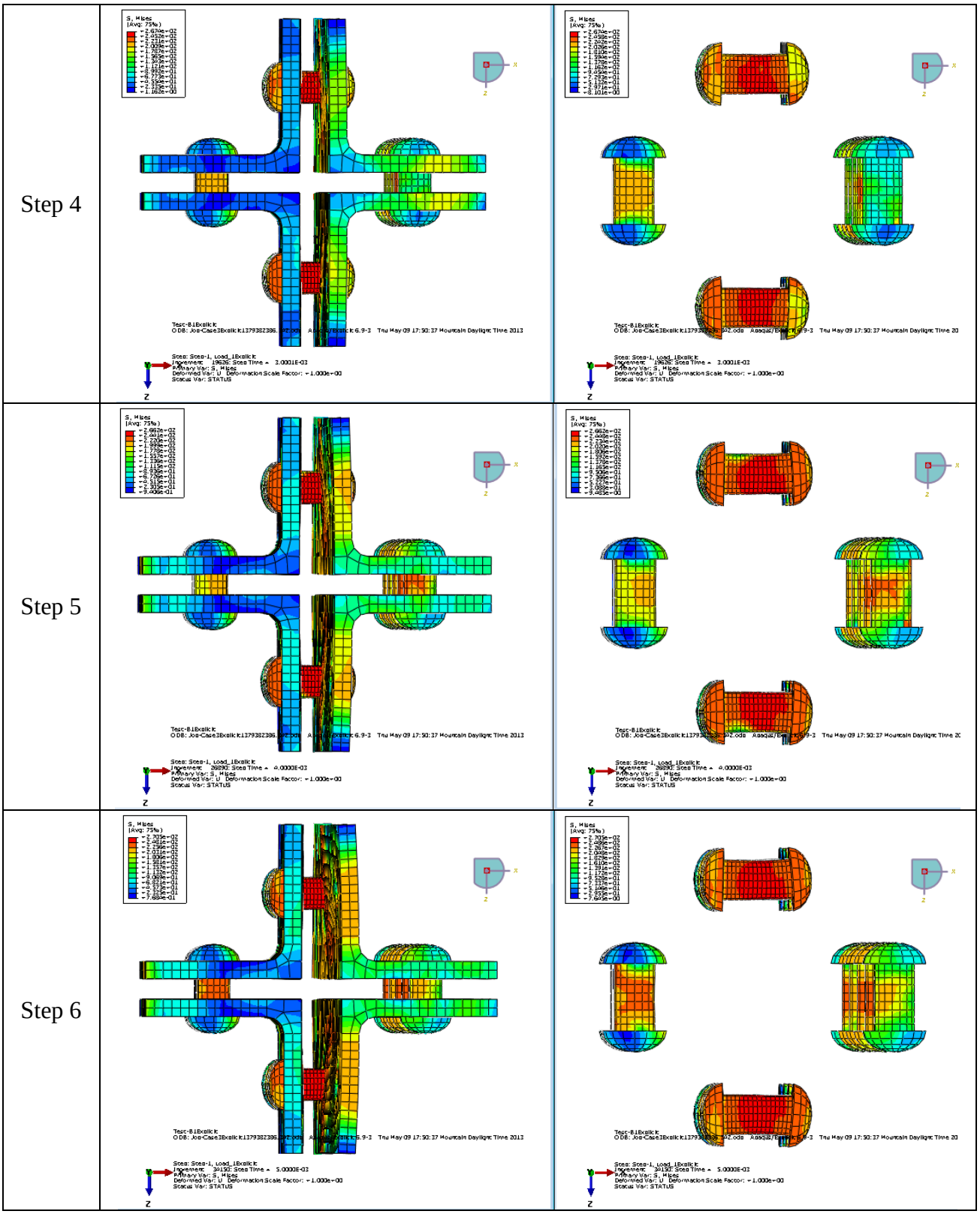

Figure D.7 cont. Stress Distribution on the Connection under Applied Load – Top View

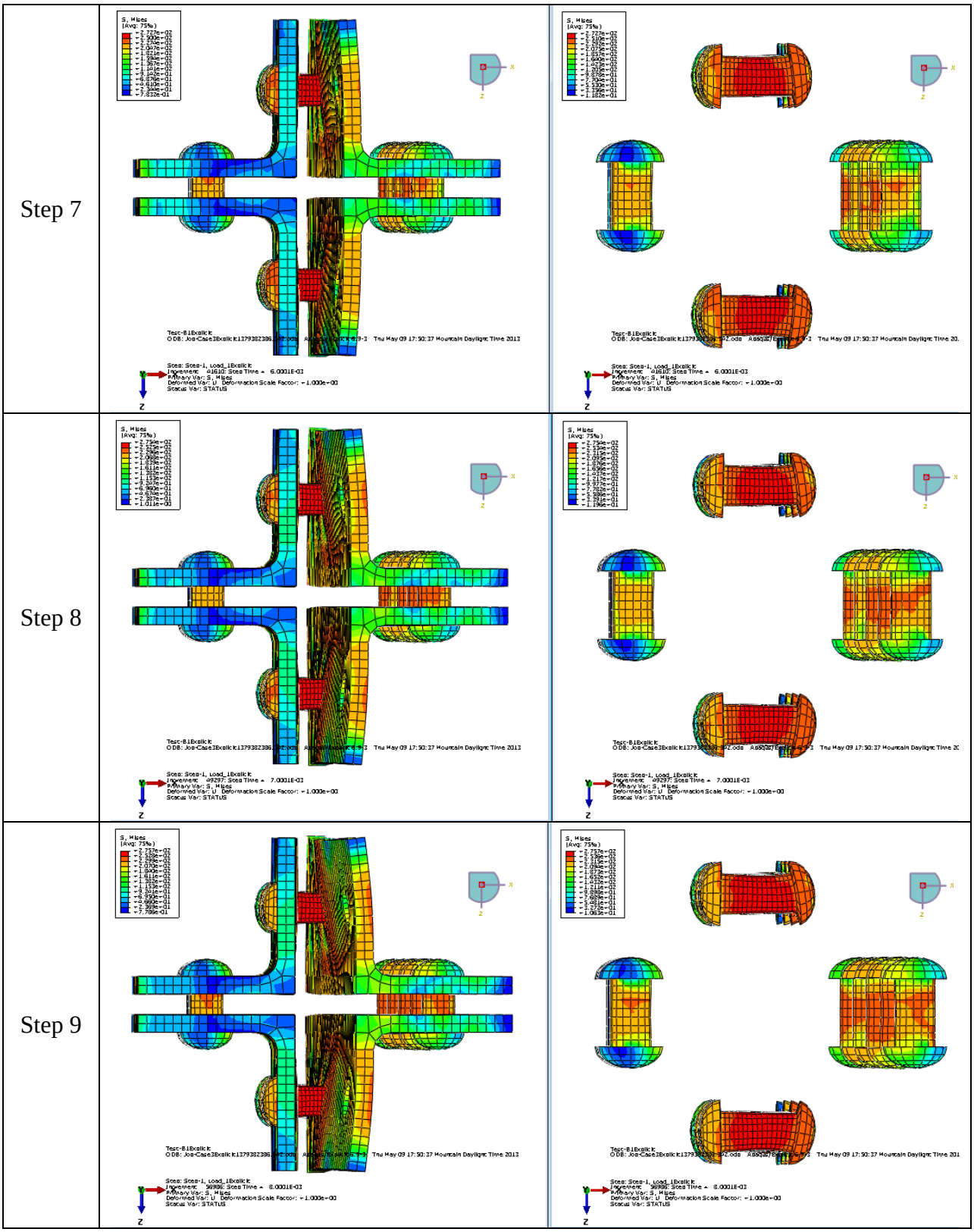

Figure D.7 cont. Stress Distribution on the Connection under Applied Load – Top View

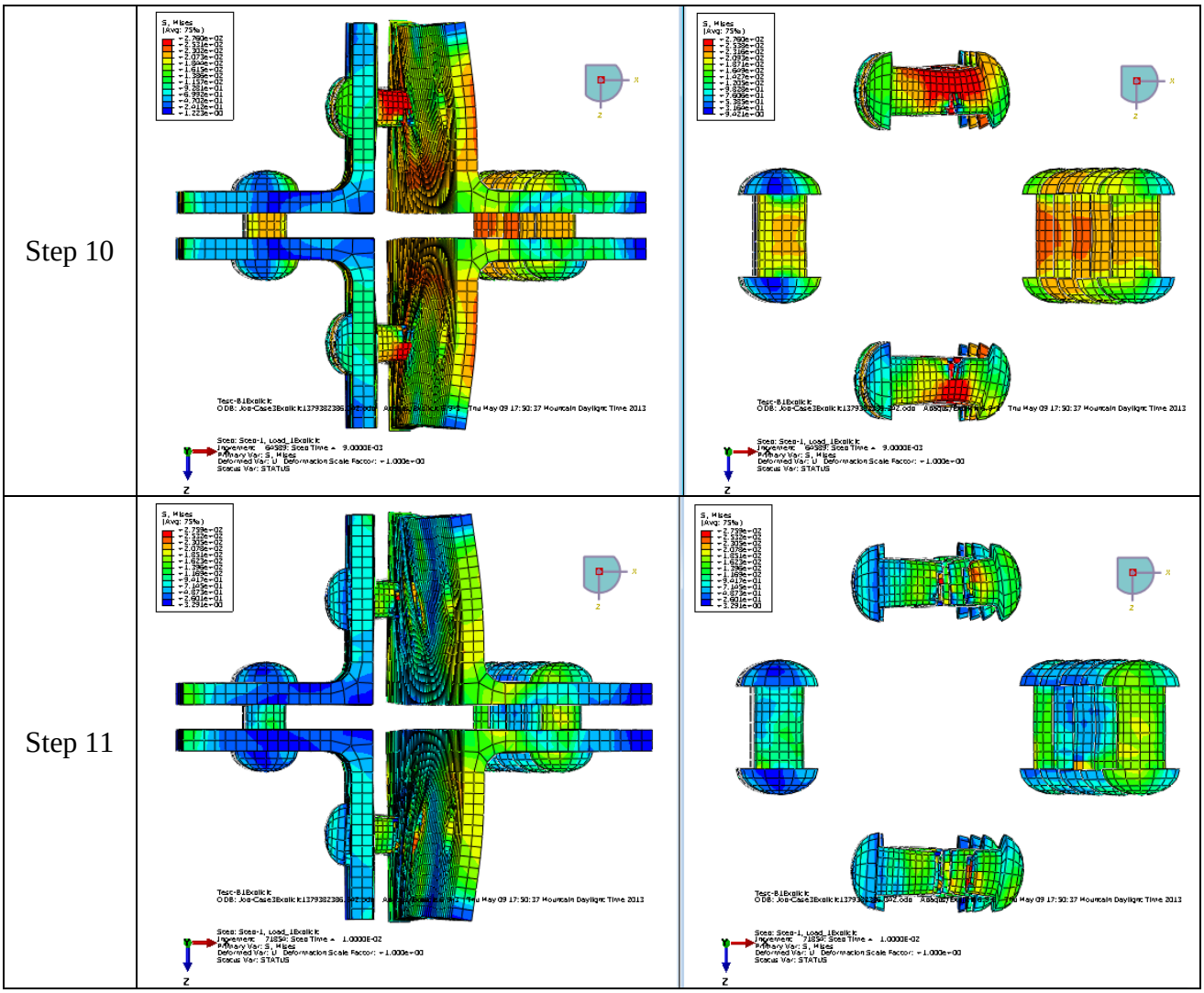

Figure D.7 cont. Stress Distribution on the Connection under Applied Load – Top View

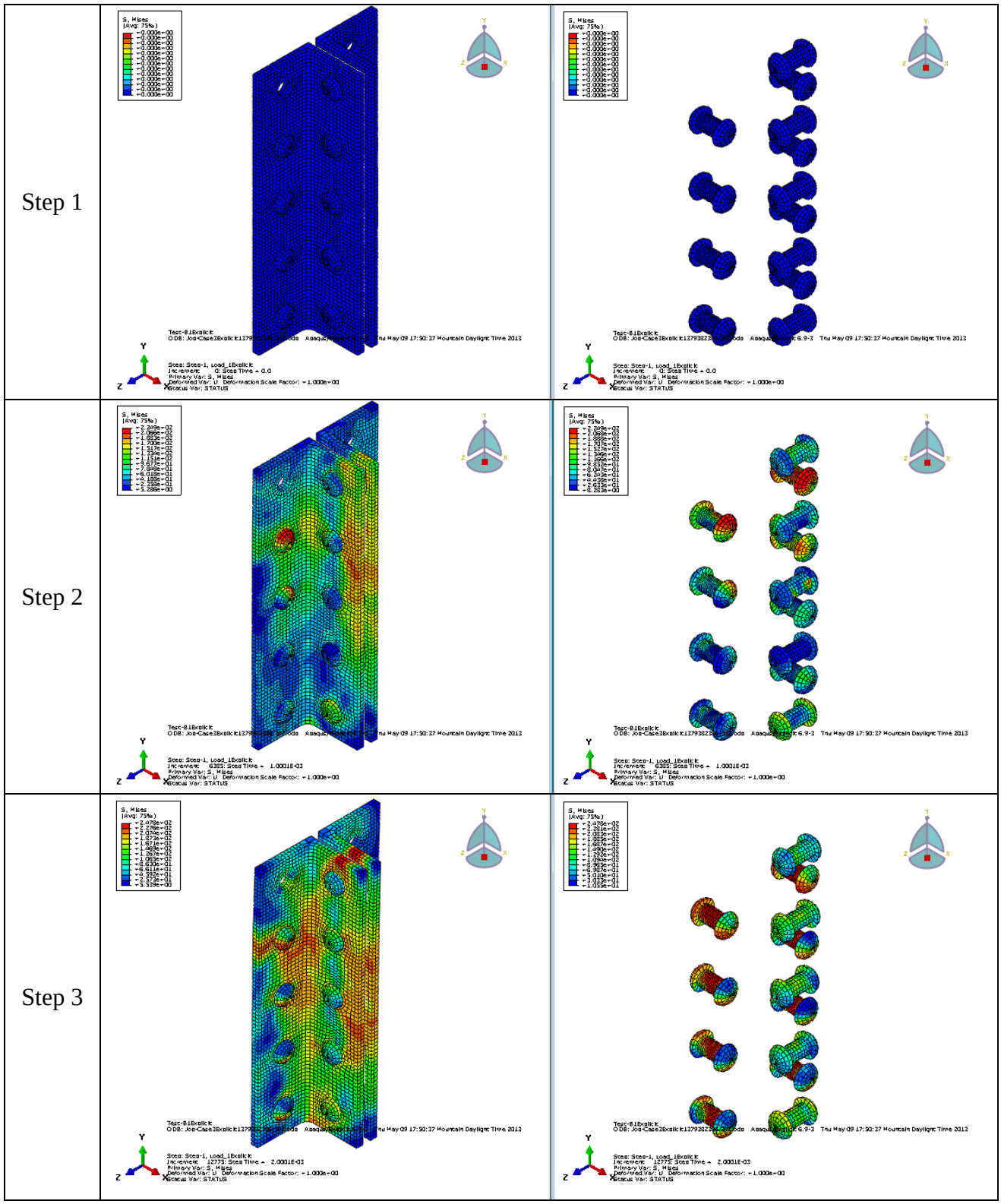

Figure D.8 Stress Distribution on the Connection under Applied Load – Isometric View

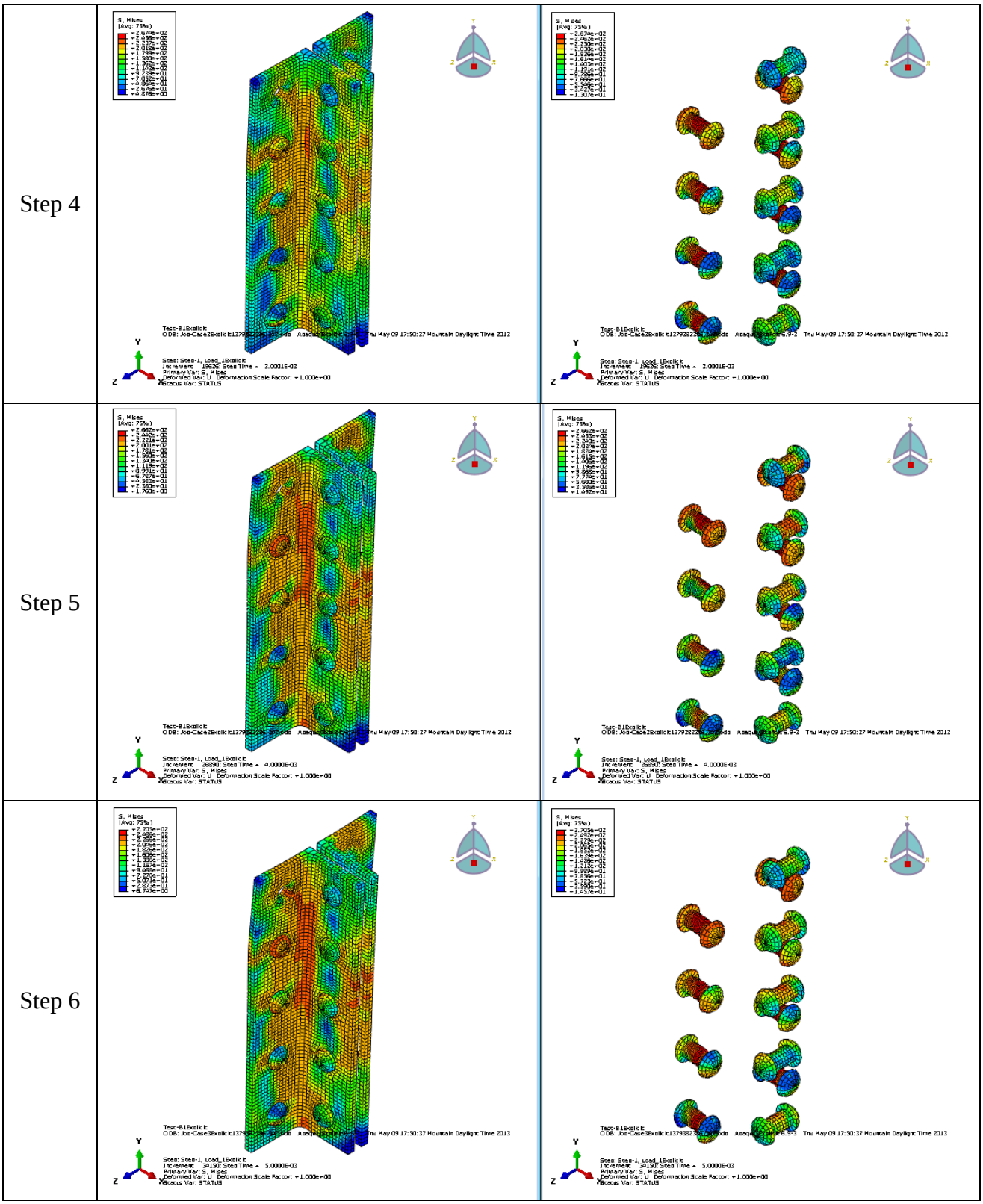

Figure D.8 cont. Stress Distribution on the Connection under Applied Load – Isometric View

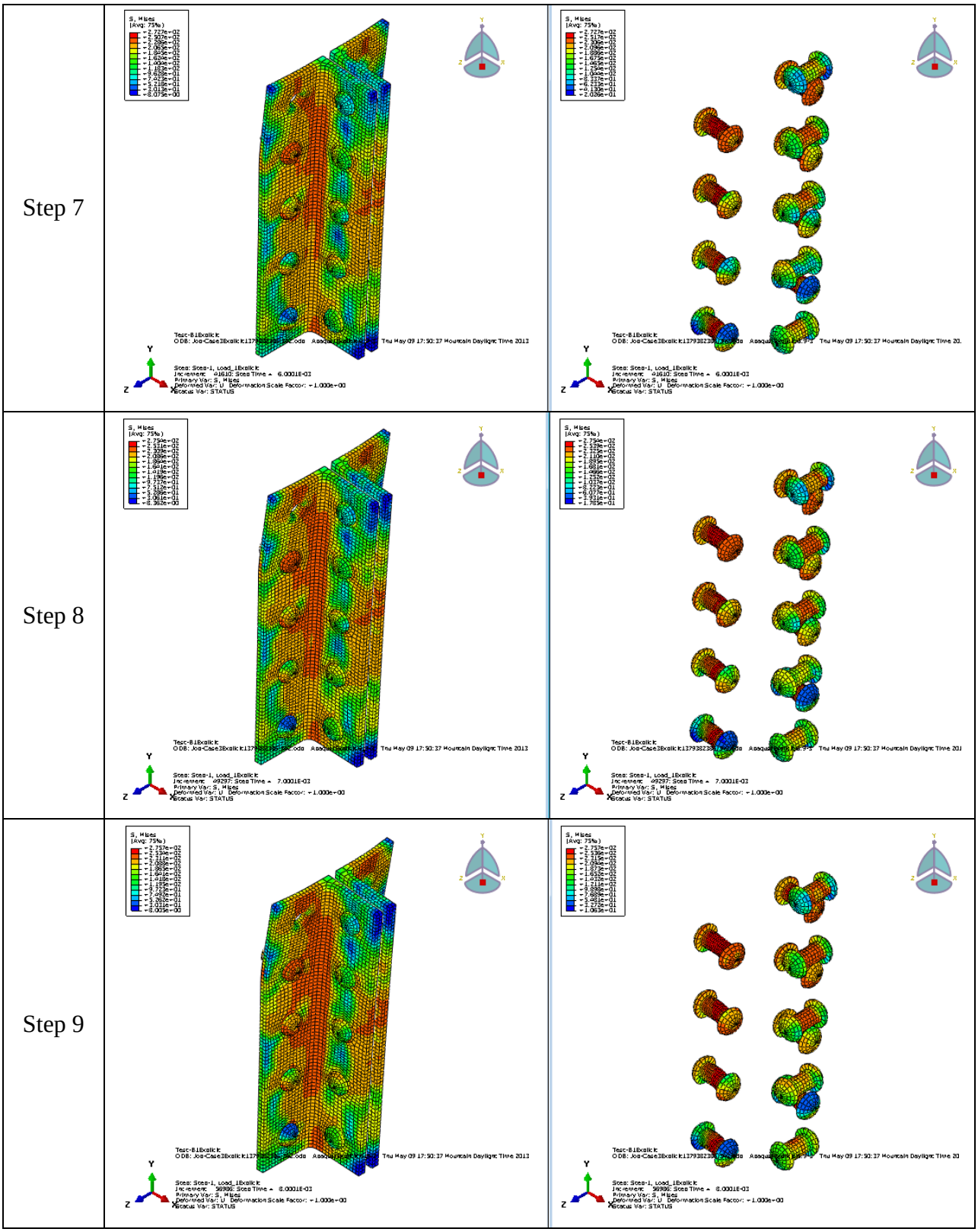

Figure D.8 cont. Stress Distribution on the Connection under Applied Load – Isometric View

Step 10	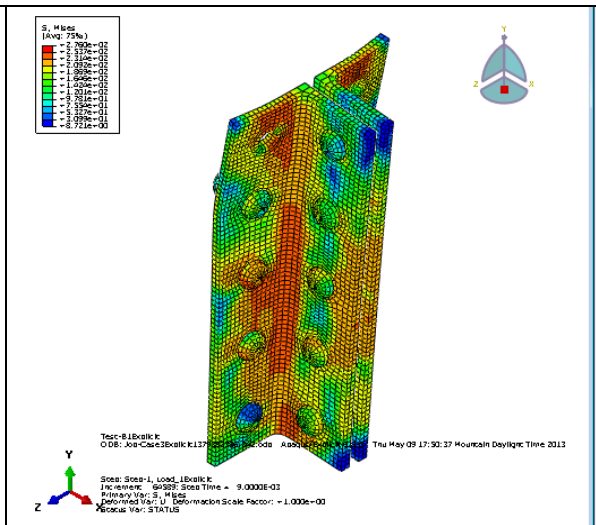	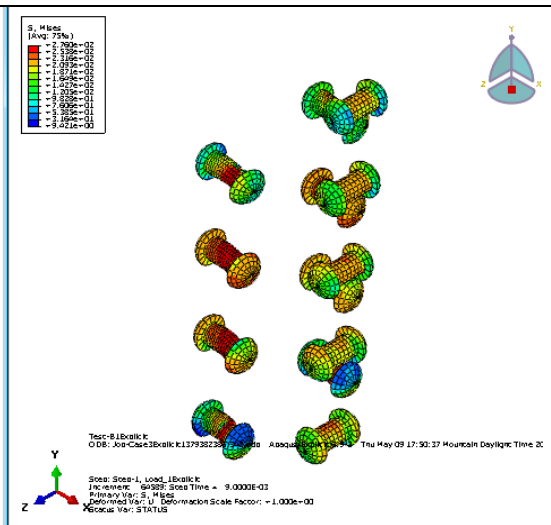
Step 11	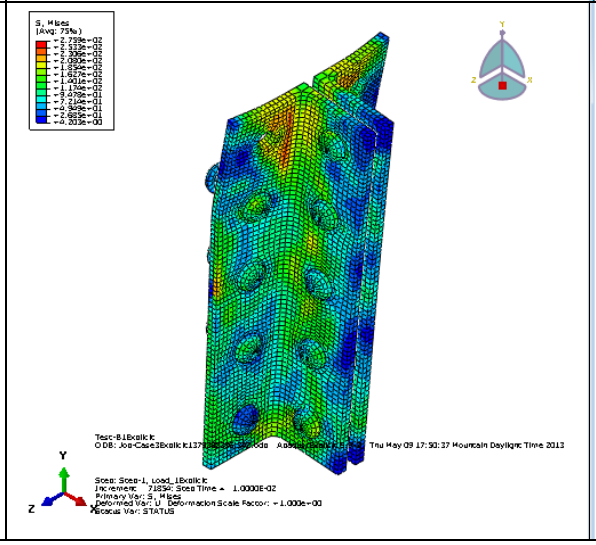	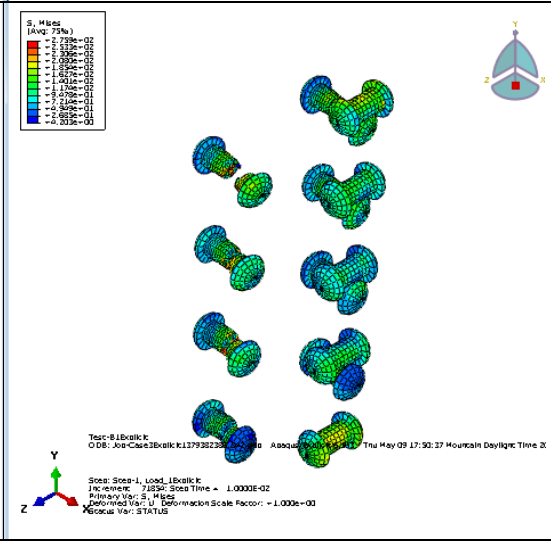

Figure D.8 cont. Stress Distribution on the Connection under Applied Load – Isometric View